Progressive Design and Self-Assembly of Supramolecular Architectures

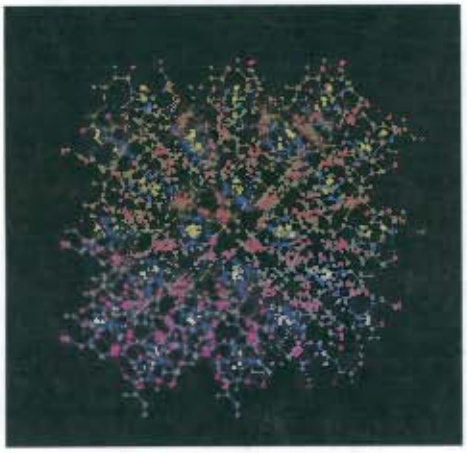

Based on Metallamacrocyclic Nickel(II) Complexes with Bipodal Tetra-alkylaroylbis(thioureas)

By

Oren Hallale

A thesis presented to the

University of Cape Town

for the degree of

Doctor of Philosophy

Department of Chemistry, University of Cape Town

Rondebosch, 7701

Cape Town, South Africa

August 2004

Acknowledgements

This thesis would never have been written, were it not for the following:

My supervisors: Prof. Susan Bourne and Prof. Klaus Koch, who gave me the best of their superb advice, guidance, inspiration, enthusiasm and support. These few lines cannot do justice to the vast amounts of time and resources that they have invested in me.

All the members of the UCT Supramolecular Chemistry Unit: lecturers, researchers, staff and students, who without hesitation: gave me good advice (when asked for), lent a helping hand (when needed), shared ideas freely, and made good conversation around the red corduroy couch.

All the members of the old PGM Research Group at UCT; we may have gone separate ways, but the time together was very well spent. All the members of the new PGM Research Group at Stellenbosch University; although I met with them only seldom, the interaction always proved enjoyable and fruitful.

All the other professors, post-docs and students at UCT with whom I have had the pleasure of interacting and whose lives I have frequently interrupted for various reasons.

All the administrative and technical staff of the UCT Chemistry department. They are the ones who keep everything running smoothly and without them, we would all be lost.

My many other friends whom I know in a non-chemical capacity. They have all put up with my rambling about molecules and crystals for far longer than anyone should have to endure. Whether they listened or not, they have all enriched my life.

Amy, for all her love and support and for keeping me sane. Good job!

Finally, my family: my parents, David and Marcelle, my brothers, Aviv and Nicky, for all their love, support, patience and good humour – and a good kick in the backside when needed.

Thank you all very much.

Publications and Conferences

Part of the work presented in this dissertation has been previously published:

"Self-assembly of 2:2 metallomacrocyclic complexes of Ni^{II} and Pd^{II} with 3,3,3',3'-tetraalkyl1,1'isophthaloylbis(thioureas). Crystal and molecular structures of *cis*-$[Pd(L^2\text{-}S,O)]_2$ and the adducts of the corresponding Ni^{II} complexes: $[Ni(L^1\text{-}S,O)(pyridine)_2]_2$ and $Ni(L^1\text{-}S,O)(4\text{-}dimethylaminopyridine)_2]_2$" K.R. Koch, O. Hallale, S.A. Bourne, J. Miller and J. Bacsa, *Journal of Molecular Structure*, **2001**, 561, 185

Another part has been accepted for publication:

"Hydrogen-bonding networks in a bipodal acyl-thiourea and its Ni(II) 2:2 metallamacrocyclic complex." S.A. Bourne, O. Hallale and K.R. Koch, *Crystal Growth & Design*, **2004**, *in press*.

Parts of this thesis have been presented as a poster:

"Self-assembly of Planar 2:2 and 3:3 Metallamacrocyclic Complexes of Bipodal *N',N',N''',N'''*-tetraalkyl-*N,N''*-phenylenedicarbonylbis(thioureas) with d^8 Metal Ions. Building Blocks for 3-Dimensional Molecular Arrays."

at the following conferences:

1.) XXV International Symposium on Macrocyclic Chemistry, University of St. Andrews, Scotland 2 – 7 July 2000

2.) 35th Convention of the South African Chemical Institute, University of Potchefstroom, September 25 – 29, 2000.

Abstract

Rationally designed bipodal 3,3,3',3'-tetraalkyl-1,1'-benzoylbis(thioureas) are used as pre-programmed chelating ligands to form metallamacrocyclic square planar nickel(II) complexes via self-assembly. Metal : ligand stoichiometries of either 2:2 or 3:3 can be achieved by using *meta*- or *para*- substituted ligands. The metallamacrocyclic complexes are subsequently converted into octahedral adducts via the addition of monodentate nitrogen donor ligands. Metallamacrocycles are further employed as secondary building units in the self-assembly of 1-dimensional double- or triple-connected coordination polymers. The synthesis of these polymers is achieved with the use of exo-bidentate nitrogen donor ligands.

The synthesized compounds have been variously studied by techniques including elemental analysis, IR and NMR spectroscopy and x-ray powder diffractometry. The thermal behaviours of the octahedral adducts and coordination polymers have also been studied. Crystal structures of two chelating ligands, one metallamacrocycle and four octahedral adducts have been elucidated.

One of the octahedral adducts, *cis*-[Ni(I-EtOH-*S,O*)(Pyridine-*N*)$_2$]$_2$, self-assembles into a 3-dimensional infinite supramolecular framework via hydrogen bonding to water guest molecules as well as aromatic interactions between pyridine ligands and guests. Guest-filled channels run continuously through the structure.

One specific coordination polymer, {*cis*-[Ni(I-Et-*S,O*)(DPE-*N,N'*)]$_2$}$_n$, has been found to act as a powerful sensor of chlorinated solvents by way of a mechanism in which a reversible coordination of exo-bidentate ligand to the nickel centres is induced by the sorption of solvent molecules into the crystal structure. This process is visibly manifested as a reversible colour change.

Abbreviations and Symbols

Compounds

Solvents

$CDCl_3$	Deuterated chloroform
DMF	N,N-dimethylformamide
DMSO	Dimethylsulfoxide
$DMSO\text{-}_{d6}$	Deuterated dimethylsulfoxide

Ligands

I-Et	3,3,3',3'-Tetraethyl-1,1'-isophthaloylbis(thiourea)
T-Et	3,3,3',3'-Tetraethyl-1,1'-terephthaloylbis(thiourea)
I-EtOH	3,3,3',3'-Tetra(2-hydroxyethyl)-1,1'-isophthaloylbis(thiourea)
T-EtOH	3,3,3',3'-Tetra(2-hydroxyethyl)-1,1'-terephthaloylbis(thiourea)
Py	Pyridine
DMAP	4-Dimethylaminopyridine
Bipy	4,4'-Bipyridine
BPE	1,2-Bis(4-pyridyl)ethane
DPE	1,2-Di(4-pyridyl)ethylene

Metallamacrocycles

***Cis*-[Ni(I-Et-*S,O*)]$_2$**

Cis-[bis-μ-(3,3,3',3'-tetraethyl-1,1'-isophthaloylbis(thioureato-*S,O*))-di-nickel(II)]

***Cis*-[Ni(T-Et-*S,O*)]$_3$**

Cis-[tris-μ-(3,3,3',3'-tetraethyl-1,1'-terephthaloylbis(thioureato-S,O))-tri-nickel(II)]

***Cis*-[Ni(I-EtOH-*S,O*)]$_2$**

Cis-[bis-μ-(3,3,3',3'-tetra(2-hydroxyethyl)-1,1'-isophthaloylbis(thioureato-*S,O*))-di-nickel(II)]

***Cis*-[Ni(T-EtOH-*S,O*)]$_3$**

Cis-[tris-μ-(3,3,3',3'-tetra(2-hydroxyethyl)-1,1'-terephthaloylbis(thioureato-*S,O*))-tri-nickel(II)]

Octahedral Adducts of Metallamacrocycles

***Cis*-[Ni(I-Et-*S,O*)(pyridine-*N*)$_2$]$_2$**

[*Cis*-(bis-μ-(3,3,3',3'-tetraethyl-1,1'-isophthaloylbis(thioureato-*S,O*))-di-nickel(II))-tetra(pyridine-*N*)]

***Cis*-[Ni(I-Et-*S,O*)(DMAP-*N*)$_2$]$_2$**

[*Cis*-(bis-μ-(3,3,3',3'-tetraethyl-1,1'-isophthaloylbis(thioureato-*S,O*))-di-nickel(II))-tetrakis(4-dimethylaminopyridine-*N*)]

***Cis*-[Ni(T-Et-*S,O*)(pyridine-*N*)$_2$]$_3$**

[*Cis*-(tris-μ-(3,3,3',3'-tetraethyl-1,1'-terephthaloylbis(thioureato-*S,O*))-tri-nickel(II))-hexa(pyridine-*N*)]

***Cis*-[Ni(I-EtOH-*S,O*)(pyridine-*N*)$_2$]$_2$**

[*Cis*-(bis-μ-(3,3,3',3'-tetra(2-hydroxyethyl)-1,1'-isophthaloylbis(thioureato-*S,O*))-di-nickel(II))-tetra(pyridine-*N*)]

***Cis*-[Ni(T-EtOH-*S,O*)(pyridine-*N*)$_2$]$_3$**

[*Cis*-(tris-μ-(3,3,3',3'-tetra(2-hydroxyethyl)-1,1'-terephthaloylbis(thioureato-*S,O*))-tri-nickel(II))-hexa(pyridine-*N*)]

Coordination Polymers

{*Cis*-[Ni(I-Et-*S,O*)(pyrazine-*N,N'*)]$_2$}$_n$

Poly-[*cis*-(bis-μ-(3,3,3',3'-tetraethyl-1,1'-isophthaloylbis(thioureato-*S,O*))-di-nickel(II))-bis-μ-(pyrazine-*N,N'*)]

{*Cis*-[Ni(I-Et-*S,O*)(bipy-*N,N'*)]$_2$}$_n$

Poly-[*cis*-(bis-μ-(3,3,3',3'-tetraethyl-1,1'-isophthaloylbis(thioureato-*S,O*))-di-nickel(II))-bis-μ-(4,4'-bipyridine-*N,N'*)]

{*Cis*-[Ni(I-Et-*S,O*)(BPE-*N,N'*)]$_2$}$_n$

Poly-[*cis*-(bis-μ-(3,3,3',3'-tetraethyl-1,1'-isophthaloylbis(thioureato-*S,O*))-di-nickel(II))-bis-μ-(1,2-bis(4-pyridyl)ethane-*N,N'*)]

{*Cis*-[Ni(I-Et-*S,O*)(DPE-*N,N'*)]$_2$}$_n$

Poly-[*cis*-(bis-μ-(3,3,3',3'-tetraethyl-1,1'-isophthaloylbis(thioureato-*S,O*))-di-nickel(II))-bis-μ-(1,2-di(4-pyridyl)ethylene-*N,N'*)]

{*Cis*-[Ni(T-Et-*S,O*)(pyrazine-*N,N'*)]$_2$}$_n$

Poly-[*cis*-(tris-μ-(3,3,3',3'-tetraethyl-1,1'-terephthaloylbis(thioureato-*S,O*))-tri-nickel(II))-tris-μ-(pyrazine-*N,N'*)]

{*Cis*-[Ni(T-Et-*S,O*)(bipy-*N,N'*)]$_3$}$_n$

Poly-[*cis*-(tris-μ-(3,3,3',3'-tetraethyl-1,1'-terephthaloylbis(thioureato-*S,O*))-tri-nickel(II))-tris-μ-(4,4'-bipyridine-*N,N'*)]

{*Cis*-[Ni(T-Et-*S,O*)(DPE-*N,N'*)]$_3$}$_n$

Poly-[*cis*-(tris-μ-(3,3,3',3'-tetraethyl-1,1'-terephthaloylbis(thioureato-*S,O*))-tri-nickel(II))-tris-μ-(1,2-di(4-pyridyl)ethylene-*N,N'*)]

Techniques

HSM	Hot stage microscopy
IR	Infrared spectroscopy
MALDI-TOF MS	Matrix-assisted laser desorption / ionisation – time of flight mass spectroscopy
NMR	Nuclear magnetic resonance spectroscopy
TGA	Thermogravimetric analysis
XRD	X-ray powder diffractometry

Other Abbreviations and Symbols

1D / 2D / 3D	One, two, and three dimensional
A	Hydrogen bond acceptor
Å	Angstrom (10^{-10} metres)
D	Hydrogen bond donor
e	Electron
F	Structure factor
F(000)	Number of electrons in the unit cell
L.S.	Least squares
μ	Absorption coefficient
Rms.	Root mean square
Z	Number of structural units in the unit cell

Contents

Chapter 1

Introduction

1.1. Acyl- and- aroylthioureas: Synthesis, Coordination and Uses

1.1.1. Classification of 1-acyl-3,3-dialkylthiourea based compounds

The fundamental chemical unit of this project is the *1-acyl-3,3-dialkylthiourea* (sometimes shortened to *acylthiourea*) moiety, shown in Figure 1.1.1(a). In essence, the 1-acyl-3,3-dialkylthiourea group consists of an amino unit bonded to a thiocarbonyl group that is in turn linked through a central secondary nitrogen atom to an acyl moiety.

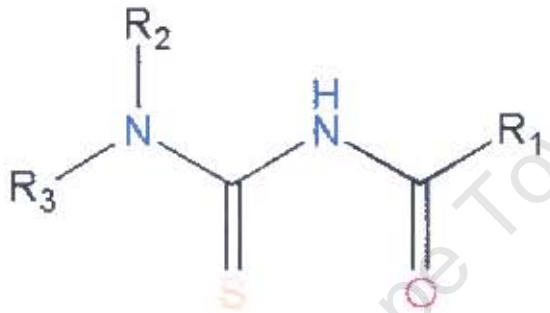

Figure 1.1.1(a). General structure of a 1-acyl-3,3-dialkylthiourea

A large variety of different compounds of this class may be synthesised simply by varying the terminal side chains (labelled R_1, R_2 and R_3). This project is based on one specific variation on the theme: the bipodal acylthiourea, more correctly termed the 3,3,3',3'-tetraalkyl-1,1'-acylbis(thiourea). This is a compound containing two acylthiourea moieties that are linked together by a central spacer unit. This spacer could be any of a vast number of groups (see Figure 1.1.1(b).), but for the purposes of this project, the spacer used in each case is a phenyl ring. The relative substitution of the phenyl ring can be either *meta-* or *para-*, classed as *isophthaloyl* (I) and *terephthaloyl* (T), as they are synthesised from isophthaloyl dichloride and terephthaloyl dichloride respectively.

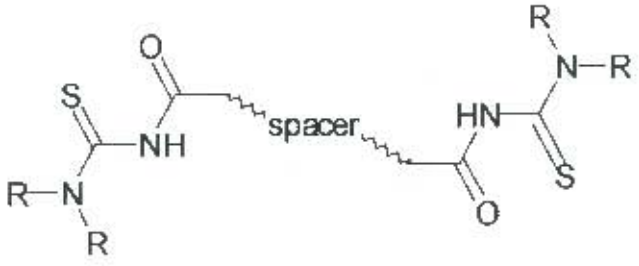

Figure 1.1.1(b). General structure of a 3,3,3',3'-tetraalkyl-1,1'-acylbis(thiourea)

Figure 1.1.1(c) below illustrates the two types of bipodal benzoylthioureas. The difference in geometry of these two types of compound is vital – as it is the exploitation of these geometries that leads to the 'pre-programming' of these compounds to self-assemble into metallamacrocyclic square planar complexes with the d^8 metal ions Pt(II), Pd(II) and Ni(II).

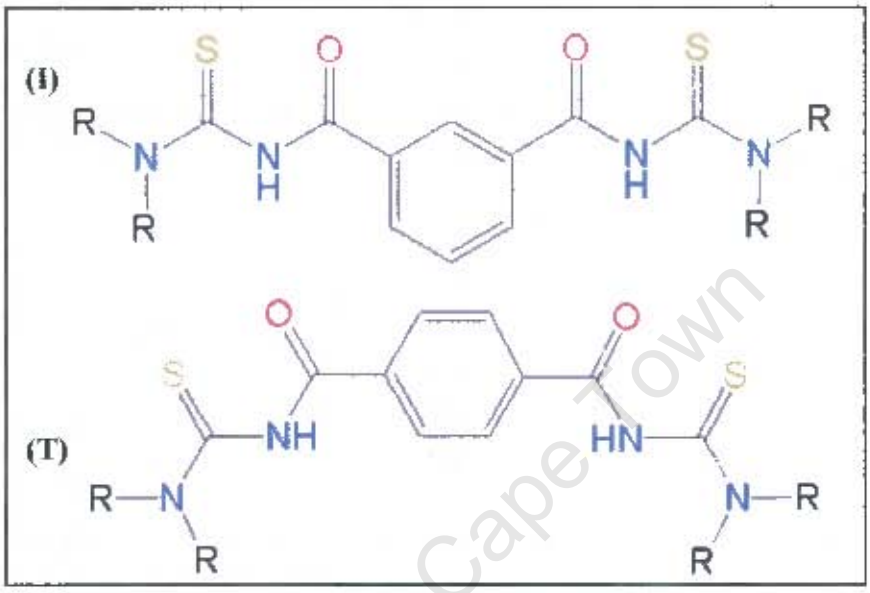

Figure 1.1.1(c). Structures of two types of bipodal benzoylthiourea: 3,3,3',3'-tetraalkyl-1,1'-isophthaloylbis(thiourea) (I) and 3,3,3',3'-tetraalkyl-1,1'-terephthaloylbis(thiourea) (T)

In the isophthaloylbis(thioureas), the acylthiourea groups are oriented in the same direction, while in the case of the terephthaloylbis(thioureas) the acylthiourea groups' orientations are offset by 60°. This difference and its consequences will be discussed below in great detail.

1.1.2. Synthesis of acylthiourea-based compounds

It is possible to synthesise a vast array of compounds based on the acylthiourea moiety by a variety of methods. The simplest method is that of Douglass and Dains[1]. This is a 2-step 1-pot reaction in which, firstly, one molar equivalent of an acid chloride (possessing the desired acyl or aroyl group) is added to one molar equivalent of potassium thiocyanate and refluxed in dry solvent under a nitrogen atmosphere to avoid undesired side reactions. The intermediate is an acyl isothiocyanate. After

cooling, one molar equivalent of an amine is added to the mixture, which is refluxed under nitrogen again. The final product is the desired 1-acyl-3-alkylthiourea or 1-acyl-3,3-dialkylthiourea (depending on whether a primary or secondary amine is used in the second step). The mechanism of this reaction is relatively simple and is illustrated below in Figure 1.1.2(a).

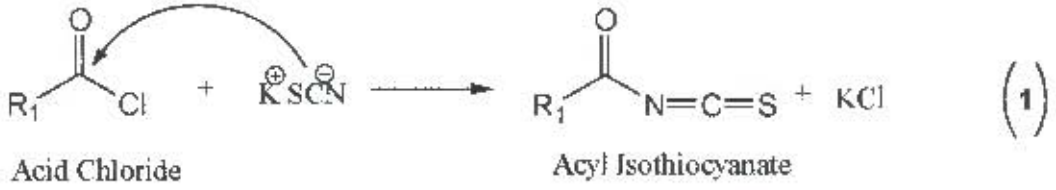

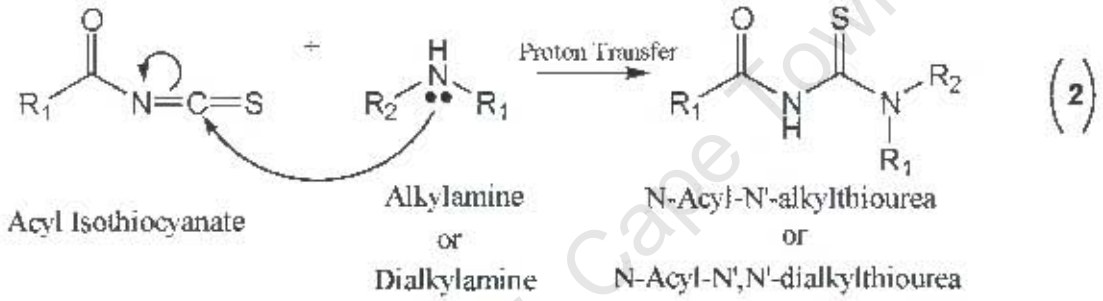

Figure 1.1.2(a). General reaction scheme of the Douglass and Dains reaction

The negatively charged thiocyanate ion attacks the acid chloride at the electrophilic carbonyl carbon via the nucleophilic nitrogen, displacing the chloride ion to form an isothiocyanate. This is in effect the same as the aminolysis of an acid chloride. This type of reaction proceeds rapidly and usually results in good yields. Following the formation of the isothiocyanate, an alkyl or dialkylamine is added. The nucleophilic amino nitrogen can attack either the carbonyl carbon (giving rise to an amide moiety) or the isothiocyanato carbon (resulting in the desired acylthiourea), both carbons being electron deficient.

In practice, the undesired amide formation does not occur when reacting an aroyl isothiocyanate with an amine containing an ethyl or longer alkyl chain. It is believed that the alkyl chains sterically impede the path of the amine to the carbonyl carbon, which is itself in a sterically shielded position[2]. This regioselectivity, in which only the isothiocyanato carbon is attacked by the amine, makes the aroylthiourea the sole product – provided that all solvents and reagents are dry and that the reaction is

performed under an inert atmosphere. In the case of a bipodal aroylthiourea, the starting material would be an aroyl dicarboxylic chloride. Two molar equivalents each of potassium thiocyanate and the desired amine would be used. Figure 1.1.2(b) gives the reactions that result in the two types of bipodal benzoylthiourea.

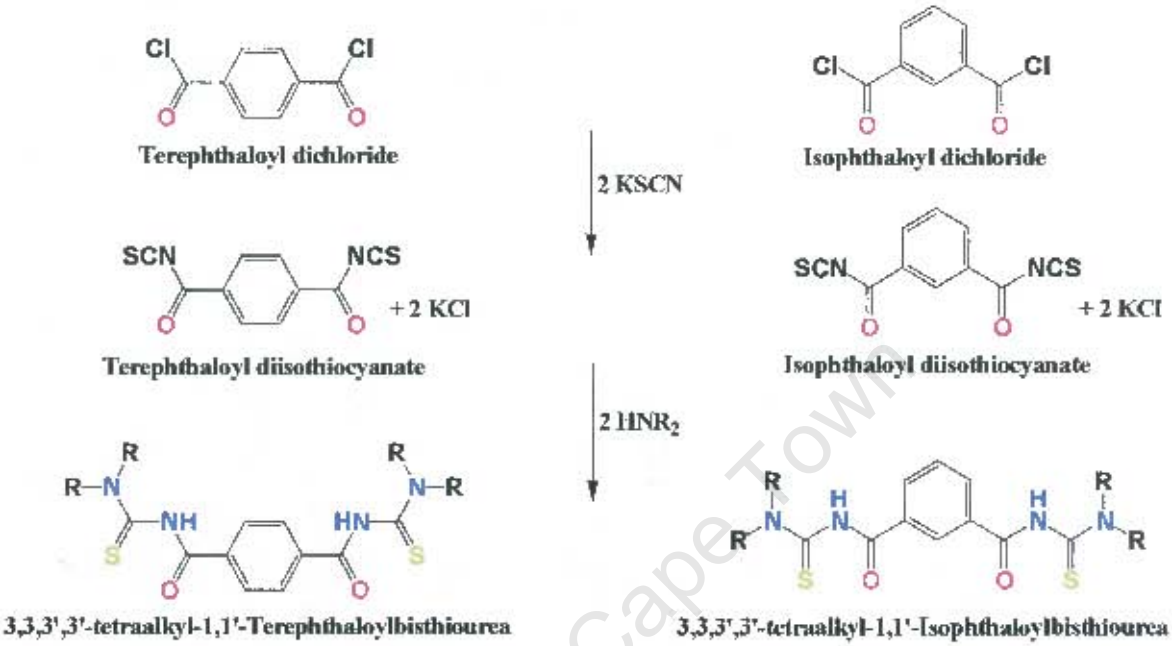

Figure 1.1.2(b). General reaction schemes to synthesise bipodal benzoylthioureas with different relative substitutions

1.1.3. Modes of coordination of acylthioureas to metals

The acylthiourea moiety contains at least three potential donor atoms (N, O and S). Any of these nucleophilic centres may be involved in coordination to metal cations. To date, only certain coordination modes have been observed.

These trends are not rigid rules, but are well adhered to, allowing one to make fairly accurate predictions about the products of acylthiourea to metals. In general, the coordination of an acylthiourea to a metal through a nitrogen atom does not occur, but at least two examples are known: the *N,S*- chelate complex *trans*-bis(1-butanoyl-3-propylthioureato) platinum(II)[2] and the *N,S,O*-coordination of 1-benzoyl-3-phenylthiourea to two Rhodium(I) centres to form a bridged dinuclear complex.[3] The majority of cases of acylthiourea complexes fall into two categories of coordination: monodentate *S*-coordinated complexes or bidentate *S,O*-coordinated

chelate complexes. Although there are only a relatively small number of papers in the literature reporting the coordination of 1-acyl-3-alkylthioureas, they suggest that these compounds preferentially undergo monodentate *S*-coordination. This behaviour is due to the 'locking' of the carbonyl oxygen in a stable 6-membered ring by an intramolecular hydrogen bond to the thioamido nitrogen as shown in Figure 1.1.3(a) below. [4,5,6,7]

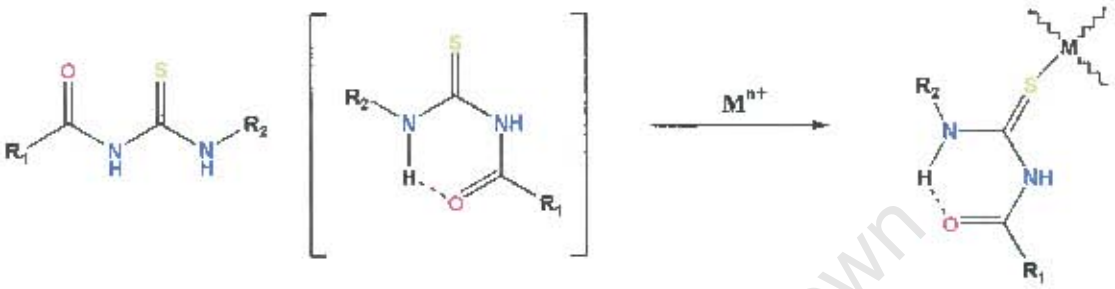

Figure 1.1.3(a). Representation of the preferential coordination mode of 1-acyl-3-alkylthiourea to a metal centre due to 'locking' of carbonyl oxygen in an intramolecular H-bond

The study of the coordination of this class of compound has been limited mainly to reactions with Platinum Group Metals, although a reported attempt to coordinate one such ligand to Ni(II) did not yield any product.[8] In each of the reactions with PGMs, both *cis*- and *trans*- square planar bis-thioureato complexes were observed.

There is much scope for further research into the properties of the 1-acyl-3-alkylthioureas as they have not been studied to the same extent as the dialkyl-substituted variants. This project however, only deals with dialkyl-substituted acylthioureas, which – with their well-studied and predictable coordination behaviour – are good candidates for components in self-assembly reactions.

The 1-acyl-3,3-dialkylthioureas have been used as ligands in coordination compounds with a variety of transition metals over the last three decades. Early work done by Hoyer and Beyer included acylthiourea complexes with such metal ions as Ni(II) and Pd(II), along with several others.[9,10,11,12,13] This research demonstrated that the 1-acyl-3-3-dialkylthioureas most often acted as *S,O*-chelating ligands. This was later found to also be the case in complexes of Ru(III)[14], Rh(III)[15] and Pt(II).[16]

Overall, it was shown that 1-acyl, 3,3-dialkylthioureas readily form *S,O*-chelate complexes with a variety of metals. Moreover, when reacted with the d^8 metals Ni(II), Pd(II) and Pt(II), the result was almost invariably a square planar bis-chelate complex with *cis*-configuration around the metal centre. Such chelate complexes are greatly stabilised by the high degree of electron delocalisation in the 6-membered chelate ring, which can be detected by the significant changes in bond lengths in the ligand upon complexation [9, 16]. In most cases, a prerequisite for the formation of these chelate complexes is the deprotonation of the central nitrogen atom (see Figure 1.1.3(b)), and it has been shown at least for dialkyl-substituted aroylthioureas that the chelate ring can be broken by reprotonating the nitrogen atom with a strong acid to yield a complex in which the aroylthiourea acts as a monodentate ligand [17]

The predominant tendency of 1-aroyl-3,3-dialkylthioureas to form *cis*- square planar complexes with d^8 metals is of huge importance to this project, as it is another element of the 'pre-programming' of the system that allows self-assembly to occur. In most cases, the exclusive product of the reaction is the *cis*- bis- chelate complex.

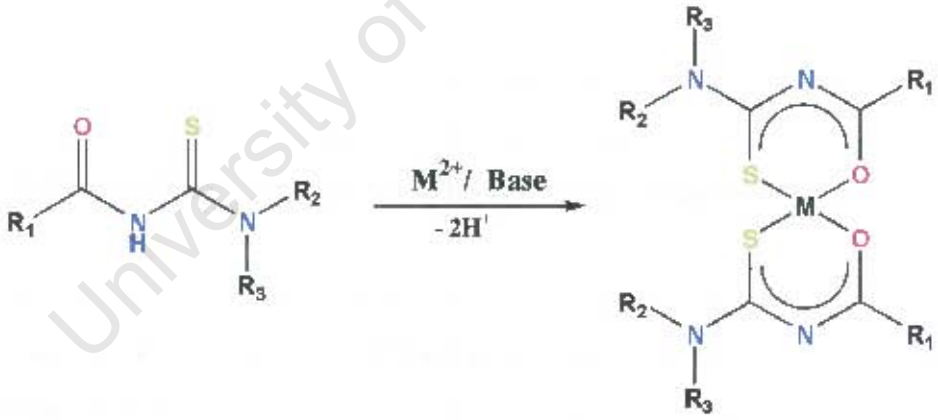

Figure 1.1.3(b) Representation of the preferred coordination mode of 1-acyl-3,3-dialkylthioureas with d^8 M(II) ion to form a *cis*- bis- *S,O*-chelate complex with electron delocalised chelate rings

It is very interesting to note that there is only one published example of a *trans*-chelate complex of a dialkyl-substituted aroylthiourea: a platinum(II) complex with 1-naphthoyl-3,3-di(*n*-butyl)thiourea[18]. In fact, a mixture of *cis*- and *trans*- complexes in the ratio 85: 15 was obtained – indicating that even in this case the *cis*- product is the preferred one.

As mentioned above, the bis- chelate products are thermodynamically very stable due to the electron delocalisation in the 6-membered chelate rings. This would apply to both *cis*- and *trans*- chelate complexes. It is therefore believed that the effect that inhibits the obtaining of the *trans*- isomer as a final product is a kinetic effect. However the reaction mechanism that gives rise to the phenomenon of predominant – and often exclusive – *cis*- chelation is not yet well elucidated.

The mechanism of coordination is most likely associative – typically observed for coordinatively unsaturated metal ions such as Ni(II), Pd(II) and Pt(II) in 16 electron square planar complexes. Therefore, the *trans* effect must be taken into account and can be used to explain the outcome of such a reaction.

In terms of the Hard / Soft Acid / Base (HSAB) theory, [19] one may consider the d^8 2+ metals to be soft Lewis acids (Ni^{2+}, being a harder acid than Pd^{2+} and Pt^{2+} due to its smaller ionic radius, is considered borderline between hardness and softness). The potential electron donor atoms in an acylthiourea differ in terms of their hardness, with the thiocarbonyl sulfur atom considered to be a softer base than the carbonyl oxygen.

Since soft acids have a greater affinity for soft bases than for hard bases, it is thought that the initial coordination of the acylthiourea to the metal ion is via the S atom. The harder carbonyl oxygen atom of the same ligand molecule is then able to coordinate in a position *cis*- to the S atom, and, as a strong σ-donor, is able to exert a considerable *trans*- effect, kinetically enhancing substitution at the position *trans*- to the oxygen atom with the S atom of the second acylthiourea ligand. Subsequently the second chelate ring is closed by the coordination of the final O atom – giving rise to a thermodynamically stable *cis*- bis- chelate complex.

This proposed process is illustrated by the example of 1-benzoyl-3,3-diethylthiourea coordinating to [tetrachloroplatinum(II)] $^{2-}$ in Figure 1.1.3(c).

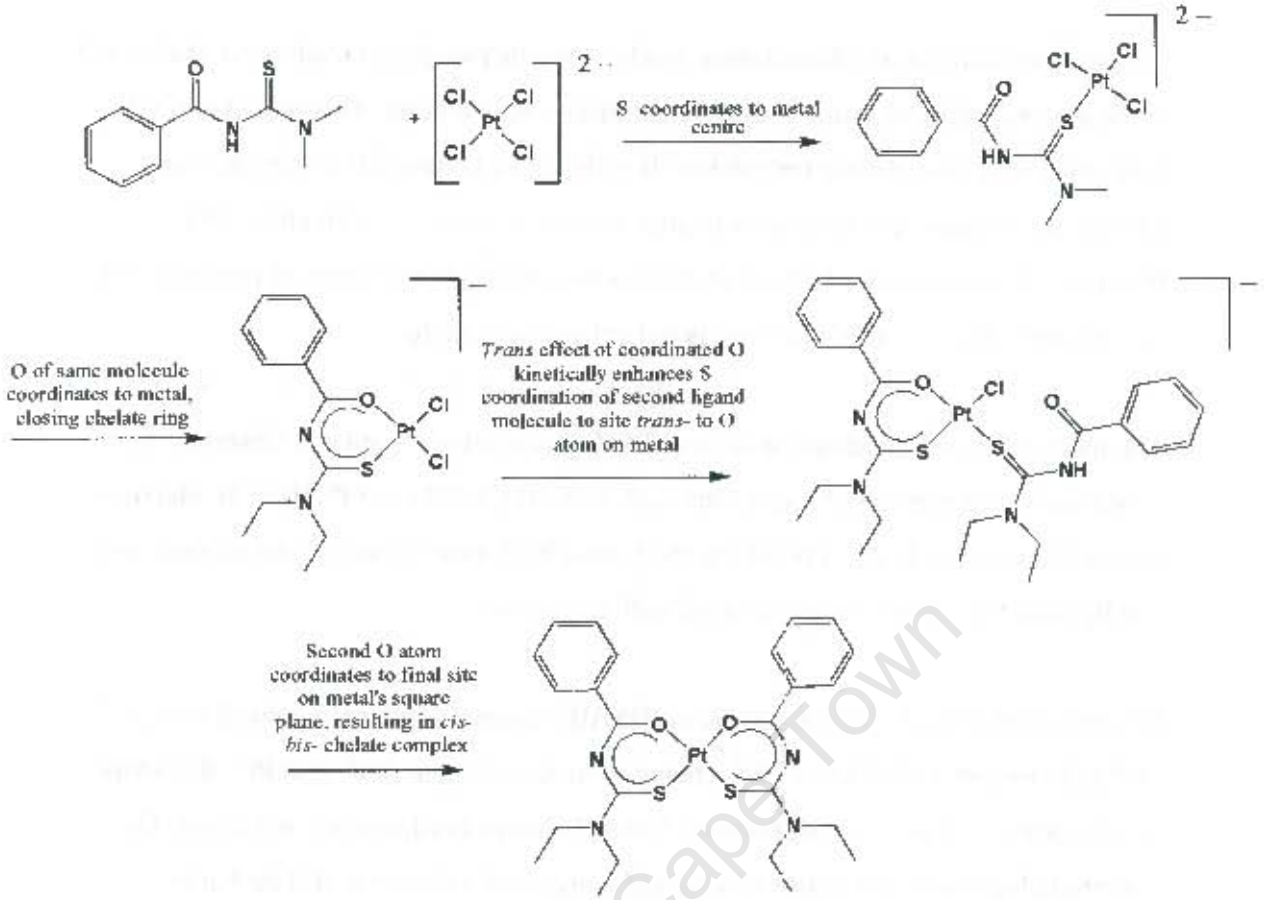

Figure 1.1.3(c). Illustration of proposed process by which *cis*- bis- chelate aroylthiourea complexes are preferentially formed using example of 1-benzoyl-3,3-diethylthiourea coordinating to Pt(II).

The proposed process by which complexation occurs does not satisfactorily explain why in most cases the *cis*- complex is the exclusive product rather than merely the preferentially formed one. However, if one considers the case of a ligand possessing a large aromatic system, such as 1-naphthoyl-3,3-di(*n*-butyl)thiourea, it can be argued that electron delocalisation from the carbonyl oxygen into the aromatic system could result in a weakening of the *trans* effect that would decrease the kinetic favourability of the *cis*- product and allow the formation of the *trans*- complex – albeit as the minor product. It must be stated however, that this argument is speculative. New research indicates that the processes of formation of *cis*- and *trans*- complexes and transformation from one to the other are far more complicated than this, involving photochemical reaction mechanisms.[20]

The exact mechanism for exclusive *cis*- complex formation is outside the scope of this project (as will be discussed below), although the phenomenon itself is exploited as a key facet of the work reported herein.

1.1.4. Potential uses of acylthioureas

In general terms, acylthioureas have demonstrated much utility in increasing our understanding of coordination chemistry, because of their versatile coordination behaviour and virtually limitless variety. However, it must also be noted that such compounds have also been studied for specific practical purposes. These potential uses are worth discussing briefly.

Since acylthioureas have a specific affinity for soft metals like platinum and other PGMs, they have been of great interest as potentially useful compounds in various aspects of the PGM mining industry. Since being identified as highly selective complexing agents for the PGMs, [21, 22] they have been utilised in the solvent extraction of PGMs [21, 23, 24, 25, 26] as well as the efficient chromatographic separation of PGMs [27, 28, 29] and in ultra trace determination of PGMs by pre-concentration [28, 29, 30]. Related thiourea derivatives containing chromophoric and fluorescent groups have been effectively synthesised and coordinated to Pt(II)[31], potentially providing another means of highly sensitive analysis of precious metals – a concept that can easily be extended from thioureas to acylthioureas. Clearly, in the areas of PGM extraction, separation and analysis, the acylthioureas are invaluable compounds with many realised and potential applications.

There are other areas in which these versatile compounds may be used. Most prominent are the potential medicinal applications of thiourea and acylthiourea derivative complexes. There are references to such compounds exhibiting anticancer properties [32, 33] – a pathway that was originally explored because these complexes bear some similarity to the square planar Pt(II) complex *cisplatin* – a proven anticancer drug.[34] Similar complexes have been reported to possess antifungal,[35, 36] antimalarial [37] and antibiotic properties.[38]

1.1.5. Bipodal aroylthioureas and their complexes

The use of bipodal aroylthioureas as chelating ligands immediately allows the possibility of polymeric or oligomeric multinuclear complexes, as one ligand molecule is able to coordinate simultaneously to two metal centres. The first reported complex of this type was the Ni(II) complex with 3,3,3',3'-tetraethyl-1,1'-terephthaloylbis(thiourea) by Hoyer *et al.* in 1986.[39] The crystal structure of this complex clearly showed that it was a trimeric metallamacrocyclic complex with a metal: ligand ratio of 3:3. Other complexes of Cu(II), Zn(II), Hg(II) and Pd(II) were also synthesised but were not characterised as well as the Ni(II) complex. The latter three were reported to be polymeric.

A year later, a paper by Konig *et al.* reported the use of 3,3,3',3'-tetraalkyl-1,1'-alkanedicarbonyl-bis(thiourea) ligands in complexation reactions with Ni(II), Cu(II), Pd(II) and Pt(II).[40] This paper did not report any structural details, but did report that in the case of 3,3,3',3'-tetraethyl-1,1'adipoylbisthiourea, a Pd(II) complex possessed a metal: ligand ratio of 3:3, while a Pt(II) complex did not appear to do so.

A decade later, Pt(II) complexes of the two ligand types (isophthaloyl and terephthaloyl) were first characterised by x-ray diffractometry.[41] The difference in relative substitution between 3,3,3',3'-tetraalkyl-1,1'-isopthaloylbis(thioureas) and 3,3,3',3'-tetraalkyl-1,1'-terephthaloylbis(thioureas) was found to be the key in synthesising metallamacrocyclic complexes of Pt(II) with two different stoichiometries: the isophthaloyl ligands gave rise to 2:2 metallamacrocycles, while the terephthaloyl ligands formed 3:3 metallamacrocycles. Crystal structures of complexes of each type were reported. It was stated that the strong tendency of aroylthioureas to form *cis*- chelates with Pt(II) coupled with the geometry of the acylthiourea moieties' alignments (due to the relative substitution around the phenyl ring), imposes very specific outcomes on the various reactions – hence resulting in the exclusive formation of metallamacrocycles of specific stoichiometry. These outcomes can be predicted by using simple molecular models or molecular drawings. Figure 1.1.5(a) below illustrates this principle, showing how 3,3,3',3'-tetraethyl-1,1'-terephthaloylbis(thiourea) is directed to form a 3:3 metallamacrocycle while 3,3,3',3'-tetraethyl-1,1'-isophthaloylbis(thiourea) is directed to form either a 2:2 or a 6:6

metallamacrocycle – depending on the conformation of the ligand molecules. In practice, isophthaloyl-based ligands appear to give rise to 2:2 metallamacrocycles exclusively and, to date no 6:6 metallamacrocyclic complex has been isolated.

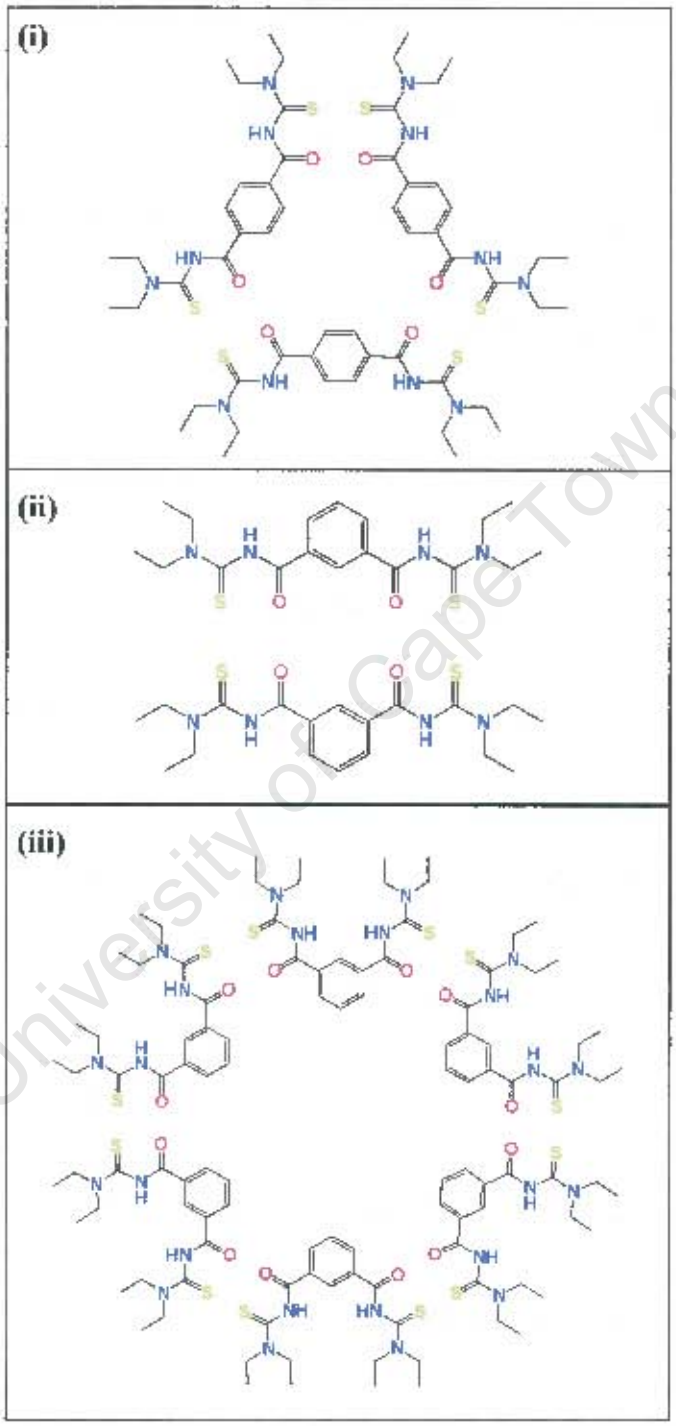

Figure 1.1.5(a). Molecular model sketches indicating how terephthaloyl-based bipodal aroylthioureas are directed to form 3:3 metallamacrocycles, while isophthaloyl-based bipodal aroylthioureas are directed to form either 2:2 or 6:6 metallamacrocycles.

Since it was conclusively shown by these papers that the outcome of bipodal benzoylthiourea complexation with d^8 metals is predetermined by the preferred *cis*-*S,O* mode of coordination and the relative substitution of the phenyl ring, it follows that one can regard the individual components as being 'pre-programmed' to form specific products, according to the definition of J.-M. Lehn.[42] This type of reaction is thus considered to be an example of self-assembly.

1.2. Aspects of Supramolecular Chemistry

The field of supramolecular chemistry is vast and is growing even more so at a rapid rate. Certain aspects of this field of chemistry are applicable to this project. A review of all the work done in the applicable areas is clearly not possible. An attempt is made to give many representative examples of the work that has been done and is ongoing in these areas. For a detailed review of the subject, the series *Comprehensive Supramolecular Chemistry* is highly recommended.[43]

1.2.1. Examples of self-assembled metallamacrocyclic complexes

Several groups have reported self-assembled metallamacrocyclic systems. The tetranuclear molecular squares synthesised by Stang *et al.*[44] are essentially 4:4 metallamacrocycles, since their structures are dependent on 4 metal centres linked by 4 bridging ligands. This system has become more sophisticated by different routes, e.g. having two different metals (Pt and Pd) in the same complex [45] or creating metallamacrocyclic arrays using porphyrins,[46] calixarenes or crown ethers.[47] Other geometries have been exploited to form other planar shapes e.g. hexagons[48] and triangles,[49] but the metallamacrocyclic motif is central to each such example, as is the mode of synthesis: self-assembly controlled by pre-designed ligands and carefully selected coordination behaviour around metal centres.

The self-assembly research of Fujita, Biradha and Aoyagi includes similar complexes with Pd(II) and Pt(II)[50]. Matthews *et al.* have reported non-planar molecular square tetranuclear diazine complexes with Cu(II) and Ni(II),[51] while a paper by Rojo *et al.* discusses the synthesis of another system of non-planar tetranuclear Co(II) and Zn(II) metallamacrocycles by self-assembly based upon variation of ligand substituents and utilising specific coordination geometry around the metal centres.[52] Some other examples of self-assembled metallamacrocyclic systems include hexanuclear manganese metallamacrocycles,[53] a dodecanuclear hexameric Zn metallamacrocycle[54] and a trinuclear ruthenium metallamacrocycle that can extract LiCl from H_2O.[55] One other recent example that ought to be mentioned is the 3:3 metallamacrocyclic complexes of 1,4-bis(3-phenyl-1,3-propandion)benzene[56], which are remarkably

similar in structure to the 3:3 complexes of bipodal aroylthioureas. However, 1,4-bis(3-phenyl-1,3-propandion)benzene can also form polymeric complexes with certain metal cations. This contrast with the aroylthiourea system is at least partly due to the fact that all the coordinating atoms are oxygens, and thus the imposed mode of *cis*-chelation that ensures aroylthiourea metallamacrocycle formation is absent in this system.

Certainly, there are more examples of self-assembled metallamacrocyclic complexes in the literature, but the examples given here are ample to demonstrate the commonality in the synthesis of these complexes: ligand geometry coupled with mode of coordination around a metal centre are exploited to pre-program the components of a system to self-assemble into multinuclear metallamacrocyclic coordination complexes.

1.2.2. Concepts in supramolecular chemistry related to self-assembly

The chemistry of the category into which metallamacrocycle synthesis falls, i.e. utilising coordination chemistry to create inorganic self-assembled systems, has been termed *metallosupramolecular chemistry* by Lehn[57]. It is a subset of the much broader field of *supramolecular chemistry* – 'chemistry beyond the molecule' which deals with all manner of non-covalent interactions between components.[58] The importance of the self-assembly concept within supramolecular chemistry cannot be overstated. The understanding that higher order structures beyond the molecule can be tailor-made by use of coordination, hydrogen bonding, π-π interactions and other non-covalent interactions has opened many avenues in chemistry over a relatively short period of time. One of the major appeals of self-assembly is that this approach allows one to envisage a highly complex system by reducing the problem to the rational design of *supramolecular synthons*: "structural units within supermolecules, which can be formed and/or assembled by known or conceivable synthetic operations involving intermolecular interactions"[59] – in other words the building blocks of supramolecular architectures, which may be existing or conceptualised molecules, molecular fragments, ions or pre-assembled supramolecular units that can be incorporated into higher order supramolecular structures. The literature also contains many papers that prefer the term *tectons* [60] for the basic building blocks of self-

assembled systems. The main difference between the terms *tecton* and *synthon* is that the former refers to actually existing molecules whereas the latter may also refer to conceptualised molecules or fragments

Self-Organisation

Beyond self-assembly is the concept of self-organisation, which has been defined in one paper as "the spontaneous formation of a well-defined supramolecular structure from simple molecular building blocks."[61] The authors (Machado, Baxter and Lehn) go on to say: "In these (self-organised) systems, each complementary block contains precise information to generate, *via* self-assembly (each step of the self-organized process),[62] the correct final structure within all possible structures." The implication is that systems of specifically designed synthons can undergo multiple self-assemblies in a particular order to produce highly ordered supramolecular architectures reproducibly – or, as stated elsewhere by Lehn: "Multilevel hierarchical self-organization enables the progressive buildup of more and more complex systems in a sequential temporally ordered fashion." [63]

What is so fascinating about such processes is that the information to produce these supramolecular architectures by self-assembly is contained within the components of the system themselves. Merely by placing simple yet carefully programmed synthons together, the spontaneous assembly of the supramolecular structure is brought about. In the case of metallosupramolecular assemblies: "the important information leading to an expected supramolecular structure may be 'sculptured' in the ligand, and the reading is carried out by a metal ion containing a suitable coordination algorithm."[61] This type of process is the key to the evolution of complex biological systems. If we are to mimic Nature's complexity, it will be by fully understanding and exploiting self-assembly. Again, to quote Lehn: "Understanding, inducing, and directing such self processes are key to unraveling the progressive emergence of complex matter. Self-organization is the driving force that led to the evolution of the biological world from inanimate matter."[63]

Discrete and infinite supramolecular assemblies

One can consider self-assemblies as falling into two broad categories [64]. In the case of large solution-based assemblies, one may think of each supramolecular unit as being discrete. There are many examples of this type. The metallamacrocyclic complexes discussed in Section 1.2.1 above would fall into this category – with coordination bonds being the mode of non-covalent interaction [65] that maintains the structure. Such polygonal assemblies can be considered to be 2-dimensional closed structures. Examples of a more complex order are the polyhedral discrete metallosupramolecular architectures. Such structures are often composed of polygons that are linked by their edges to assemble into 3-dimensional units with diameters in the multiple nanometer range. Nano-architectures of this type have been reported by the research groups of Fujita[66], Saalfrank[67], Stang[68], Yaghi[69] Zaworotko[70], and others.

The second category of self-assembly comprises systems of infinite polymers and networks. In such cases, intermolecular forces direct building blocks to assemble into infinite repeating patterns in one, two or three dimensions. The resulting products are often highly crystalline as a result of the symmetry that the systems assume. The rational design and synthesis of such systems constitute a very important part of the relatively new field of *crystal engineering*. The term crystal engineering was originally applied only to the synthesis of organic solids, but has now broadened to include non-covalent frameworks of all kinds. In the words of Desiraju, crystal engineering is: "the understanding of intermolecular interactions in the context of crystal packing and in the utilisation of such understanding in the design of new solids with desired physical and chemical properties."[71] Clearly, self-assembly is a necessary and powerful tool for crystal engineers, as it is the means of creation of tailor-made crystalline materials (which can essentially be considered as supramolecular structures). An extremely thorough review on advances in crystal engineering – citing hundreds of publications – by Moulton and Zaworotko[72] is particularly enlightening and informative.

The potential fruits of crystal engineering are new materials with a considerable range of macroscopic physical and chemical properties. New materials created by crystal engineering are set to revolutionise many areas of technology that will impact on the

everyday world e.g. electronics, catalysis, medicine and separation science [73] to name a few.

When the intermolecular interaction that holds the building blocks of an infinite repeating system is a coordination bond, the product is termed a *coordination polymer* A related term is *metal-organic framework*, which James describes in a clear and useful review as a "class of porous polymeric material, consisting of metal ions linked together by organic bridging ligands"[74]. Other types of infinite supramolecular structures include organic hydrogen-bonded and, aromatic π-π stacked networks. A review by Zaworotko discusses crystal engineering utilising both coordination polymerisation and organic non-covalent networks.[75] Of course, hybrid frameworks that are held together by any combination of metal-organic ligand coordination, H-bonding or π-π interactions are also possible.[76]

A recent review by Roesky and Andruh discusses the way these types of coordination and non-covalent interactions are used in infinite supramolecular architecture [77]. The ways in which the interactions of components give rise to the overall structures of such architectures are well known. A system derived by Wells [78] for describing the various topologies of 'chemical nets' is of great use and has been applied by Batten and Robson in their authoritative description of interpenetrating supramolecular networks of varying dimensionality [79] as well as by Decurtins *et al.* in their excellent review: *Multifunctional coordination compounds: design and properties.*[80]

One can consider each repeating unit in an infinite structure as a *node* or group of connected nodes in a network [80, 70]. By looking at the number of connections that a node or collection of nodes has available for connection to other nodes, one can determine what type of supramolecular architecture will be built up.

Nodes with two connections will only give rise to one-dimensional chains and depending on the relative geometry between connections in successive nodes, linear, zigzag or helical chains may arise. Linear chains arise if the nodes are aligned so that all connections are directed in a collinear manner; zigzag chains are formed by connections that are coplanar but not collinear and helical chains are based upon successive nodes being aligned so that their connections are neither collinear nor

coplanar, thus inducing a 3-dimensional 'twist' into the built structure while maintaining overall growth in only one dimension.

In the case of *p*-connected nodes with $p > 2$, the components will be able to assemble into networks in 2 or 3 dimensions. The Wells (*n*, *p*) notation is applied to these networks. The variable *p* indicates how many connections to neighbouring nodes can be made, while the variable *n* indicates the number of nodes there are in the shortest cyclical path within the net (i.e. the shortest path that will take one back to the node at which one originated).

A common approach in coordination polymer assembly is to use *exo*-bidentate ligands (i.e. ligands with divergent directionality of donor atoms) as connectors between metal centres. The metals are thus considered the nodes of the chain or net and the value of *p* can be manipulated by choosing metals with different coordination modes and using monodentate or *endo*-multidentate ligands to block connectivity in certain directions. A recently reported and demonstrative example of this is a paper by Choi *et al.*[81] In this example, the potentially 6-connected Ni(II) cation is bound by square planar coordination to a tetraaza macrocyclic ligand, thus allowing connection to neighbouring nodes only by the two remaining octahedral coordination sites. The resulting 2-connected node is bound by *exo*-bidentate 2,6-pyridinedicarboxylate anions to neighbouring nodes in a linear fashion.

Pyridine-based compounds are well known and commonly used *exo*-bidentate ligands in coordination polymer assemblies. The number of publications that report the use of such ligands is exceedingly large. The most common N-donor connector molecule is probably 4,4'-bipyridine[82], which the review by Roesky and Andruh [77] refers to as the "the classical molecular rod in constructing supramolecular polymetallic architectures". Pyrazine is also used as a connector in infinite supramolecular architectures.[83] Where pyrazine and 4,4'-bipyridine are rigid bidentate bridging ligands, flexible analogues may be of use as well. 1,2-bis(4-pyridyl)ethane is well used for this purpose[84].

There is much more detail that can be given about the types of infinite supramolecular architectures that have been created particularly with respect to their design and

topologies (including network interpenetration). The various types of coordination polymers and networks in 1,2,or 3-dimensions are well known. They include linear, zigzag and helical 1D chains, honeycomb, brick wall and square grid 2D nets and cubic, diamondoid and prismatic 3D frameworks of various sizes and with various metals and ligands. The reader is directed to the excellent reviews mentioned in this section for further reading [72, 74, 75, 77, 79, 80].

One other detail in the section on discrete and infinite supramolecular architectures that should be mentioned is the ability to combine the two. It may seem fairly obvious that discrete nano-architectures can be designed in such a way that they are able to assemble further into infinite networks that give rise to interesting crystalline materials. However, this development is fairly recent and references to it are all within the last few years[85]. The approach essentially utilises discrete self-assemblies as secondary building units (SBUs) in infinite frameworks. Yaghi *et al.* name this approach *reticular synthesis*[86] and have designed several systems in this manner [87] including a framework of adjustable pore size that is up to 91.1% of the total volume of the crystal and is capable of storing large amounts of methane [87(b)]. Zaworotko *et al.* have reported square shaped dicarboxylate metal clusters that assemble in groups of four into curved molecular bowls. These discrete architectures act as nanoscale secondary building units (nSBUs) that in turn self-assemble into an infinite undulating sheet structure, with guest molecules included in the bowl-like indentations of the nSBUs and trapped there by the bottom of the nSBU located directly above.[88] The Zaworotko group has also reported infinite assemblies using polyhedral 'nanoballs' as nodes in the network[89]. Others employing similar strategies include Brammer *et al.*, who have employed Ag(I) carboxylate dimers as secondary building units,[90] and Lah et al.[91] who have used their hexanuclear manganese metallamacrocycles[53] as secondary building units.

Although not so closely related to this project, the work of Stoddart *et al.* should also be mentioned, as their large output of publications features many examples of self-assembly of rotaxanes and catenanes and other structures as well as their use as secondary building units in higher order assemblies.[92] The goal of Stoddart *et al.* to produce working molecular machines with useful applications such as switches in molecular computers clearly shows how achievements in supramolecular chemistry

are set to provide technologies that may have a huge impact on the life of the common person in the near future.

Host-guest chemistry in supramolecular assemblies

One other fundamental aspect of supramolecular chemistry that must be discussed in relation to self-assembled architectures is guest inclusion. It has already been alluded to in the preceding portion of this introduction and warrants some more detailed explanation. The inclusion, within a crystal structure, of some compound (the guest) other than the main constituent of the structure (the host) is very common and well studied and is a fundamental concept within supramolecular chemistry – often playing a role in the various sub-fields of supramolecular chemistry mentioned above.[43] Included guests are in many cases solvent molecules trapped in cavities within the main crystal structure and often, strong intermolecular attractions are responsible for holding guests in place within a structure.

The term *clathrate* is used to describe a system in which guest molecules are encaged in cavities within the host framework.[93] The Werner clathrates (of the form MX_2A_4 – where M is a divalent metal ion, X is an anionic ligand and A is a neutral coordinating ligand derived from pyridine or related compounds), particularly the $Ni(NCS)_2A_4$ type are of interest with respect to this project, as they bear some structural and behavioural similarity to the octahedral pyridine adducts of Ni(II) metallamacrocycles discussed in Section 3.3. Self-assembled polymeric complexes similar to the Werner clathrates and their formation of cavities and channels that can accommodate guests have been reported [76(i), 83(b), 83(c)].

An important ability that many host compounds display is guest sorption and desorption and the observation of these processes by thermal analytical methods is ubiquitous in supramolecular chemistry. Desorptive processes can result in disturbances of the host structure, often-irreversible phase transitions and possibly even complete collapse of the host structure to a different phase. The reversible diffusion of guests into and out of a host crystal structure is a desired property, particularly if crystal structures of both states can be obtained. Crystal to crystal guest desorption transformations in metal organic frameworks are rare, but have been

observed [94] and it is increasingly clear that guests play a vital role in determining the crystal structures of inclusion complexes.

Application of supramolecular concepts to aroylthiourea metallamacrocycles

By looking at the work done by others with similar systems, it is immediately evident that the system of self-assembled 2:2 and 3:3 square planar metallamacrocyclic units could be extended further into the realm of supramolecular architecture in several different directions. That is – in essence – the aim of this project. A detailed discussion of the project's aims is given below in Section 1.3. Briefly, the different directions explored involve linking discrete metallamacrocycles by H-bonding and *exo*-bidentate coordination into infinite arrays. Related issues that have been discussed arise in the execution of this exploration. Host-guest interactions and their importance in determining crystal structures are one of the focuses of this project – as will be shown in several cases in Chapter 3. Different types of host framework including a layered/channel-type system have been created and studied. Remarkable guest sorption and molecular recognition properties are observed in one particular case. Overall, it will be shown that the 2:2 and 3:3 aroylthiourea metallamacrocycles offer areas of exploration in various exciting directions, touching on many different facets of supramolecular chemistry.

1.3. Scope, Aims and Motivation

1.3.1. Potential directions for development of aroylthiourea metallamacrocycles

In Section 1.1.5 above, the self-assembly of 2:2 and 3:3 metallamacrocyclic complexes of 3,3,3',3'-tetraalkyl-1,1'-aroylbisthioureas was introduced and recognition of the potential for exploration of chemistry utilising these units was mentioned. In this section, some possible paths of exploration are considered.

Spacer modification

By varying the chemical group that comprises the central spacer of the bipodal acyl/aroylthiourea, other types of metallamacrocycle might be synthesised. All that is required is a rational consideration of the geometry and coordination behaviour of the ligands. Higher order than 2:2 and 3:3 metallamacrocycles might be possible.

A simple route would be to use naphthoyl-spaced thioureas with various relative substitutions. Figure 1.3.1(a) shows the possible metallamacrocyclic products that may be produced. These possible products include three types of 2:2 metallamacrocycle, three types of 3:3 metallamacrocycle and one 6:6 metallamacrocycle. Note that the 1,3-substituted and 1,4-substituted varieties are essentially the same as 1,3- (isophthaloyl) and 1,4- (terephthaloyl) substituted benzoylthioureas respectively. Also note that each of the proposed products would arise from exclusively *cis*-coordination around the metal centres, but it has been shown that *trans*-coordination can occur with a naphthoylthiourea [18]. Thus there is the possibility that bipodal naphthoylbis(thioureas) could also give rise to 1-dimensional polymeric chains.

Similar geometries could be achieved with other fused benzene ring aromatic spacers. The appeal of this route for further exploration is the possibility of large metallamacrocycles with cavitation abilities in the manner of crown ethers and cyclodextrins. This idea could then be further advanced by the addition of intra-cavity directed functional groups in the ligand design, allowing precise manipulation of cavity size, shape and internal chemical environment. The potential applications of

2:2 Metallamacrocycles

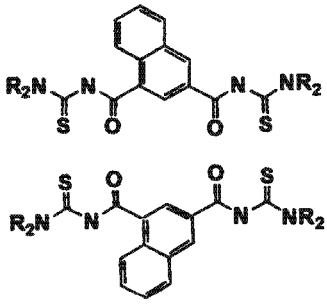

1,3-substituted

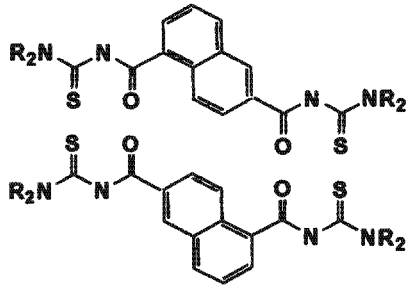

1,6-substituted

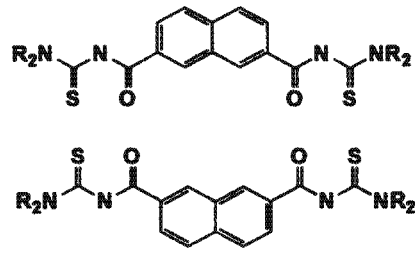

2,7-substituted

3:3 Metallamacrocycles

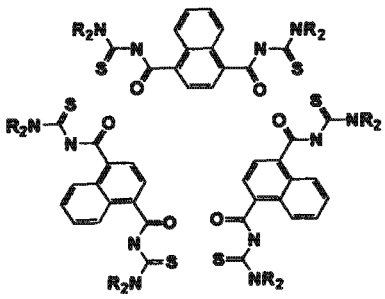

1,4-substituted

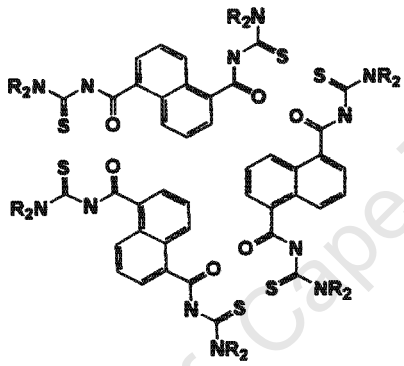

1,5-substituted

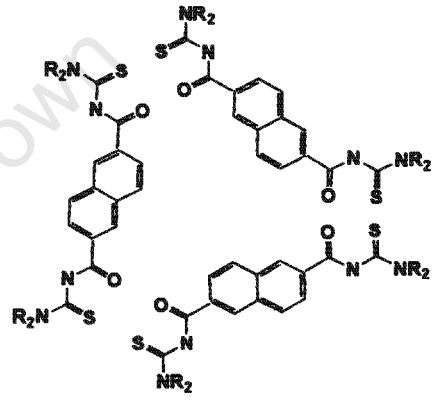

2,6-substituted

6:6 Metallamacrocycle

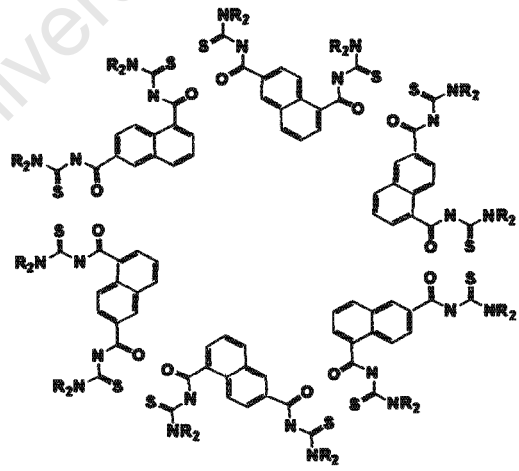

1,6-substituted (alternate)

Figure 1.3.1(a). Molecular drawings indicating possible metallamacrocyclic complexes of 3,3,3',3'-tetraalkyl-1,1'-naphthoylbisthioureas

compounds containing rationally designed cavities runs from guest-specific hosts for highly efficient separations through to nano-chambers for catalysis and enantioselective chemical reactions.

Alkyl chain customisation

Variation of the side chains of the aroylthiourea ligands is another possible route to synthesising metallamacrocyclic complexes with different properties. As shown above in Section 1.1.3, ligands synthesised from primary amines do not undergo chelate complexation. Thus one restriction on the alkyl chain variation is that the ligands must be derived from dialkylamines. The alkyl chains could be of considerable length, giving rise to hydrophobic interactions between neighbouring molecules. Molecules composed of a flat rigid core and long alkyl chains are well known for their use as discotic mesogens in liquid crystal formation[95] A recent paper by Choi and Suh reports a nickel macrocyclic complex with a hexadecyl pendant chain, which possesses hydrophobic, electrically insulative and anion exchange properties.[96] The authors draw attention to work done in the area of organic compounds with long alkyl chains and the properties of such compounds. The utilisation of hydrophobic properties in self-organisation of supramolecular architectures [97] is of particular interest.

An alternative design feature added to the side branches of a metallamacrocycle is achieved by using di(hydroxyalkyl)amines in the bipodal ligand synthesis. This imparts hydrogen-bonding abilities to the metallamacrocycle. As discussed above, H-bonding ability is one of the most powerful tools in directing self-assembly reactions. H-bonding side branches should allow discrete metallamacrocyclic units to link into 1- or 2-dimensional networks. The synthesis of a monopodal aroylthiourea with hydroxyethyl side chains has been reported, as have bis-chelate complexes of this ligand with Pt(II), Pd(II) and Ni(II)[98] – although crystal structures of the complexes were not reported. At the outset of this project, the H-bonding side chain route was one of the most appealing options for exploration, as it offers the simplest method of using metallamacrocyclic complexes as secondary building units in higher order supramolecular assemblies.

Coordination polymerisation of metallamacrocyclic units

There are, generally speaking, two modes of coordination polymerisation available for aroylthiourea metallamacrocyclic complexes: polymerisation directed parallel to the metallamacrocyclic plane and polymerisation directed perpendicular to the plane. A simple method to achieve the former is to use tripodal or tetrapodal aroylthiourea ligands. The metallamacrocyclic structure could form normally by engaging two chelating moieties of each ligand molecule in complexation to two metal atoms, as observed in metallamacrocycle formation, while the remaining chelating groups could participate in complexation to other metal centres in such a manner that an infinite chain or network would result. Figure 1.3.1(b) illustrates two possible examples. Molecular modelling indicates that an anthracenoyl spacer would be ideal for a tetrapodal aroylthiourea to be synthesised with two pairs of 1,3-substituted thiourea groups. These ligands should self-assemble with d^8 metal ions into a 1D coordination polymer of 2:2 metallamacrocyclic units. The use of a pentacenoyl spacer to form a tetrapodal aroylthiourea with two pairs of 1,4-substituted thiourea groups is also feasible in principal. This ligand is expected to assemble into a 2D planar coordination network with d^8 metals. Note that this network consists of 3:3 metallamacrocyclic subunits, and also 6:6 metallamacrocyclic arrangements. Also note that the alkyl side chain that is *cis*- to the sulfur atom across the C – N bond protrudes into the 6:6 metallamacrocyclic cavity. It has been shown conclusively that this C – N bond possesses a degree of double-bond character that restricts rotation and allows configurational isomerism when unsymmetrically substituted dialkyl acylthioureas are synthesised.[5] This suggests that unsymmetrically substituted ligands may be used to alter the environment within the 6:6 metallamacrocyclic cavity while avoiding the large cost in steric interference in the more crowded region around the central fused rings of the pentacene spacer.

Other fused ring aromatic spacers may also be employed to produce multipodal aroylthiourea ligands, which should in turn be able to assemble into planar polymeric complexes. The molecular modelling approach to ligand design is a powerful and proven tool for this purpose.[41]

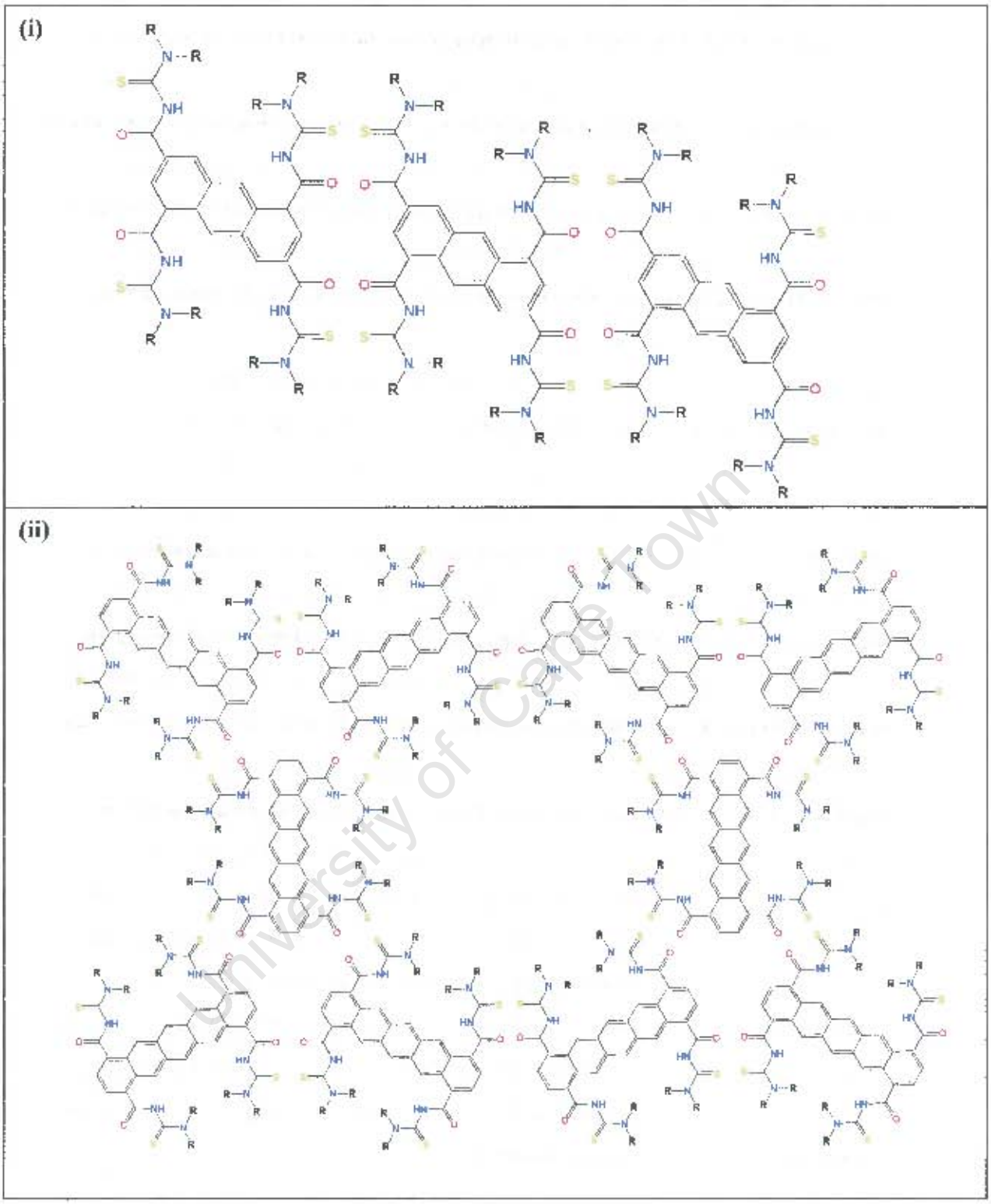

Figure 1.3.1(b). Proposed arrangement of (i) 1,3,5,7-anthracenoyltetrakis(thiourea) ligands giving rise to a 1D polymeric array of 2:2 metallamacrocyclic subunits and (ii) 1,4,8,11-pentacenoyltetrakis(thiourea) ligands giving rise to a 2D polymeric array containing 3:3 and 6:6 metallamacrocycles.

To achieve polymerisation directed orthogonally to the metallamacrocyclic plane, axial bridging ligands can be employed. Since Ni(II) readily undergoes octahedral coordination, the Ni(II) metallamacrocycles are ideal candidates for use in this type of polymerisation. Part of this project involves the study of the axial coordination of pyridine to the Ni(II) centres of a 2:2 metallamacrocycle.[99] This was done en route to using exo-bidentate pyridine-based ligands to achieve coordination polymerisation. An analysis of the possible outcomes of such polymerisation is discussed in some detail in Section 3.4 of this thesis.

Hybrid supramolecular architectures based on metallamacrocyclic units

Any of the variable design features discussed above can be used in combination. For example, a 3D supramolecular framework consisting of coordination linkages orthogonal to the metallamacrocycle planes and H-bonded linkages roughly parallel to the planes is feasible, as is a 2D coordination polymer synthesised from tetrapodal aroylthiourea ligands and bidentate pyridine based ligands. Polymers based on axial coordination of exo-bidentate ligands could be fashioned from metallamacrocycles (possibly with tailored nanoscale cavity sizes) resulting in nanotube structures. H-bonding could link such tubes laterally as could multipodal planar coordination, giving rise to new metal organic frameworks (see Figure 1.3.1(c).)

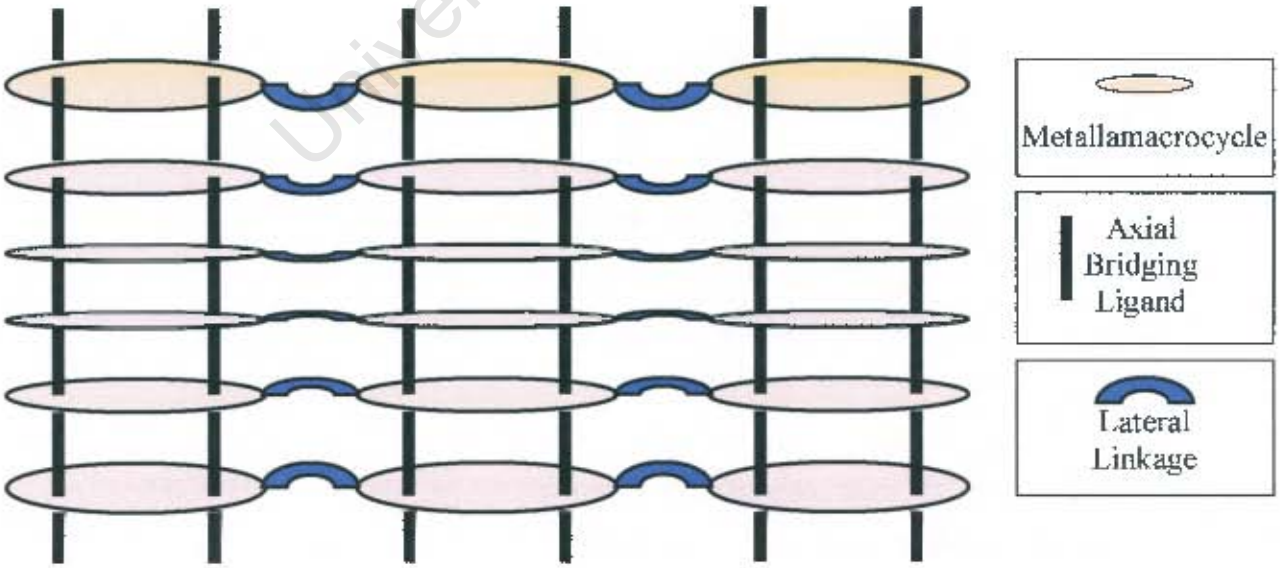

Figure 1.3.1(c) Schematic representation of a laterally linked array of nanotubes based on stacked metallamacrocyclic subunits held in place by axially coordinated bidentate bridging ligands

The bipodal aroylthiourea metallamacrocycle system appears to be highly versatile, possessing features that can be fine-tuned – either individually or in combination – to yield a range of supramolecular architectures.

1.3.2 Aims of this research project

The aims of this project were divided into four stages based on the initially envisaged process of building up from simple components into successively more complex architectures.

First stage aims: ligand synthesis and characterisation

The synthesis and characterisation of isomeric isophthaloyl and terephthaloyl ligand pairs was the first step of this project. The 3,3,3',3'-tetra*ethyl*-1,1'*benzoyl*bis(thioureas) were selected as the archetypal ligands. The bulk synthesis of 2:2 and 3:3 metallamacrocycles for later use required large stocks of both the isophthaloyl and terephthaloyl isomers. Since no crystal structure of an isophthaloylbis(thiourea) had been reported before this project began, the full determination of the crystal and molecular structure of 3,3,3',3'-tetraethyl-1,1'-isophthaloylbis(thiourea) was a major initial aim.

The synthesis of isophthaloyl and terephthaloyl ligands with appended hydrogen-bonding groups was also set as an aim. This pair of isomeric ligands should be as close to the archetypes as possible. Hydroxyethyl side chains were selected as the simplest modification. Full crystal and molecular structures were aimed at, with the expectation that the customised H-bonding ability should give rise to interesting crystal structures for the ligands as well as for any metallamacrocycles synthesised from these ligands.

These four ligands were considered sufficient for the purposes of diversity at this stage of the project.

Second stage: metallamacrocyclic Ni(II) complexes

In general, a major aim of this project was the extension of what is known about Pt(II) and Pd(II) aroylthiourea metallamacrocycles to Ni(II). Furthermore, Ni(II) is considered ideal for the purposes of progressive building, as it can be converted from a square planar to an octahedral coordination mode without the complication of a change in oxidation state. The formation of Ni(II) metallamacrocycles from each of the ligands synthesised in the first stage was required, as was the characterisation of these complexes. Since, only a 3:3 Ni(II) metallamacrocycle had been reported prior to this research,[39] the structural elucidation by single crystal x-ray diffractometry of at least one 2:2 Ni metallamacrocycle – constituting definitive proof of the existence of this species – was set as a goal. Crystal and molecular structures of at least one of the (hypothetically) H-bond capable metallamacrocycles was another major aim of this stage. It was expected that crystal structures of the H-bonding complexes would reveal 2D supramolecular arrays of metallamacrocyclic units. A thorough comparison of H-bond active complexes with their H-bond inactive analogues was also desired.

Third stage: octahedral adducts of metallamacrocycles

Following the synthesis of metallamacrocycles, a logical next step is the synthesis of octahedral adducts of 2:2 and 3:3 metallamacrocycles using pyridine and its derivatives. The extension of the square planar metallamacrocycles into octahedral adducts was considered to be a major goal, as it would fit into the progression of building more complex supramolecular architectures from the metallamacrocyclic motif. The thorough study and comparison of any synthesised adducts was of course a high priority aim, particularly the host-guest interactions and thermal stability of these complexes, which were to be studied by thermal analytical techniques – in particular thermogravimetric analysis. The obtaining of good quality single crystals and the subsequent crystallographic analysis was also required. A comparison of 2:2 and 3:3 adducts – if both were obtained – was particularly desirable, as was the comparison of adducts using different axial ligands. The ligands that were selected for this purpose are pyridine and some of its derivatives. The comparison of H-bond capable pyridine adducts with their H-bond inactive analogues was another vital aim, as this would serve to further demonstrate the dramatic differences in supramolecular structure that

were expected to arise from the implementation of hydrogen-bonding capability. In general, the expected and desired outcome for this portion of the project was the self-assembly of new porous or channel-type products. This expectation was not considered to be unrealistic, particularly in view of the many previous reports of channel-type H-bonded supramolecular architectures

Fourth stage: polymerisation of metallamacrocycles using bidentate bridging ligands

The successive phase in the progressive design project was the use of bidentate bridging ligands to axially link metallamacrocyclic units. The compounds chosen for this purpose were ones that are well known as either rigid or flexible exo-bidentate ligands: pyrazine, 4,4'-bipyridine and other di(4-pyridyl) compounds. Two parallel series of coordination polymers were envisaged based on 2:2 and 3:3 metallamacrocycles. Full characterisation was required with an emphasis on thermal analysis and any other techniques allowing insight into any host-guest interactions, as was a thorough comparison of the structures and properties of the various products. An important goal set for this phase of the project was the elucidation of the crystal structures of at least two coordination polymers: one 2:2- and one 3:3-based product.

The wide spectrum of interesting physical properties reported for various coordination polymers could lead one to anticipate that some of the products proposed here could exhibit such properties. Any evidence of such behaviour was to be investigated further as this might lead to the development of useful new materials.

Beyond this point, a further aim for this project was the synthesis of axial coordination polymers of metallamacrocycles, linked laterally by H-bonding. Such products would constitute new 3D infinite hybrid supramolecular architectures derived from secondary building units. Following this, attempts to synthesise larger metallamacrocycles and employ them in the formation of 3D architectures were also aimed for. However, these last two aims were deemed inessential for the purposes of this project, and were set aside for a later research project. The potential for the development of new materials in that phase of research is even greater, and even though this project did not pursue such aims, it is highly recommended that such routes be investigated.

1.3.3 Motivation for this project

These aims, if achieved, would place the work done on metallamacrocyclic aroylthiourea complexes close to the frontiers of current supramolecular research. As the number and complexity of supramolecular systems investigated increases, it is highly desirable to study systems composed of simple, easily obtained components that interact and self-assemble in predictable fashions. Furthermore, a system with components that possess multiple, easily tuned chemical features is even more attractive for exploitation, because these allow the supramolecular chemist to engineer a variety of new materials while working in the same general framework. The aroylthioureas and their complexes constitute such a system. The versatility of the aroylthioureas ensures that the scope for new chemistry utilising this motif is virtually limitless. Even if no direct technological application were to arise eventually from the plethora of potential products, which is unlikely, the contribution of knowledge obtained from their study has its place in the rapidly advancing progression of self-assembly, crystal engineering and supramolecular chemistry in general.

The first step in realising the value of the aroylthioureas in supramolecular chemistry was recognising that the exclusive formation of metallamacrocycles is indeed self-assembly. The next steps into this realm are those undertaken by this project. The work done in this project – by creating and studying a number of new compounds and supramolecular architectures with complex and intriguing crystal structures and host-guest interactions – provides a solid platform for further research that can advance this system right into the forefront of current supramolecular chemistry.

Furthermore, the use of acylthiourea complexes as antifungal, anticancer and antibiotic agents and the acylthioureas themselves as selective PGM complexing ligands has been demonstrated – as discussed above. These previous findings are all compelling reasons to study acylthiourea-based chemistry, as they offer the promise of potential application in the pharmaceutical and mining industries. The analytical, waste-recovery and environmental benefits in the latter may prove to be considerable in the very near future, and even though the synthesis of new Ni(II) complexes does not directly benefit the PGM mining industry, it is thought that such complexes may be useful models for improving our understanding of PGM complexation to

acylthioureas and may lead to the eventual development of supramolecular architectures with technological application in the precious metal industry.

This concludes the introduction, which it is hoped has given the reader some idea of the nature of this project, where it fits in the context of contemporary chemical research and ultimately, sufficient motivation for its effectuation. From here, this dissertation progresses to discussing the experimental work carried out during this project, the results that were obtained from these experiments, and finally, the conclusions that can be drawn from these results.

Chapter 2

Experimental Section

2.1. Ligand Synthesis

These compounds were synthesized according to the Douglass and Dains method.[1] Throughout the synthesis, care was taken to expose all reagents and solvents to air for as short a period as possible. The solvent used (acetone) was freshly dried and distilled.

2.1.1. 3,3,3',3'-tetraethyl-1,1'-isophthaloylbis(thiourea) (I-Et)

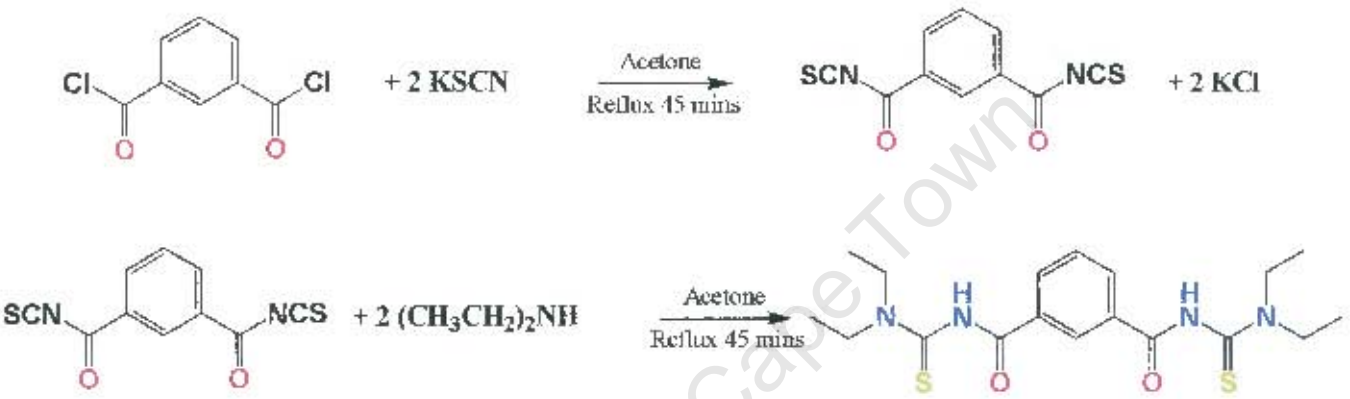

Figure 2.1.1(a). Reaction scheme for synthesis of 3,3,3',3'-tetraethyl-1,1'-isophthaloylbis(thiourea)

5.15g (25.4mmol.) isophthaloyl dichloride, dissolved in 200 ml acetone, was placed in a pressure-compensated dropping funnel and added drop-wise with stirring to 4.96g (51.0 mmol.) dry potassium thiocyanate dissolved in 200 ml acetone, under an inert atmosphere (N_2), in a three-necked round bottom flask. During addition, a pale yellow precipitate formed in the reaction vessel. The mixture was heated to reflux for 45 minutes and then allowed to cool. 3.74g (51.1 mmol.) of dry, distilled diethylamine was dissolved in 100ml acetone and added drop-wise from a pressure-compensated dropping funnel to the reaction mixture under N_2 atmosphere. The mixture was heated to reflux for another 45 minutes, after which it was allowed to cool. A pale orange solution with an off white precipitate was observed. The mixture was transferred to a large beaker containing 500 ml water. The precipitate was observed to dissolve in the water. The mixture was left to stand in a fume cupboard to allow the evaporation of acetone. After 48 hours, off white crystals of the product had formed in the beaker.

The product was recrystallised from a chloroform / acetone solution by slow evaporation.

Yield: 8.50g, 21.5 mmol. 85%. M.p. 141 – 143 °C. Found: 54.74% C, 6.77% H, 14.06% N, 16.01% S. $C_{18}H_{26}N_4O_2S_2$ requires 54.78% C, 6.65%H, 14.20% N, 16.25%S. δ^1H/ppm (200 MHz, $CDCl_3$): 1.28 (t, 6H), 1.32 (t, 6H), 3.58 (q, 4H), 4.00 (q, 4H), 7.50 (t, 1H), 7.96 (d, 2H), 8.25 (s, 1H), 9.38 (s, 2H); δ^{13}C/ppm (50 MHz, CDCl3): 11.4 (-CH_3), 13.3(-CH_3), 47.5 (-NCH_2-), 47.8(-NCH_2-), 126.6, 129.4, 132.6, 132.8, 163.3(-C(O)-), 179.2(-C(S)-). The crystals thus obtained were found to be suitable for single crystal x-ray diffractometry.

2.1.2. 3,3,3',3'-tetraethyl-1,1'-terephthaloylbis(thiourea) (T-Et)

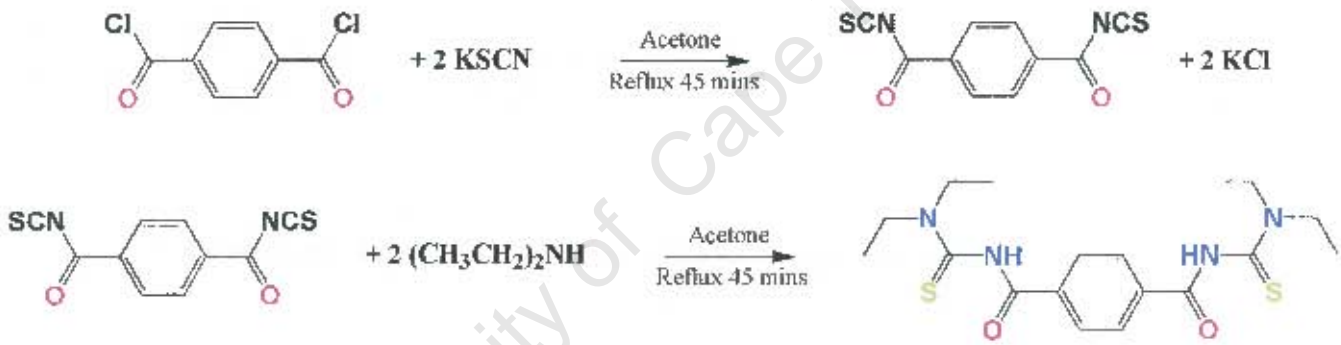

Figure 2.1.2(a). Reaction scheme for synthesis of 3,3,3',3'-tetraethyl-1,1'-terephthaloylbis(thiourea)

5.09g (25.1 mmol.) terephthaloyl dichloride, dissolved in 200 ml acetone, was placed in a pressure-compensated dropping funnel and added drop-wise with stirring to 4.96g (51.0 mmol.) dry potassium thiocyanate dissolved in 200 ml acetone, under an inert atmosphere (N_2), in a three-necked round bottom flask. During addition, a pale yellow precipitate formed in the reaction vessel. The mixture was heated to reflux for 45 minutes and then allowed to cool. 3.73g (51.0 mmol.) of dry, distilled diethylamine was dissolved in 100ml acetone and added drop-wise from a pressure-compensated dropping funnel to the reaction mixture under N_2 atmosphere. The mixture was heated to reflux for another 45 minutes, after which it was allowed to cool. An orange solution with an off white precipitate was observed. The mixture was transferred to a

large beaker containing 500 ml water. The precipitate was observed to dissolve in the water. The mixture was left to stand in a fume cupboard to allow the evaporation of acetone. After 48 hours, orange crystals of the product had formed in the beaker. The product was recrystallised from a chloroform / acetone solution by slow evaporation to yield pale yellow crystals.

Yield: 8.71g, 22.1 mmol. 87%. M.p. 154 – 156 °C. Found: 54.90% C, 6.71% H, 14.04% N, 16.12% S. $C_{18}H_{26}N_4O_2S_2$ requires 54.78% C, 6.65%H, 14.20% N, 16.25%S. δ^1H/ppm (200 MHz, $CDCl_3$): 1.29 (t, 6H), 1.33 (t, 6H), 3.57 (q, 4H), 3.98 (q, 4H), 7.87 (s, 4H) 8.88 (s, 2H); δ^{13}C/ppm (50 MHz, CDCl3): 11.4 (-CH_3), 13.3(-CH_3), 47.7 (-NCH_2-), 47.9(-NCH_2-), 128.3, 136.1, 162.9(-C(O)-), 178.9 (-C(S)-).

2.1.3. 3,3,3',3'-tetra(2-hydroxyethyl)-1,1'-isophthaloylbis(thiourea) (I-EtOH)

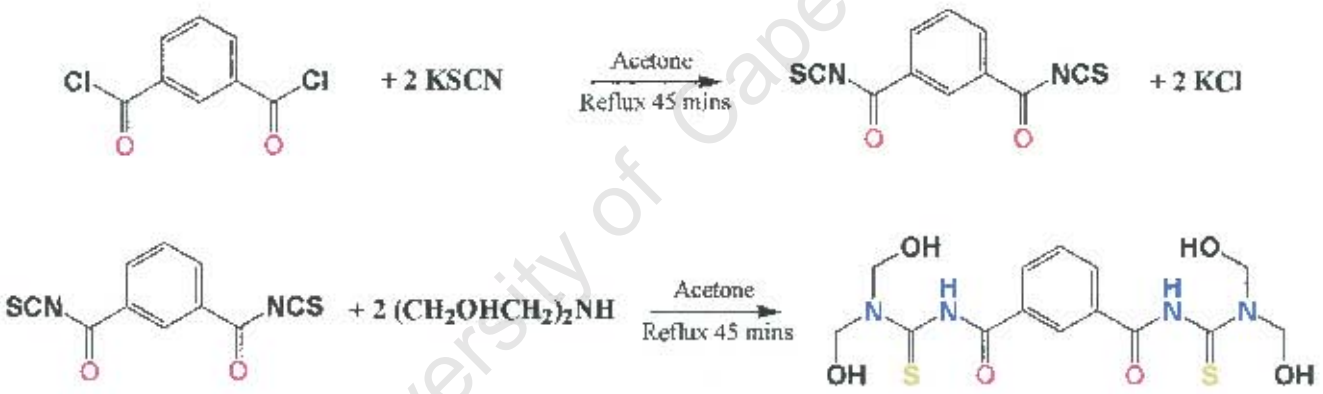

Figure 2.1.3(a) Reaction scheme for synthesis of 3,3,3',3'-tetra(2-hydroxyethyl)-1,1'-isophthaloylbis(thiourea)

5.12g (25.2 mmol.) isophthaloyl dichloride, dissolved in 200 ml acetone, was placed in a pressure-compensated dropping funnel and added drop-wise with stirring to 4.86g (50.0 mmol.) dry potassium thiocyanate dissolved in 200 ml acetone, under an inert atmosphere (N_2), in a three-necked round bottom flask. During addition, a white precipitate formed in the reaction vessel. The mixture was heated to reflux for 45 minutes and then allowed to cool. 5.40g (51.4 mmol.) of dry, distilled diethanolamine was dissolved in 100ml acetone and added drop-wise from a pressure-compensated dropping funnel to the reaction mixture under N_2 atmosphere. The mixture was heated

to reflux for another 45 minutes, after which it was allowed to cool. A pale yellow solution with an off white precipitate was observed. The mixture was transferred to a large beaker containing 500 ml water. The precipitate was observed to dissolve in the water. The mixture was left to stand in a fume cupboard to allow the evaporation of acetone. After 48 hours the product had precipitated as a pale yellow powder. The product was found to be far less soluble than 1-Et and T-Et in chlorinated solvents, alcohols, water and acetone. A solvent system of dimethylformamide (DMF) / water was used to recrystallise the compound as a fine white powder.

Yield: 6.83g, 14.9 mmol. 59%. M.p. 151 – 155 °C. Found: 47.35% C, 5.78 % H, 12.34% N, 13.73% S. $C_{18}H_{26}N_4O_6S_2$ requires 47.15% C, 5.71% H, 12.22% N, 13.98% S. δ^1H/ppm (200 MHz, DMSO-d_6): 3.72 (s, 16H), 4.01 (s, 4H), 4.85 (s, 2H), 7.63 (t, 1H), 8.05(d, 2H), 8.36 (s, 1H), δ^{13}C/ppm (50 MHz, DMSO-d_6): 39.08 (-*N*CH_2-), 39.92 (-*N*CH_2-), 59.10 (-CH_2OH), 57.46 (-CH_2OH), 127.59, 128.72, 131.19, 133.84, 163.84 (-*C*(O)-), 181.08 (-*C*(S)-).

Crystals suitable for single crystal x-ray diffractometry were obtained from a solution of the product in dimethylsulfoxide (DMSO) / water by slow evaporation of solvent over several weeks.

2.1.4. 3,3,3',3'-tetra(2-hydroxyethyl)-1,1'-terephthaloylbis(thiourea) (T-EtOH)

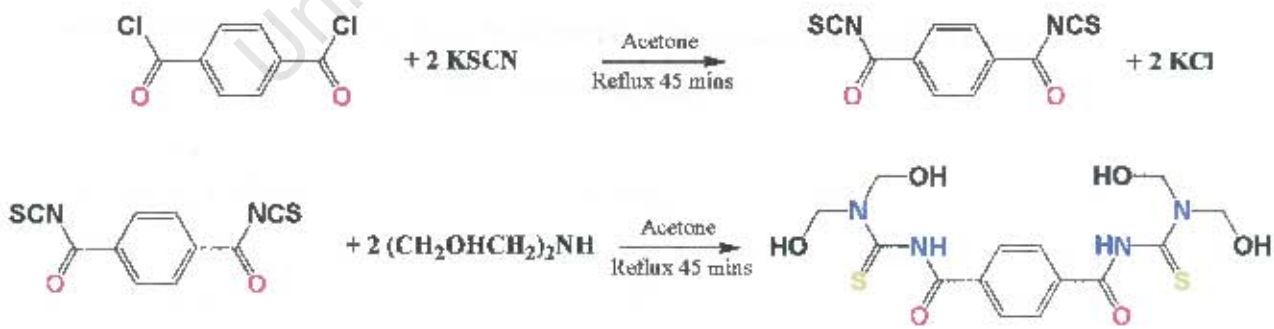

Figure 2.1.4(a). Reaction scheme for synthesis of 3,3,3',3'-tetra(2-hydroxyethyl)-1,1'-terephthaloylbis(thiourea)

5.11g (25.2 mmol.) terephthaloyl dichloride, dissolved in 200 ml acetone, was placed in a pressure-compensated dropping funnel and added drop-wise with stirring to 4.86g (50.0 mmol.) potassium thiocyanate, dissolved in 200 ml acetone, under an inert atmosphere (N_2), in a three-necked round bottom flask. During addition, a pale yellow precipitate formed in the reaction vessel. The mixture was heated to reflux for 45 minutes and then allowed to cool. 5.40g (5.14 mmol.) of dry, distilled diethanolamine was dissolved in 100ml acetone and added drop-wise from a pressure-compensated dropping funnel to the reaction mixture under N_2 atmosphere. The mixture was heated to reflux for another 45 minutes, after which it was allowed to cool. A pale yellow solution and precipitate was observed. The mixture was transferred to a large beaker containing 500 ml water. The precipitate was observed to dissolve in the water. The mixture was left to stand in a fume cupboard to allow the evaporation of acetone. After 48 hours the product had precipitated as a yellow powder, which was found to be soluble in DMF or DMSO. The product was recrystallised from DMF / water to yield a fine, pale yellow powder. The obtained yield was quite low (38%) but was not optimised.

Yield: 4.40g, 9.60 mmol., 38%. m.p. 159 – 162 °C. Found: 47.48% C, 5.58% H, 12.31% N, 13.76%S. $C_{18}H_{26}N_4O_6S_2$ requires 47.15% C, 5.71% H, 12.22% N, 13.98% S. δ^1H/ppm (200 MHz, DMSO-d_6): 3.73 (s, 16H), 4.00 (s, 4H), 4.33 (s, 2H), 7.93 (s, 4H), δ^{13}C/ppm (50 MHz, DMSO-d_6): 39.07 (-*N*CH_2-), 39.91 (-*N*CH_2-), 57.49 (-CH_2OH), 59.15 (-CH_2OH), 127.89, 136.56, 164.02 (-*C*(O)-), 180.09 (-*C*(S)-).

Crystals suitable for single crystal x-ray diffractometry could not be obtained, despite many attempts using solvent mixtures of DMF or DMSO with acetone, water, alcohols or chlorinated solvents.

2.2. Synthesis of Metallamacrocyclic Complexes

2.2.1. *Cis*-[bis-μ-(3,3,3',3'-tetraethyl-1,1'-isophthaloylbis(thioureato-*S,O*))-di-nickel(II)] (*cis*-[Ni (I-Et-*S,O*)]$_2$)

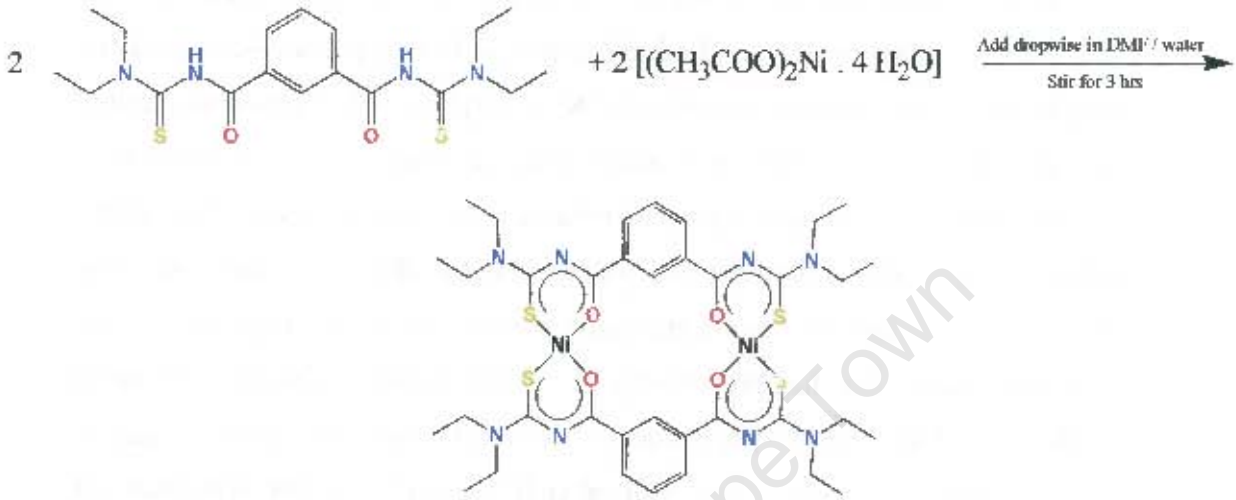

Figure 2.2.1(a). Reaction scheme for synthesis of *cis*-[Ni(I-Et-*S,O*)]$_2$

0.3946g (1.00 mmol.) of I-Et was dissolved in DMF to which $Ni(CH_3COO)_2.4H_2O$ (0.2489g, 1.00 mmol.), dissolved in 20 cm^3 H_2O and 15 cm^3 DMF, was added drop-wise while stirring vigorously, at room temperature. The mixture was stirred for a further 3 h, followed by addition of 100 cm^3 of H_2O. On cooling to 4 °C in a refrigerator for 24 hours, the dark solid product was collected by centrifugation and washed several times with small portions of water. The product, *cis*-[Ni(I-Et-*S,O*)]$_2$ was recrystallised from chloroform / acetone to give a deep purple powder.

Yield: 0.394g, 0.436 mmol., 87%, m.p. 310 – 313 °C. Found: 48.29% C, 5.47% H, 12.18% N, 13.94% S. $C_{36}H_{48}N_8O_4S_4Ni_2$ requires 47.91% C, 5.36% H, 12.42% N, 14.21% S; δH (200 MHz, CDCl3): 1.24 (m, 24H), 3.78 (m 16H), 8.26 (m, 6H), 8.78 (s, 2H); δ^{13}C (50 MHz, $CDCl_3$): 12.6 (-*C*H$_3$), 13.1 (-*C*H$_3$), 45.3 (-*N*CH$_2$-), 45.9 (-*N*CH$_2$-), 126.8, 130.0, 132.5, 136.9, 170.0(-*C*(S)-), 172.3(-*C*(O)-). IR (KBr, 1000 – 300 cm^{-1}): 943, 920, 896, 822, 779, 755, 730, 698, 679, 661, 566, 520, 487. The complex was recrystallised from a variety of solvent mixtures in an attempt to grow

crystals suitable for x-ray analysis. Eventually, such crystals were grown from a solvent mixture of DMF / H_2O.

2.2.2. *Cis*-[tris-μ-(3,3,3',3'-tetraethyl-1,1'-terephthaloylbis(thioureato-*S,O*))-tri-nickel(II)] (*cis*-[Ni(T-Et-*S,O*)]$_3$)

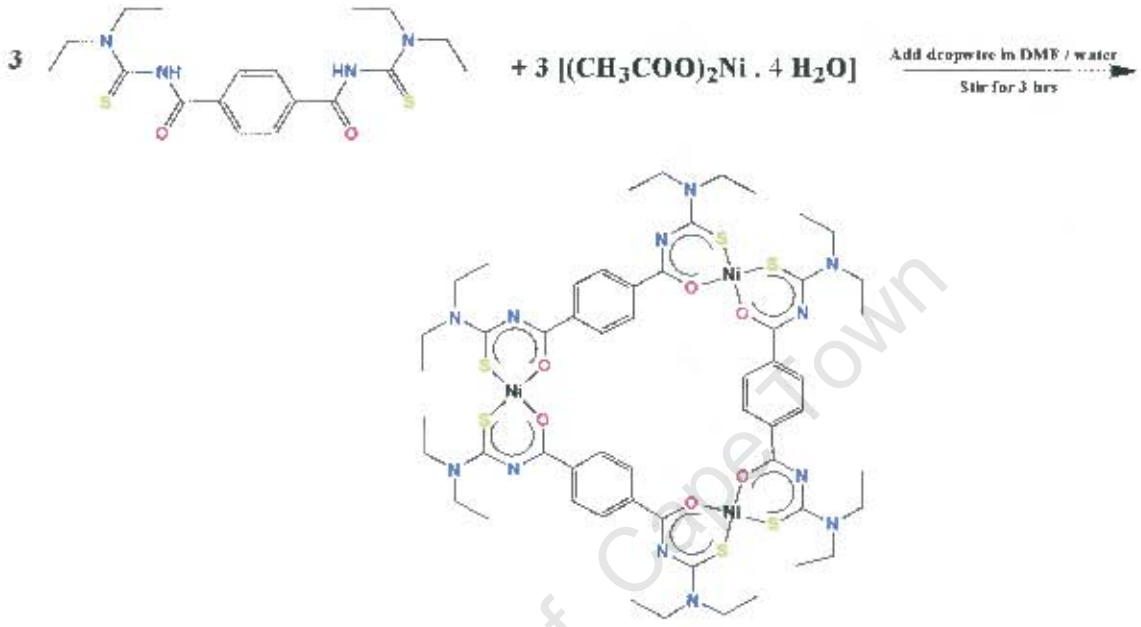

Figure 2.2.2(a). Reaction scheme for synthesis of *cis*-[Ni (T-Et-*S,O*)]$_3$

0.3946g (1.00 mmol.) of T-Et was dissolved in DMF to which $Ni(CH_3COO)_2.4H_2O$ (0.2489g, 1.00 mmol.), dissolved in 20 cm^3 H_2O and 15 cm^3 DMF, was added drop-wise while stirring vigorously, at room temperature. The mixture was stirred for a further 3 h, followed by addition of 100 cm^3 of H_2O. On cooling to 4 °C in a refrigerator for 24 hours, the dark brown solid product was collected by centrifugation and washed several times with small portions of water. The product, *cis*-[Ni(T-Et-*S,O*)]$_3$, was recrystallised from chloroform / acetone to give a fine dark brown powder.

Yield: 0.413g, 0.305 mmol., 92%. m.p. 285 – 289 °C. Found: 47.47% C, 5.47% H, 12.36% N, 13.97% S. $C_{54}H_{72}N_{12}O_6S_6Ni_3$ requires 47.91% C, 5.36% H, 12.42% N, 14.21% S; δH (200 MHz, CDCl3): 1.24 (m, 36H), 3.78 (m 24H), 8.10 (s, 12H); $\delta^{13}C$ (50 MHz, $CDCl_3$): 12.6(-CH_3), 13.2(-CH_3), 45.4(-NCH_2-), 46.0(-NCH_2-), 128.7,

139.3, 172.1(-*C*(O)-),172.2(-*C*(S)-). IR (KBr, 1000 – 300 cm^{-1}): 938, 898, 872, 836, 824, 790, 730, 684, 656, 625, 558, 530, 487, 432. The complex was recrystallised from a variety of solvent mixtures in an attempt to grow crystals suitable for x-ray analysis. These various attempts were unsuccessful.

2.2.3. *Cis*-[bis-μ-(3,3,3',3'-tetra(2-hydroxyethyl)-1,1'-isophthaloylbis(thioureato-*S,O*))-di-nickel(II)] (*cis*-[Ni(I-EtOH-*S,O*)]$_2$)

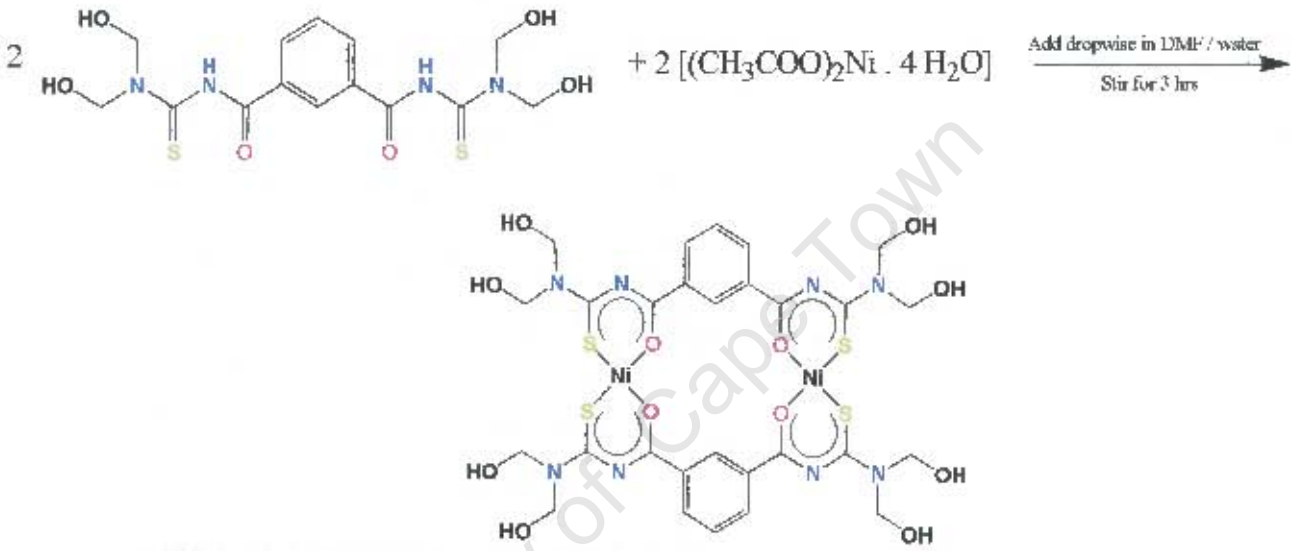

Figure 2.2.3(a). Reaction scheme for synthesis of *cis*-[Ni(I-EtOH-*S,O*)]$_2$

0.500g (1.09 mmol.) of I-EtOH was dissolved in DMF to which 0.275g (1.10 mmol.) of $Ni(CH_3COO)_2.4H_2O$, dissolved in 20 ml water and 15 ml DMF, was added drop-wise while stirring vigorously, at room temperature. The mixture was stirred for a further 3 h, followed by addition of 100 cm^3 of H_2O. On cooling to 4 °C in a refrigerator for 24 hours, the dark purple solid product was collected by centrifugation and washed several times with small portions of water. The product, *cis*-[Ni(I-EtOH-*S,O*)$_2$], was recrystallised from DMF / water to give a fine purple powder.

Yield: 0.522g, 0.506 mmol, 93%. m.p. 213 – 215 °C. Found: 41.79% C, 4.85% H, 10.81% N, 12.15% S. $C_{36}H_{48}N_8O_{12}S_4Ni_2$ requires 41.96% C, 4.70% H, 10.87% N, 12.45% S. NMR was not performed because of the low solubility of the product. Crystals suitable for single crystal x-ray diffractometry could not be obtained, despite

many attempts using solvent mixtures of DMF or DMSO with acetone, water, alcohols or chlorinated solvents.

2.2.4. *Cis*-[tris-μ-(3,3,3',3'-tetra(2-hydroxyethyl)-1,1'-terephthaloylbis(thioureato-*S,O*))-tri-nickel(II)] (*cis*-[Ni(T-EtOH-*S,O*)]$_3$)

Figure 2.2.4(a) Reaction scheme for synthesis of *cis*-[Ni(T-EtOH-*S,O*)]$_3$

0.4586g (1.00 mmol.) of T-EtOH was dissolved in DMF to which 0.2489g (1.00 mmol.) of $Ni(CH_3COO)_2.4H_2O$, dissolved in 20 ml water and 15 ml DMF, was added drop-wise while stirring vigorously, at room temperature. The mixture was stirred for a further 3 h, followed by addition of 100 cm^3 of H_2O. On cooling to 4 °C in a refrigerator for 24 hours, the dark brown solid product was collected by centrifugation and washed several times with small portions of water. The product, *cis*-[Ni(T-EtOH-*S,O*)]$_3$, was recrystallised from DMF / water to give a fine dark brown powder.

Yield: 0.474g, 0.307 mmol, 92%. Found: 42.19% C, 4.83% H, 10.77% N, 12.08% S $C_{54}H_{72}N_{12}O_{18}S_6Ni_3$ requires 41.96% C, 4.70% H, 10.87% N, 12.45% S. NMR was not performed because of the low solubility of the product. Crystals suitable for single crystal x-ray diffractometry could not be obtained, despite many attempts using solvent mixtures of DMF or DMSO with acetone, water, alcohols or chlorinated solvents.

2.3. Synthesis of Octahedral Adducts

In general, the octahedral adducts of metallamacrocycles were synthesised by dissolving the metallamacrocyclic complex in a suitable solvent and then adding the desired N-donor ligand in solution in excess. However, the compound chosen as the archetypal donor ligand was pyridine, which is liquid and also a powerful solvent. Thus in most cases, pyridine acted a dual role as the solvent of the reaction mixture and as coordinating ligand. This has important implications for the crystal structures that were obtained for these adducts. It should also be noted that, generally speaking, these adducts were found to be unstable upon removal from the mother liquor. This prevented further analysis by certain techniques, e.g. elemental analysis. Furthermore, it was found that the paramagnetic nature of the octahedral Ni(II) prevented the use of NMR techniques to analyse the products. In cases where crystalline material was obtained, appropriate measures were taken to prevent decomposition of single crystals during x-ray diffraction analysis.

2.3.1. [*Cis*-(bis-μ-(3,3,3',3'-tetraethyl-1,1'-isophthaloylbis(thioureato-*S,O*))-di-nickel(II))-tetra(pyridine-*N*)] (*cis*-[Ni(I-Et-*S,O*)(pyridine-*N*)$_2$]$_2$)

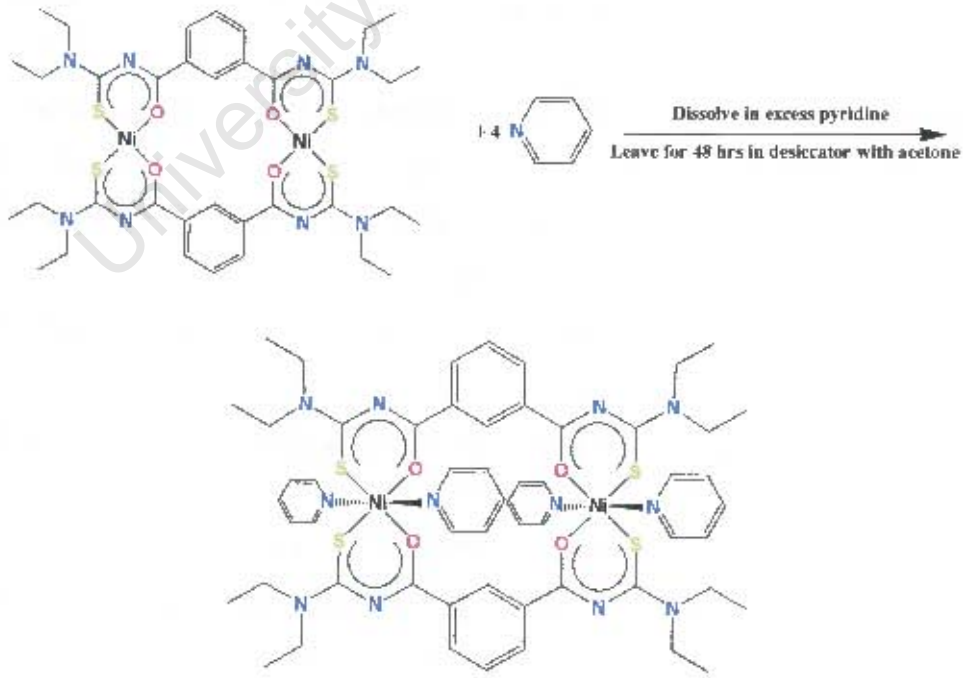

Figure 2.3.1(a). Reaction scheme for synthesis of *cis*-[Ni(I-Et-*S,O*)(pyridine-*N*)$_2$]$_2$

0.50 g of the purple complex *cis*-[Ni(I-Et-*S,O*)]$_2$ was dissolved in an excess (20 ml) of pyridine to give a bright green solution. This solution was filtered through a 0.45-micron nylon filter and left to crystallise by slow evaporation. After several days, although the volume of the solution had decreased, the formation of crystalline material was not observed. This solution was placed in a desiccator together with a beaker containing 50 cm^3 of acetone, after which the desiccator was partially evacuated to encourage the slow diffusion of acetone into the green pyridine solution. After 48 hours green crystals suitable for the purpose of x-ray diffraction analysis had formed. These crystals were found to be very friable, disintegrating rapidly into a purple powder on removal from the pyridine mother liquor, making characterisation by conventional means very difficult. The disintegration of a suitable crystal could however be arrested by immediately covering a green crystal with a drop of silicone oil prior to x-ray diffraction analysis. A small quantity of dry crystalline product, immediately after removal from the mother liquor, was subjected to thermogravimetric analysis

2.3.2. [*Cis*-(bis-μ-(3,3,3',3'-tetraethyl-1,1'-isophthaloylbis(thioureato-*S,O*))-di-nickel(II))-tetrakis(4-dimethylaminopyridine-*N*)] (*cis*-[Ni(I-Et-*S,O*)(DMAP-*N*)$_2$]$_2$)

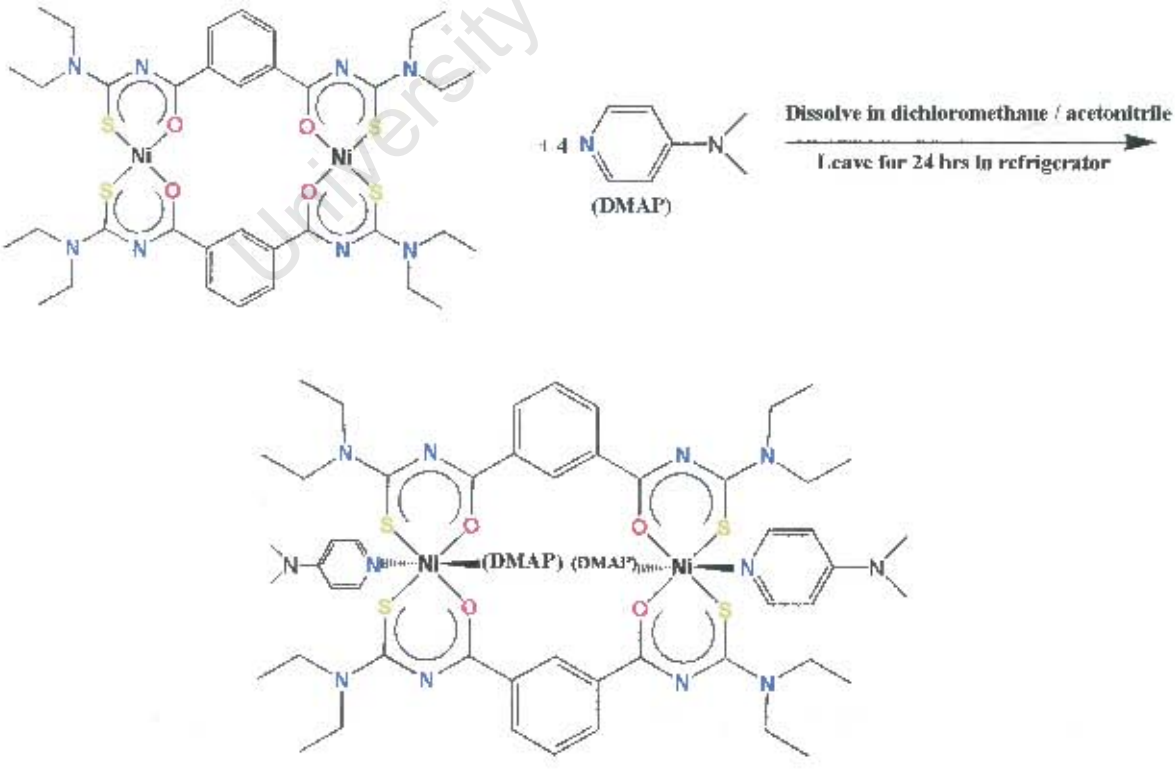

Figure 2.3.2(a). Reaction scheme for synthesis of *cis*-[Ni(I-Et-*S,O*)(DMAP-*N*)$_2$]$_2$

0.15g of purple complex *cis*-[Ni(I-Et-*S,O*)]$_2$ was dissolved together with an excess (0.10g) of 4-dimethylaminopyridine in a dichloromethane / acetonitrile mixture on gentle heating to give a brown-green solution. This solution was filtered through glass-fibre wool to remove any un-dissolved *cis*-[Ni(I-Et-*S,O*)]$_2$. Attempts to grow crystals of the product by slow evaporation of solvent at room temperature were unsuccessful. A sample of the solution was placed in a refrigerator at ~ 4 °C to encourage crystallisation. Shortly after cooling (> 90 minutes), the solution was found to have changed colour to a pale green. After 24 hours, green crystals suitable for x-ray diffraction analysis had formed from the solution. These crystals proved to be relatively stable once removed from their mother liquor, unlike those of *cis*-[Ni(I-Et-*S,O*)(pyridine-*N*)$_2$]$_2$. A small quantity of dry crystalline product was subjected to thermogravimetric analysis.

2.3.3. [*Cis*-(tris-μ-(3,3,3',3'-tetraethyl-1,1'-terephthaloylbis(thioureato-*S,O*))-tri-nickel(II))-hexa(pyridine-*N*)] (*cis*-[Ni(T-Et-*S,O*)(pyridine-*N*)$_2$]$_3$)

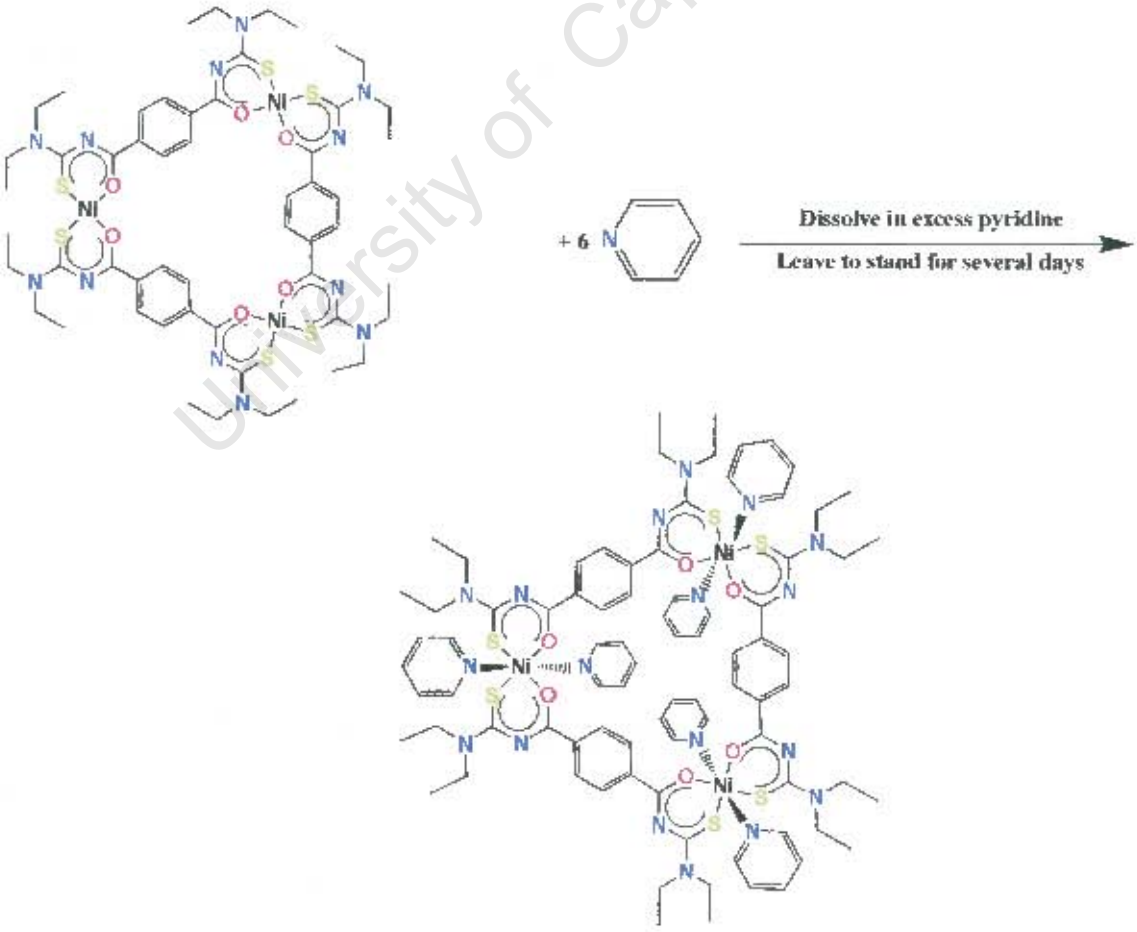

Figure 2.3.3(a) Reaction scheme for synthesis of *cis*-[Ni(T-Et-*S,O*)(pyridine-*N*)$_2$]$_3$

0.50 g of the brown complex *cis*-[Ni(T-Et-*S,O*)]$_3$ was dissolved in an excess (20 ml) of pyridine to give a dark yellow -- brown solution. This solution was filtered through a 0.45-micron nylon filter and left to crystallise by slow evaporation. After several days, dark brown crystals suitable for x-ray diffraction analysis had formed. Observation under a microscope indicated that these crystals disintegrated over time when removed from their mother liquor. Thus characterisation by conventional methods was found to be difficult. The disintegration of a suitable crystal could be arrested by immersing in a drop of silicone oil prior to x-ray diffraction analysis. A small quantity of dry crystalline product, immediately after removal from the mother liquor, was subjected to thermogravimetric analysis.

2.3.4. [*Cis*-(bis-μ-(3,3,3',3'-tetra(2-hydroxyethyl)-1,1'-isophthaloylbis(thioureato-*S,O*))-di-nickel(II))-tetra(pyridine-*N*)] (*cis*-[Ni(1-EtOH-*S,O*)(pyridine-*N*)$_2$]$_2$)

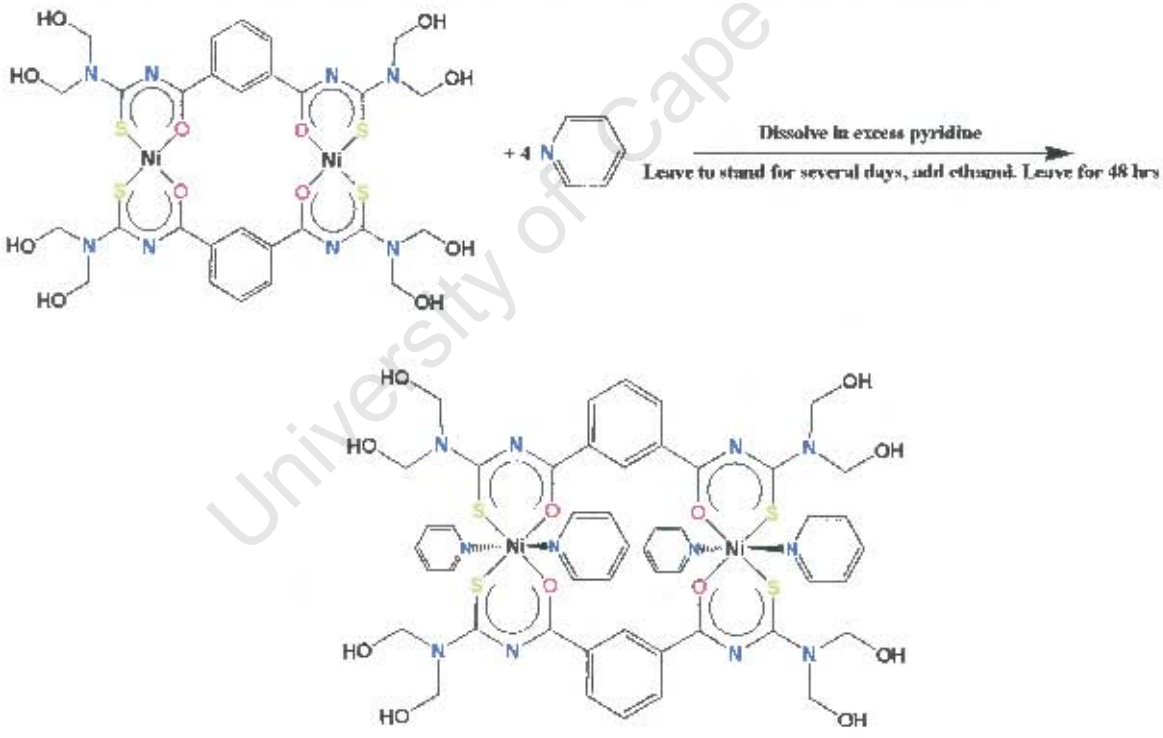

Figure 2.3.4(a) Reaction scheme for synthesis of *cis*-[Ni(1-EtOH-*S,O*)(pyridine-*N*)$_2$]$_2$

0.20 g of the purple complex *cis*-[Ni(I-EtOH-*S,O*)]$_2$ was dissolved in an excess (10 ml) of pyridine to give a bright lime green solution. This solution was filtered through a 0.45-micron nylon filter and left to crystallise by slow evaporation. After several

days the volume of solution was found to have decreased considerably, but the presence of crystalline material was not observed. 10 ml of ethanol was added to the solution, which was filtered a second time, as described above. The solution was again left to crystallise. After 48 hours, green crystals suitable for single crystal x-ray diffraction had formed. These crystals were found to decompose slowly into a purple powder on removal from the pyridine / ethanol mother liquor at room temperature. Thus, as with *cis*-[Ni(1-Et-*S,O*)(pyridine-*N*)$_2$]$_2$, characterisation of this product by conventional means was complicated. The disintegration of a suitable crystal could be arrested by immersing in a drop of silicone oil prior to x-ray diffraction analysis. A small quantity of the crystalline product, immediately after removal from the mother liquor, was subjected to thermogravimetric analysis.

2.3.5. [*Cis*-(tris-μ-(3,3,3',3'-tetra(2-hydroxyethyl)-1,1'-terephthaloylbis(thioureato-*S,O*))-tri-nickel(II))-hexa(pyridine-*N*)] (*cis*-[Ni(T-EtOH-*S,O*)(pyridine-*N*)$_2$]$_3$)

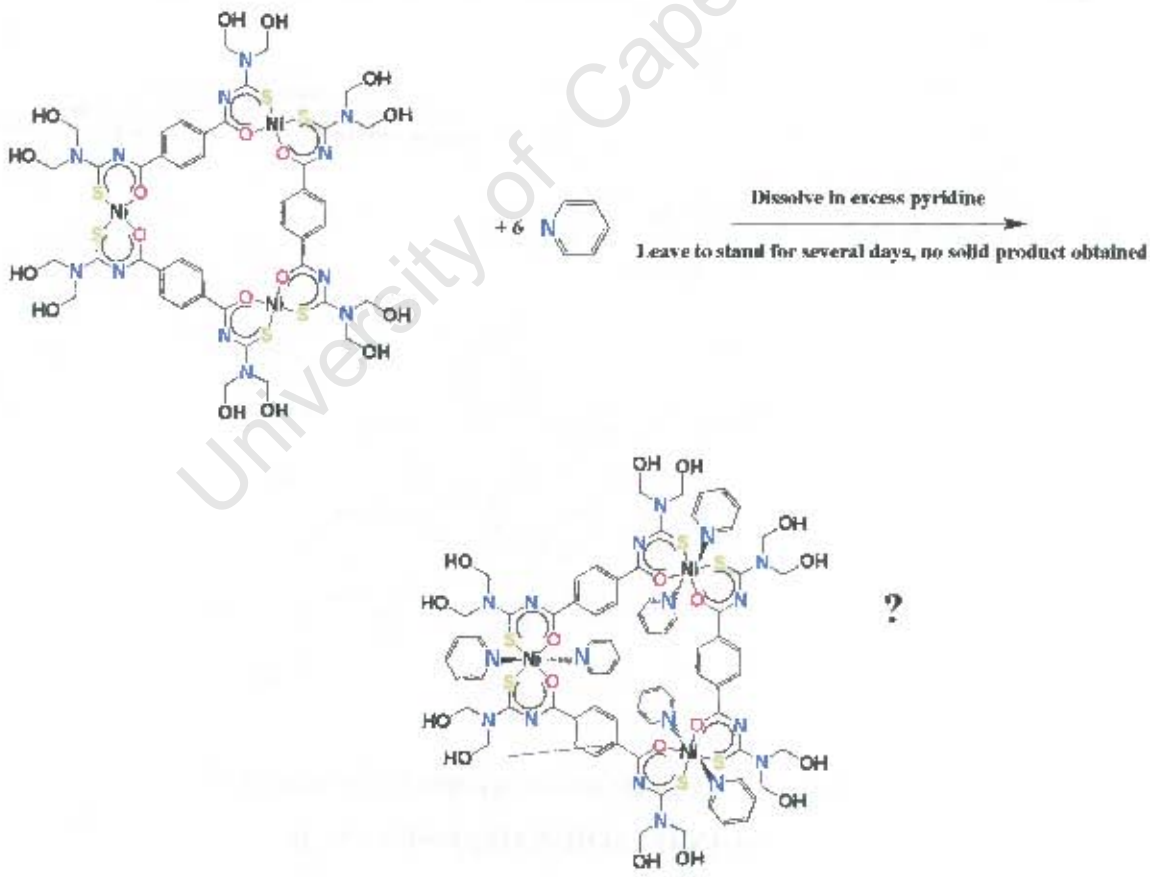

Figure 2.3.5(a) Reaction scheme for synthesis of *cis*-[Ni(T-EtOH-*S,O*)(pyridine-*N*)$_2$]$_3$; no solid product obtained

0.50 g of the brown complex *cis*-[Ni(T-EtOH-*S,O*)]$_3$ was dissolved in an excess (20 ml) of pyridine to give a dark yellow – brown solution. This solution was filtered through a 0.45-micron nylon filter and left to crystallise by slow evaporation. No crystalline material and indeed no solid material of any kind was found to have formed. After several weeks, the solution was found have reduced to a dark brown paste owing to the gradual evaporation of pyridine. Several attempts to crystallise the product at lower temperatures and from mixtures of pyridine and other solvents (ethanol, chloroform, *N*, *N*-dimethylformamide) were also unsuccessful –yielding similar results. This unexpected outcome has given rise to complications in the determination of the nature of this product.

2.4. Synthesis of Co-ordination Polymers

2.4.1. Poly-[*cis*-(bis-μ-(3,3,3',3'-tetraethyl-1,1'-isophthaloylbis(thioureato-*S,O*))-di-nickel(II))-bis-μ-(pyrazine-*N,N'*)] ({*cis*-[Ni(I-Et-*S,O*)(pyrazine-*N,N'*)]$_2$}$_n$)

0.20 g (0.22 mmol.) of the purple complex *cis*-[Ni(I-Et-*S,O*)]$_2$ was dissolved in 50 ml of dichloromethane. The resultant solution was filtered through a 0.45-micron nylon filter to remove traces of solid particles. A quantity of pyrazine (0.16 g; 2.0 mmol.) was similarly dissolved in dichloromethane and subsequently filtered. The two solutions were heated gently, and then mixed together in a beaker. The reaction mixture was left to stand. After a few minutes it was noted that the initially clear purple mixture had developed a murky quality. After a further time (ca. 30 minutes) an orange-green suspension was observed. Following a further half hour, it was found that the suspension had thickened and separated from the mother liquor, which retained a slight tinge of purple. After another 2 hours, the mother liquor was found to be clear and colourless, while the suspension was observed to be lime green. The product was centrifuged, resulting in the packing of the suspended particles into a thick disc that, after centrifugation, was found to be resting on the upper surface of the mother liquor. The latter was decanted after which the glass centrifuge tube, still containing the lime green solid, was placed in an oven at 60 °C to evaporate residual solvent. The product was removed from the oven and collected as a flaking light green layer from the walls of the centrifuge tube. The product was pulverised and then washed briefly with suction in a Buchner funnel with small amounts of ethanol / water, after which it was dried and stored as a green powder. The product, predicted to be a co-ordination polymer, [*cis*-[Ni(I-Et-*S,O*)]$_2$-(pyrazine-*N,N'*)$_2$]$_n$(pyrazine)$_2$, was not recrystallised, as attempts to dissolve the compound in dichloromethane resulted in the formation of a clear purple solution. This seems to indicate dissociation into the product's original components. Subsequent attempts to resynthesise the product with a slower mixing of the starting materials in order to encourage the formation of crystalline material were met with no success.

Yield 0.198 g; 84.6 % - assuming a *cis*-[Ni(I-Et-*S,O*)]$_2$: pyrazine stoichiometry of approximately 1:2. The thermal decomposition of the product was investigated using

hot-stage microscopy – decomp. > 90 °C. Found: 49.10% C, 5.28% H, 15.49% N, 11.77% S. IR (KBr, 1000 – 300 cm^{-1}): 957, 945, 917, 885, 848, 831, 804, 783, 755, 726, 673, 655, 532, 486, 450, 415, 381, 302. A small quantity of the product was subjected to thermogravimetric analysis. The product was also analysed by x-ray powder diffraction (XRD).

2.4.2. Poly-[*cis*-(bis-μ-(3,3,3',3'-tetraethyl-1,1'-isophthaloylbis(thioureato-*S,O*))-di-nickel(II))-bis-μ-(4,4'-bipyridine-*N,N'*)] ({*cis*-[Ni(I-Et-*S,O*)(bipy-*N,N'*)]$_2$}$_n$)

0.20 g (0.22 mmol.) of the purple complex *cis*-[Ni(I-Et-*S,O*)]$_2$ was dissolved in 50 ml of dichloromethane. The resultant solution was filtered through a 0.45-micron nylon filter. 0.31 g (2.0 mmol.) of 4,4'-bipyridine was similarly dissolved in dichloromethane and then filtered. The two solutions were heated gently, and then mixed together in a beaker. The reaction mixture was left to stand. As was the case with {*cis*-[Ni(I-Et-*S,O*)(pyrazine-*N,N'*)]$_2$}$_n$ above, the formation of a green suspension was noted after a certain amount of time (in this case ca. 1 hour). Following the same procedure as with {*cis*-[Ni(I-Et-*S,O*)(pyrazine-*N,N'*)]$_2$}$_n$, this product was separated from the mother liquor by centrifugation, dried in an oven, collected as solid green flakes, pulverised, then washed with ethanol/ water in a Buchner funnel, dried and finally stored as a green powder. Attempts to recrystallise the product were met with dissociation to the starting compounds as indicated by the transformation of the green solid to a clear purple solution. Subsequent attempts to resynthesise the product with a slower mixing of the starting materials in order to encourage the formation of crystalline material were unsuccessful.

Yield: 0.215 g; 80% - assuming a *cis*-[Ni(I-Et-*S,O*)]$_2$: 4,4'- bipyridine stoichiometry of 1:2. The thermal decomposition of the product was investigated using HSM – decomp. > 160 °C. Found: 54.76% C, 5.34% H, 13.77% N, 9.86% S. IR (KBr, 1000 – 300 cm^{-1}) 956, 942, 915, 887, 847, 810, 781, 754, 723, 695, 674, 654, 627, 605, 570, 528, 493, 446, 302. A small quantity of the product was subjected to thermogravimetric analysis. The product was also analysed by means of x-ray powder diffraction (XRD) as well as MALDI-TOF mass spectrometry.

2.4.3. Poly-[*cis*-(bis-μ-(3,3,3',3'-tetraethyl-1,1'-isophthaloylbis(thioureato-*S,O*))-di-nickel(II))-bis-μ-(1,2-bis(4-pyridyl)ethane-*N,N'*)] ({*cis*-[Ni(I-Et-*S,O*)(BPE-*N,N'*)]$_2$}$_n$)

0.20 g (0.22 mmol.) of the purple complex *cis*-[Ni(I-Et-*S,O*)]$_2$ was dissolved in 50 ml of dichloromethane. The resultant solution was filtered through a 0.45-micron nylon filter. 0.37 g (2.0 mmol.) of 1,2-bis(4-pyridyl)ethane (BPE) was similarly dissolved in dichloromethane and subsequently filtered. The two solutions were heated gently, and then mixed together in a beaker. The reaction mixture was left to stand. After approximately 1 hour, the formation of a green suspension was observed. Following the same procedure as with {*cis*-[Ni(I-Et-*S,O*)(pyrazine-*N,N'*)]$_2$}$_n$, this product was separated from the mother liquor by centrifugation, dried in an oven at 60 °C, collected as solid green flakes, pulverised, then washed with ethanol / water in a Buchner funnel, dried and finally stored as a green powder. Attempts to recrystallise the product were met with dissociation to the starting compounds as indicated by the transformation of the green solid to a clear purple solution. Subsequent attempts to resynthesise the product with a slower mixing of the starting materials in order to encourage the formation of crystalline material were not successful.

Yield: 0.212 g; 76% - assuming a (*cis*-[Ni(I-Et-*S,O*)]$_2$: 1,2-bis(4-pyridyl)ethane) stoichiometry of 1:2. The thermal decomposition of the product was investigated using HSM – decomp. > 100 °C. Found: 56.75% C, 5.97% H, 12.84% N, 9.13% S. IR (KBr, 1000 – 300 cm^{-1}): 951, 918, 893, 867, 845, 827, 780, 755, 723, 693, 673, 652, 529, 486, 440, 387. A small quantity of the product was subjected to thermogravimetric analysis. The product was also analysed by means of x-ray powder diffraction (XRD)

2.4.4. Poly-[*cis*-(bis-μ-(3,3,3',3'-tetraethyl-1,1'-isophthaloylbis(thioureato-*S,O*))-tri-nickel(II))-bis-μ-(1,2-di(4-pyridyl)ethylene-*N,N'*)] ({*cis*-[Ni(I-Et-*S,O*)(DPE-*N,N'*)]$_2$}$_n$)

0.20 g (0.22 mmol.) of the purple complex *cis*-[Ni(I-Et-*S,O*)]$_2$ was dissolved in 50 ml of dichloromethane. The resultant solution was filtered through a 0.45-micron nylon filter. 0.36 g (2.0 mmol.) of 1,2-di(4-pyridyl)ethylene (DPE) was similarly dissolved

in dichloromethane and subsequently filtered. The two solutions were heated gently, and then mixed together in a beaker. The reaction mixture was left to stand. After approximately 1 hour, a green suspension was observed to have formed. Following the same procedure as with {*cis*-[Ni(I-Et-*S,O*)(pyrazine-*N,N'*)]$_2$}$_n$ above, this product was separated from the mother liquor by centrifugation and dried in an oven at 60 ° C. The dry, flakes of solid product were found to be a dull orange – pink in colour as opposed to the green colour of the product when suspended in the mother liquor. The product was pulverised and washed with suction in a Buchner funnel with ethanol / water. Attempts to recrystallise the compound from dichloromethane yielded a very interesting result. On exposure of the product to fumes of dichloromethane, the powdered substance was observed to change colour to a bright green. On removal of the source of solvent fumes, the green powder reverted to the orange – pink colour within a few seconds. This colour change was found to be reproducible on re-exposure to fumes of dichloromethane. This phenomenon was replicated with the use of chloroform, although a longer period of exposure to the fumes was required. It was seen that this product possesses the remarkable property of vapochromism with especially high sensitivity to chlorinated solvents. The process has been seen to be highly reversible. The product, when dissolved in a quantity of liquid dichloromethane or chloroform, initially transformed in colour to green, but then quickly dissociated to its starting materials – indicated by the clear purple colour of the resultant solution. Subsequent attempts to resynthesise the product with a slower mixing of the starting materials in order to encourage the formation of crystalline material were met with no success

Yield: 0.254 g; 91% - assuming a (*cis*-[Ni(I-Et-*S,O*)]$_2$: 1,2-di(4-pyridyl)ethylene) stoichiometry of 1:2. The thermal decomposition of the product was investigated using HSM – decomp. ca. > 110 °C. Found: 56.89% C, 5.50% H, 13.29% N, 9.84% S. IR, (KBr, 1000 cm^{-1} – 300 cm^{-1}): 966, 951, 920, 891, 849, 821, 785, 751, 724, 695, 671, 553, 487, 446, 323. IR (KBr with DMF, 1000 – 300 cm^{-1}): 983, 949, 918, 889, 865, 831, 783, 752, 725, 660, 556, 446, 408, 354, 323. A small quantity of the product was subjected to thermogravimetric analysis. The product was also analysed by means of x-ray powder diffraction (XRD) as well as MALDI-TOF mass spectrometry. An experiment to determine the rate and extent of solvent inclusion associated with the colour change was conducted using a levitating balance.

2.4.5. Poly-[*cis*-(tris-μ-(3,3,3',3'-tetraethyl-1,1'-isophthaloylbis(thioureato-*S,O*))-tri-nickel(II))-tris-μ-(pyrazine-*N,N'*)] ({*cis*-[Ni(T-Et-*S,O*)(pyrazine-*N,N'*)]$_2$}$_n$)

0.30 g (0.22 mmol.) of the brown complex *cis*-[Ni(T-Et-*S,O*)]$_3$ was dissolved in 50 ml of chloroform and then filtered through a 0.45-micron nylon filter to remove traces of solid particles. 0.25 g (3.1 mmol) of pyrazine was similarly dissolved in chloroform and filtered. The two solutions were heated gently and then mixed together in a beaker. The mixture was left to stand. After 1 hour a gel-like orange – brown suspension had formed. The product was centrifuged, resulting in the packing of the suspended particles into a thick disc resting on the upper surface of the mother liquor. The latter was decanted after which the glass centrifuge tube, still containing the brown solid, was placed in an oven at 60 °C to evaporate residual solvent. The product was removed from the oven and collected as a flaking brown layer from the walls of the centrifuge tube. The product was pulverised and then washed briefly with suction in a Buchner funnel with small amounts of ethanol / water, after which it was dried and stored as an orange-brown powder. Attempts to recrystallise the product were unsuccessful as were any attempts to produce crystalline material by re-synthesising the product with a slower mixing of the starting materials.

Yield: 0.271 g; 77% - assuming a *cis*-[Ni(T-Et-*S,O*)]$_3$: pyrazine stoichiometry of 1:3. The thermal decomposition of the product was investigated using HSM – decomp. > 90 °C. Found: 49.66% C 5.34% H 15.33% N 12.57% S. IR (KBr, 1000 – 300 cm^{-1}): 939, 899, 875, 837, 822, 792, 731, 689, 658, 625, 533, 483. A small quantity of the product was subjected to thermogravimetric analysis. The product was also analysed by means of XRD.

2.4.6. Poly-[*cis*-(tris-μ-(3,3,3',3'-tetraethyl-1,1'-isophthaloylbis(thioureato-*S,O*))-tri-nickel(II))-tris-μ-(4,4'-bipyridine-*N,N'*)] ({*cis*-[Ni(T-Et-*S,O*)(bipy-*N,N'*)]$_3$}$_n$)

0.30 g (0.22 mmol.) of the brown complex *cis*-[Ni(T-Et-*S,O*)]$_3$ was dissolved in 50 ml of chloroform. The resultant dark brown solution was then filtered through a 0.45-micron nylon filter. 0.40 g (2.6 mmol.) of 4,4'-bipyridine was similarly dissolved in chloroform and subsequently filtered. The two solutions were gently heated and then mixed together in a beaker. The reaction mixture was allowed to stand. After ca. 2

hours a dark brown gel-like suspension had formed. Following the same procedure as with {*cis*-[Ni(T-Et-*S,O*)(pyrazine-*N,N'*)]$_2$}$_n$, this product was separated from the mother liquor by centrifugation, dried in an oven at 60 °C, collected as solid brown flakes, pulverised, then washed with ethanol / water in a Buchner funnel, dried and finally stored as a fine dark brown powder. Attempts to recrystallise the product and to produce crystalline material by re-synthesising the product with a slower mixing of the starting materials were unsuccessful.

Yield: 0.316 g; 79% - assuming a *cis*-[Ni(T-Et-*S,O*)]$_3$: 4,4'-bipyridine stoichiometry of 1:3. The thermal decomposition of the product was investigated using HSM – decomp. > 100 °C. Found: 53.98% C, 5.18% H, 13.20% N, 9.66% S. IR (KBr, 1000 – 300 cm^{-1}): 896, 875, 835, 805, 730, 628, 617, 606, 575, 531, 432. A small quantity of the product was subjected to thermogravimetric analysis. The product was also analysed by means of XRD, as well as MALDI-TOF mass spectrometry.

2.4.7. Poly-[*cis*-(tris-μ-(3,3,3',3'-tetraethyl-1,1'-isophthaloylbis(thioureato-*S,O*))-tri-nickel(II))-tris-μ-(1,2-di(4-pyridyl)ethylene-*N,N'*)] ({*cis*-[Ni(T-Et-*S,O*)(DPE-*N,N'*)]$_3$}$_n$)

0.30 g (0.22 mmol.) of the brown complex *cis*-[Ni(T-Et-*S,O*)]$_3$ was dissolved in 50 ml of chloroform. The dark brown solution was then filtered through a 0.45-micron nylon filter. 0.45 g (2.5 mmol.) of 1,2-di(4-pyridyl)ethylene was similarly dissolved in chloroform and subsequently filtered. The two solutions were gently heated and then mixed together in a beaker. The reaction mixture was allowed to stand. After approximately 1 hour, the formation of an orange suspension was noted. Following the same procedure as with {*cis*-[Ni(T-Et-*S,O*)(pyrazine-*N,N'*)]$_2$}$_n$, this product was separated from the mother liquor by centrifugation, dried in an oven at 60 °C, collected as solid orange – brown flakes, pulverised, then washed with ethanol / water in a Buchner funnel, dried and finally stored as an orange powder. Attempts to recrystallise the product were unsuccessful as were any attempts to produce crystalline material by re-synthesising the product with a slower mixing of the starting materials.

Yield: 0.361 g; 86 % - assuming a *cis*-[Ni(T-Et-*S,O*)]$_3$: 1,2-di(4-pyridyl)ethylene stoichiometry of 1:3. The thermal decomposition of the product was investigated using HSM – decomp. > 180 °C. Found: 56.74% C, 5.60% H, 13.05% N, 9.62% S. IR (KBr, 1000 – 300 cm^{-1}): 969, 896, 875, 821, 792, 729, 552, 480, 385 A small quantity of the product was subjected to thermogravimetric analysis. The product was also analysed by means of x-ray powder diffraction (XRD), as well as MALDI-TOF mass spectrometry.

2.5. Instrumental and Computational Methods

2.5.1. Elemental analysis

All synthesised compounds that could survive removal from the mother liquor were analysed by elemental analysis. All elemental analyses were performed on a Carlo Erba elemental analyzer Model 1106.

2.5.2. Nuclear magnetic resonance (NMR) spectroscopy

All synthesised ligands and some metallamacrocyclic compounds were analysed by NMR spectroscopy. The initial analysis of *cis*-[Ni(I-Et-*S,O*)(pyridine-*N*)$_2$]$_2$ by NMR gave rise to a spectrum that was distorted by a very high paramagnetic shift. Since all octahedral Ni(II) complexes are paramagnetic, similar distortions were expected for all octahedral adducts and coordination polymers. As a result, these compounds were not subjected to NMR

All ^{1}H and ^{13}C NMR spectra were recorded on a Varian VXR-200 spectrometer. The deuterated solvents used were chloroform and dimethylsulfoxide (DMSO-d_6). ^{1}H spectra were measured at a frequency of 200 MHz in the range.0 – 12 ppm. ^{13}C spectra were measured at a frequency of 50 MHz in the range 0 – 200 ppm.

2.5.3. Infrared (IR) spectroscopy

All coordination polymers were analysed by IR spectroscopy. Samples were prepared as KBr pellets and analysed on a Perkin-Elmer 983 IR spectrometer in the 1000 cm^{-1} – 300 cm^{-1} range. The compound {*cis*-[Ni(I-Et-*S,O*)(DPE-*N,N'*)]$_2$}$_n$, which undergoes a colour change in the presence of solvents was subjected to an additional IR analysis, mixed with *N,N*-dimethylformamide (DMF) and prepared as a KBr pellet. The lists of absorption peaks for both analyses are reported above.

2.5.4. Melting point determination and hot stage microscopy (HSM)

Visual observation of the behaviour of ligands and metallamacrocyclic compounds on heating was conducted on a Reichert-Jung Thermovar hot stage microscope. All coordination polymers were heated on a Linkam THMS 600 hot stage, which was controlled by a Linkam TP92 central processor. Digital photographs were taken through a Nikon SMZ-10 binocular microscope using a Sony Hyper HAD digital video camera.

2.5.5. Thermogravimetric analysis (TGA)

All octahedral adducts and coordination polymers were subjected to TGA with a heating rate of 20 °C min^{-1} under an atmosphere of dry N_2 (flow rate 30 cm^3 min^{-1}) using a Mettler Toleda TGA/sDTA 851^e. Raw data from these analyses were plotted graphically using Microsoft Excel.

2.5.6. X-ray powder diffraction (XRD)

All coordination polymers were subjected to XRD analysis using a HUBER-Guinier 670 Imaging Plate x-ray powder diffractometer using Cu Kα x-rays (1.5405 Å). Graphs of x-ray reflection intensity vs. angle (2θ) were plotted from the raw data using Microsoft Excel.

2.5.7. Single crystal x-ray diffractometry

All data for crystal and molecular structures determination were measured on a Nonius KappaCCD diffractometer using graphite-monochromated Mo Kα radiation (0.7107 Å) at decreased temperatures (either 173K or 193K). In each case, a series of frames were recorded, each of width 1° in ϕ or in ω (with $\kappa \neq 0$) to ensure completeness of the data collected to θ>28°. The unit cell was indexed from the first ten frames and positional data were refined along with diffractometer constants to give the final cell parameters. Integration and scaling (DENZO, Scalepack[100]) resulted in unique data sets corrected for Lorentz-polarization effects and for the

effects of crystal decay and absorption by a combination of averaging of equivalent reflections and an overall volume and scaling correction. The structures were solved using SHELXS-97 [101] and refined using full-matrix least squares methods (with the exception of *cis*-[Ni(T-Et-*S,O*)(pyridine-*N*)$_2$]$_3$) in SHELXL-97 [101], with the aid of the program XSEED.[102] Additional information pertaining to individual structure determinations is given in the appropriate places in Chapter 3. If not otherwise specified, all non-hydrogen atoms were modelled anisotropically, while all hydrogen atoms were assigned an isotropic thermal parameter 1.2 times that of their parent atom and refined using a 'riding' model. All images of crystal and molecular structures were rendered using the program POV-Ray. Additional modifications to these images, such as labelling atoms, were performed using Microsoft PowerPoint.

2.5.8. Levitation balance sorption studies

The product {*cis*-[Ni(1-Et-*S,O*)(DPE-*N,N'*)]$_2$}$_n$, which displays vapochromic behaviour, was subjected to levitation balance analysis. A sample of the product was placed in a chamber, which was subsequently evacuated. Vapours of dichloromethane were then admitted into the chamber. A computer-controlled valve maintained constant CH_2Cl_2 pressure. Gains in sample mass due to vapour sorption were measured by a sensitive system, in which a sample pan is attached to a permanent magnet which is coupled across the chamber boundary to an external electromagnet suspended from an analytical balance. This coupling is effected by maintaining the equilibrium between the upward electromagnetic and downward gravitational forces acting on the permanent magnet. Electronic feedback of the position of the permanent magnet is used to control the current through the electromagnet in order to balance the forces. Position feedback is achieved by means of optical sensing. Mass gains at various constant pressures of CH_2Cl_2 were measured over time (at room temperature). The raw data were plotted graphically using Microsoft Excel.

2.5.9. Matrix-assisted laser desorption / ionisation time of flight mass spectroscopy (MALDI-TOF MS)

Selected coordination polymers were submitted for MALDI-TOF MS analysis, a technique that accurately measures molecular masses of large molecules such as

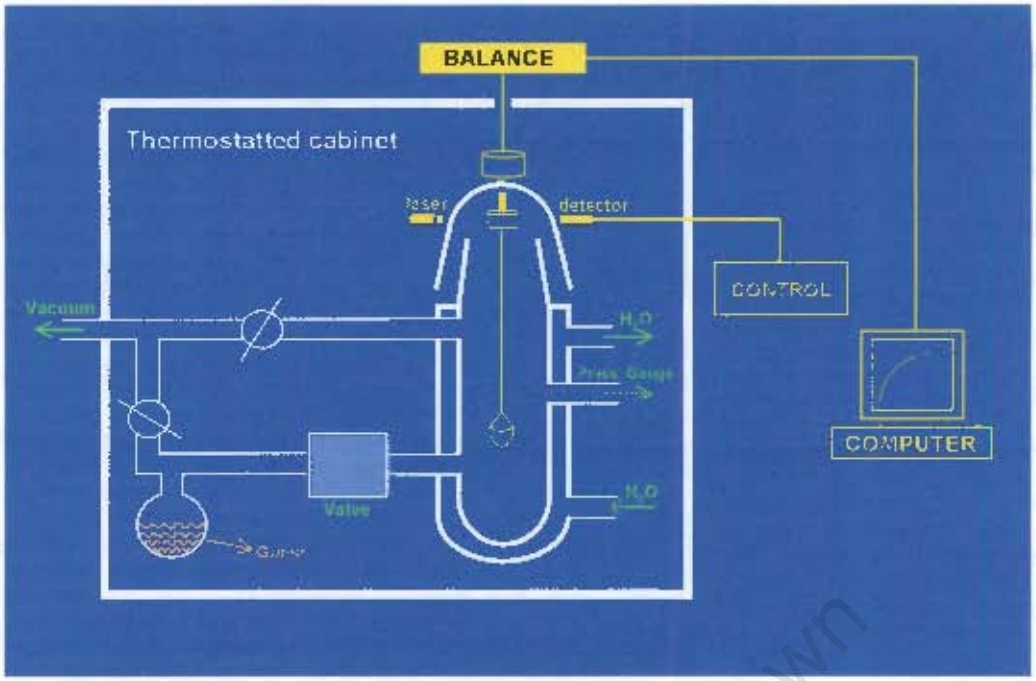

Figure 2.5.8(a) Schematic diagram of levitation balance used in sorption studies of coordination polymer {*cis*-[Ni(I-Et-*S,O*)(DPE-*N,N'*)]$_2$}$_n$.

proteins. The instrument used was a Perseptive Biosystems Voyager DE-PRO Biospectrometry Workstation possessing Delayed Extraction Technology. The matrix used was a saturated solution of dithranol (DIT) in $CHCl_3$. 2µl of the matrix/sample mixture was applied to a MALDI P100 gold sample plate and allowed to completely dry under a gentle stream of air. The drying process allowed crystallisation of the matrix and the sample was trapped in the crystals. After confirming crystal formation by light microscopy, the plate was inserted into the instrument. The sample was then analysed using the preset method HCD1005 in the positive ion mode, which has an accelerating voltage of 20kV, grid voltage of 94%, Guide Wire Voltage of 0.05%, delayed extraction at 1500ns and laser intensity of ~2000-2500. Spectra were captured using Perseptive Grams/32(R) v.4.14.

The analysis was done to determine the number of repeating units in the coordination polymers. In each case, the only mass peaks observed were those corresponding with single metallamacrocyclic units. It is believed that the solvent used in the technique caused the polymers to dissociate into their separate components, as there is other compelling evidence to suggest that the products are indeed polymeric. As a result of this phenomenon, MALDI-TOF MS proved not to be useful in analysing these products.

Chapter 3

Results and Discussion

3.1. Chelating Ligands

The bipodal benzoylthioureas, synthesised by the Douglass and Dains method were all recrystallised and characterised by elemental analysis, NMR spectroscopy and melting point determination. The ethyl-branched compounds were found to possess markedly different solubility properties from those of the hydroxyethyl-branched ligands.

The hydrogen-bonding ability of the acylthioureas via the N-H group is predictable. However, the abstraction of the N-H proton during co-ordination of the ligand to a metal centre precludes this mode of H-bonding from occurring in complexes of acylthioureas. The synthesis of hydroxyethyl-branched ligands gives rise to the possibility of new and interesting modes of H-bonding in the ligand crystal structure. Furthermore, this H-bonding ability should be carried over into co-ordination complexes based on these ligands.

While only structural data for isophthaloyl ligands have been determined crystallographically in this study, certain general speculations about their terephthaloyl analogues (based upon results from this and other studies) will be discussed.

The structural similarities and differences of the two isophthaloyl ligands I-Et and I-EtOH will be discussed in some detail. Certain values (i.e. bond lengths and angles) for these compounds require direct numerical comparison. For convenience in this regard, these are tabulated together and reported prior to the subsections (3.1.1. and 3.1.2.) devoted specifically to each of the compounds. References are made back to these tables throughout the two subsections.

Table 3.1(a). Selected bond lengths in synthesized bipodal isophthaloyl chelating ligands compared with published data for analogous compounds.

Bond Type	Average Bond Lengths (Å)			
	I-Et	I-EtOH	1-(2-chlorobenzoyl)-3,3-diethyl thiourea [103]	1-naphthoyl-3,3-di(n-butyl) thiourea [5]
C = O	1.218(4)	1.213(2)	1.218(2)	1.215(3)
(O)C – N	1.381(4)	1.370(2)	1.360(2)	1.376(4)
(OC)N – C(S)	1.428(4)	1.404(2)	1.428(2)	1.420(6)
C = S	1.671(4)	1.676(1)	1.658(2)	1.676(2)
C(S) – NR_2	1.318(4)	1.334(2)	1.327(2)	1.320(3)

Table 3.1(b). Comparison of bond angles in acylthiourea moieties of I-Et and I-EtOH.

Bonds	Bond Angles (°)	
	I-Et	I-EtOH
C – C(O) = O	122.3(3)	121.8(1)
C – C(O) – N	115.1(3)	124.9(1)
O = C(O) – N	122.5(3)	113.2(1)
C(O) – N – C(S)	119.8(3)	126.7(1)
N – C(S) = S	118.6(3)	121.7(1)
N – C(S) – NR2	115.0(3)	113.6(1)
S = C(S) – NR2	126.4(3)	124.6(1)

3.1.1. 3,3,3',3'-tetraethyl-1,1'-isophthaloylbis(thiourea) (I-Et)

Table 3.1.1(a). Crystal Data and Refinement* Parameters for I-Et

Molecular Formula	$C_{18}H_{26}N_4O_2S_2$
Formula Weight ($g.mol^{-1}$)	394.55
Temperature (K)	293
Wavelength (Å)	0.71070
Crystal System	Orthorhombic
Space Group	$Pna2_1$
a (Å)	20.439(1)
b (Å)	6.979(1)
c (Å)	29.324(2)
$\alpha = \beta = \gamma$ (°)	90
Volume ($Å^3$)	4182.9(7)
Z	8
Calculated Density ($g.cm^{-3}$)	1.253
μ (mm^{-1})	0.274
F(000)	1680
Crystal Size	0.30 x 0.40 x 0.20 mm
θ Range Scanned (°)	3.08 – 25.35
Index Range	$-23 \leq h \leq 24$, $-8 \leq k \leq 7$, $-5 \leq l \leq 35$
No. Reflections Collected	15652
No. Unique Reflections	7311 [R(int) = 0.0398]
Completeness	97.4 %
Refinement Method	Full-matrix L.S. on F^2
Data / Restraints / Parameters	7311 / 1 / 494
Goodness-of-fit on F^2	1.019
Final R Indices [$I>2\sigma(I)$]	$R_1 = 0.0455$, $wR_2 = 0.0992$
R Indices (all data)	$R_1 = 0.0742$, $wR_2 = 0.1103$
Largest Diff. Peak and Hole	0.852 and -0.200 e. $Å^{-3}$

* Flack parameter (0.43) indicates a racemic twin (see CIF file in appendix B). Structure was refined as such.

Single crystal diffractometry

Figure 3.1.1(a) shows the molecular structure of I-Et. Inspection of the molecular structure indicates that the two acylthiourea moieties assume non-planar conformations with respect to the phenylene ring and are in an '*anti*' orientation relative to each other, similar to that observed in the related structures on 1,1'-di(n-butyl)-3-naphthoylthiourea [5] and 1,1-diethyl-3-(2-chlorobenzoyl)thiourea [103]. The important bond lengths within I-Et are very similar to the corresponding values observed for the compound 1,1-diethyl-3-(2-chlorobenzoyl)-thiourea and 1,1'-di(n-butyl)-3-naphthoylthiourea as well as for I-EtOH. (Table 3.1(a)). The bond lengths, C4A – N4A (1.318(4) Å) C2A – N3A (1.381(4) Å) and C4A – N3A (1.428(4) Å), are significantly shorter than the average length of a C(sp^3) – N(sp^3) bond (1.472 ± 0.016 Å) [104], reflecting a degree of double bond character in these C – N bonds and following a trend typical for this class of compound.[5, 16, 18, 103] It is interesting to note the effects of electron delocalisation on these bond lengths upon complexation. Specifically, it will be shown (see Section 3.2 below) that the C = O and C = S lengthen, indicating a decrease in bond order, while the C – N bonds that form part of the chelate ring shorten, indicating a shift towards greater double bond character.

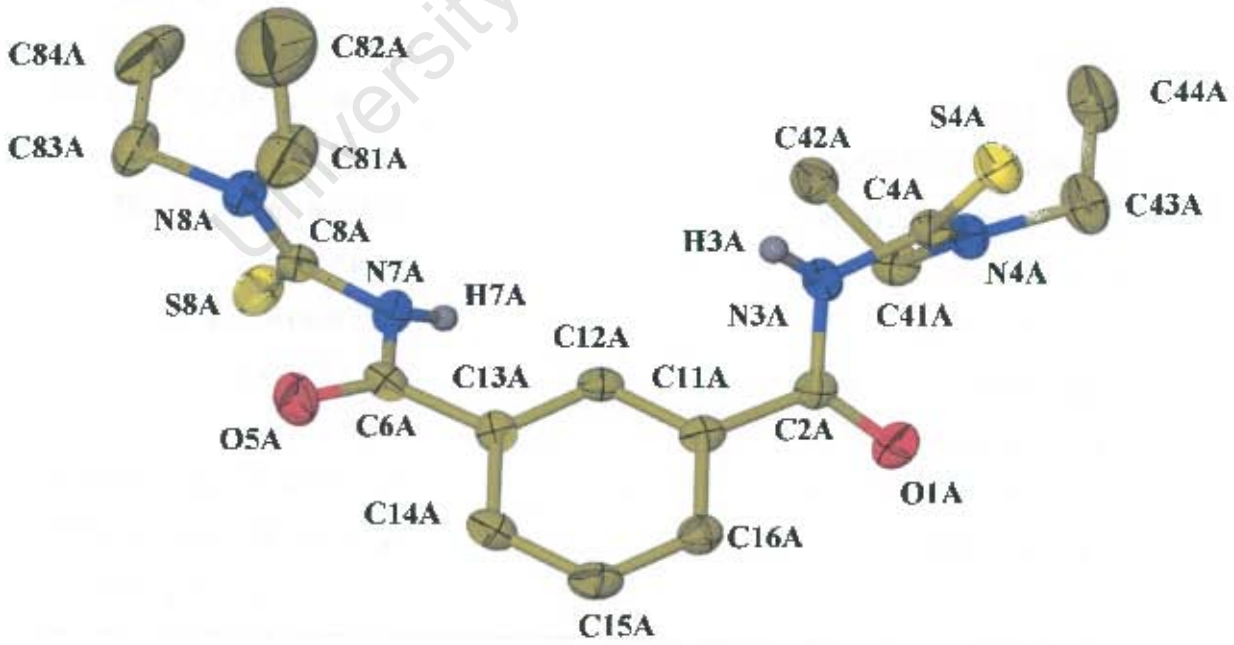

Fig. 3.1.1(a). Molecular Structure of I-Et (Molecule A). Thermal ellipsoids drawn at 50% probability

At first, it appears that the molecule possesses a 2-fold rotation axis through C12A and C15A However, on closer inspection, it is seen that one half of the molecule differs slightly from the other (compare bond angles O1A – C2A – C11A 122.32° and O5A – C6A – C13A 122.12° as well as angles N3A – C4A N4A 115.00° and N7A – C8A – N8A 116.45°.) In theory, it would be possible for the asymmetric unit for this crystal structure to consist of one half of this symmetrical molecule. The experimental evidence proves otherwise.

Furthermore, figure 3.1.1(b) shows that there are two molecules of I-Et in the asymmetric unit (A and B), which are not related by symmetry and which assume somewhat different conformations. This can be seen by comparing torsion angles involving the ethyl branches in molecule A: C(4A) – N(4A) – C(41A) – C(42A) 69.1(4)°; C(4A) – N(4A) – C(43A) – C(44A) -97.6(4)°; C(8A) – N(8A) – C(81A) – C(82A) 139.9(5)°; C(8A) – N(8A) – C(83A) – C(84A) -87.0(5)° with the corresponding angles in molecule B: C(4B) – N(4B) – C(41B) – C(42B) 86.9(4)°; C(4B) – N(4B) – C(43B) – C(44B) -110.1(4)°; C(8B) – N(8B) – C(81B) – C(82B) 90.9(5)°; C(8B) – N(8B) – C(83B) – C(84B) 86.9(4)°.

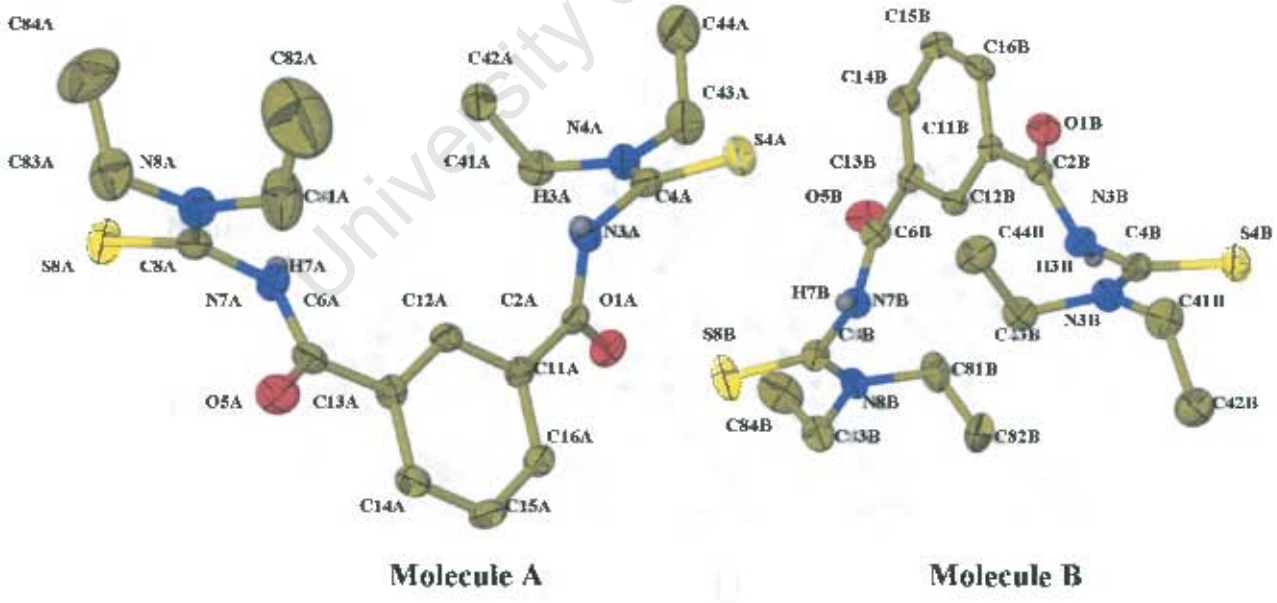

Fig. 3.1.1(b). Asymmetric Unit of I-Et Crystal Structure Thermal ellipsoids drawn at 50% probability

The crystal packing of I-Et molecules consists of chains of symmetry related molecules (A linked to A and B linked to B) interconnected by hydrogen bonds between N-H and S moieties (Table 3.1.1(b)). Thus each molecular link in the chain is doubly H-bonded to the next. These chains run parallel to the b-axis of the unit cell (i.e. in the [010] direction) as indicated in figure 3.1.1(c). By comparing torsion angles O1A – C2A – N3A – C4A (-9.95°) and C2A – N3A – C4A – S4A (-106.05°), it can be seen that the carbonyl (C2A-O1A) and thiocarbonyl (C4A-S4A) moieties are virtually orthogonal to one another, held in that position by a hydrogen bond to a nitrogen atom in an adjacent molecule.

Table 3.1.1(b). List of Hydrogen bonds in crystal structure of I-Et

Atoms in Hydrogen Bond (D-H---A)	Donor – Acceptor Distance (Å)	H-Bond Angle (°)	Symmetry Operator
N3A – H3A --- S8A$1	3.410	159.8	$1: (x; y + 1; z)
N7A – H7A --- S4A$2	3.405	170.9	$2: (x; y - 1; z)
N3B H3B --- S8B$1	3.305	172.7	$1: (x; y + 1; z)
N7B – H7B --- S4B$2	3.428	163.0	$2: (x; y - 1; z)

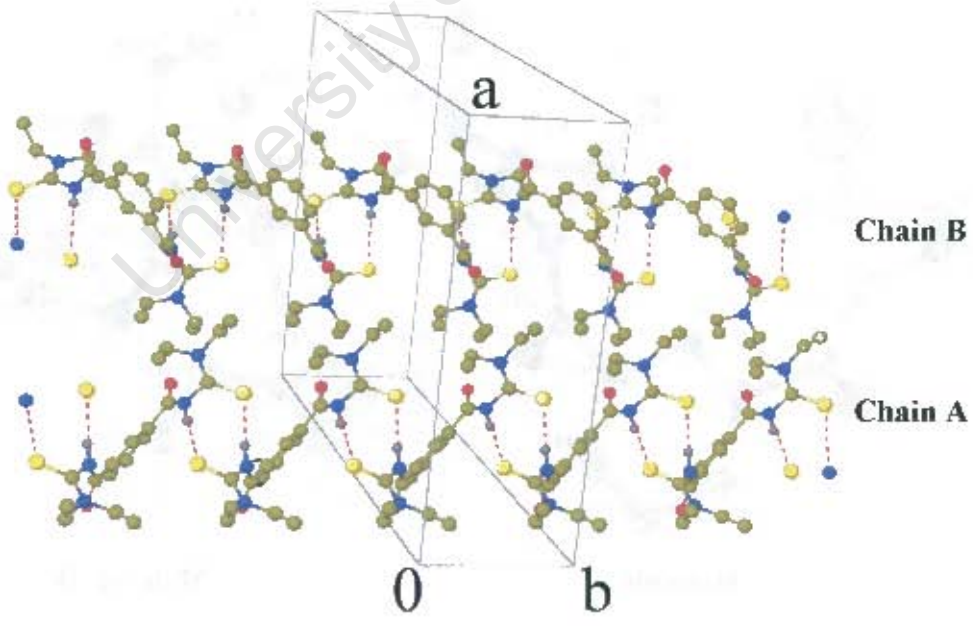

Fig. 3.1.1(c). Crystal Structure of I-Et: H-bonded Chains of I-Et Molecules

The full crystal packing of I-Et is illustrated by stereo diagrams viewed along the [100], [010] and [001] directions (figure 3.1.1(d)).

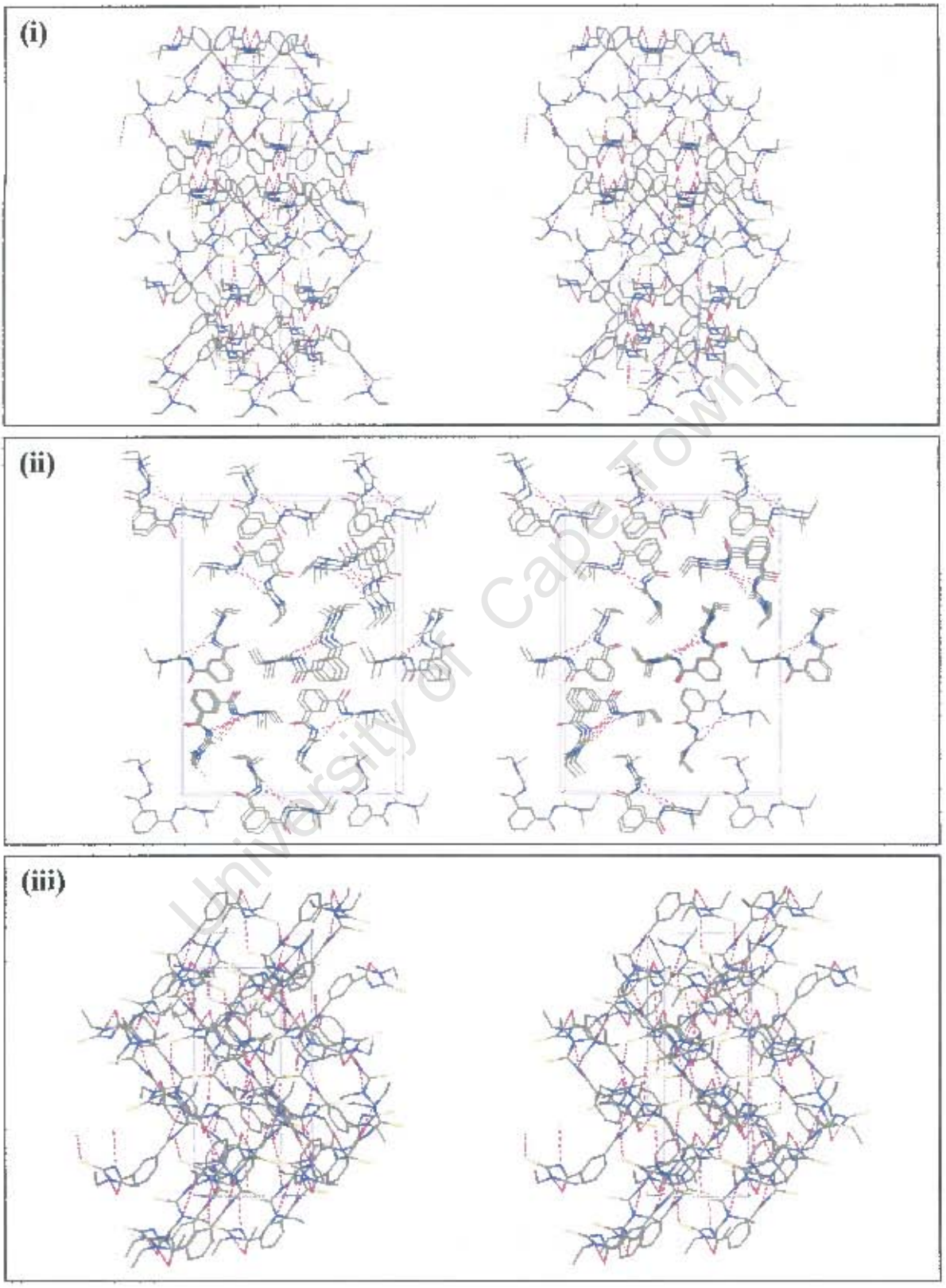

Fig. 3.1.1(d). Stereo crystal packing diagrams of I-Et viewed down principle directions [100] (i), [010] (ii) and [001] (iii).

By viewing the crystal packing in the [010] direction the H-bonded chains of molecules are clearly seen to run parallel and to be separate from one another. When viewing along the other principle directions in the crystal, one can see that the molecules within a particular chain are in identical orientations, while molecules in neighbouring chains differ in orientation. The angle made between the phenylene ring planes of two molecules is a good indicator of relative orientation. In the asymmetric unit, the phenylene ring planes of molecules A and B make an angle of 84.51 ° with one another. Despite having phenylene rings almost perpendicular to each other, both of these molecules are links in chains that run parallel with one another. The distance between phenylene rings in successive molecules is b = 6.979Å. This is far greater than the accepted distance for strong π-π interactions (3.3 – 3.8 Å) [105]. Thus the H-bonds are the dominant factor in determining the mode of crystal packing.

It is interesting to note that there is an apparent relationship between type A molecules in one asymmetric unit and type B molecules in a different asymmetric unit (e.g. generated by symmetry operator (½ + x, ½ - y, z)). They appear to have identical orientations, with one molecule able to be generated from the other by pseudo 2-fold screw axis symmetry, as shown in figure 3.1.1(e).

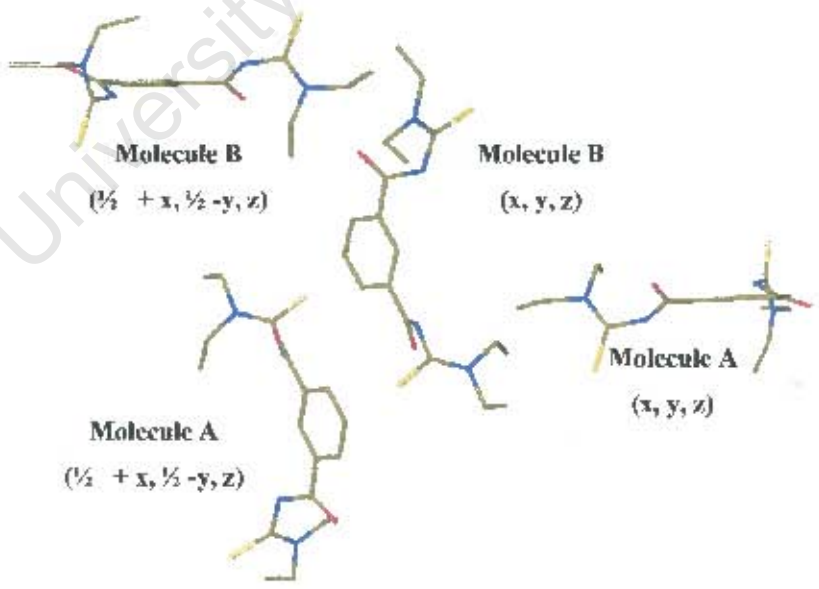

Fig. 3.1.1(e). Relative orientation of I-Et molecules in 2 asymmetric units

The phenyl ring planes of two such molecules appear at first glance to be parallel. However, the angle between these planes is calculated to be 3.95 °. Furthermore, the

small, yet significant, differences in conformation of molecules A and B mentioned above strengthen the argument that there is no symmetry-based relationship between type A and type B molecules.

3.1.2. 3,3,3',3'-tetra(2-hydroxyethyl)-1,1'-isophthaloylbis(thiourea) (I-EtOH)

Table 3.1.2(a). Crystal Data and Refinement Parameters for I-EtOH

Molecular Formula	$C_{18}H_{26}N_4O_6S_2$
Formula Weight ($g.mol^{-1}$)	458.56
Temperature (K)	193
Wavelength (Å)	0.71073
Crystal System	Tetragonal
Space Group	$P4_32_12$
a = b (Å)	9.289(1)
c (Å)	25.028(5)
$\alpha = \beta = \gamma$ (°)	90
Volume ($Å^3$)	2159.6(6)
Z	4
Calculated Density ($g.cm^{-3}$)	1.410
μ (mm^{-1})	0.289
F(000)	968
Crystal Size	0.60 x 0.40 x 0.40 mm
θ Range Scanned (°)	3.93 – 28.28
Index Range	$-12 \leq h \leq 12$, $-8 \leq k \leq 12$, $-31 \leq l \leq 33$
No. Reflections Collected	12620
No. Unique Reflections	2660 [R(int) = 0.0266]
Completeness	98.2 %
Refinement Method	Full-matrix L.S. on F^2
Data / Restraints / Parameters	2660 / 0 / 149
Goodness-of-fit on F^2	1.074
Final R Indices [$I>2\sigma(I)$]	$R_1 = 0.0264$, $wR_2 = 0.0708$
R Indices (all data)	$R_1 = 0.0285$, $wR_2 = 0.0723$
Absolute Structure Parameter	0.01(6)
Largest Diff. Peak and Hole	0.169 and -0.186 e. $Å^{-3}$

Single Crystal Diffractometry

Figure 3.1.2(a) shows the molecular structure of the I-EtOH molecule. The asymmetric unit comprises one half of the I-EtOH molecule. The other half of the molecule is generated by a 2-fold rotational symmetry operation that transforms the coordinate (x, y, z) into (1-y, 1-x, ½-z). Other axes of this type exist at intervals of ¼ along the [001] direction. The atoms C12, H12, C14 and H14 lie on the 2-fold rotation axis at special positions (x, 1-x, ¼). In other words, the rotation axis is a diagonal of the square made by taking a transverse section of the tetragonal unit cell at z = ¼.

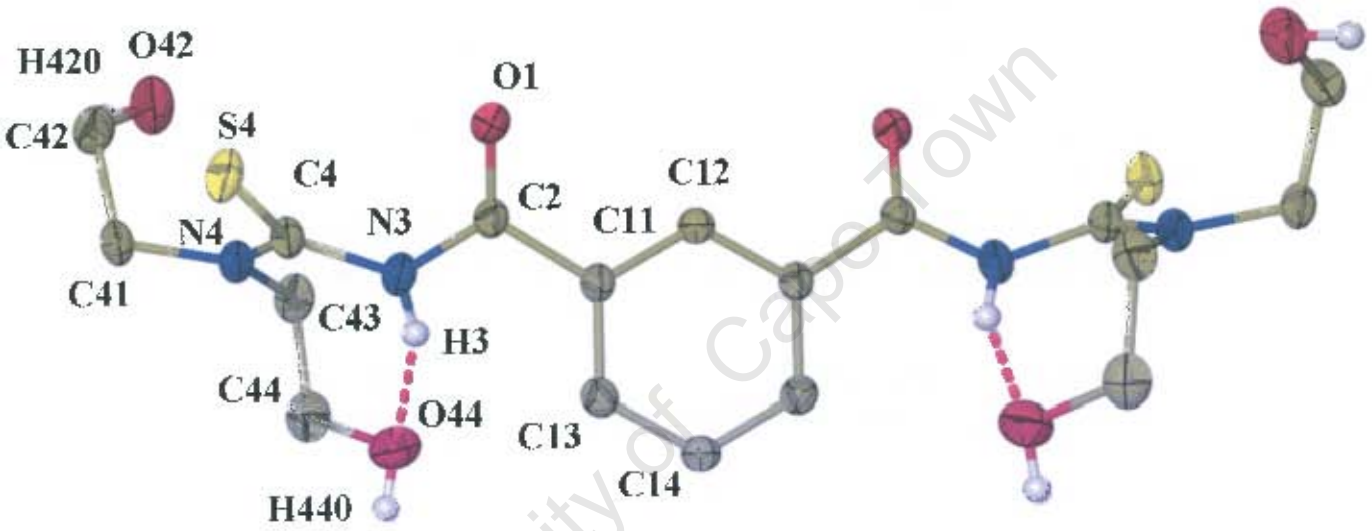

Figure 3.1.2(a). Molecular structure of I-EtOH with N-H and O-H hydrogen atoms and intramolecular H-bonds indicated. Thermal ellipsoids drawn at 50% probability.

It is immediately evident that the structure is analogous to that of I-Et. However, not unexpectedly, there are differences between the structural details of the two compounds. These differences are of varying degree. The I-EtOH acylthiourea bond lengths differ only slightly from the corresponding bond lengths in I-Et (see Table 3.1(a)), while the bond angles within the acylthiourea moieties of the two compounds (see Table 3.1(b)) differ by up to 10° (C11 – C2 – O1 124.9° in I-EtOH and C11A – C2A – O1A 115.1°).

As is the case for I-Et, the acylthiourea moieties of I-EtOH do not lie coplanar with the phenylene ring. However, the conformation of this functional group is greatly

different from its counterpart in I-Et. For 1-Et, the carbonyl and thiocarbonyl moieties were shown to be almost perpendicular; for I-EtOH, the torsion angles O1 – C2 – N3 – C4 (-5.4°) and C2 – N3 – C4 – S4 (-46.0°) show that the C - O and C - S groups are in an oblique orientation with respect to each other.

This conformational difference is a result of the difference in hydrogen-bonding modes between 1-Et and 1-EtOH. For the former, the N-H groups were shown to act as donor groups for intermolecular H-bonds to carbonyl oxygens. In the case of I-EtOH, the N-H group is engaged in an intramolecular interaction with the hydroxyl oxygen atom O44. This hydroxyl group in turn acts as a donor in an intermolecular hydrogen bond to sulphur atom S4 of a neighbouring asymmetric unit generated by the symmetry operator (½ + x, ½ -y, ¼ -z). The atom O1 acts as a hydrogen bond acceptor in an intermolecular interaction with the hydroxyl group O42 – H420 of the asymmetric unit in symmetry-generated position (½ + x, 3/2 - y, ¼ -z). Table 3.1.2(b) lists the unique hydrogen bonds present in the crystal structure of 1-EtOH.

Table 3.1.2(b). List of Hydrogen bonds in crystal structure of I-EtOH

Atoms in Hydrogen Bond (D-H---A)	Donor – Acceptor Distance (Å)	H-Bond Angle (°)	Symmetry Operator
N3 – H3 --- O44	2.706	162.4	
O44 – H44O --- S4$1	3.164	157.8	$1: (½ + x, ½ -y, ¼ -z)
O42 – H42O --- O1$2	2.791	141.0	$2: (½ + x, 3/2 - y, ¼ -z)

The modes of hydrogen bonding exhibited by I-EtOH in the crystal structure differ somewhat from those observed for the monopodal analogue 1-benzoyl-3,3-di(2-hydroxyethyl)thiourea.[98] In both cases, a N – H --- O(H) intramolecular hydrogen bond, as well as an O – H --- O(C) intermolecular interaction are observed. However, where an O – H --- O(H) intermolecular hydrogen bond is observed for the monopodal compound, 1-benzoyl-3,3-di(2-hydroxyethyl)thiourea, an O – H --- S(C) intermolecular interaction is observed in the case of I-EtOH.

In the crystal structure of 1-benzoyl-3,3-di(2-hydroxyethyl)thiourea, the molecules were described as packing "in stacks of alternating orientation and (the molecules) are hydrogen bonded in a ribbon-like fashion approximately parallel to the z-axis. This is a consequence of the symmetry of the space group ($P2_12_12_1$) in which this compound crystallises. Note that this description of linear H-bonded chains is to some extent reminiscent of what is observed for the bipodal ethyl-branched compound I-Et (section 3.1.1 above).

It will now be shown that the higher order symmetry of the bipodal, hydroxyethyl-branched I-EtOH crystal structure gives rise to a wholly different mode of packing that is far more complicated than what was observed for the monopodal hydroxyethyl-branched compound, 1-benzoyl-3,3-di(2-hydroxyethyl)thiourea, or the bipodal ethyl-branched compound, I-Et.

The $P4_32_12$ space group possesses multiple symmetry elements, the most characteristic of which is the 4-fold screw axis. Three symmetry operators will generate asymmetric units that are connected to the original (either half of the same molecule or joined by intermolecular H-bond), meaning that the crystal structure is in fact a network of hydrogen-bonded molecules of I-EtOH. The crystal packing diagrams (Fig 3.1.2(b)) indicate these two characteristic features of this crystal structure.

The complex hydrogen-bonded network and 4-fold screw axis symmetry are evident in the crystal packing when viewing in the [001] direction. However some closer examination is worthwhile, as the high order of symmetry of the tetragonal space group suggests that interesting symmetry-generated patterns of molecules can be found. To view these, we must start with a single asymmetric unit and grow each pattern singly, for if all possible symmetry generated patterns are viewed simultaneously, we observe the full packing of the system, while much of the beauty of the crystal's symmetry is hidden.

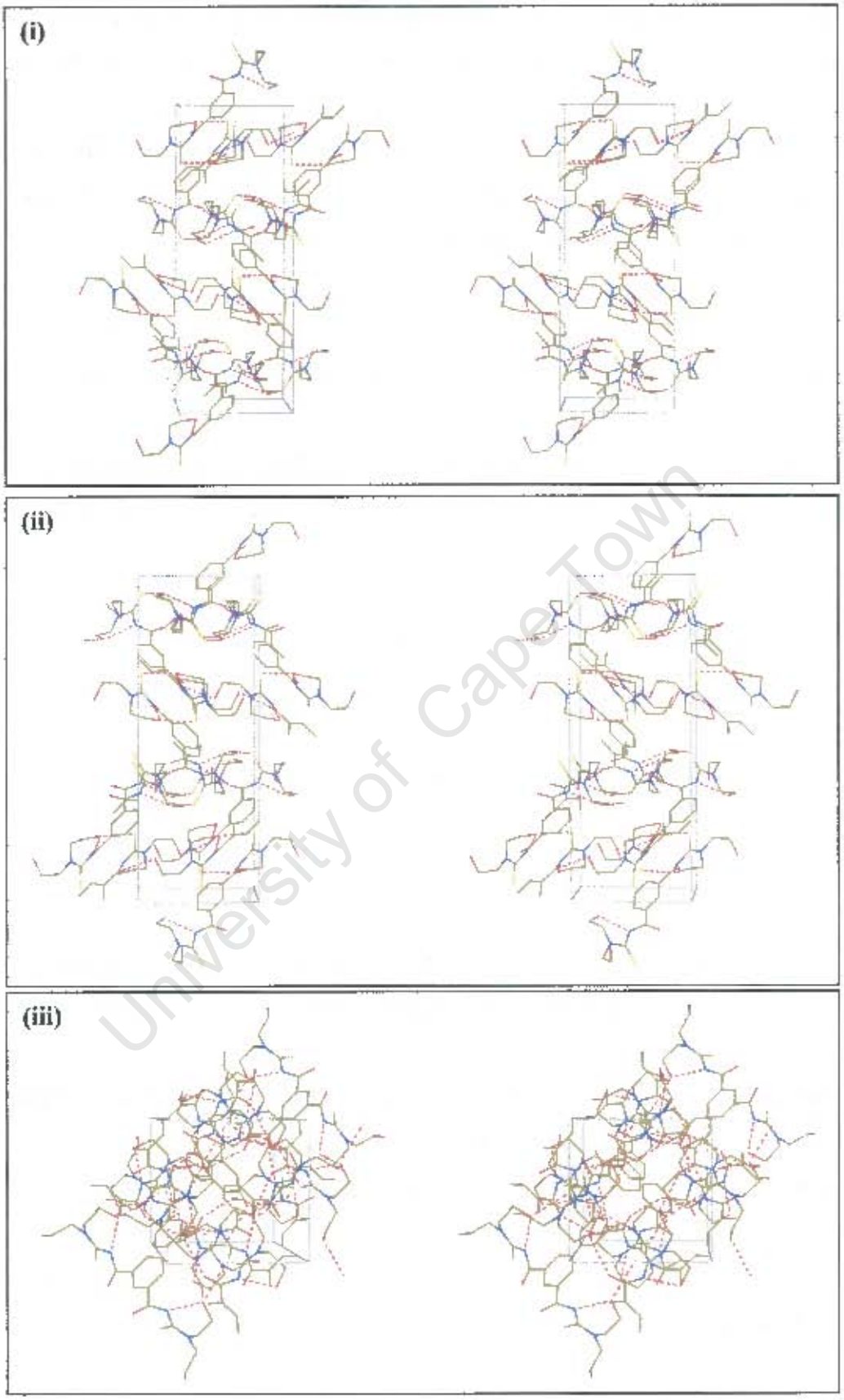

Fig. 3.1.2(b). Stereo crystal packing diagrams of I-EtOH viewed down principle directions [100] (i), [010] (ii) and [001] (iii).

Fig. 3.1.2(c) illustrates the growth of the asymmetric unit into a symmetrical pattern. Take a single asymmetric unit. It is half a molecule of I-EtOH. By 2-fold rotation symmetry, the other half of the molecule is grown. Let the original asymmetric unit be arbitrarily named A and the other B. (Of course, as these units are indistinguishable, these labels are meaningless and are only used here for the sake of convenience in description.) This is Step 1.

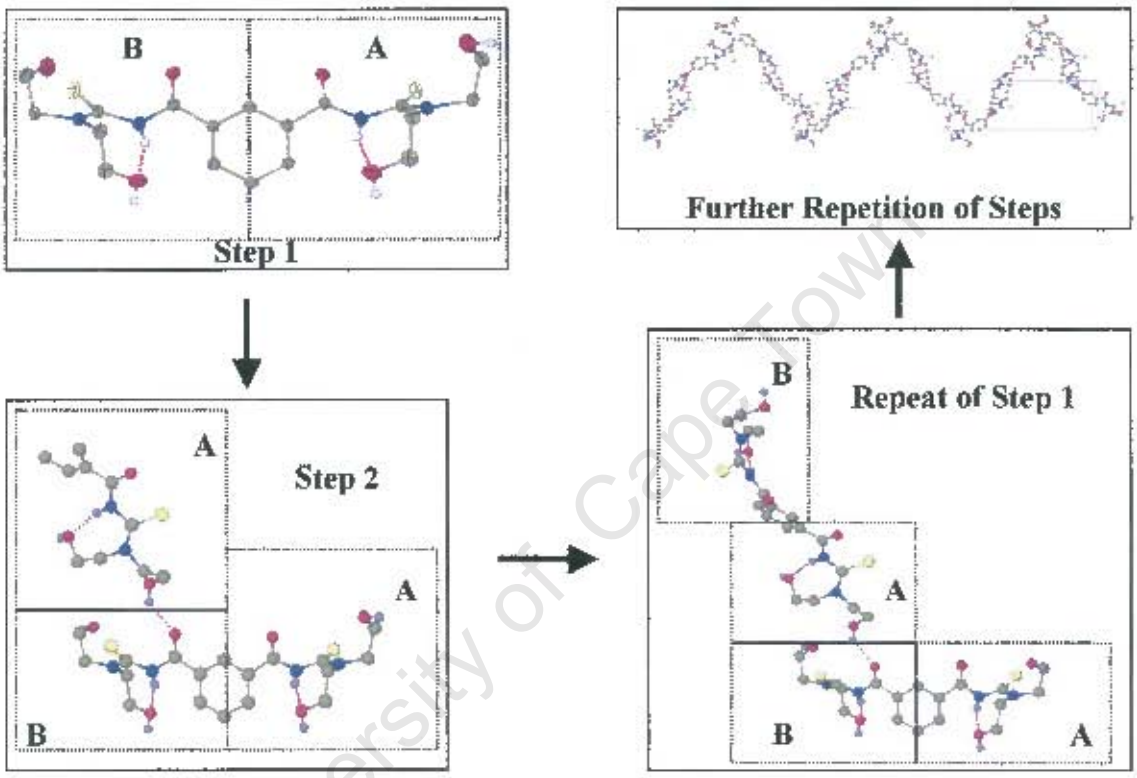

Figure 3.1.2(c). Growing O – H --- O hydrogen-bonded helical chain of I-EtOH by 4-fold screw-axis symmetry operation.

The asymmetric unit whose atom O42 is H-bonded to atom O1 of unit B is now grown by 4-fold screw axis symmetry. This newly grown unit is labelled as A. This is Step 2.

It therefore follows that this unit will be attached to another unit B to give a second complete molecule of I-EtOH (repeating Step 1).

If the process is repeated of continuously growing unit A H-bonded to the last grown unit B as in Step 2 (O42A – H42A ---- O1B), followed by growing the other half (B) of this new molecule (i.e. repeating step 1) it can be seen that the molecules of I-EtOH

are being grown by way of a 4-fold screw axis. The result is a helical H-bonded chain of molecules whose axis runs parallel to the c-axis of the unit cell. Fig. 3.1.2(d) shows this helix as viewed down each of the unit cell axes. This helix is chiral: winding anti-clockwise in the +z direction.

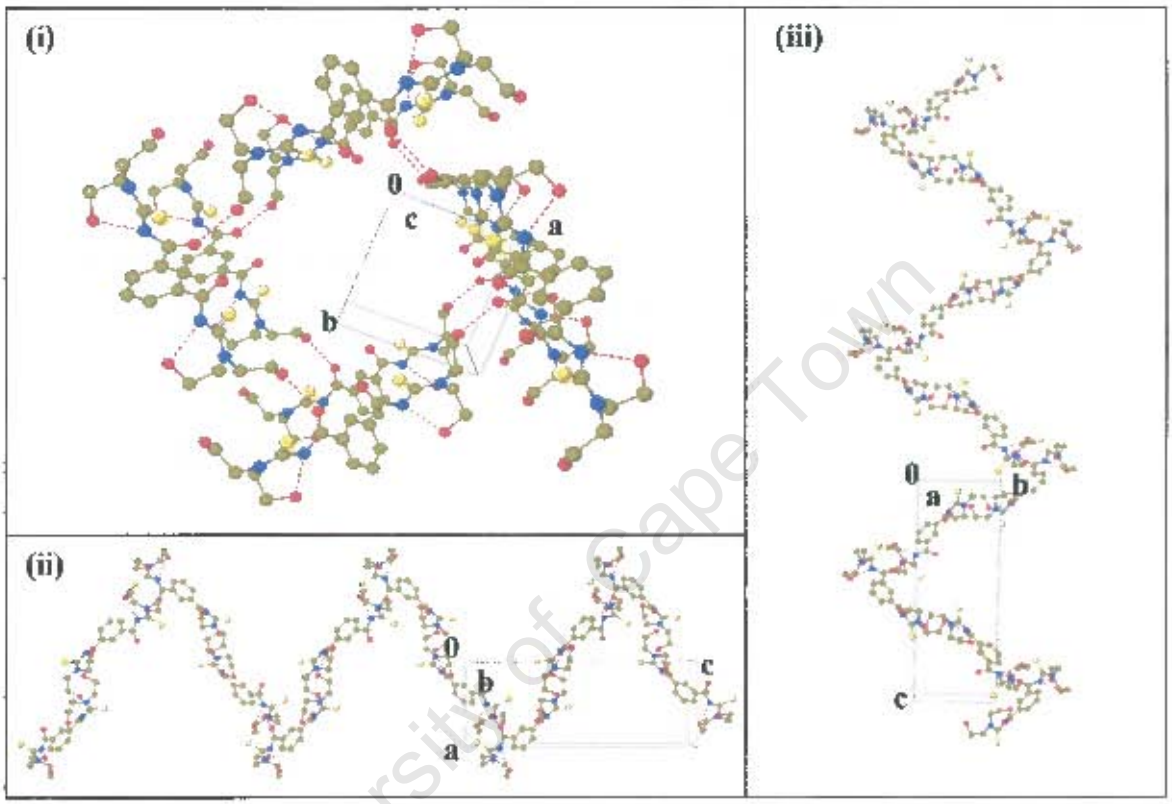

Figure 3.1.2(d). Single 4-fold helical O – H --- O hydrogen-bonded chain viewed down principle unit cell directions: [100] (i), [010], (ii) and [001] (iii). Hydrogen atoms omitted; H-bonds shown as D --- A connections.

Clearly, one could instead follow a similar process by growing the unit B whose atom O42 is H-bonded to O1 of unit A as Step 2. Then the produced result would be an identical 4-fold helix of the same chirality parallel to the c-axis, but one that is not a continuation of the helix described above. In fact, each molecule of I-EtOH is the junction of two separate, yet identical helices. This is clearly illustrated in Fig. 3.2(e), which shows two views of a molecule of I-EtOH with all four O – H --- O hydrogen bonded neighbours. These neighbours are shown in different colours. The green molecules are part of one helical chain. The blue molecules are part of another. The central molecule is part of both helices.

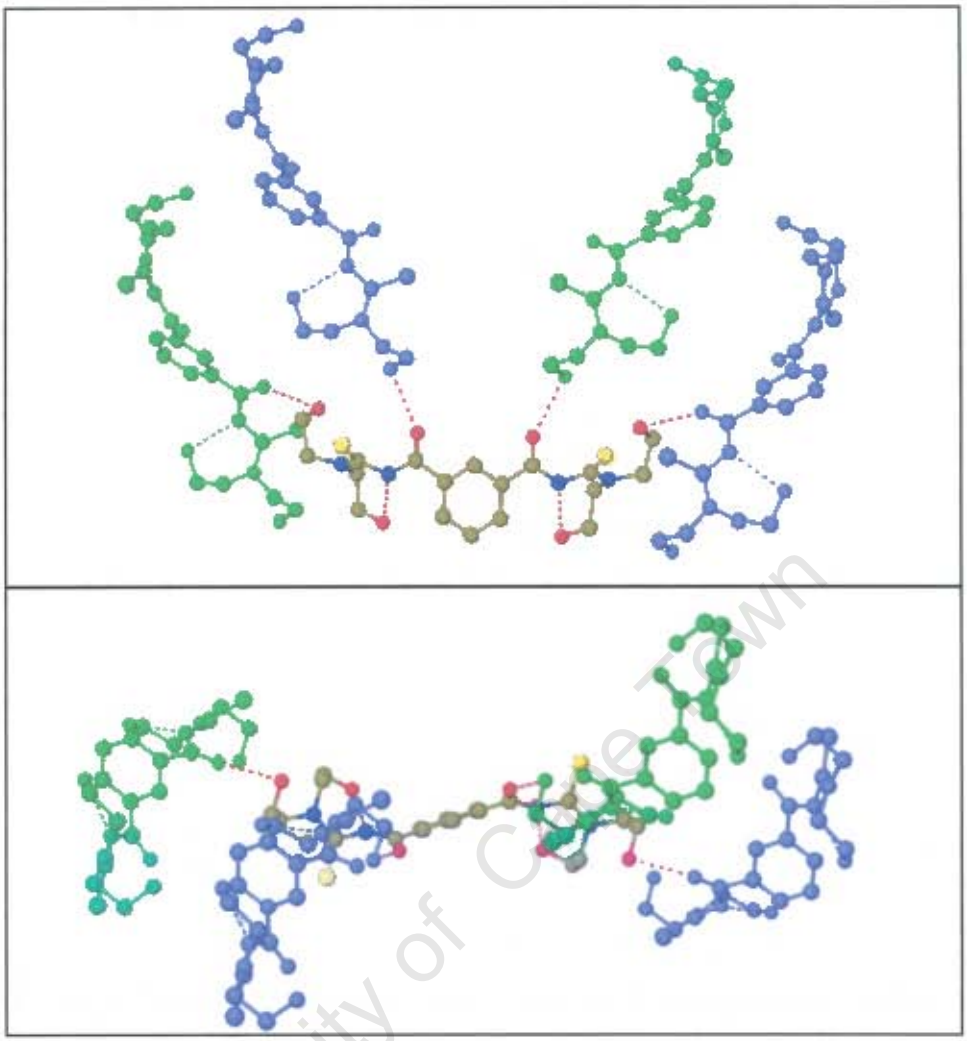

Figure 3.1.2(e). Two views of I-Et-OH molecule shown as intersection of two helical O – H --- O hydrogen-bonded chains. Hydrogen atoms omitted; H-bonds shown as D --- A connections.

By further growth of both helices, we arrive at the pattern illustrated in Fig. 3.2(f). Two helical chains share an intersecting molecule. At an interval of 4 I-EtOH molecules further along both chains, there is another junction molecule. This pattern of intersecting double helices continues parallel to the c-axis throughout the crystal. The figure is colour-coded: green and blue for molecules in separate helices, orange for molecules that are junctions of the helices.

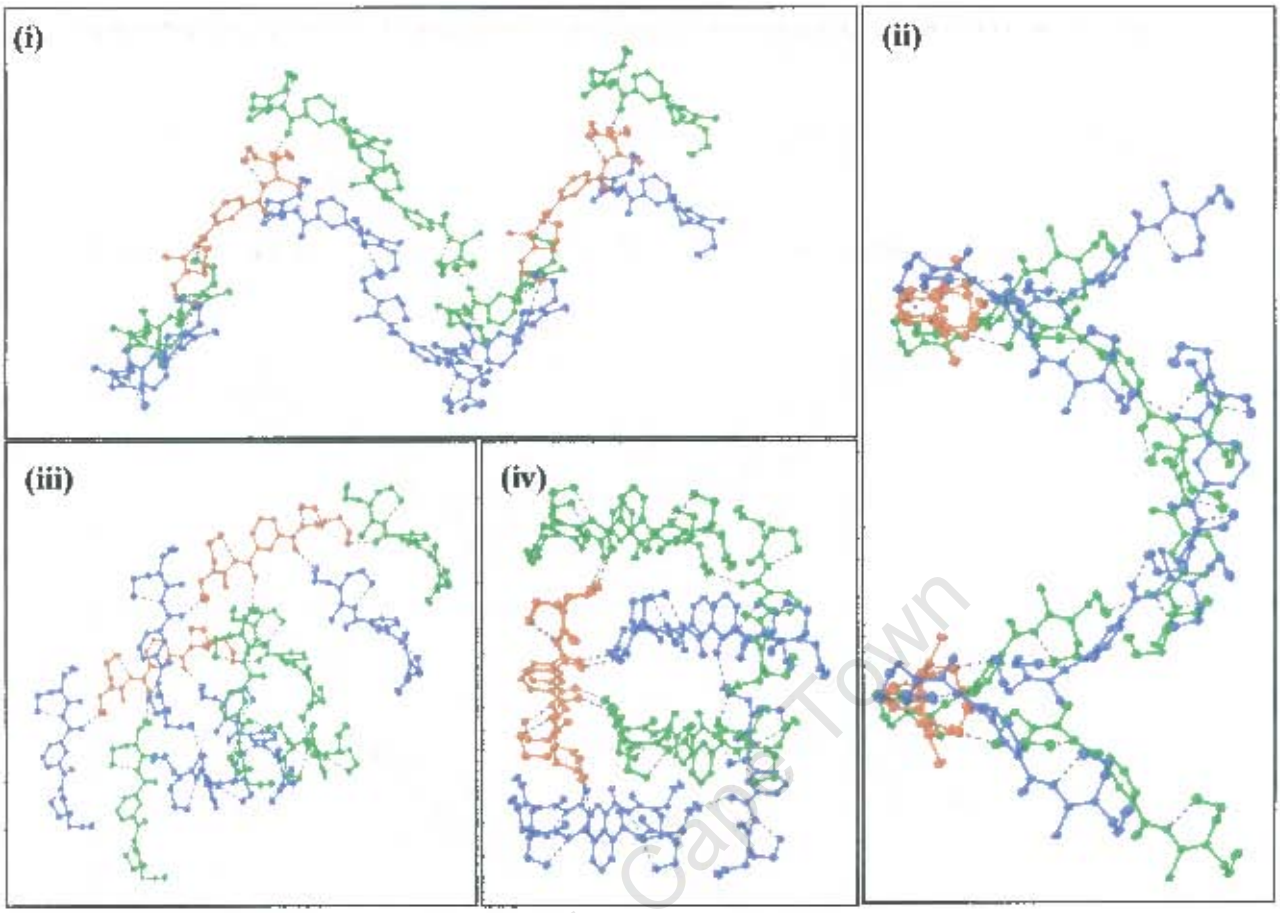

Figure 3.1.2(f). Views of intersecting O-H --- O hydrogen-bonded helical chains of I-EtOH molecules. Hydrogen atoms omitted; H-bonds shown as D --- A connections.

Even though in Fig. 3.2(f) the green and blue molecules are shown as being part of only one chain, each of these molecules is also a link in another chain not shown. The crystal structure is thus made up of a network of H-bonded molecules running in 4-fold helical chains parallel to the c-axis. These chains are all interconnected and thus the crystal structure of I-EtOH is in fact a 3D H-bonded network. Compare this with the H-bonded molecular chains in the crystal structure of I-Et, where individual chains of molecules are not interconnected and thus the crystal structure is a 1D network. Furthermore, the H-bonding capability of I-Et is lost on deprotonation of the N-H hydrogens prior to complexation. Any chelate complexes of I-Et will be incapable of hydrogen bonding. In the case of I-EtOH, the hydroxyl groups will remain intact after complexation to a metal cation. The H-bonding capability demonstrated by the uncoordinated ligand therefore mirrors the H-bonding ability that

should be available to metallamacrocycles based on I-EtOH. This will be illustrated in the crystal structure of *cis*-[Ni(I-EtOH-*S,O*)(pyridine-*N*)$_2$]$_2$ (subsection 3.3.3 below). Another way to view the crystal structure is by a similar process centred on the O44 – H44O --- S4$1 hydrogen bonds. Figure 3.1.2(g) demonstrates this process. Starting from asymmetric unit A, the other half of the I-EtOH molecule is generated (labelled unit B). The second step is to generate the asymmetric unit whose atom O44 is H-bonded to S4 of unit B. This new unit is labelled A. By repetition of steps 1 and 2, a H-bonded 4-fold helical structure is grown.

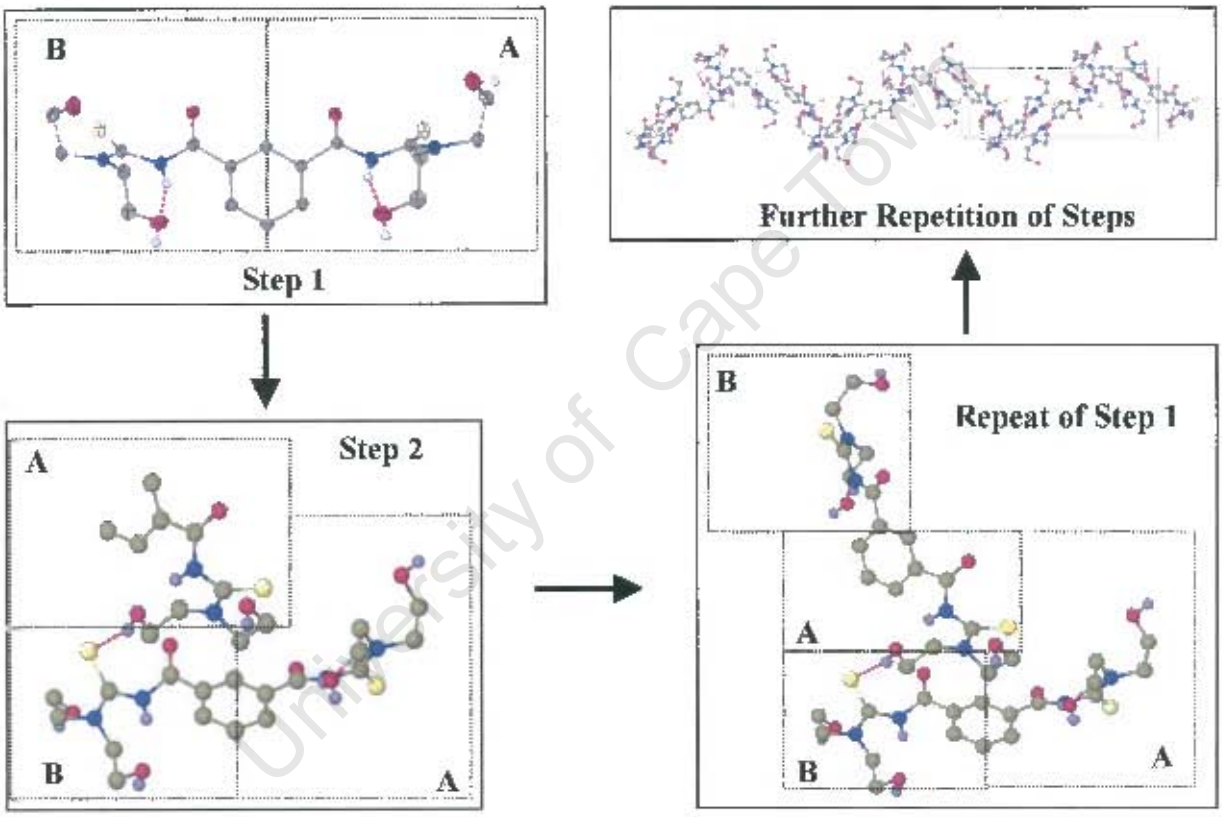

Figure 3.1.2(g). Growing O – H --- S hydrogen-bonded helical chain of I-EtOH by 4-fold screw-axis symmetry operation.

The resulting helical chain is represented in Figure 3.1.2(h). The 4-fold screw axis symmetry can clearly be seen in this diagram. The O – H --- S hydrogen bonds are found quite close to the screw-axis, thus the central 'well' around which the helix is wound is much narrower than that of the analogous O – H --- O helical pattern as shown in Figure 3.1.2(d), giving the patterns markedly different appearances.

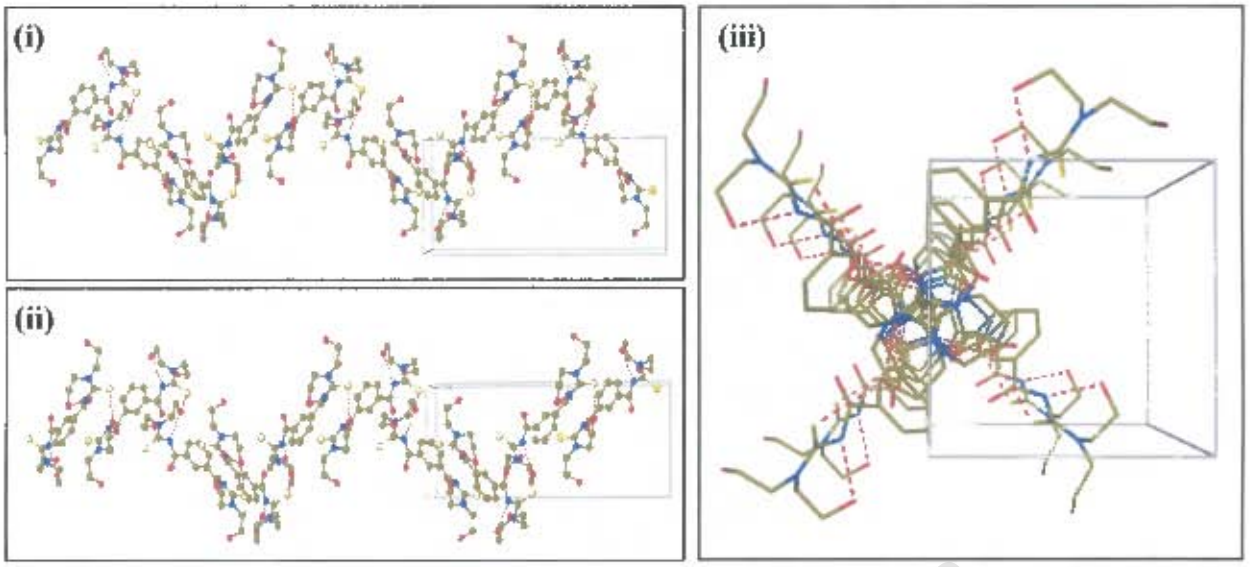

Figure 3.1.2(h). Single 4-fold helical O – H --- S hydrogen-bonded chain viewed down principle unit cell directions: [100] (i) (ball and stick), [010] (ii) (ball and stick), and [001] (iii) (stick). Hydrogen atoms omitted; H-bonds shown as D --- A connections.

As is the case for the O – H --- O helical pattern, an alternative mode of growing asymmetric units gives rise to an identical pattern, but one that is not a continuation of the same helical structure. This is done simply by growing the asymmetric unit whose S4 is H-bonded to O44 of unit B as step 2. Each molecule of I-EtOH can be seen as the junction of two O – H --- S helical structures. Figure 3.1.2(i) shows a central I-EtOH molecule and the 4 neighbouring molecules connected to it via the O44 – H44O --- S4 intermolecular hydrogen bonds. The green-coloured molecules are part of one helical pattern, while the blue-coloured molecules are part of the other. Compare this figure with Figure 3.1.2(e) above.

By further growth of both H-bonded chains, the intersecting double-helical pattern illustrated in Figure 3.1.2(j) is generated. The figure is colour-coded as in Figure 3.1.2(f) above. The junctions between the two helices occur every four molecules in either chain.

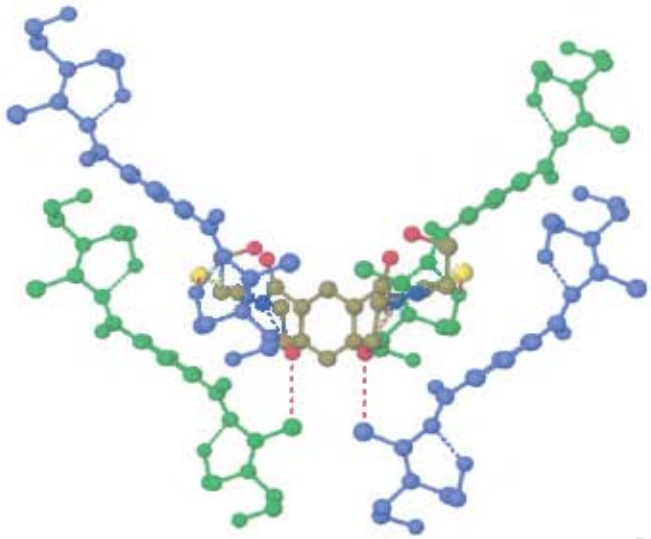

Figure 3.1.2(i). I-EtOH molecule shown as intersection of two helical O – H --- S hydrogen-bonded chains. Hydrogen atoms omitted; H-bonds shown as D --- A connections.

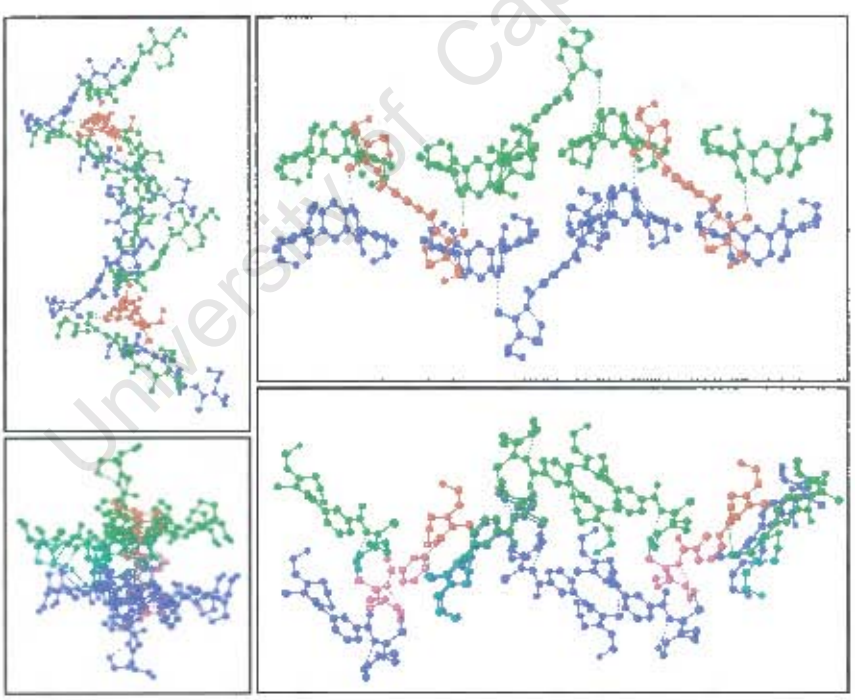

Figure 3.1.2(j). Views of intersecting O – H --- S hydrogen-bonded helical chains of I-EtOH molecules. Hydrogen atoms omitted; H-bonds shown as D --- A connections.

The packing of the I-EtOH crystal structure can be described as the superposition of the helical H-bonded chains described above. Clearly, this is a crystal structure of

great complexity, which arises from the high order of symmetry of the space group in which the compound crystallises, as well as the multiple modes of connection between asymmetric units. This contrasts with the crystal structure of the compound I-Et, in which only one mode of hydrogen bonding exists, and far fewer symmetry elements are present. The I-EtOH crystal packing also contrasts with the crystal structure of the monopodal hydroxyethyl-branched 1-benzoyl-3,3-di(2-hydroxyethyl)thiourea [98], which exhibits H-bonded 'ribbons' rather than an intricate interconnection of helices. It seems that a ligand possessing a combination of features (hydrogen bond-capable hydroxyethyl groups and a bipodal molecule) gives rise to a far more complicated type of crystal packing than the compounds that possess either one of these features alone.

The comparison between the two isophthaloyl bipodal ligands must continue as one examines the products of their complexation with nickel and the subsequent formation of octahedral adducts by the addition of pyridine. Whereas the supramolecular interactions of the complexes based on I-Et will be seen to be relatively simple, the 3D hydrogen bonded network of molecules described here for I-EtOH adumbrates the intricate supramolecular structure of the octahedral nickel complex *cis*-[Ni(I-EtOH-*S*,*O*)(pyridine-*N*)$_2$]$_2$ that is synthesised from this compound.

3.2. Metallamacrocyclic Complexes

Although a total of four metallamacrocyclic complexes were synthesised, the crystal structure of only one such compound was obtained. As a result, this section deals mainly with that particular compound – *cis*-[Ni(I-Et-*S,O*)]$_2$.

The other three metallamacrocyclic compounds were characterised by techniques such as elemental analysis or NMR spectroscopy. The results of these techniques have been reported in the Experimental Section above and confirm to a certain extent that these compounds are indeed 2:2 or 3:3 metallamacrocycles. More conclusive evidence indicating the metallamacrocyclic nature of these complexes will be given by the crystal structures of the various octahedral adducts of these complexes in Section 3.3 below.

The need to grow crystals of the metallamacrocyclic complexes in order to conclusively prove their existence is obviated if crystals of their octahedral adducts can be obtained. Because of this, and since it has proven far simpler to grow crystals of the adducts rather than the metallamacrocyclic complexes themselves, it turns out that Section 3.2 is short, where Section 3.3 is far longer and more detailed.

However, the single square planar metallamacrocyclic crystal structure described in this section is exceedingly important. Much information about the metallamacrocyclic complexes can be inferred from the crystal structures of their adducts, assuming that the metallamacrocyclic structures are not altered greatly after undergoing octahedral coordination by N-donor ligands. The hypothesis that the metallamacrocyclic structure does not vary greatly upon octahedral coordination will be employed when considering the possible outcomes of polymerisation of metallamacrocycles in Section 3.4 below.

This hypothesis is confirmed by the comparison of the square planar 2:2 metallamacrocycle *cis*-[Ni(I-Et-*S,O*)]$_2$, with its octahedral adducts *cis*-[Ni(I-Et-*S,O*)(pyridine)$_2$]$_2$ and *cis*-[Ni(1-Et-*S,O*)(DMAP)$_2$]$_2$, as will be clearly shown below.

3.2.1. *Cis*-[bis-μ-(3,3,3',3'-tetraethyl-1,1'-isophthaloylbis(thioureato-*S,O*))-di-nickel(II)] (*cis*-[Ni(I-Et-*S,O*)]$_2$)

Table 3.2.1(a). Crystal Data and Refinement Parameters for *cis*-[Ni(I-Et-*S,O*)]$_2$

Molecular Formula	$C_{36}H_{48}N_8O_4S_4Ni_2$
Formula Weight (g.mol^{-1})	902.51
Temperature (K)	173
Wavelength (Å)	0.71070
Crystal System	Triclinic
Space Group	P-1
a (Å)	8.3237(1)
b (Å)	9.6149(1)
c (Å)	12.8717(1)
α (°)	81.090(1)
β (°)	82.799(1)
γ (°)	84.601(1)
Volume (Å^3)	1006.75(2)
Z	1
Calculated Density (g.cm^{-3})	1.489
μ (mm^{-1})	1.192
F(000)	472
Crystal Size	0.30 x 0.18 x 0.15 mm
θ Range Scanned (°)	1.61 – 27.49
Index Range	$-10\leq h\leq 10$, $-12\leq k\leq 12$, $-15\leq l\leq 16$
No. Reflections Collected	8648
No. Unique Reflections	4625 [R(int) = 0.0147]
Completeness	99.8 %
Refinement Method	Full-matrix L.S. on F^2
Data / Restraints / Parameters	4625 / 0 / 248
Goodness-of-fit on F^2	1.048
Final R Indices [I>2σ(I)]	$R_1 = 0.0232$, $wR_2 = 0.0593$
R Indices (all data)	$R_1 = 0.0283$, $wR_2 = 0.0617$
Largest Diff. Peak and Hole	0.342 and -0.272 e. Å^{-3}

Single crystal diffractometry

The elucidation of the molecular structure of *cis*-[Ni(I-Et-*S,O*)]$_2$ confirms that the complex is a 2:2 metallamacrocycle (Figure 3.2.1(a)). The asymmetric unit consists of one half of a *cis*-[Ni(I-Et-*S,O*)]$_2$ molecule. The other half of the molecule is generated by a centrosymmetric operation. The complex exhibits the characteristic square planar *cis*-*S,O* chelate coordination of the acylthiourea moieties to the nickel(II) centres, although there is some deviation from ideal square planar behaviour: the *cis*- bond angles around the nickel centre all deviate from 90° (O1A – Ni1 – O1B 85.80°, O1A – Ni1 – S4A 96.15°, S4A – Ni1 – S4B 83.60° and O1B – Ni1 – S4B 94.68°) and the *trans*-bond angles across the nickel centre both deviate from 180° (O1A – Ni1 – S4B 175.47° and O1B – Ni1 – S4A 176.52°).

Furthermore, these atoms are not coplanar. The root mean square (rms) deviation of these atoms from their least squares plane is 0.0586 Å, which is significant, being an order of magnitude greater than the rms deviation of the benzoyl atoms of the same molecule from their l.s. plane (0.0051Å). The two unique 6-membered chelate rings in the compound namely O1A – C2A – N3A – C4A – S4A Ni1 – O1A and O1B – C2B – N3B – C4B – S4B – Ni1 – O1B, should in theory be planar rings. In fact, neither ring is truly planar, but it is evident that the atoms of the former chelate ring are far closer to being coplanar than those of the latter (rms deviations of 0.0433 Å and 0.1635 Å respectively). In the case of the latter, it is the atom S4B that deviates most greatly from the theoretical plane, giving this ring a 'buckled' appearance.

The entire molecule (with the exception of the ethyl branches) could also, in theory, be planar, but inspection of the atoms of the asymmetric unit (excluding hydrogen atoms and alkyl carbon atoms) for planarity reveals that these atoms have a rms deviation from the l.s. plane of 0.2201 Å. This value is reduced to 0.1419 Å by omitting the single atom S4B from the planarity calculation. Even with this omission, the calculation shows that the metallamacrocyclic ring is not completely planar. Nonetheless, the structure of *cis*-[Ni(I-Et-*S,O*)]$_2$ is quasi-planar as shown in figure 3.2.1(a(ii)).

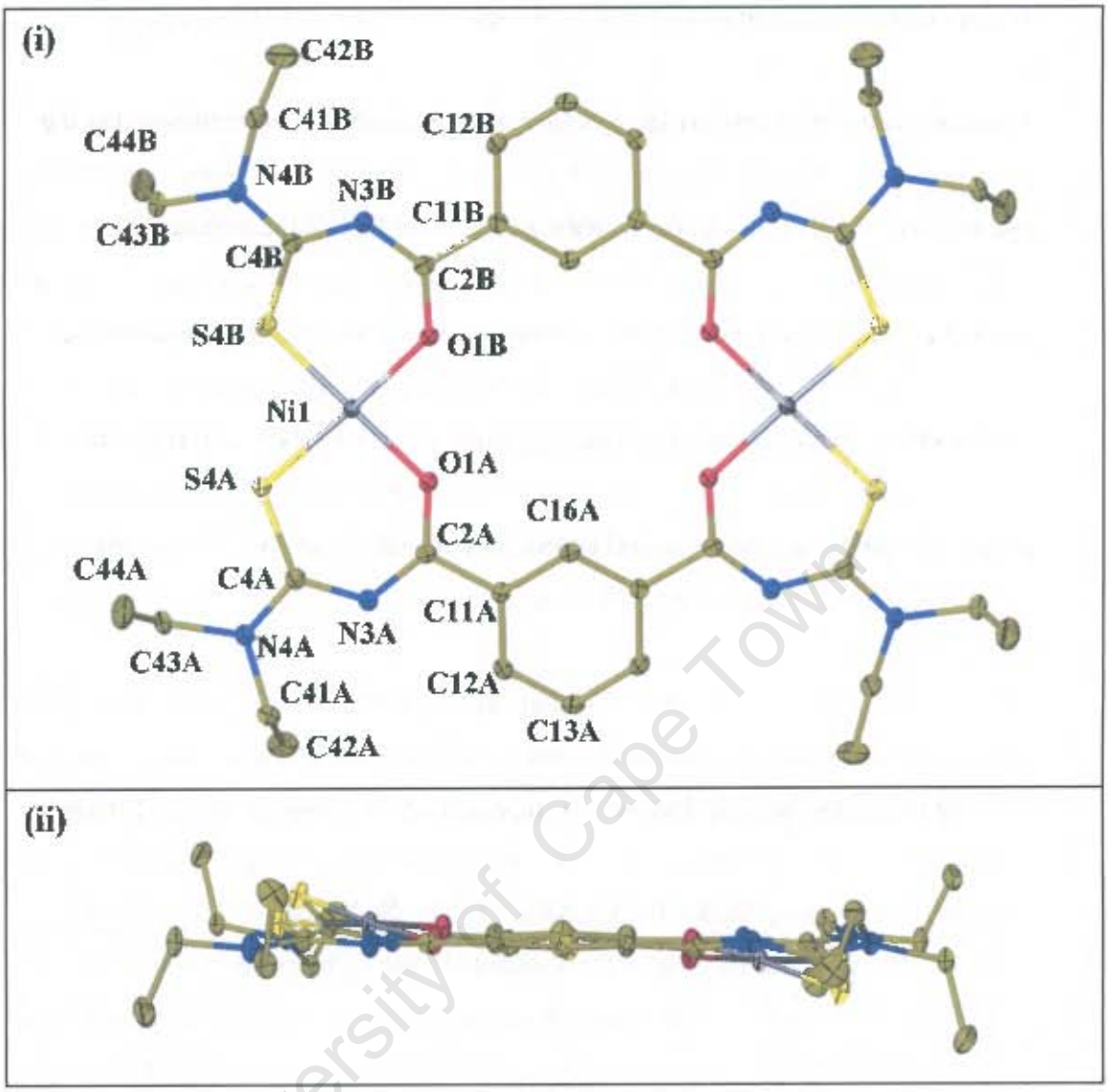

Fig. 3.2.1(a) Molecular Structure of *cis*-[Ni(I-Et-*S,O*)]$_2$ viewed from perspectives (i) normal and (ii) parallel to the benzoyl ring planes. Thermal ellipsoids drawn at 50% probability.

The important bond lengths of *cis*-[Ni(1-Et-*S,O*)]$_2$ are listed in Table 3.2.1(b). They are compared with the corresponding bond lengths of the ligand 1-Et (where applicable) as well as with those of an analogous Pd(II) metallamacrocycle,[99] the mononuclear complex bis(1-benzoyl-3,3-di(n-butyl)-thioureato) Pt(II) [16]and the mononuclear complex bis(1-benzoyl-3,3-diethylthioureato) Ni(II) [9]. The data in the table reveal that there is a significant lengthening of the carbonyl and thiocarbonyl bonds of I-Et upon complexation with a concomitant shortening of both types of C – N bond within the newly formed chelate ring. This points to a certain degree of electron delocalisation within the chelate rings. Although the table refers to the

carbonyl and thiocarbonyl bonds as C – O and C = S bonds respectively, it is important to note that these bonds have lost a significant degree of the double bond character with which they are characterised in the crystal structure of I-Et. On the other hand, the carbon – nitrogen (partially) single bonds that existed in the free ligand have now gained an even greater amount of double bond character, as evidenced by their shortening in length (with the exception of the C(S) – NR_2 bond, which lies outside of the chelate ring and has lengthened.) A prerequisite for the establishment of electron resonance within the chelate rings is the deprotonation of the N-H hydrogen atoms of I-Et, effected by the acetate ions present during the reaction. Although hydrogen atoms are not indicated in Figure 3.2.1(a), the deprotonation is confirmed by the absence of the N-H signal from the ^{1}H NMR spectrum of *cis*-[Ni(I-Et-*S,O*)]$_2$ (see the section on the characterisation of *cis*-[Ni(I-Et-*S,O*)]$_2$ in Chapter 2).

Table 3.2.1(b) Comparison of important bond lengths of *cis*-[Ni(I-Et-*S,O*)]$_2$ with corresponding bond lengths of free ligand I-Et and analogous Pd(II) metallamacrocyclic and mononuclear Ni(II) complexes

Bond	Average Bond Lengths (Å)				
	cis-[Ni(I-Et-*S,O*)]$_2$	I-Et	(*cis*-[Pd(L^2-*S,O*)]$_2$)[*99]	Bis(1-benzoyl-3,3-di(n-butyl) thioureato) Pt(II) [16]	Bis(1-benzoyl-3,3-diethyl thioureato) Ni(II) [9]
C = O	1.274(1)	1.218(4)	1.267(4)	1.261(7)	1.252(4)
C(O) – N	1.320(2)	1.381(4)	1.323(4)	1.305(6)	1.327(6)
C(S) – N(CO)	1.344(1)	1.428(4)	1.338(4)	1.343(9)	1.339(6)
C = S	1.730(6)	1.671(4)	1.740(3)	1.717(13)	1.731(4)
C(S) – NR2	1.340(1)	1.318(4)	1.346(4)	1.350(11)	1.332(7)
O – Metal	1.880(1)	–	2.028(2)	2.022(6)	1.863(3)
S – Metal	2.147(12)	–	2.433(9)	2.232(3)	2.123(2)

[*] L^2 = 3,3,3',3'-tetra(*n*-butyl-1,1'-isophthaloylbis(thiourea)

Table 3.2.1(b) also shows that the intra-ligand bond lengths are all similar to those of analogous complexes, both mononuclear and metallamacrocyclic – although it should be noted that some of the bonds in the Pt(II) complex (namely the thiocarbonyl bond and the C(O) – N bond) are significantly shorter than the analogous bonds in the other complexes. The O – Ni and S – Ni bonds of *cis*-[Ni(I-Et-*S,O*)]$_2$ are shorter than the corresponding bonds of the palladium(II) metallamacrocycle and the platinum(II) mononuclear complex (which is of course to be expected owing to the greater atomic radii of palladium and platinum), and are comparable in length to the corresponding bonds in the mononuclear complex bis(3,3-diethyl-1-benzoylthioureato) Ni(II).

The molecular structure shown in Figure 3.2.1(a) possesses a central cavity. This feature of the structure could be of interest in that it suggests the possibility that *cis*-[Ni(I-Et-*S,O*)]$_2$ is a porous or channel-type material. However this representation is misleading. The internuclear distances between identical atoms across the centre of symmetry (and thus across the cavity) of the complex are as follows: Ni1 – Ni1 7.673Å, C16A – C16A 5.153Å, O1A – O1A 5.603Å and O1B – O1B 5.500Å. However if one takes into account the van der Waals radii of each type of atom, it can be shown that the central cavity is far too small to admit any atoms or ions. Figure 3.2.1(b) is a space-filling depiction of the complex *cis*-[Ni(I-Et-*S,O*)]$_2$. In this figure, it is clear that there is no possibility of pores or channels of sufficient size to permit the trapping or transportation of particles.

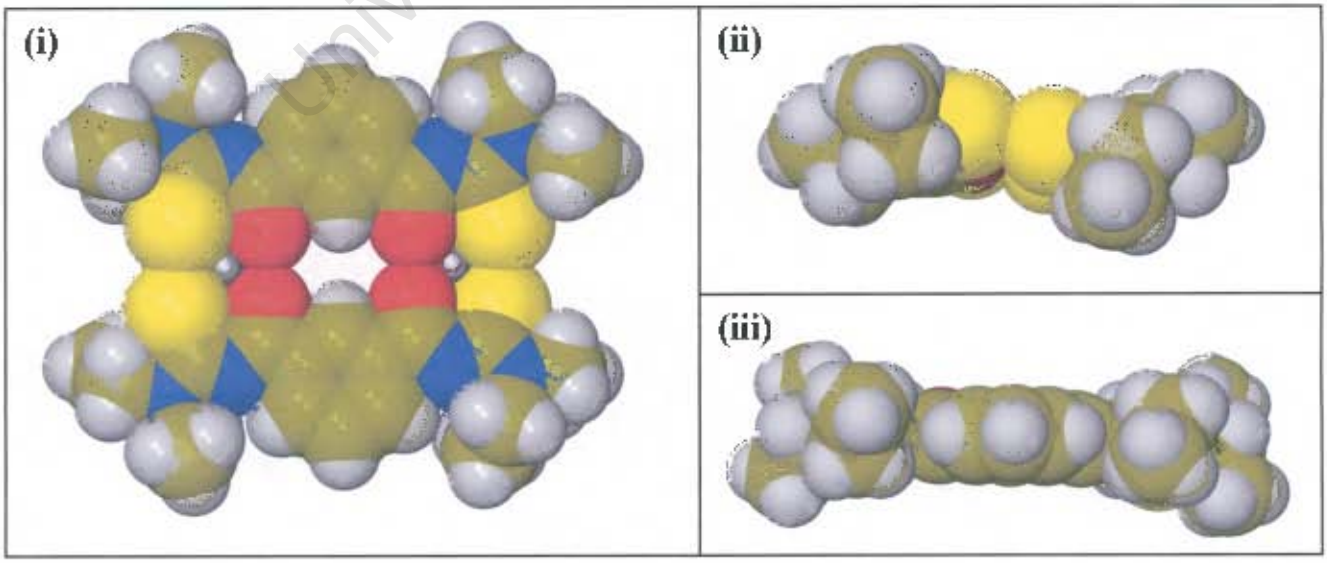

Fig. 3.2.1(b). Space fill representations of the 2:2 metallamacrocycle *cis*-[Ni(I-Et-*S,O*)]$_2$: viewed (i) normal to the face of the molecule and viewed (ii), (iii) edge-on.

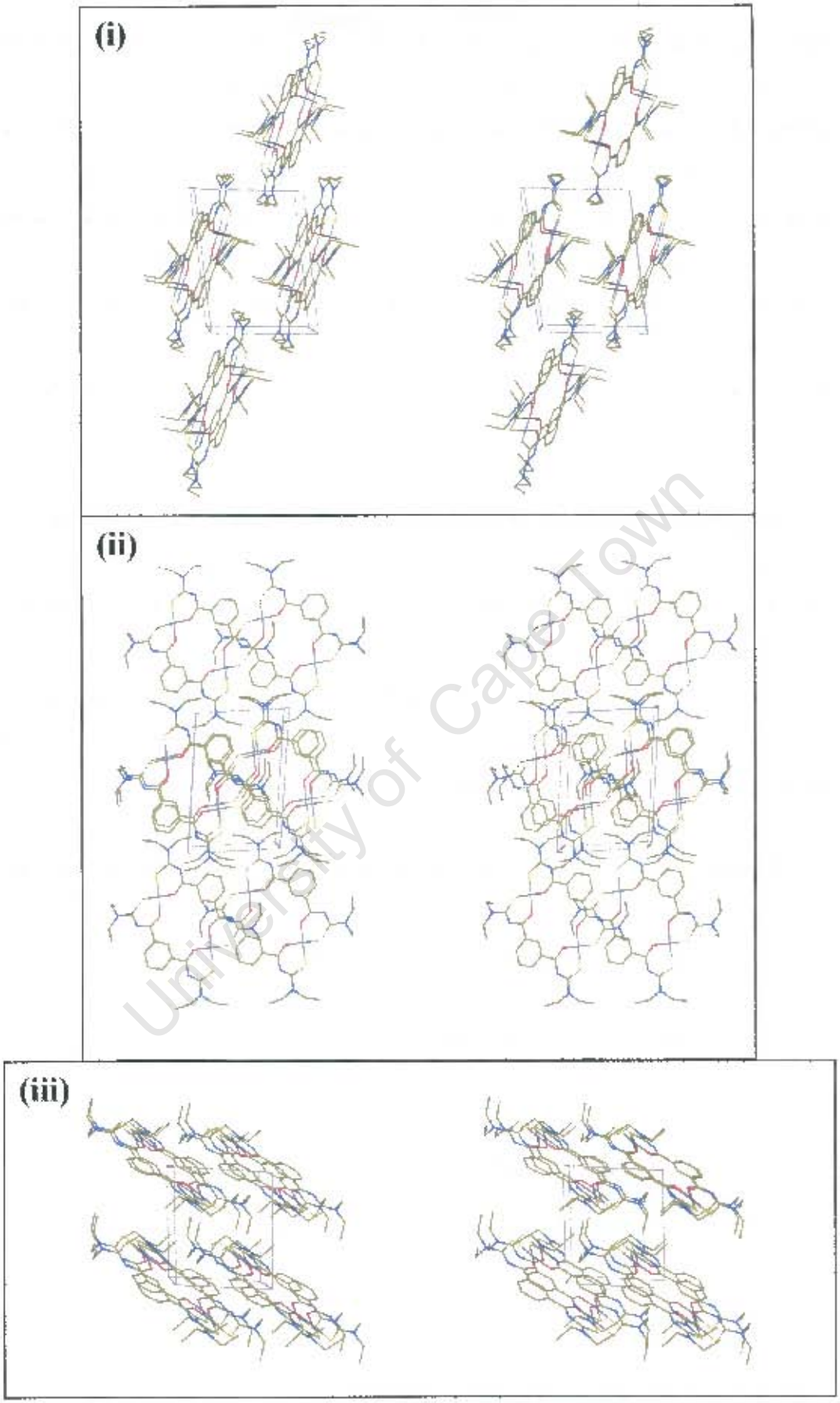

Fig. 3.2.1(c). Stereo crystal packing diagrams of *cis*-[Ni(I-Et-*S,O*)]$_2$ viewed down principle directions [100] (i), [010] (ii) and [001] (iii).

The crystal packing of *cis*-[Ni(I-Et-*S,O*)]$_2$ is depicted in Figure 3.2.1(c). The centres of symmetry in the unit cell transform each half of a molecule into the other half. The low symmetry of the P-1 space group is evidenced by the fact that each molecule of *cis*-[Ni(I-Et-*S,O*)]$_2$ in the crystal is generated by translation operations only. The repetition of a molecule occurs at intervals of one unit cell length in each of the axial directions. As a result, the molecules are all in parallel orientations. The packing diagrams reveal one important feature of the crystal structure: the presence of an intermolecular π-π interaction. A better perspective for viewing this feature is given in Figure 3.2.1(d).

One benzoyl ring of a *cis*-[Ni(I-Et-*S,O*)]$_2$ molecule associates with the six-membered chelate ring: Ni1B – O1B – C2B – N3B – C4B – S4B of the adjacent molecule generated by a translation of one unit cell length in the [100] direction (i.e. (x + 1, y, z)), while the specified chelate ring of the former molecule, associates with a benzoyl ring of the latter. This interaction causes the complex molecules to form offset stacks running in the [100] direction. This finding is consistent with the prediction of the theoretical study by Hunter and Sanders[106] that an offset cofacial interaction will be more stable than a fully superimposed interaction.

The distance between the centroids of associated rings is found to be 3.804Å. This value, as well as the offset parallel orientation agree with the trend observed by Janiak for π-π interactions[105]. A similar type of interaction was found for the previously reported Pt(II) metallamacrocycle synthesised with the same ligand (I-Et),[41] although in that publication it was not explicitly described as a π-π interaction.

The 2:2 metallamacrocyclic complex *cis*-[Ni(I-Et-*S,O*)]$_2$ displays marked similarity to its previously reported Pd(II) and Pt(II) analogues[99, 41] in terms of their molecular structural features such as bond lengths and deviations from ideal square planar configuration about the metal centre. It should perhaps be mentioned that this finding is not as straightforward as it would seem. No prior reports of the successful synthesis of such a 2:2 Ni(II) complex were to be found in the literature and it is believed that this project is the first to demonstrate that the pre-programmed conditions for self-assembly of the 2:2 Ni(II) metallamacrocycle are present in this system, hence the

trend observed from the synthesis of 2:2 Pd and Pt metallamacrocycles is now confirmed by the characterisation of the corresponding Ni complex.

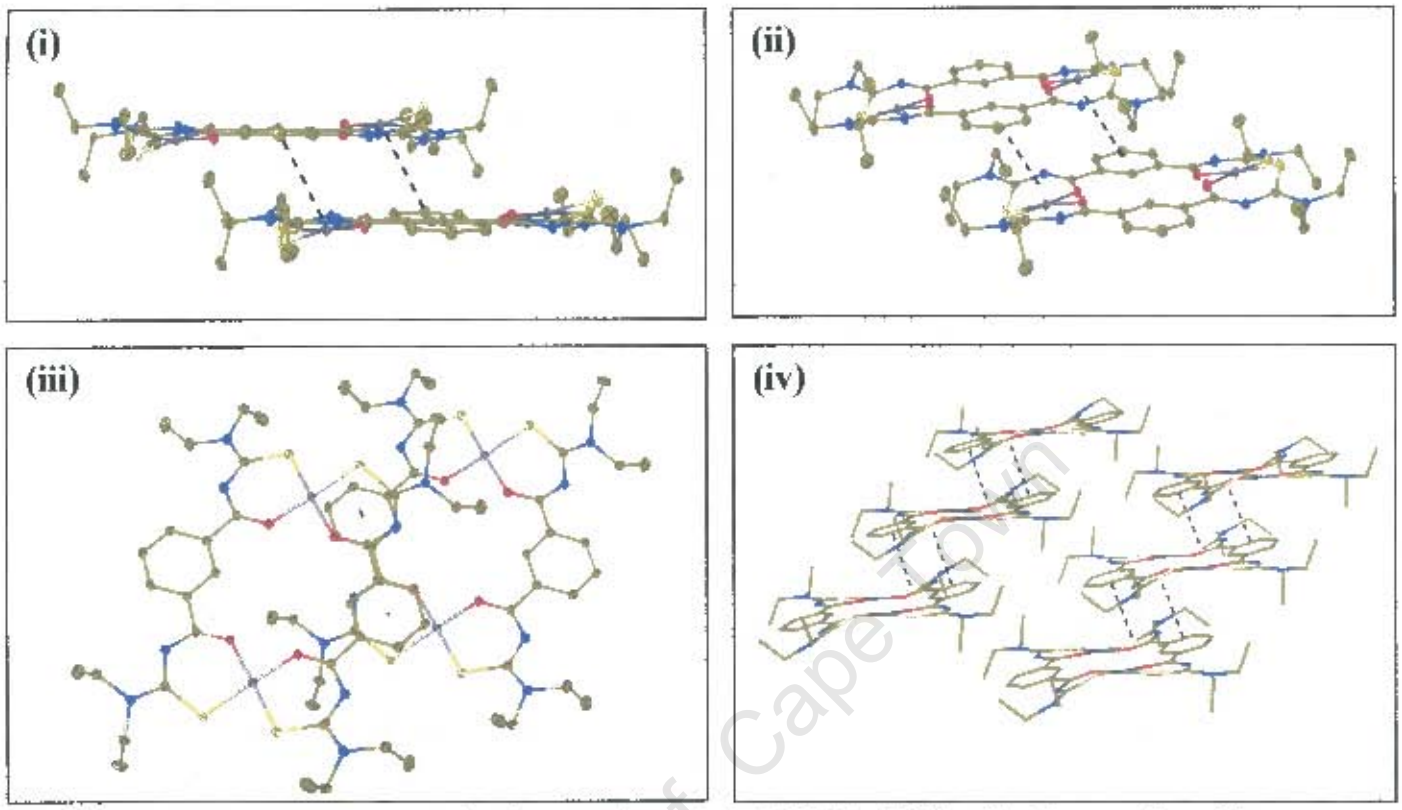

Fig 3.2.1(d). π-π stacking interactions of *cis*-[Ni(I-Et-*S,O*)]$_2$: (i) edge-on view, (ii) oblique view, (iii) face-on view and (iv) view of parallel molecular stacks. Dashed lines join centroids of associated ring moieties.

The similarities between the crystal packing modes of the nickel(II), palladium(II) and platinum(II) metallamacrocycles are also worthy of note. The main difference between *cis*-[Ni(I-Et-*S,O*)]$_2$ and the preceding PGM analogues is its ability to be transformed from a square planar complex into an octahedral complex via the simple addition of electron donor ligands. The platinum(II) metallamacrocycle has been shown to undergo a similar transformation, although this requires the additional complication of oxidising the platinum(II) to platinum(IV) [107].

The ease with which the nickel-based metallamacrocycle accepts ligands into the nickel atoms' axial coordination sites makes this complex ideal as an intermediate in the assembly of new supramolecular architectures.

3.3 Octahedral Adducts of Metallamacrocycles

On addition of pyridine or some of its derivatives, the metallamacrocycle *cis*-[Ni(1-Et-*S,O*)]$_2$ undergoes a rapid and visually striking colour change from purple to bright green. This is an indication that the pyridines act as donor ligands. Attempts to co-ordinate 2,6-dimethylpyridine to the complex *cis*-[Ni(1-Et-*S,O*)]$_2$ produced no colour change, indicating that no octahedral co-ordination takes place. This effect is certainly due to the steric crowding of the methyl moieties around the nitrogen atom, preventing the donation of the nitrogen's lone pair of electrons to the nickel metal centre. In the cases of sterically unhindered pyridines, the resultant green colour of the solution strongly suggests that octahedral co-ordination via the nitrogen atom is occurring.

There are certain broad predictions that can be made regarding the crystal structures of these adducts. It is expected that solvent molecules may be included in the unit cells of such complexes by virtue of weak van der Waals interactions. Hydrogen bonding ability incorporated into the design of an octahedral adduct could allow a honing of this prediction inasmuch as one might expect a H-bond accepting solvent molecule to be located around an H-bond donor moiety within the accepted limits of D – H --- A radii. Experimental techniques must be utilised to confirm (or contradict) these suggestions. The most powerful tool at our disposal is single-crystal x-ray diffractometry. The obtaining of high-quality single crystals is often quite challenging and various techniques to do so were employed for these adducts. They were not always successful. In the case of *cis*-[Ni(T-EtOH-*S,O*)(pyridine-*N*)$_2$]$_3$, even the obtaining of a solid powder was not achieved, thus excluding the use, in that case, of the other powerful characterising technique at our disposal – thermal analysis. TGA was utilised to determine the contents of the crystal structures of the other octahedral adducts.

The data obtained from the structural elucidation of *cis*-[Ni(1-Et-*S,O*)(pyridine-*N*)$_2$]$_2$, *cis*-[Ni(1-Et-*S,O*)(DMAP-*N*)$_2$]$_2$ and *cis*-[Ni(1-EtOH-*S,O*)(pyridine-*N*)$_2$]$_2$ require direct numerical comparison. For convenience in this regard, the bond lengths, bond angles and regional planarities of these complexes are tabulated together and reported prior

to the subsections (3.3.1 – 3.3.3) devoted to each of the compounds individually. References are made back to these tables throughout the two subsections. These tables also contain data pertaining to *cis*-[Ni(I-Et-*S,O*)]$_2$, the parent complex of *cis*-[Ni(I-Et-*S,O*)(pyridine-*N*)$_2$]$_2$ and *cis*-[Ni(I-Et-*S,O*)(DMAP-*N*)$_2$]$_2$.

Table 3.3(a) Comparison of important bond lengths of octahedral adducts *cis*-[Ni(I-Et-*S,O*)(pyridine-*N*)$_2$]$_2$, *cis*-[Ni(I-Et-*S,O*)(DMAP-*N*)$_2$]$_2$ and *cis*-[Ni(I-EtOH-*S,O*)(pyridine-*N*)$_2$]$_2$ and of parent 2:2 metallamacrocycle *cis*-[Ni(I-Et-*S,O*)]$_2$ (where applicable)

Bond Type	Average Bond Lengths (Å)			
	cis-[Ni(I-Et-*S,O*)]$_2$	*cis*-[Ni(I-Et-*S,O*)(pyridine-*N*)$_2$]$_2$	*cis*-[Ni(I-Et-*S,O*)(DMAP-*N*)$_2$]$_2$	*cis*-[Ni(I-EtOH-*S,O*)(pyridine-*N*)$_2$]$_2$
C=O	1.274(1)	1.265(2)	1.252(9)	1.250(4)
C(O)–N	1.320(2)	1.338(8)	1.336(9)	1.335(5)
C(S)–N(CO)	1.344(1)	1.34(1)	1.344(6)	1.346(4)
C=S	1.730(6)	1.727(8)	1.727(8)	1.723(2)
C(S)–NR2	1.340(1)	1.353(1)	1.35(1)	1.352(2)
O – Ni	1.880(1)	2.06(1)	2.043(2)	2.030(2)
S – Ni	2.15(1)	2.38(2)	2.40(2)	2.40(2)
N – Ni	-	2.14(1)	2.118(7)	2.132(1)

Table 3.3(b) List of Ni(II) bond angles of *cis*-[Ni(I-Et-*S,O*)]$_2$, and 2:2 octahedral adducts

Bonds	Bond Angles (°)			
	cis-[Ni(I-Et-*S,O*)]$_2$	*cis*-[Ni(I-Et-*S,O*)(pyridine-*N*)$_2$]$_2$	*cis*-[Ni(I-Et-*S,O*)(DMAP-*N*)$_2$]$_2$	*cis*-[Ni(I-EtOH-*S,O*)(pyridine-*N*)$_2$]$_2$
	cis- Angles (°)			
O1A – Ni1 – O1B	85.80	93.09	89.59	88.15
O1A – Ni1 – S4A	96.15	90.91	91.64	89.41
O1B – Ni1 – S4B	94.68	89.08	88.69	89.97
S4A – Ni1 – S4B	83.60	87.01	90.03	92.48
N5A – Ni1 – O1A	-	84.00	88.54	85.83
N5A – Ni1 – O1B	-	85.20	85.79	86.93
N5B – Ni1 – O1A	-	87.40	87.27	86.89
N5B – Ni1 – O1B	-	85.85	85.70	86.82
N5A – Ni1 – S4A	-	96.97	95.68	93.18
N5A – Ni1 – S4B	-	93.20	93.08	92.72
N5B – Ni1 – S4A	-	84.00	92.92	92.77
N5B – Ni1 – S4B	-	95.76	90.86	94.35
	Trans- Angles (°)			
O1A – Ni1 – S4B	175.47	176.29	177.55	177.68
O1B – Ni1 – S4A	176.52	175.63	178.10	177.55
N5A – Ni1 – N5B	-	167.22	170.54	170.55

Table 3.3(c) List of regional planarities for *cis*-[Ni(I-Et-*S,O*)]$_2$, and 2:2 adducts

Atoms in Plane	Root Mean Square Deviation from Planarity (Å)			
	cis-[Ni(I-Et-*S,O*)]$_2$	*cis*-[Ni(I-Et-*S,O*)(pyridine-*N*)$_2$]$_2$	*cis*-[Ni(I-Et-*S,O*)(DMAP-*N*)$_2$]$_2$	*cis*-[Ni(I-EtOH-*S,O*)(pyridine-*N*)$_2$]$_2$
O1A, C2A, N3A, C4A, S4A, Ni1	0.0432	0.1454	0.0866	0.2413
O1B, C2B, N3B, C4B, S4B, Ni1	0.1632	0.2208	0.2587	0.2233
Ni1, O1A, O1B, S4A, S4B	0.0581	0.0423	0.0127	0.0143
Benzoyl Ring Carbons	0.0055	0.0069	0.0046	0.0152

3.3.1. [*Cis*-(bis-μ-(3,3,3',3'-tetraethyl-1,1'-isophthaloylbis(thioureato-*S,O*))-di-nickel(II))-tetra(pyridine-*N*)] (*cis*-[Ni(I-Et-*S,O*)(pyridine-*N*)$_2$]$_2$)

Thermal Analysis

Fairly large green crystals grown from a solution of *cis*-[Ni(I-Et-*S,O*)]$_2$ in pyridine / acetone (by solvent cross-diffusion in an evacuated desiccator) were subjected to TGA. Figure 3.3.1(a) shows the results of this experiment. A mass loss of 25.49 % is indicated in the temperature range 54 – 139 °C. A further loss of 9.50 % is recorded, ending at 162 °C, after which no further significant mass loss is observed. Since this compound has been shown to revert back to the metallamacrocycle *cis*-[Ni(I-Et-*S,O*)]$_2$ at room temperature (see Experimental Section 2.3.1.), it is logical to take this as the end product of the thermal decomposition of *cis*-[Ni(I-Et-*S,O*)(pyridine-*N*)$_2$]$_2$ at higher temperatures. The melting point of *cis*-[Ni(I-Et-*S,O*)]$_2$ (310 – 313 °C) is much higher than 139 °C. Thus the remaining 64.96 % mass is attributed to this compound, since other possible components of the green crystals (namely pyridine and acetone) are too volatile to be retained in the residue at this temperature. Table 3.3.1(a) shows the results derived from this TGA.

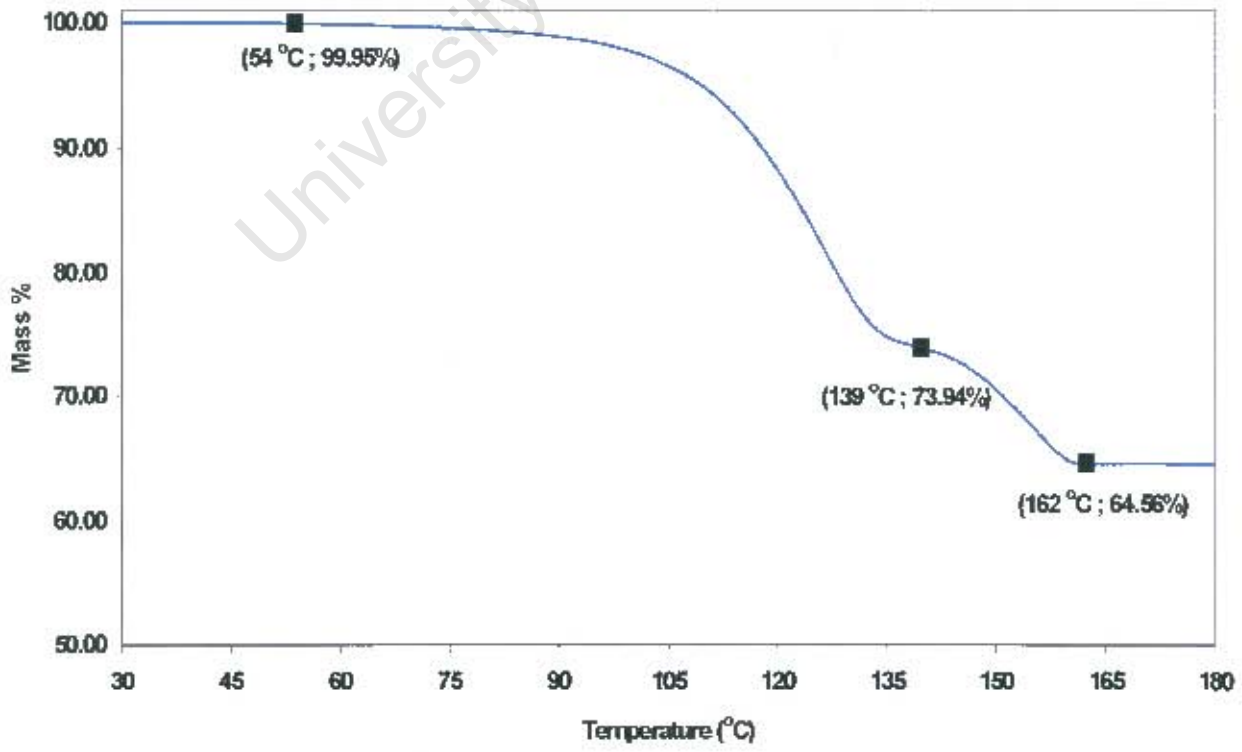

Figure 3.3.1(a) Graph of TGA results for *cis*-[Ni(I-Et-*S,O*)(pyridine-*N*)$_2$]$_2$.

Table 3.3.1(a) TGA Calculations of Mass Losses for *cis*-[Ni(I-Et-*S,O*)(pyridine-*N*)$_2$]$_2$

Reaction	Temp. Range (°C)	Experimental Mass Loss (%)	Calculated Mass Loss (%)
cis-[Ni(I-Et-*S,O*)(pyridine-*N*)$_2$]$_2$.2Py			
↓	54 – 139	25.49	22.98 (4 Py)
↓	139 – 162	9.50	11.49 (2 Py)
cis-[Ni(I-Et-*S,O*)]$_2$	Total (30 – 180)	34.99	34.47 (6 Py)

The first thermal event represents more than 4 pyridines, while the second represents fewer than 2. From this we may conclude that there are 2 pyridine guest molecules per complex molecule within the crystal. However, the decomposition of the crystal does not proceed – as might be expected – with the loss of the two guest molecules, followed by the loss of the co-ordinated (and thus more strongly bound) pyridines. Rather, it seems that the decomposition follows some other process.

TGA has given us some insight into the nature of the compound. It seems that the crystal structure consists of *cis*-[Ni(I-Et-*S,O*)(pyridine-*N*)$_2$]$_2$ with 2 pyridine guests i.e. it is of the form *cis*-[Ni(I-Et-*S,O*)(Pyridine)$_2$]$_2$.2(Pyridine).

Single crystal diffractometry

Table 3.3.1(b). Crystal Data and Refinement Parameters for *cis*-[Ni(I-Et-*S,O*)(pyridine-*N*)$_2$]$_2$. 2(pyridine)

Molecular Formula	$C_{56}H_{68}N_{12}O_4S_4Ni_2$. $2(C_5H_5N)$
Formula Weight (g.mol^{-1})	1377.08
Temperature (K)	173
Wavelength (Å)	0.71070
Crystal System	Monoclinic
Space Group	$P2_1/n$
a (Å)	9.51(1)
b (Å)	18.18(2)
c (Å)	19.74(2)
$\alpha = \gamma$ (°)	90
β (°)	94.269(5)
Volume (Å^3)	3402(6)
Z	2
Calculated Density (g.cm^{-3})	1.344
μ (mm^{-1})	0.734
F(000)	1448
Crystal Size	0.27 x 0.35 x 0.22 mm
θ Range Scanned (°)	2.45 – 27.43
Index Range	$-9 \leq h \leq 10$, $-23 \leq k \leq 23$, $-15 \leq l \leq 25$
No. Reflections Collected	12929
No. Unique Reflections	6214 [R(int) = 0.0453]
Completeness	83.1 %
Refinement Method	Full-matrix L.S. on F^2
Data / Restraints / Rarameters	6214 / 0 / 391
Goodness-of-fit on F^2	1.038
Final R Indices [I>2σ(1)]	$R_1 = 0.0548$, $wR_2 = 0.1404$
R Indices (all data)	$R_1 = 0.0831$, $wR_2 = 0.1567$
Largest Diff. Peak and Hole	0.951 and -0.567 e. Å^{-3}

The molecular structure of the octahedral metallamacrocyclic complex *cis*-[Ni(I-Et-*S,O*)(pyridine-*N*)$_2$]$_2$ is shown in Figure 3.3.1(b). The complex crystallises in the centrosymmetric space group $P2_1/n$. Consequently, the asymmetric unit consists of one half of the complex molecule, with an associated guest molecule. The complex is easily seen to be an adduct of the 2:2 metallamacrocycle *cis*-[Ni(I-Et-*S,O*)]$_2$; the one major chemical change undergone by the complex is the addition of pyridine molecules to each of the octahedral coordination sites of the nickel(II) centres. The presence of two pyridine guest molecules associated with each *cis*-[Ni(I-Et-*S,O*)(pyridine-*N*)$_2$]$_2$ molecule confirms the stoichiometric calculations that were made based upon thermogravimetric analysis data. The complex is indeed of the form *cis*-[Ni(I-Et-*S,O*)(pyridine)$_2$]$_2$.2 pyridine.

The axial addition of pyridine alters the nature of the compound drastically: at the molecular level and consequently at the macroscopic level. The change in electronic configuration at the Ni(II) centres from the 16-electron diamagnetic square planar system to a 20-electron paramagnetic octahedral system is manifested by a transition in the UV-visible absorption spectrum of the complex (qualitatively observed in the characteristic purple to green colour change) and a change in the magnetic properties of the complex. Although no magnetic susceptibility studies were conducted, the onset of paramagnetism is qualitatively confirmed by very large shifts in the NMR spectrum of the octahedral complex.

Another prominent feature in the molecular structure is the disorder of the terminal CH_3 group of one of the ethyl moieties. The disordered carbon is modelled as C44A and C45A with site occupancies of 53% and 47% respectively.

The unbound pyridine molecule in the asymmetric unit is shown with the nitrogen atom occupying a specific position in the ring. However, the refinement parameters obtained when the structure is refined with this particular site occupancy in the guest are only marginally better than those obtained for other possible occupancies, which is perhaps to be expected in view of the similar electron densities of C and N atoms. The possibility of slight disorder for the unbound pyridines in this structure could result from varying positions of the nitrogen atom in the ring from one asymmetric unit to the next. The true locations of the pyridinyl hydrogens would signal the

location of the nitrogen, but these cannot be determined owing to the very large thermal parameters of the guest molecule's atoms, which translate as a fine positional disorder or 'blurring' of the atoms in the guest molecule, regardless of whether the gross positions of individual atoms are disordered or not. This increased uncertainty in the positions of the guest atoms renders anisotropic modelling of these atoms meaningless, hence their isotropic thermal ellipsoids.

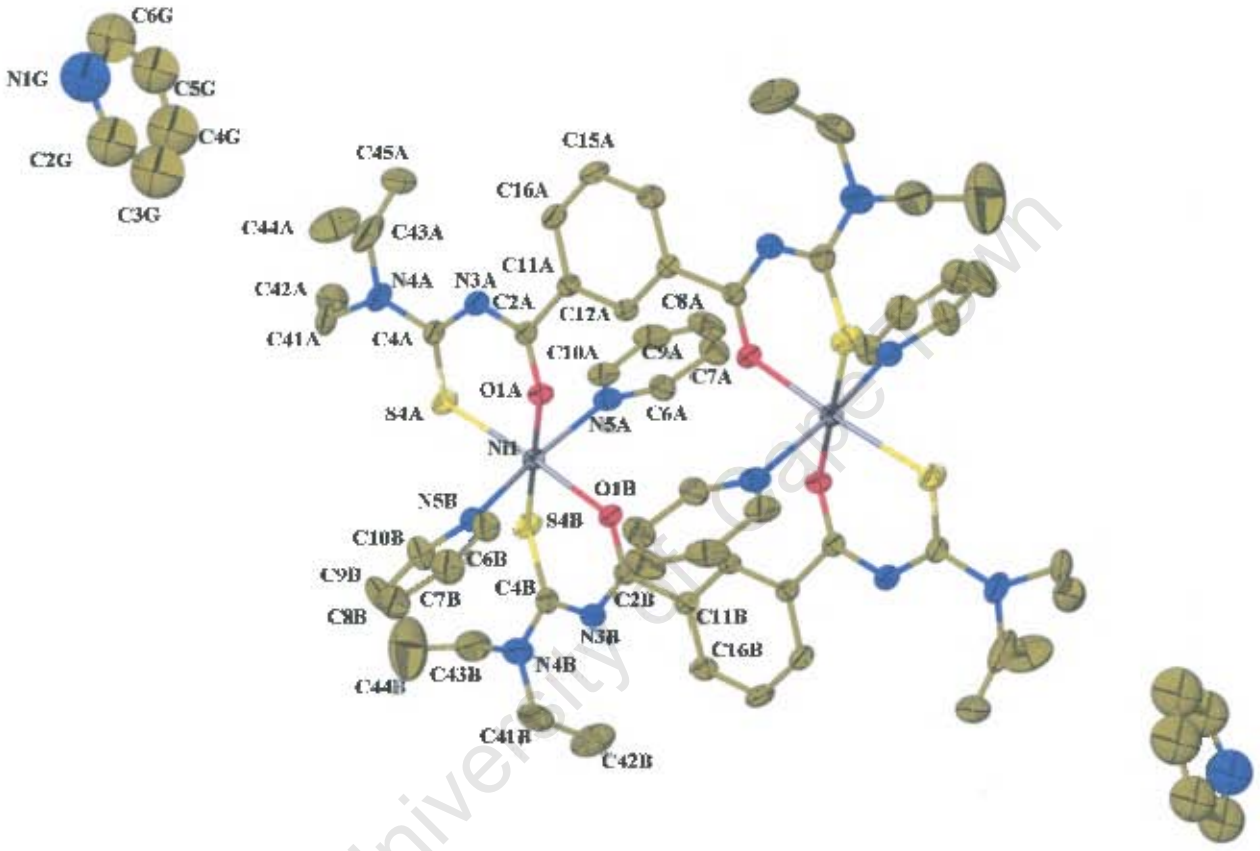

Figure 3.3.1(b) Molecular Structure of *cis*-[Ni(I-Et-*S,O*)(pyridine-*N*)$_2$]$_2$ with isotropically modelled unbound pyridine guest molecules indicated. Thermal ellipsoids shown at 50% probability.

The coordination around the nickel(II) centres is of great interest. For important bond lengths and coordination bond angles refer back to Tables 3.3(a) and 3.3(b) (pp. 97-98). The axial coordination of the pyridine molecules causes a substantial lengthening of the S – Ni bonds (> 0.2Å) and O -- Ni bonds (> 0.17Å). This is consistent with a decrease in tetragonal distortion (i.e. shortening z-axis metal – ligand distance from infinity with concomitant lengthening of metal -- ligand distances along the x- and y-axes) to form an octahedral adduct from a square planar complex. Some of the other

average bond lengths within the chelate rings also change significantly upon addition of pyridine: the carbonyl bonds become shorter, while the C(O) – N bonds lengthen, as do the C(S) – NR_2 bonds. The thiocarbonyl bonds and the C(S) – N(CO) bonds do not change significantly in length. It is evident that some rearrangement occurs and the bond angles within the chelate rings are perhaps better indicators of this change than are the bond lengths. The distortion in the square planar configuration of *cis*-[Ni(I-Et-*S,O*)]$_2$ has already been noted (Section 3.2.1). Table 3.3(b) shows that the coordination of pyridine decreases this distortion by shifting the *cis*- bond angles of the square plane closer to 90°. The calculated root mean square deviations from planarity for certain regions of the molecule are also useful indicators of distortion (refer to Table 3.3(c). above). The root mean square deviation from planarity for atoms that make up the theoretical square plane of the complex (namely O1A, O1B, S4A, S4B and Ni1A) is 0.0423Å – a small but significant shift towards planarity when compared with the corresponding value for the atoms of the *cis*-[Ni(I-Et-*S,O*)]$_2$ square plane: 0.0581Å. Thus it can be seen that distortions from square planar coordination of the thiourea ligands have diminished in *cis*-[Ni(I-Et-*S,O*)(pyridine-*N*)$_2$]$_2$ as compared to *cis*-[Ni(I-Et-*S,O*)]$_2$.

However, this does not imply that *cis*-[Ni(I-Et-*S,O*)(pyridine-*N*)$_2$]$_2$ approximates ideal octahedral behaviour. The co-ordinated pyridines in these complexes are not perpendicular to the plane of the *cis*-[Ni(I-Et-*S,O*)]$_2$ cores, but are tilted inwards toward the cavity with an N(5B) – Ni(1) – N(5A) angle of 167.2°. Note that the planes of the axially bound pyridine molecules are not parallel (compare for example the torsion angles O(1A) – Ni(1) – N(5A) – C(6A): 53.1(3)° and O(1A) – Ni(1) – N(5A) – C(10A): -127.9(3)° with O(1A) – Ni(1) – N(5B) – C(6B): -38.0(3)° and O(1A) – Ni(1) – N(5B) – C(10B): 142.7(3)°.

Another interesting observation is the deviation from planarity of the chelate rings. The root mean square deviations of the two chelate rings are: 0.1454Å for O1A – C2A – N3A – C4A – S4A – Ni1 and 0.2208Å for O1B – C2B – N3B – C4B – S4B – Ni1. Compare these values for those found for the corresponding rings in *cis*-[Ni(I-Et-*S,O*)]$_2$: 0.0433Å and 0.1635Å respectively. Both rings are substantially more distorted from planarity in the octahedral adduct than in the square planar *cis*-[Ni(I-Et-*S,O*)]$_2$. The square plane around the nickel(II) centre makes an angle of 27.33° with the

benzoyl ring planes thus detracting from the overall planarity of the entire molecule. Figure 3.3.1(c) shows the *cis*-[Ni(I-Et-*S,O*)(pyridine-*N*)$_2$]$_2$ molecule from two side-on views. These perspectives allow one to observe the increased 'buckled effect' in the chelate rings as well as the skewing of the Ni(II) square planes out of plane with the benzoyl rings and also the tilting of the pyridines towards the centre of the metallamacrocycle.

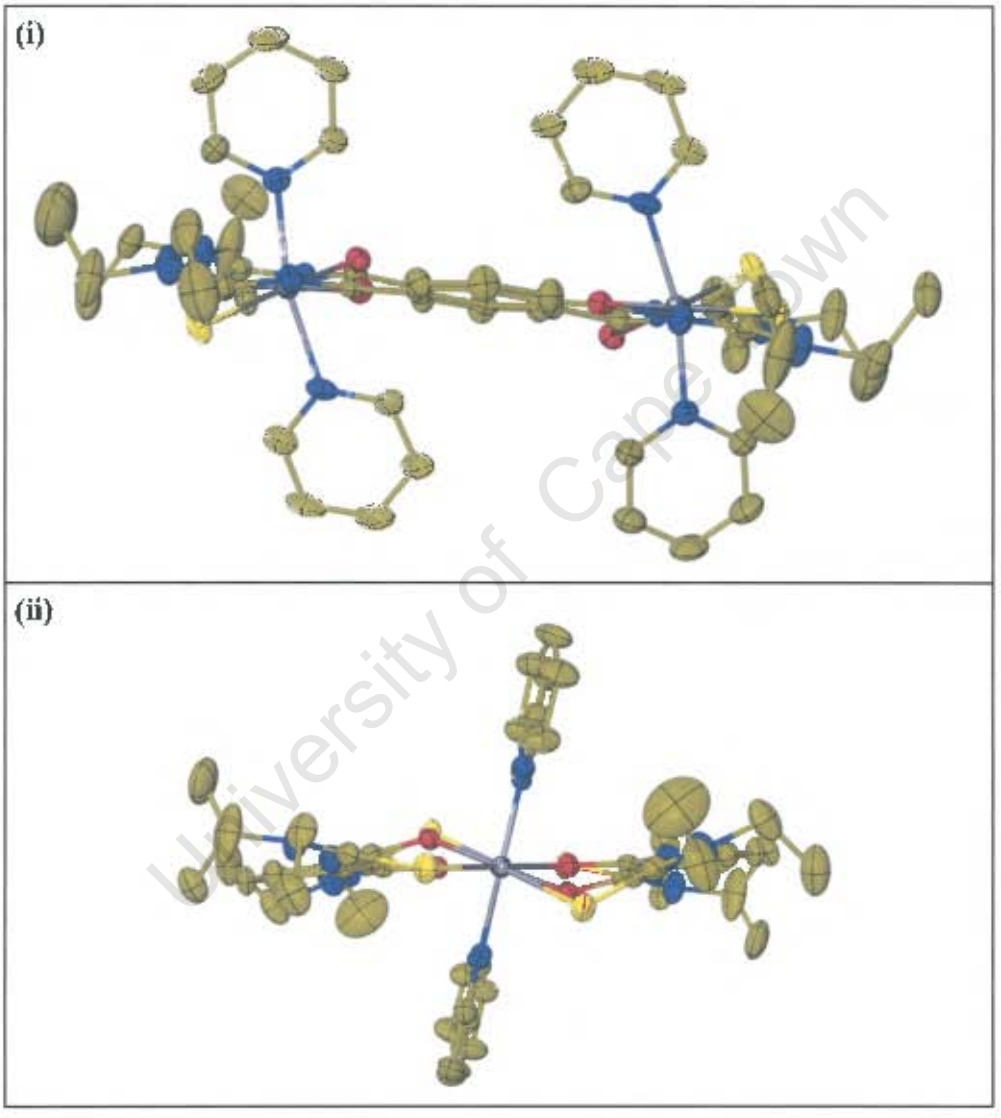

Figure 3.3.1(c). Two side-on perspectives of *cis*-[Ni(I-Et-*S,O*)(pyridine-*N*)$_2$]$_2$ illustrating distortion from ideal octahedral behaviour. Thermal ellipsoids shown at 50% probability.

The crystal packing of *cis*-[Ni(I-Et-*S,O*)(pyridine-*N*)$_2$]$_2$ is shown in the stereo diagrams below (Figure 3.3.1(d).) There is little to say about the packing of this

adduct; there is no hydrogen bonding or π-π stacking interactions between neighbouring complex molecules. The absence of π-π interactions similar to those observed in the crystal structure of *cis*-[Ni(I-Et-*S,O*)]$_2$ is due to the axial pyridine rings. They prevent metallamacrocycles from approaching each other closely enough to undergo any such non-bonded interactions. However these pyridines do take part in an edge-to-face interaction with the benzoyl rings of a neighbouring complex molecule: the distance between H8A and the centroid of the benzoyl ring of the asymmetric unit generated by symmetry operator (-x, -y, -z) is 2.698Å. The coordinated pyridine rings do not appear to have any face-to-face overlap with those of neighbouring complex molecules and do not lie closer to each other than 4.7Å.

The pyridine guest molecules are not aligned face-to-face or edge-to-face with any π-delocalised moieties of the *cis*-[Ni(I-Et-*S,O*)(pyridine-*N*)$_2$]$_2$ molecules and are thus only very weakly held in place in the crystal. This is most probably the cause of the friable nature of the crystals once removed from the mother liquor. Figure 3.3.1(d) shows the crystal packing of *cis*-[Ni(I-Et-*S,O*)(pyridine-*N*)$_2$]$_2$ with the guest molecules in space-fill representation. From the three different views down the principal cell axes, it can be seen that there are sizeable gaps between *cis*-[Ni(I-Et-*S,O*)(pyridine-*N*)$_2$]$_2$ molecules, which are filled by guest molecules. These gaps can be seen to form parallel continuous channels that run in the [100] direction. In the [010] and [001] directions, the rows of guest molecules are not continuous, being interrupted by *cis*-[Ni(I-Et-*S,O*)(pyridine-*N*)$_2$]$_2$ molecules. *Cis*-[Ni(I-Et-*S,O*)(pyridine-*N*)$_2$]$_2$ can thus be said to possess a channel structure that is held intact by weak intermolecular interactions.

The complex *cis*-[Ni(I-Et-*S,O*)(pyridine-*N*)$_2$]$_2$ is the archetype of a new class of compounds. The results and discussions of the analogous adducts *cis*-[Ni(I-Et-*S,O*)(DMAP-*N*)$_2$]$_2$, *cis*-[Ni(I-EtOH-*S,O*)(pyridine-*N*)$_2$]$_2$ and *cis*-[Ni(T-Et-*S,O*)(pyridine-*N*)$_2$]$_3$ are related in the following sections of this chapter. In each case, comparisons are made with *cis*-[Ni(I-Et-*S,O*)(pyridine-*N*)$_2$]$_2$.

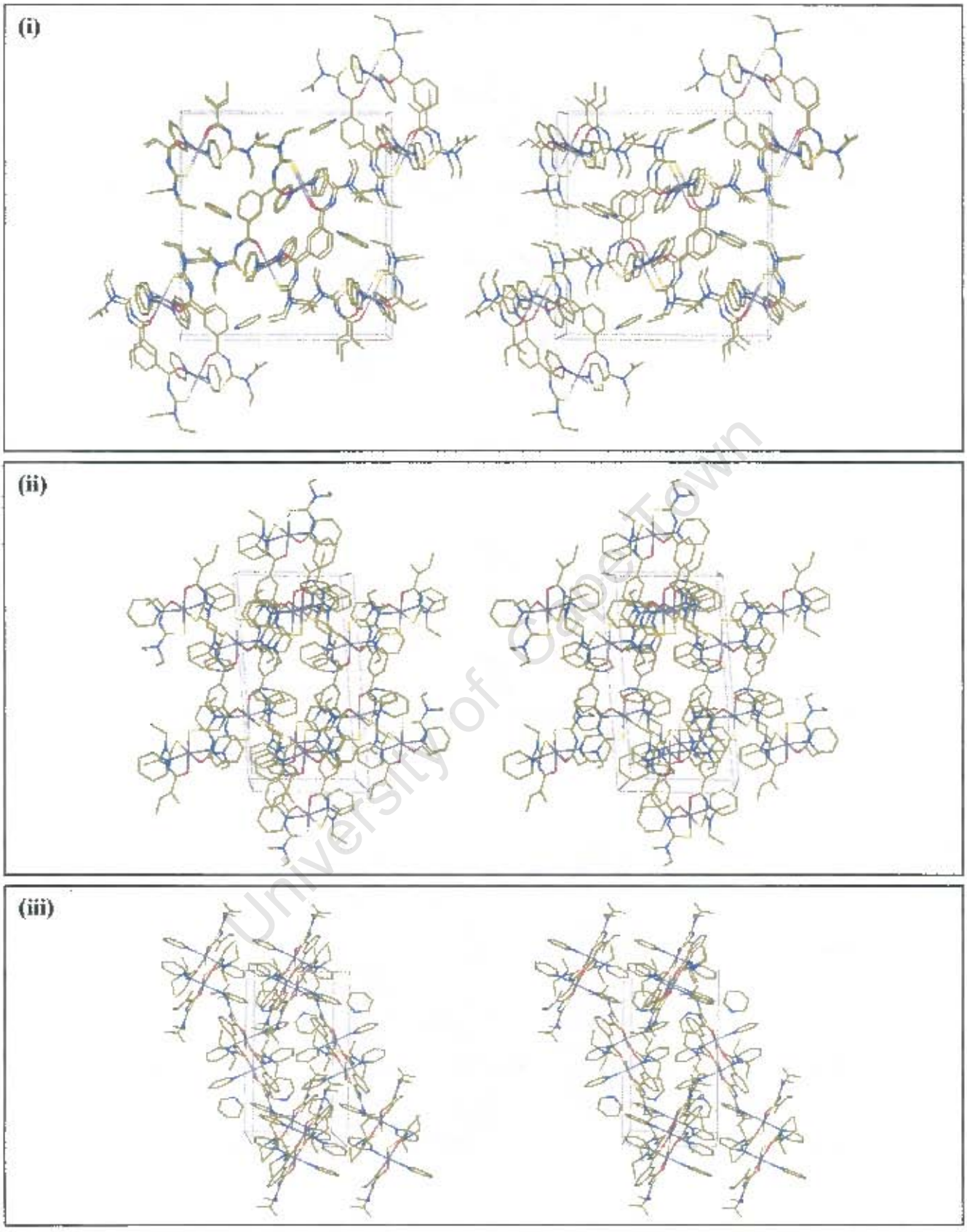

Fig. 3.3.1(d). Stereo crystal packing diagrams of *cis*-[Ni(I-Et-*S,O*)(pyridine-*N*)$_2$]$_2$ viewed down principle directions [100] (i), [010] (ii) and [001] (iii).

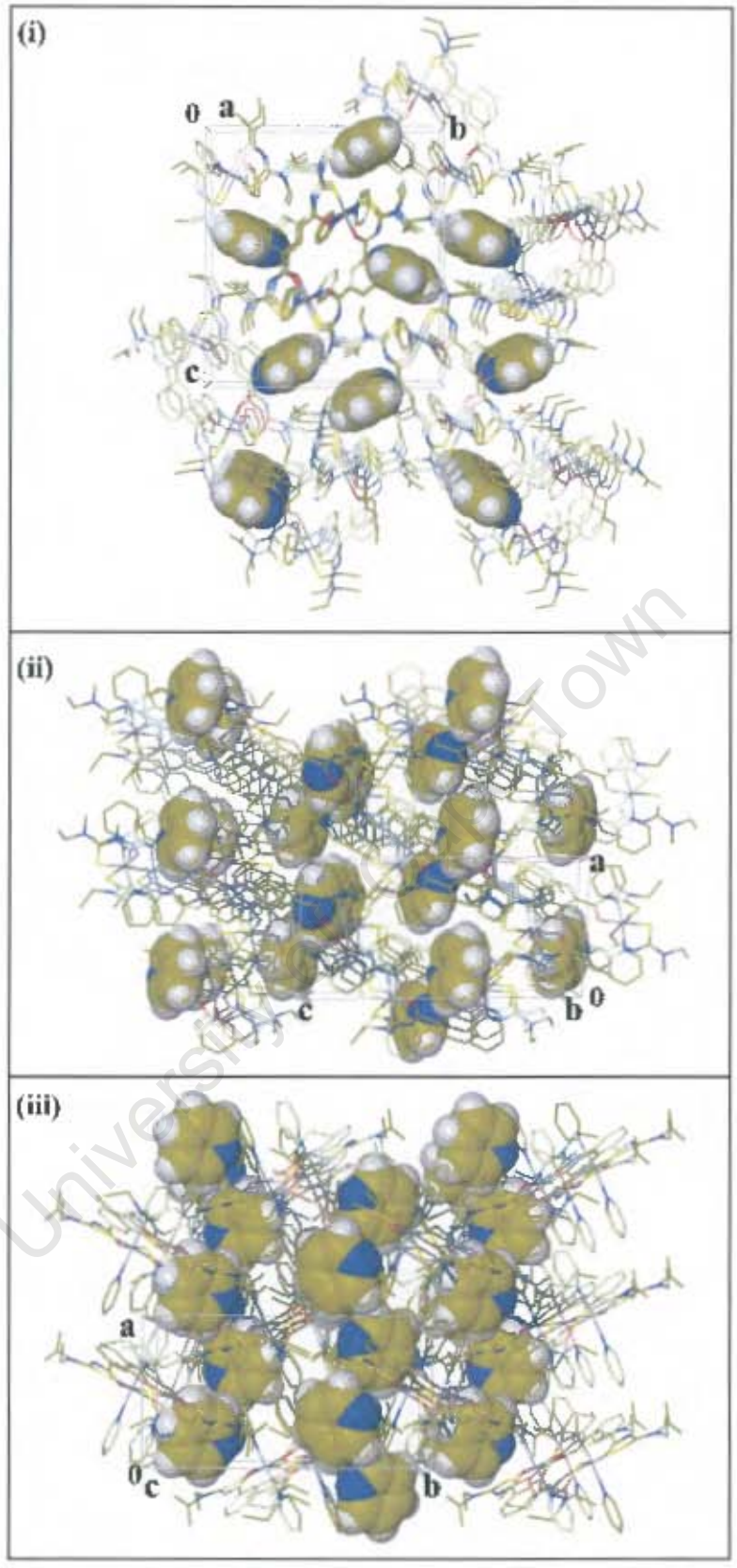

Figure 3.3.1(e). Crystal packing diagrams of *cis*-[Ni(I-Et-*S,O*)(pyridine-*N*)$_2$]$_2$ showing guests in space-fill representation revealing continuous guest-filled channels running in the [100] direction. Views given are along principal axes: (i) [100], (ii) [101] and (iii) [001].

3.3.2. [*Cis*-(bis-μ-(3,3,3',3'-tetraethyl-1,1'-isophthaloylbis(thioureato-*S,O*))-di-nickel(II))-tetrakis(4-dimethylaminopyridine-*N*)]
(*cis*-[Ni(I-Et-*S,O*)(DMAP-*N*)$_2$]$_2$)

Thermal Analysis

Suitable crystals were grown from a solution of *cis*-[Ni(I-Et-*S,O*)]$_2$ with 4-dimethylamino-pyridine (DMAP) in a mixture of dichloromethane and acetonitrile at ~ 4 °C. Figure 3.3.2(a) shows the results of TGA for this product. A loss of 6.25 % of the total mass is indicated between 74 °C and 99 °C. This is quickly followed by a second mass loss of 32.42 % ending at 152 °C. Following this, the mass remains stable. As with *cis*-[Ni(I-Et-*S,O*)(pyridine-*N*)$_2$]$_2$, this final mass is taken to represent the stable metallamacrocycle *cis*-[Ni(I-Et-*S,O*)]$_2$, hence we may determine the nature of the volatilised components of the crystal. Table 3.3.2(a) shows the results of these calculations, while a graphical representation of the TGA data is given in Figure 3.3.2(a).

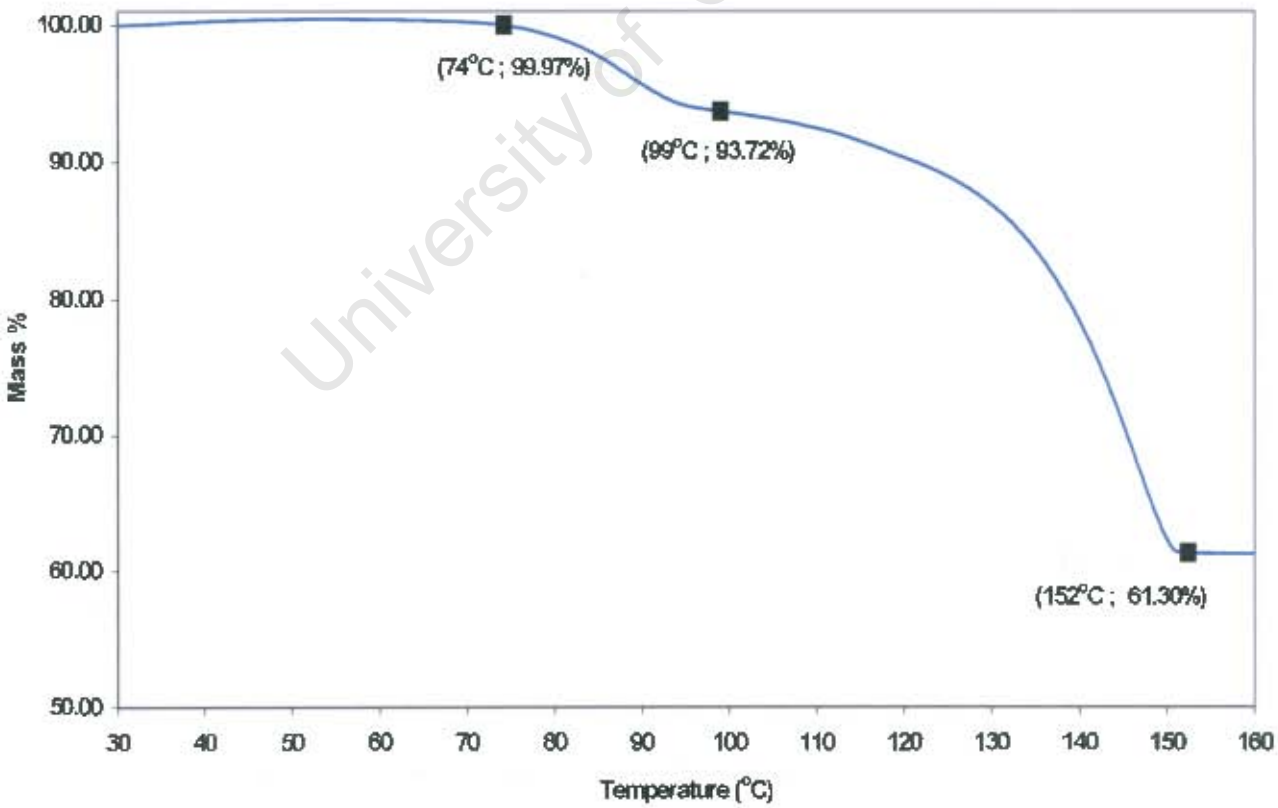

Figure 3.3.2(a) Results of TGA for *cis*-[Ni(I-Et-*S,O*)(DMAP-*N*)$_2$]$_2$

The first thermal event corresponds fairly well with the mass loss calculated for one molecule of dichloromethane, while the second event indicates the loss of four 4-dimethylamino-pyridine molecules. Thus TGA indicates that this compound is an octahedral adduct of *cis*-[Ni(I-Et-*S,O*)]$_2$, with one CH_2Cl_2 guest molecule per metallamacrocycle – i.e. *cis*-[Ni(I-Et-*S,O*)(DMAP-*N*)$_2$]$_2$.(dichloromethane). This was confirmed by crystal structure analysis. Furthermore, it is evident that the process of thermal decomposition of the crystal is more straightforward than that of *cis*-[Ni(I-Et-*S,O*)(pyridine-*N*)$_2$]$_2$. In this case, it is clear that the weakly bound guest is the first component to be removed from the crystal, followed by the axially co-ordinated ligands in two well-resolved steps.

Table 3.3.2(a) TGA Calculations of Mass Losses for *cis*-[Ni(I-Et-*S,O*)(DMAP-*N*)$_2$]$_2$

Reaction	Temp. Range (°C)	Experimental Mass Loss (%)	Calculated Mass Loss (%)
cis-[Ni(I-Et-*S,O*)(DMAP-*N*)$_2$]$_2$.CH_2Cl_2			
↓	74 – 99	6.25	5.77 (CH_2Cl_2)
	99 – 152	32.42	33.19 (4 DMAP)
cis-[Ni(I-Et-*S,O*)]$_2$	Total (30 – 160)	38.67	38.96

A comparison of the TGA graphs for *cis*-[Ni(I-Et-*S,O*)(pyridine-*N*)$_2$]$_2$ and *cis*-[Ni(I-Et-*S,O*)(DMAP-*N*)$_2$]$_2$ shows that the onset temperature of initial mass loss is higher for the latter, but the initial thermal event is more gradual for the former. It is difficult to ascertain when the axially coordinated ligands of *cis*-[Ni(I-Et-*S,O*)(pyridine-*N*)$_2$]$_2$ begin to be removed during heating (as mentioned above) but it appears that the axial ligands of either compound are removed over comparable temperature ranges.

Single Crystal Diffractometry

Table 3.3.2(b). Crystal Data and Refinement Parameters for *cis*-[Ni(1-Et-*S,O*)(DMAP-*N*)$_2$]$_2$. (CH_2Cl_2)

Molecular Formula	$C_{64}H_{88}N_{16}O_4S_4Ni_2$. ($CH_2Cl_2$)
Formula Weight (g.mol^{-1})	1476.02
Temperature (K)	173
Wavelength (Å)	0.71070
Crystal System	Monoclinic
Space Group	$P2_1/n$
a (Å)	16.3426(5)
b (Å)	11.1685(3)
c (Å)	21.4148(7)
$\alpha = \gamma$ (°)	90
β (°)	99.352 (1)
Volume (Å^3)	3856.7(2)
Z	2
Calculated Density (g.cm^{-3})	1.271
μ (mm^{-1})	0.719
F(000)	1556
Crystal Size	0.30 x 0.20 x 0.18 mm
θ Range Scanned (°)	1.46 – 27.51
Index Range	$-20 \leq h \leq 21$, $-14 \leq k \leq 14$, $-27 \leq l \leq 27$
No. Reflections Collected	20785
No. Unique Reflections	8734 [R(int) = 0.0389]
Completeness	98.3 %
Refinement Method	Full-matrix L.S. on F^2
Data / Restraints / Rarameters	8743 / 0 / 438
Goodness-of-fit on F^2	1.028
Final R Indices [I>2σ(I)]	$R_1 = 0.0592$, $wR_2 = 0.1703$
R Indices (all data)	$R_1 = 0.0884$, $wR_2 = 0.1887$
Extinction Coefficient	0.0009(3)
Largest Diff. Peak and Hole	2.224 and -0.322 e. Å^{-3}

The molecular structure of *cis*-[Ni(I-Et-*S,O*)(DMAP-*N*)$_2$]$_2$ is given in Figure 3.3.2(b). The space group in which the complex crystallises is $P2_1/n$ (as for *cis*-[Ni(I-Et-*S,O*)(pyridine-*N*)$_2$]$_2$.) Thus, like *cis*-[Ni(I-Et-*S,O*)(pyridine-*N*)$_2$]$_2$, the asymmetric unit contains only one half of the metallamacrocyclic adduct. Furthermore, a solvent guest molecule is also contained in the asymmetric unit – in this case, the solvent used was dichloromethane. The TGA results indicate that there is one dichloromethane guest molecule in the crystal for each metallamacrocycle, thus the crystal structure was modelled in this way. Aside from the fact that there is only one guest molecule for every *cis*-[Ni(I-Et-*S,O*)(DMAP-*N*)$_2$]$_2$ molecule (i.e. two asymmetric units), there is a further complication in the form of positional disorder. The dichloromethane guest was modelled in two similar positions each with site occupancy of 25%. Residual electron density in this region suggests that the disorder is even more complicated, however, attempts to further model the disorder proved unsuccessful.

The *cis*-[Ni(I-Et-*S,O*)(DMAP-*N*)$_2$]$_2$ molecule is practically identical to *cis*-[Ni(I-Et-*S,O*)(pyridine-*N*)$_2$]$_2$. Indeed, the only considerable structural difference between the two is the presence of the dimethylamino groups in *cis*-[Ni(I-Et-*S,O*)(DMAP-*N*)$_2$]$_2$. The coordinating ability of DMAP is similar to that of pyridine, although DMAP is a stronger base than pyridine (compare DMAP's pK_a (in water) of 10.1 to that of pyridine: 5.25).[108] The dimethylamino group, though bulky, offers no steric hindrance of the nucleophilic nitrogen's approach to the Ni(II) metal ion.

The bond lengths listed for the two complexes in Table 3.3(a) (p. 97) do not differ greatly. The carbonyl bonds of *cis*-[Ni(I-Et-*S,O*)(DMAP-*N*)$_2$]$_2$ are, on average, slightly shorter than those of *cis*-[Ni(I-Et-*S,O*)(pyridine-*N*)$_2$]$_2$, as are the C(S) – N(R_2) bond and the O Ni bonds, while the S · Ni bonds are somewhat longer. The axial N – Ni bonds of *cis*-[Ni(I-Et-*S,O*)(DMAP-*N*)$_2$]$_2$ are shorter, a fact attributable to the more basic nature of DMAP mentioned above.

A comparison of the central bond angles (Table 3.3(b).) of the two adducts shows that some of the *cis*- bond angles around the nickel metal centre are essentially identical, while others, namely: O1A – Ni1 – O1B; S4A – Ni1 – S4B; N5A – Ni1 – O1A; N5B – Ni1 – S4A and N5B – Ni1 – S4B differ by as much as 8.9°. Interestingly, all these significant shifts in *cis*- bond angle result in values that are closer to 90°.

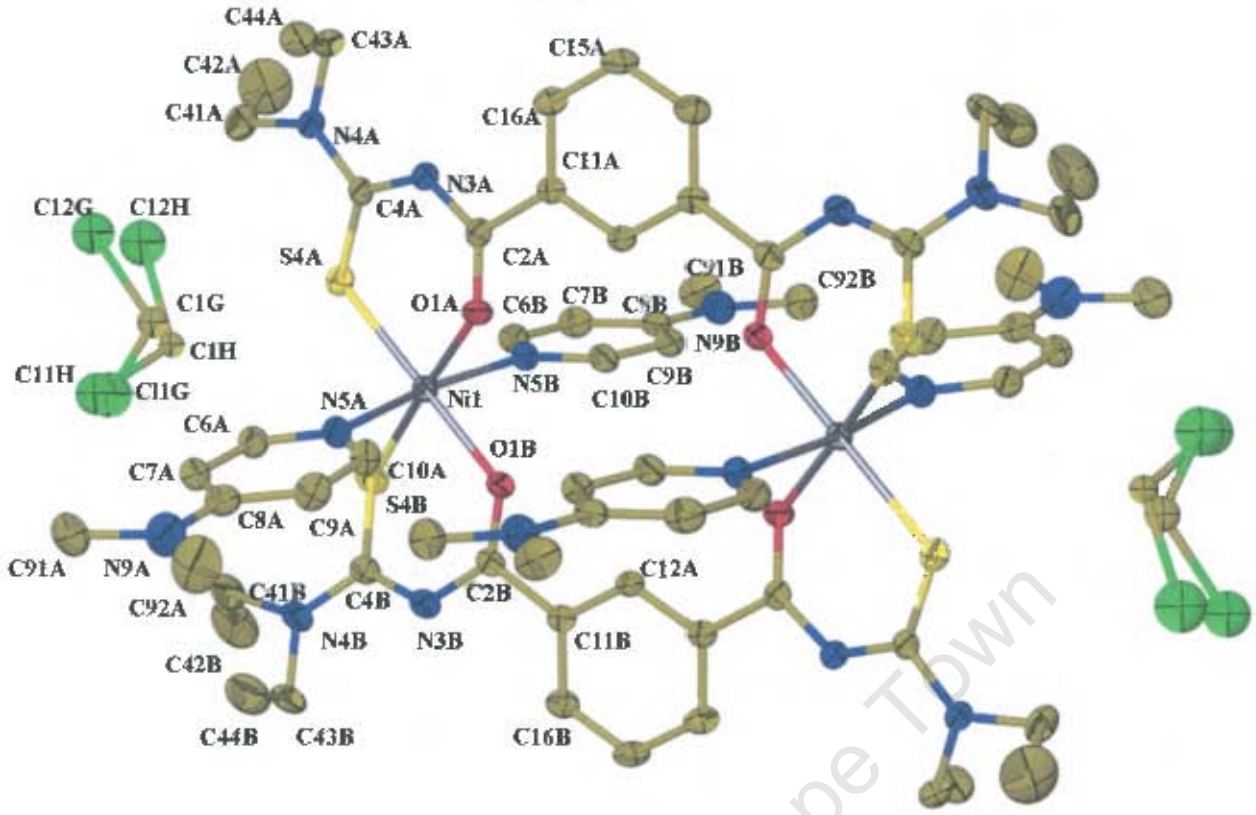

Figure 3.3.2(b). Molecular structure of *cis*-[Ni(I-Et-*S,O*)(DMAP-*N*)$_2$]$_2$ with included dichloromethane guest indicated. Guest modelled as disordered in two positions each with site occupancy 25% - giving a total of one dichloromethane guest per *cis*-[Ni(I-Et-*S,O*)(DMAP-*N*)$_2$]$_2$ molecule. Thermal ellipsoids shown at 50% probability.

The three *trans*- angles of *cis*-[Ni(I-Et-*S,O*)(DMAP-*N*)$_2$]$_2$ are all slightly nearer 180° than their *cis*-[Ni(I-Et-*S,O*)(pyridine-*N*)$_2$]$_2$ counterparts. Overall, the differences in bond angles point to a lesser deviation from ideal octahedral behaviour in *cis*-[Ni(I-Et-*S,O*)(DMAP-*N*)$_2$]$_2$. This can be seen more clearly by comparing calculated root mean square deviations from planarity in various regions of the adducts' molecular structures (refer to Table 3.3(c). above). The root mean square deviation from planarity of the atoms in the theoretical square plane (O1A, O1B, S4A, S4B, Ni1) is 0.0127. This value is substantially lower than the corresponding value for *cis*-[Ni(I-Et-*S,O*)(pyridine-*N*)$_2$]$_2$. The root mean square deviation of the chelate ring O1A – C2A – N3A – C4A – S4A – Ni1 is calculated to be 0.0866: significantly lower than the same value for *cis*-[Ni(I-Et-*S,O*)(pyridine-*N*)$_2$]$_2$, but not as low as that of *cis*-[Ni(I-Et-*S,O*)]$_2$. However the atoms of the other chelate ring (O1B – C2B – N3B – C4B –

S4B – Ni1) are shown to have a root mean square deviation from the least squares plane of 0.2587 – an increase when compared with *cis*-[Ni(I-Et-*S,O*)(pyridine-*N*)$_2$]$_2$. It seems that distortion from planarity is "ironed out" in one ring, only to manifest itself as greater distortion within the other. A consequence of this buckling of the B-chelate ring is that the ethyl group C43B – C44B is situated quite close to the aromatic ring of one of the DMAP ligands. Further more, the conformation of this ethyl branch is such that C44B partially eclipses the aromatic ring. In *cis*-[Ni(I-Et-*S,O*)(pyridine-*N*)$_2$]$_2$, this eclipsing is avoided by the conformation of the ethyl branch, which orients the terminal methyl group away from the pyridine ring.

Another feature of this complex worth comparing with the matching feature of *cis*-[Ni(I-Et-*S,O*)(pyridine-*N*)$_2$]$_2$ is the angle between the original square plane around the Ni(II) centre and the benzoyl ring plane. In this compound, that angle is 20.57°, while for *cis*-[Ni(I-Et-*S,O*)(pyridine-*N*)$_2$]$_2$, the value was reported to be 27.23°. This angle between two of the major planar features indicates a deviation from planarity of the entire molecule, though not as great a deviation as for *cis*-[Ni(I-Et-*S,O*)(pyridine-*N*)$_2$]$_2$. One other feature worth mentioning is that the planes of the two coordinated DMAP ligands are approximately parallel. The torsion angles O1A – Ni1 – N5A – C6A: 134.7° and O1A – Ni1 – N5A – C10A: -48.5° match well with the corresponding torsion angles O1A – Ni1 – N5B – C6B: -136.8° and O1A – Ni1 – N5B – C10B: 48.2°. This same comparison for the coordinated pyridine ligands of *cis*-[Ni(I-Et-*S,O*)(pyridine-*N*)$_2$]$_2$ showed that they did not adopt parallel alignments.

Overall, there is a less strained appearance to *cis*-[Ni(I-Et-*S,O*)(DMAP-*N*)$_2$]$_2$. The complex possesses much lower distortion from planarity and ideal octahedral coordination behaviour than does *cis*-[Ni(I-Et-*S,O*)(pyridine-*N*)$_2$]$_2$. Why this should be the case is not immediately evident, and an important issue is now raised. Is there some trend that can be identified so that one could predict how closely a complex will approximate ideal behaviour? This question of crystal engineering merits investigation in a further study.

A visual comparison between *cis*-[Ni(I-Et-*S,O*)(pyridine-*N*)$_2$]$_2$ and *cis*-[Ni(I-Et-*S,O*)(DMAP-*N*)$_2$]$_2$ is given in Figure 3.3.2(c) below. Many of the differences described above can be seen quite clearly.

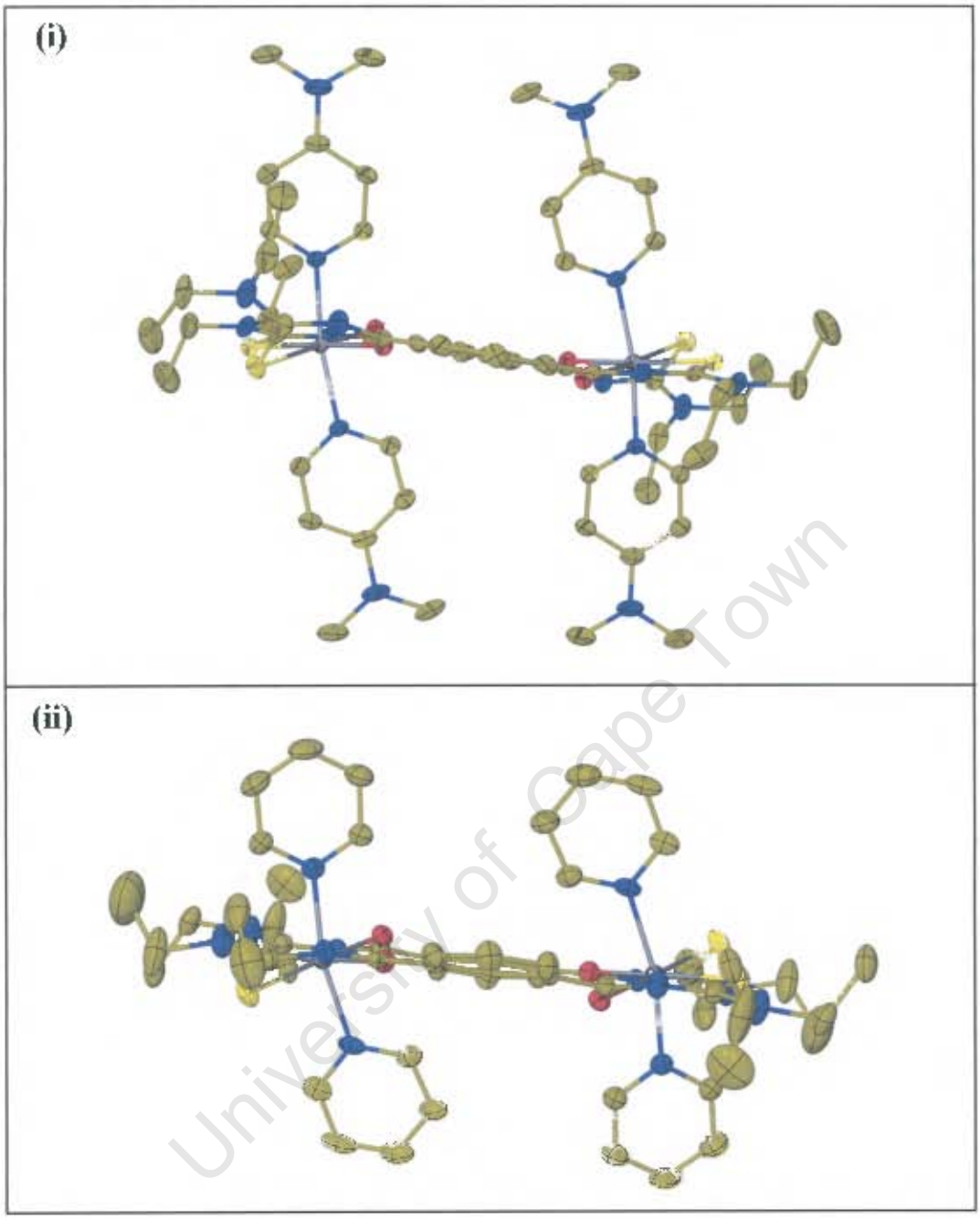

Figure 3.3.2(c). Visual comparison of the molecular structures of (i) *cis*-[Ni(I-Et-*S,O*)(DMAP-*N*)$_2$]$_2$ and (ii) *cis*-[Ni(I-Et-*S,O*)(pyridine-*N*)$_2$]$_2$. Thermal ellipsoids shown at 50% probability.

Since *cis*-[Ni(I-Et-*S,O*)(DMAP-*N*)$_2$]$_2$ shares the same space group symmetry as *cis*-[Ni(I-Et-*S,O*)(pyridine-*N*)$_2$]$_2$, it is not surprising that its mode of packing is very similar to that of *cis*-[Ni(1-Et-*S,O*)(pyridine-*N*)$_2$]$_2$. The adduct does not possess any hydrogen bonding capability and like *cis*-[Ni(1-Et-*S,O*)(pyridine-*N*)$_2$]$_2$, the axially coordinated ligands prevent any π-π stacking between moieties within neighbouring

metallamacrocycles such as that identified in the crystal structure of *cis*-[Ni(I-Et-*S,O*)]$_2$. However, it seems that certain neighbouring adduct molecules do have some type of π-π interaction between 4-dimethylaminopyridine ligands. There is a great degree of overlap between the N9A dimethylamino moiety and the N5B aromatic ring generated by symmetry operator (x, 1 + y, z), and the atoms C8A and C8B (x, 1 + y, z) are only 3.818 Å apart. If one considers that the amino nitrogen atom of DMAP is an extension of the π-delocalised system, then it is logical that such an interaction could occur. It is interesting that this interaction occurs on the face of the N5A ligand that is opposite to the eclipsing ethyl branch C43B – C44B mentioned above. This ethyl branch blocks any such π-π interactions on its side of the DMAP ligand. Figure 3.3.2(d) illustrates this effect quite clearly.

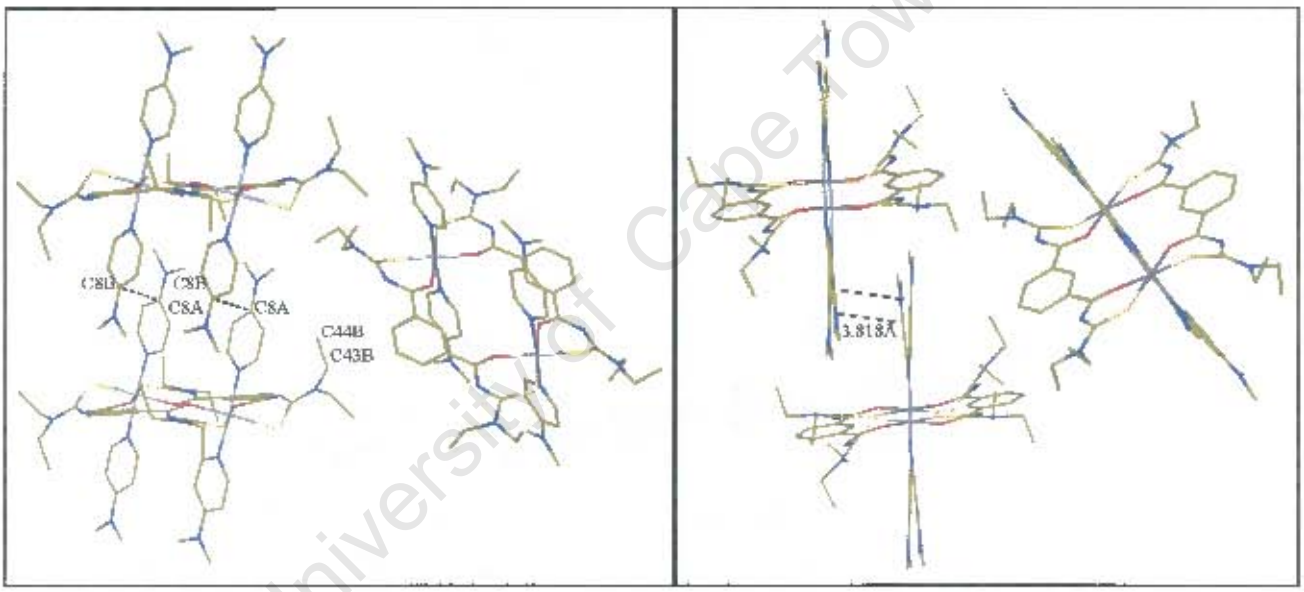

Figure 3.3.2(d). Two views of the π-π interaction of neighbouring *cis*-[Ni(I-Et-*S,O*)(DMAP-*N*)$_2$]$_2$ molecules and blocking of similar interactions by ethyl branch C43B – C44B (Guest molecules omitted for clarity).

If this blocking effect were not present, neighbouring molecules on both sides of the DMAP molecule could engage in this π-π interaction. The result would be a connection of all adduct molecules in the crystal through a network of such interactions. This would be reflected in the space group of such a crystal, which would certainly differ from what is observed here. Instead, what is observed is crystal

packing made up of discrete, non-parallel, one-dimensional chains of adduct molecules (Figure 3.3.2(e).).

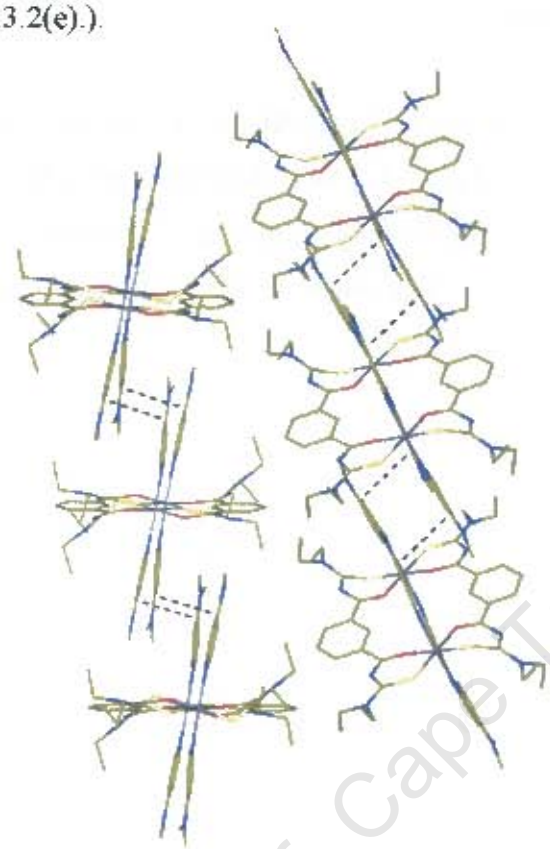

Figure 3.3.2(e). Two separate 1D chains of π-π associated *cis*-[Ni(I-Et-*S,O*)(DMAP-*N*)$_2$]$_2$ molecules. Inter-chain interactions are blocked by C43B – C44B ethyl branches.

Overall views of the crystal packing are given in Figure 3.3.2(f). The dichloromethane guest molecules are shown to be trapped between neighbouring adduct molecules. They do not seem to be held by any strong intermolecular forces. This explains why they emerge from the crystal separately from the DMAP ligands on heating and may also explain why there is not 100% site occupancy by the guest in the crystal structure. An alternate representation of the crystal packing, in which guest molecules are shown in space-fill representation, is given in Figure 3.3.2(g). The guest molecules are contained in gaps between the metallamacrocyclic adduct molecules. The representation in Figure 3.2.2(f) allows one to see that these gaps form continuous parallel channels running in the [010] direction. In other directions through the structure, the rows of guest molecules are not continuous, being interrupted by *cis*-[Ni(I-Et-*S,O*)(DMAP-*N*)$_2$]$_2$ molecules. Thus, the crystal structure

could be said to be a channel-type structure held intact by π-π interactions and weak intermolecular interactions.

The crystal structure of *cis*-[Ni(I-Et-*S,O*)(DMAP-*N*)$_2$]$_2$ has been shown to be remarkably similar to its analogue *cis*-[Ni(I-Et-*S,O*)(pyridine-*N*)$_2$]$_2$. The following crystal structure, *cis*-[Ni(I-EtOH-*S,O*)(pyridine-*N*)$_2$]$_2$, demonstrates how differently analogous molecules can crystallise simply by altering one functional group.

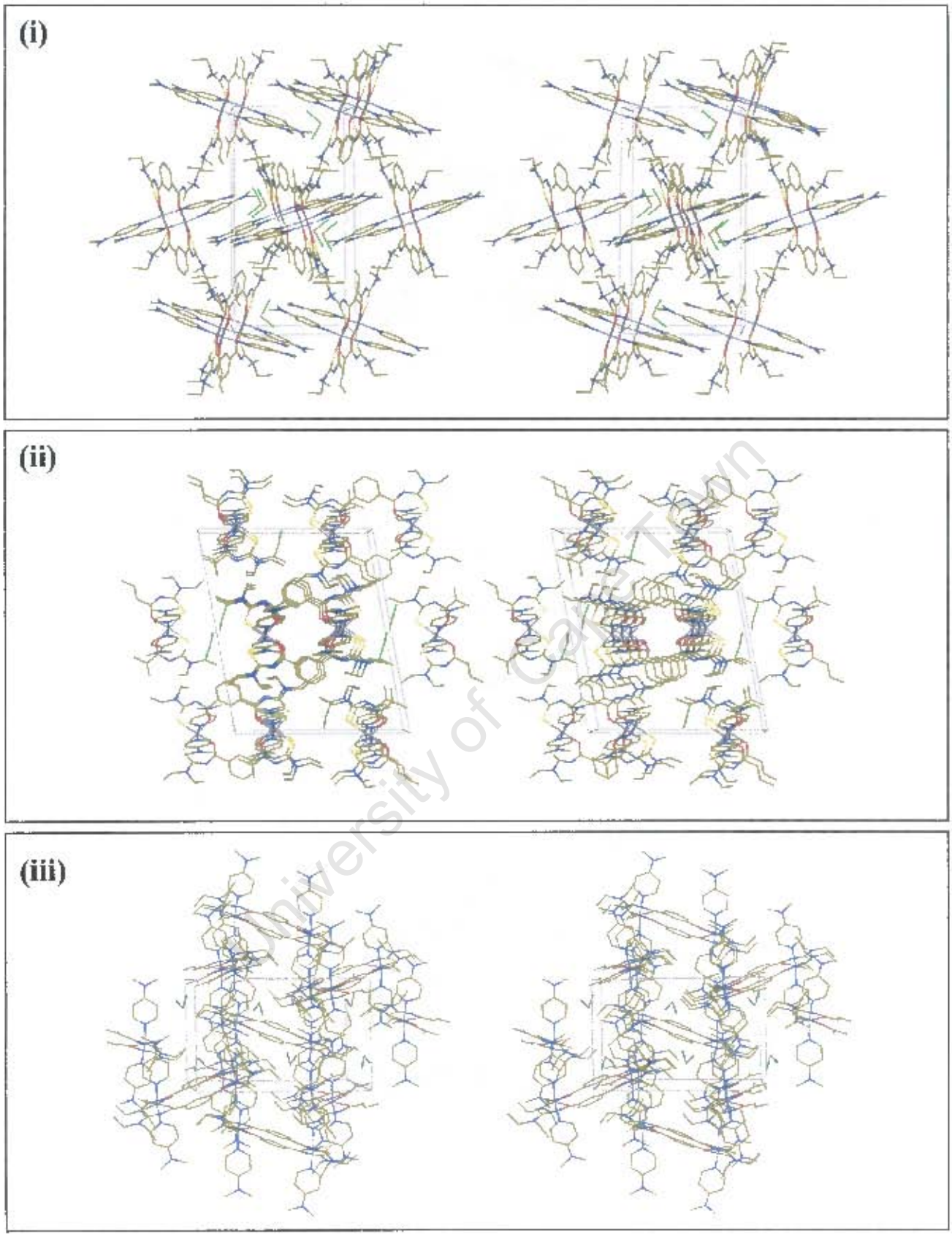

Figure 3.3.2(f). Stereo packing diagrams for *cis*-[Ni(I-Et-*S,O*)(DMAP-*N*)$_2$]$_2$ viewed down (i) [100] (ii) [010] and (iii) [001] directions. (π-π stacking interactions not shown and only one guest position indicated for clarity).

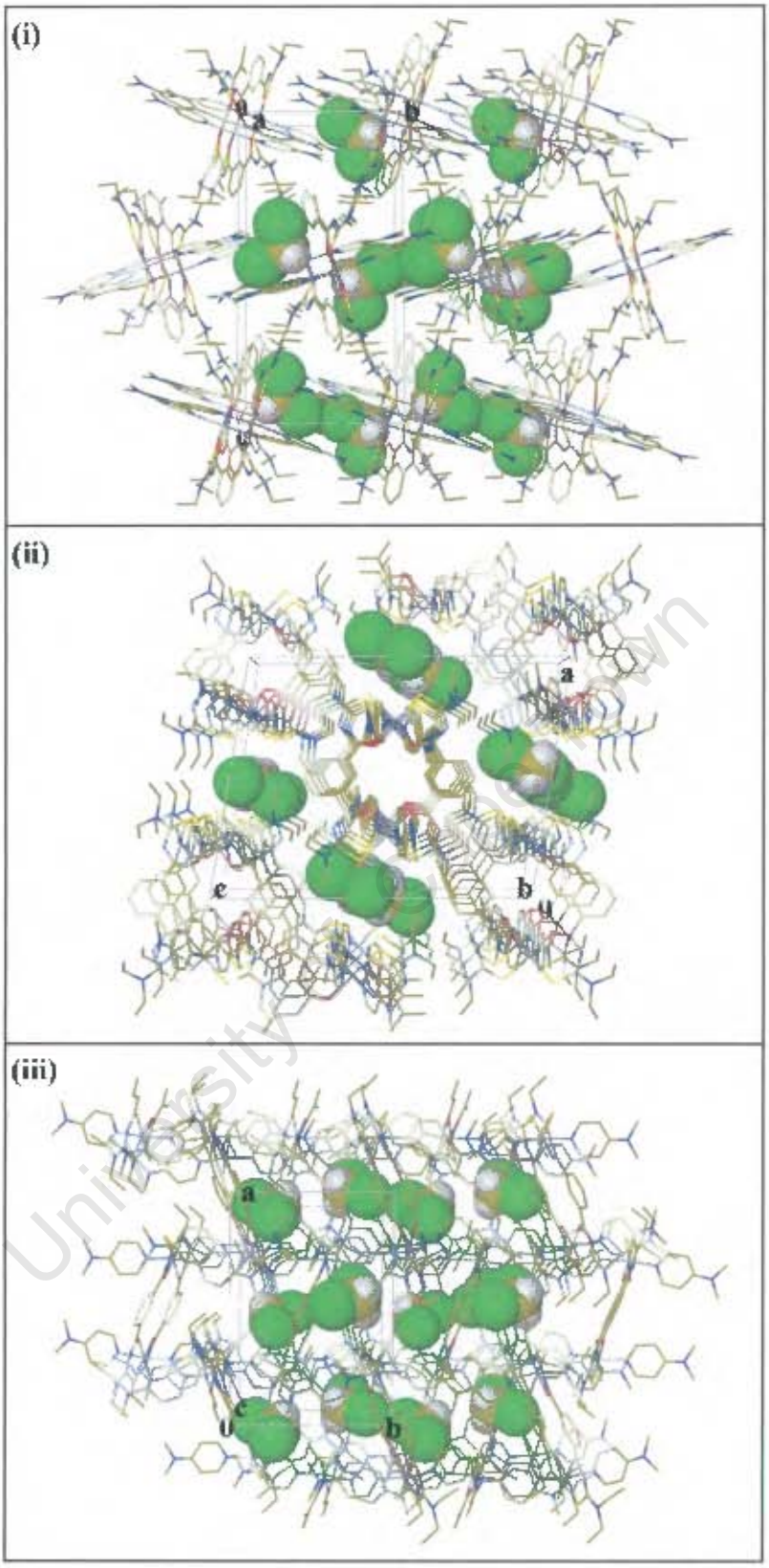

Figure 3.3.2(g). Crystal packing diagrams of *cis*-[Ni(I-Et-*S,O*)(DMAP-*N*)$_2$]$_2$ showing CH_2Cl_2 guests in space-fill representation. Guest-filled channels run in the [010] direction. Views given are along principal cell axes: (i) [100], (ii) [101] and (iii) [001]. (π-π stacking interactions not shown and only one guest position indicated for clarity).

3.3.3. [*Cis*-(bis-μ-(3,3,3',3'-tetra(2-hydroxyethyl)-1,1'-isophthaloylbis(thiourcato-*S,O*))-di-nickel(II))-tetra(pyridine-*N*)] (*cis*-[Ni(I-EtOH-*S,O*)(pyridine-*N*)$_2$]$_2$)

Thermal Analysis

The purple complex *cis*-[Ni(I-EtOH-*S,O*)]$_2$ was dissolved in pyridine, rapidly forming a green adduct in solution. The green crystals that were grown from this solution were subjected to TGA. As with the previous adducts, all TGA calculations are based on the notion that, after heating, the remaining mass is solely attributable to the parent square planar metallamacrocycle – in this case *cis*-[Ni(I-EtOH-*S,O*)(pyridine-*N*)$_2$]$_2$. This premise is strongly supported by the fact that *cis*-[Ni(1-EtOH-*S,O*)(pyridine-*N*)$_2$]$_2$ has been observed to revert to *cis*-[Ni(I-EtOH-*S,O*)]$_2$ upon removal from the pyridine based mother liquor (see Experimental Section 2.3.3). A graphical representation of these results is given in Figure 3.3.3(a), while the results of TGA are summarised in Table 3.3.3(a).

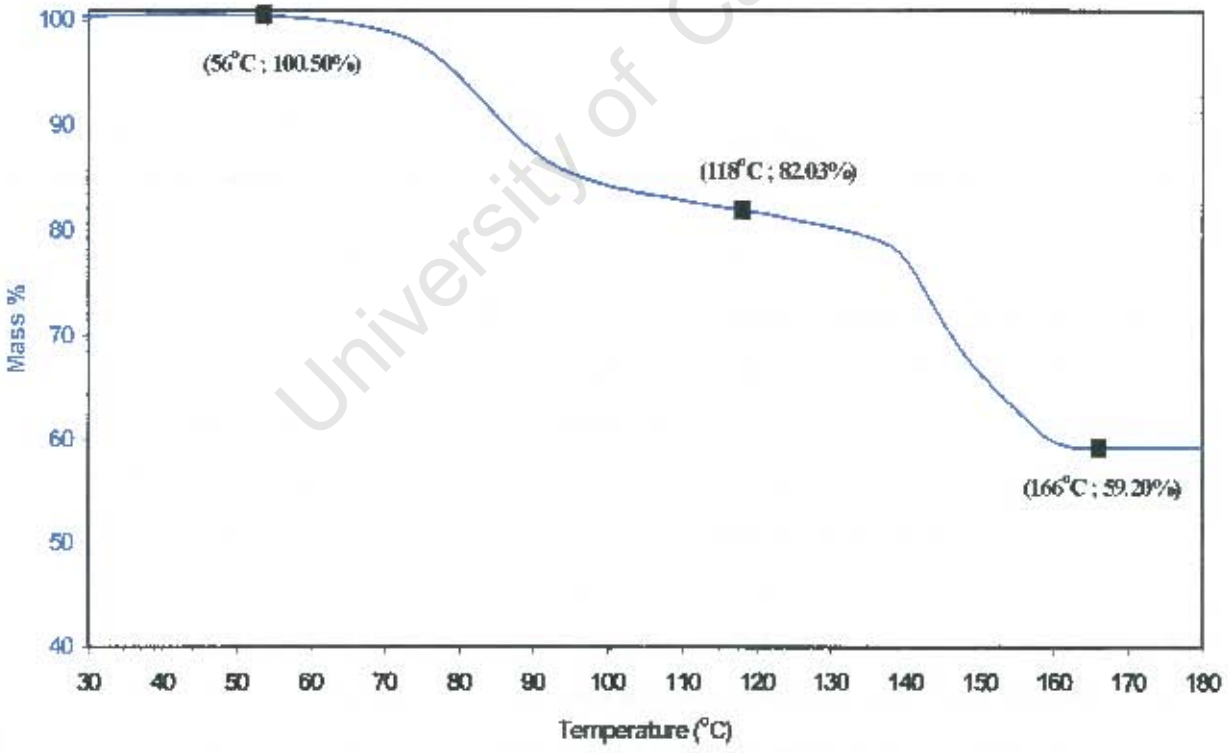

Figure 3.3.3(a) Graph of TGA results for *cis*-[Ni(I-EtOH-*S,O*)(pyridine-*N*)$_2$]$_2$

These results give the indication that the green crystals of the adduct *cis*-[Ni(I-EtOH-*S,O*)(pyridine-*N*)$_2$]$_2$ contain 5 included molecules of pyridine per adduct molecule.

This number of included molecules is quite different from the one or two guests included in the crystals of *cis*-[Ni(I-Et-*S,O*)(DMAP-*N*)$_2$]$_2$ and *cis*-[Ni(I-Et-*S,O*)(pyridine-*N*)$_2$]$_2$. This difference can be explained by the fact that the hydroxyl groups present in *cis*-[Ni(I-EtOH-*S,O*)(pyridine-*N*)$_2$]$_2$ possess strong H-bond donor capability. These groups would be expected to have a great affinity for H-bond acceptors such as pyridine. The crystal structure is thus expected to reveal the positioning of some pyridine guests in proximity to the hydroxyl groups of the metallamacrocycle.

Table 3.3.3(a) TGA Calculations of Mass Losses for *cis*-[Ni(I-EtOH-*S,O*)(pyridine-*N*)$_2$]$_2$

Reaction	Temp. Range (°C)	Experimental Mass Loss (%)	Calculated Mass Loss (%)
cis-[Ni(I-EtOH-*S,O*)(pyridine-*N*)$_2$]$_2$.5Py			
↓	56 – 118	18.47	18.18 (4 Py)
↓	118 – 166	22.83	22.72 (5 Py)
cis-[Ni(I-EtOH-*S,O*)]$_2$	Total (30 – 180)	41.30	40.90 (9 Py)

It is interesting that the first thermal event corresponds with the loss of 4 pyridine molecules, while the second event corresponds with the loss of 5. As was the case for *cis*-[Ni(I-Et-*S,O*)(pyridine-*N*)$_2$]$_2$, the individual mass losses do not conform to expected behaviour – i.e. removal of guests in the first event, followed by the loss of coordinated pyridine molecules. However, since dative covalent bonds are stronger than other non-covalent interactions (even ones as strong as hydrogen bonds), it is likely that the first event is not due to the removal of the coordinated axial ligands of the adduct, with the second event then arising from the removal of the included guests. Rather, one should conclude that the first event corresponds with the loss of 4 included pyridine guests and the second with the loss of one other pyridine guest molecule along with the 4 axially coordinated pyridine ligands.

However, the interpretation of the TGA data is not so clear-cut. There is no gravimetrically stable point in the temperature range from 100°C – 135°C, so it is

difficult to pinpoint exactly where the first thermal event ends and the second begins. Furthermore, even though the total mass lost corresponds well with the mass of 9 pyridines, there is a large enough margin for error in TGA to allow the possibility that the loss of some included guest of relatively low mass, such as water, is occurring within this range. As will be shown by the elucidation of the crystal structure of *cis*-[Ni(1-EtOH-*S,O*)(pyridine-*N*)$_2$]$_2$, this is indeed the case.

At this point, TGA gives some indication that the crystals of *cis*-[Ni(1-EtOH-*S,O*)(pyridine-*N*)$_2$]$_2$ are of the form *cis*-[Ni(I-EtOH-S,O)(Pyridine)$_2$]$_2$.5(Pyridine). The crystallographic results below confirm that this is, in part, the case. The presence of an additional guest molecule, though not immediately evident from the TGA results is shown to be of great importance in the crystal structure.

Table 3.3.3(b). Crystal Data and Refinement Parameters for *cis*-[Ni(1-EtOH-*S,O*)(pyridine-*N*)$_2$]$_2$. 5(pyridine). 2(H_2O)

Molecular Formula	$C_{56}H_{68}N_{12}O_{12}S_4Ni_2.5(C_5H_5N).2(H_2O)$
Formula Weight (g.mol^{-1})	1778.42
Temperature (K)	173
Wavelength (Å)	0.71073
Crystal System	Triclinic
Space Group	P-1
a (Å)	9.481(1)
b (Å)	12.993(3)
c (Å)	18.474(4)
α (°)	97.30(3)
β (°)	100.30(3)
γ (°)	100.52(3)
Volume (Å^3)	2171.1(8)
Z	1
Calculated Density (g.cm^{-3})	1.360
μ (mm^{-1})	0.601
F(000)	934
Crystal Size	0.50 x 0.50 x 0.50 mm
θ Range Scanned (°)	2.29 – 28.68
Index Range	$0\leq h\leq 12$, $-17\leq k\leq 17$, $-24\leq l\leq 24$
No. Reflections Collected	11143
No. Unique Reflections	11143 [R(int) – 0.0000]
Completeness	99.5 %
Refinement Method	Full-matrix L.S. on F^2
Data / Restraints / Parameters	11143 / 3 / 538
Goodness-of-fit on F^2	1.035
Final R Indices [$I>2\sigma(I)$]	$R_1 = 0.0507$, $wR_2 = 0.1177$
R Indices (all data)	$R_1 = 0.0889$, $wR_2 = 0.1338$
Largest Diff. Peak and Hole	1.004 and -0.829 e. Å^{-3}

Figure 3.3.3(b) depicts the molecular structure of *cis*-[Ni(l-EtOH-*S,O*)(pyridine-*N*)$_2$]$_2$. No guest molecules are indicated in this figure, for the sake of clarity. The asymmetric unit of the crystal contains one half of a *cis*-[Ni(l-EtOH-*S,O*)(pyridine-*N*)$_2$]$_2$ adduct molecule. The other half of the molecule is generated through a centre of symmetry at (1, 1, ½).

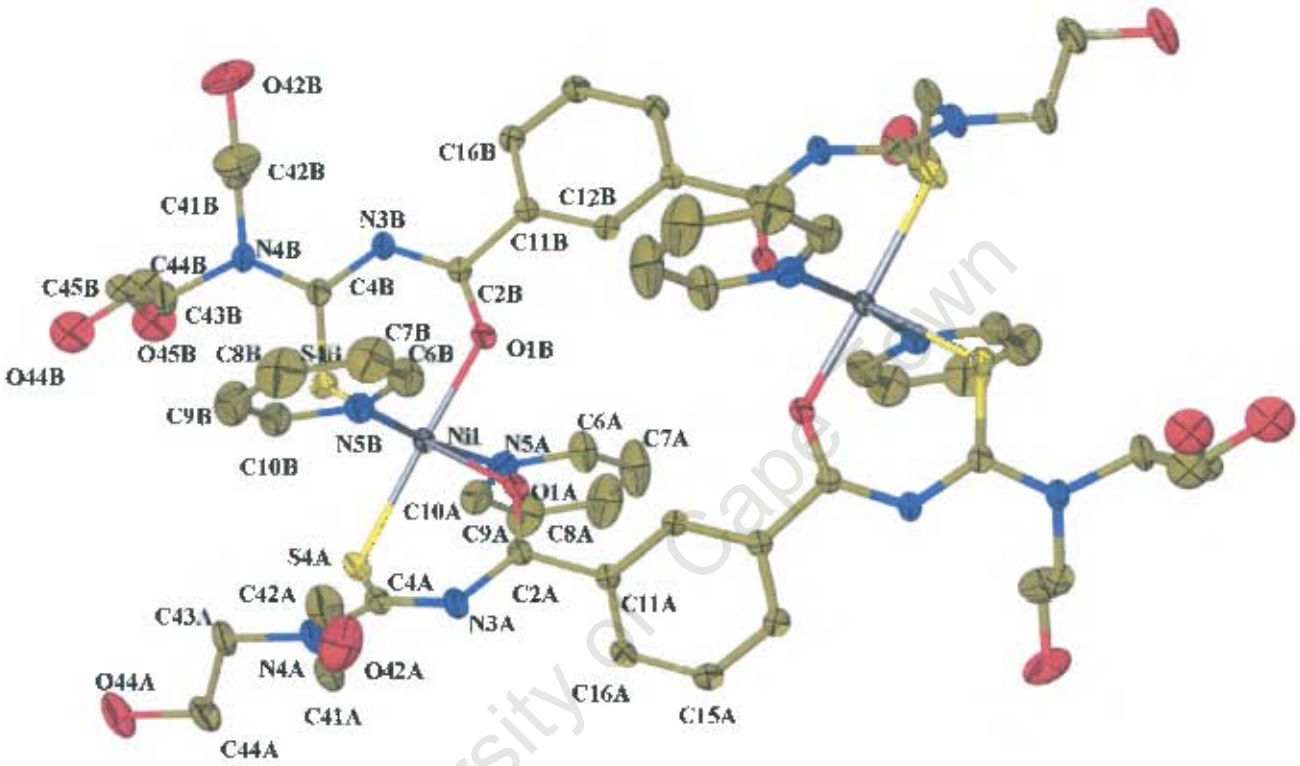

Figure 3.3.3(b). Molecular structure of *cis*-[Ni(l-EtOH-*S,O*)(pyridine-*N*)$_2$]$_2$. Thermal ellipsoids drawn at 50% probability.

The structural similarity of this complex to *cis*-[Ni(l-Et-*S,O*)(pyridine-*N*)$_2$]$_2$ is clear. Aside from the hydroxyl groups, the two adducts are identically composed. Table 3.3(a) above gives the comparison of some average bond lengths of *cis*-[Ni(l-EtOH-*S,O*)(pyridine-*N*)$_2$]$_2$ with corresponding values for the two other 2:2 metallamacrocyclic adducts. The average lengths of the intra-ligand bonds within the chelate rings do not vary significantly from those of *cis*-[Ni(l-Et-*S,O*)(DMAP-*N*)$_2$]$_2$. The O – Ni bonds are of intermediate length compared with those of the other two adducts. The average N – Ni bond lengths of *cis*-[Ni(l-EtOH-*S,O*)(pyridine-*N*)$_2$]$_2$ (2.132Å) are very close to those of *cis*-[Ni(l-Et-*S,O*)(pyridine-*N*)$_2$]$_2$ (2.14Å). In

general, the octahedral bond angles of *cis*-[Ni(I-EtOH-*S,O*)(pyridine-*N*)$_2$]$_2$ (see Table 3.3(b), p. 98.) are much the same as those of *cis*-[Ni(I-Et-*S,O*)(DMAP-*N*)$_2$]$_2$ differing by less than 2.5°, the only exceptions being N5A – Ni1 – O1A, N5A – Ni1 – S4A and N5B – Ni1 – S4B. The planarities of various regions of the molecule are listed in Table 3.3(c). It is interesting to note that both of the chelate rings of *cis*-[Ni(I-EtOH-*S,O*)(pyridine-*N*)$_2$]$_2$ have very high root mean square deviations from planarity – giving the molecule a greater buckled appearance, while the atoms that make up the original square plane around the nickel centre (O1A, O1B, S4A, S4B and Ni1) approach true coplanarity more closely than the atoms of the benzoyl rings. The angle between these two defined planes is calculated to be 22.74°. This is closer to the corresponding value for *cis*-[Ni(1-Et-*S,O*)(DMAP-*N*)$_2$]$_2$ (20.57°) than to that of *cis*-[Ni(I-Et-*S,O*)(pyridine-*N*)$_2$]$_2$ (27.33°). Most importantly though, these results show that in this case – as with both of the other 2:2 adducts – there is a distinct tilting of the equatorial Ni(II) square planes with respect to the benzoyl ring planes.

One other similarity between this adduct and *cis*-[Ni(I-Et-*S,O*)(DMAP-*N*)$_2$]$_2$ worth mentioning is the fashion in which the side chains of the acylthiourea ligands seem to interact with the axial pyridine ligands. In this case, the effect is more pronounced in two ways. Firstly, two of the hydroxyethylamine side chains (N4A to O42A and N4B to O42B) on opposite faces of the N5B pyridine ligand run virtually parallel with each other (the root mean square deviation from planarity of the atoms in these two side chains is 0.0282Å) and are held in a quasi-axial conformation with respect to the Ni(II) square plane (the angle between the least squares plane of these side chains and the Ni(II) square plane is 53.16°). Secondly, because the side chains are longer than the ethyl chains of *cis*-[Ni(1-Et-*S,O*)(DMAP-*N*)$_2$]$_2$, there is a greater degree of eclipsing of the face of the pyridine ligand. The extent of this eclipsing is best noted by the angle O42A – C8B – O42B: 172.82°. This shows that there exists an almost straight line between the two hydroxyethyl oxygens through the atom in the *para*-position of the pyridine ligand (i.e. the atom of the pyridine ligand that is 'highest above' the metallamacrocyclic platform.)

One other hydroxyethyl group is conspicuous due to the disorder that it exhibits. The atoms C44B and O44B are found to occupy more than one site. These alternative sites are labelled C45B and O45B in the molecular structure diagrams. The site

occupancies of the positions C44B and O44B are refined to 69%. There is some residual electron density around this side chain, suggesting that there exists further disorder in the atomic coordinates, but further refinement was not possible. The atoms C44B/C45B and O44B/O45B are modelled isotropically with no affixed hydrogen atoms.

The salient differences between *cis*-[Ni(l-EtOH-*S,O*)(pyridine-*N*)$_2$]$_2$ and the previous two adducts, *cis*-[Ni(l-Et-*S,O*)(pyridine-*N*)$_2$]$_2$ and *cis*-[Ni(l-Et-*S,O*)(DMAP-*N*)$_2$]$_2$, can be seen in Figure 3.3.3(c). This is a rendering of the molecular structure from the same perspective as in Figure 3.3.3(b), but with guest molecules included.

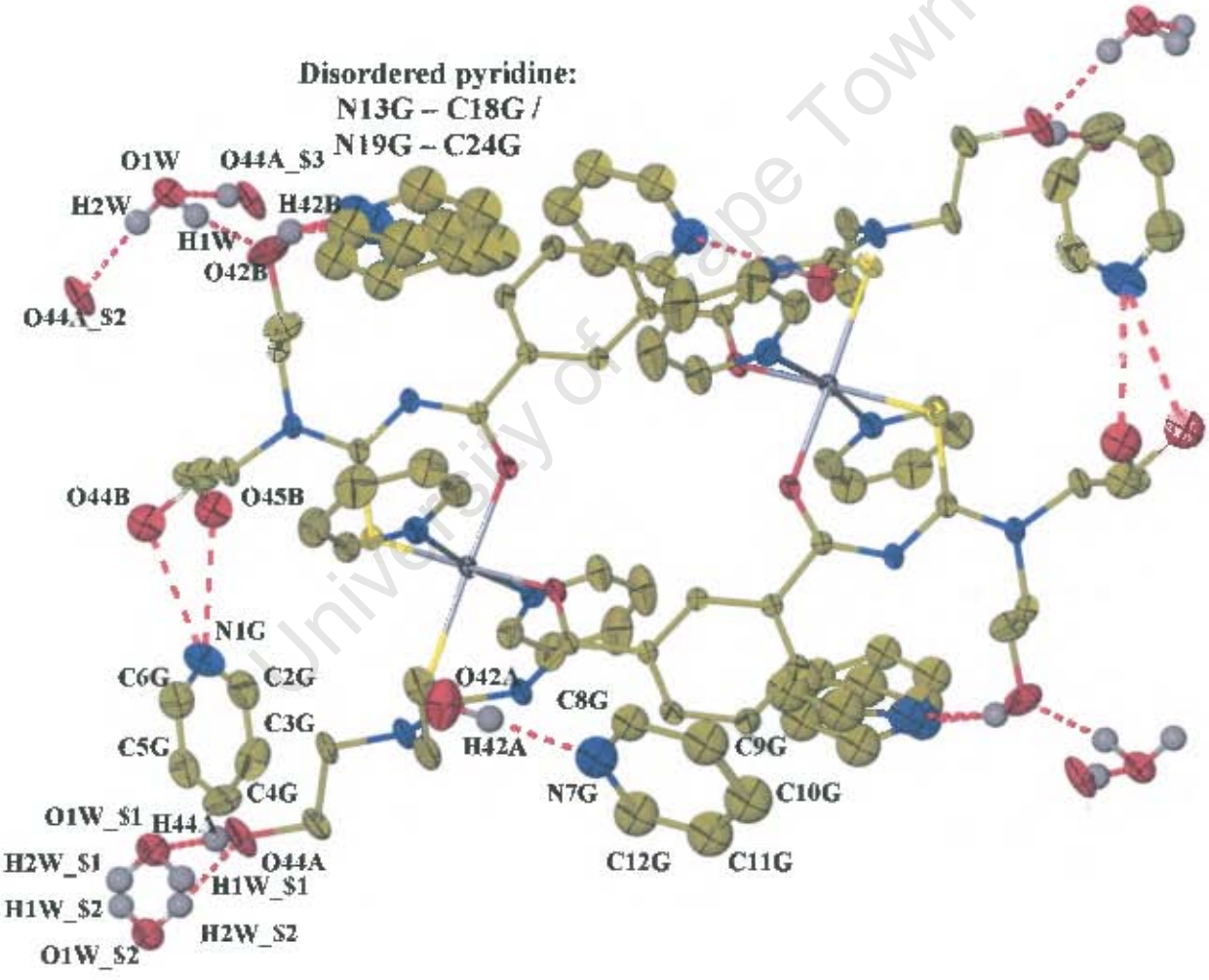

Figure 3.3.3(c). Molecular structure of *cis*-[Ni(l-EtOH-*S,O*)(pyridine-*N*)$_2$]$_2$ with associated pyridine and water guest molecules indicated. Hydrogens involved in H-bonding also shown. Thermal ellipsoids drawn at 50% probability.

From this diagram it is clear that the hydroxyl groups of this complex fundamentally affect the crystal structure. Each hydroxyl group is involved in intermolecular hydrogen bonding with one or more guest molecules. A list of all unique H-bonds with D – H --- A lengths is given in Table 3.3.3(c).

The OH group of the disordered side chain (C44B – O44B / C45B – O45B) is engaged in a hydrogen bond with a pyridine guest molecule (with N1G being the H-bond acceptor). It is interesting to note that despite the disorder, this interaction exists for both of the possible positions of the group. Furthermore, the possible donor – acceptor distances (O44B --- N1G 2.889Å and O45B --- N1G 2.971Å) listed in Table 3.3.3(c) show that in the O44B position, the OH group has a slightly closer interaction with the guest than in the O45B position. This finding corresponds with the relative site occupancies (O44B: O45B 69%: 31%), showing that the preferentially occupied site is the one that has a closer intermolecular interaction with the guest.

Table 3.3.3(c) List of hydrogen bonds in crystal structure of *cis*-[Ni(I-EtOH-*S,O*)(pyridine-*N*)$_2$]$_2$.

Atoms in Hydrogen Bond (D-H---A)	Donor – Acceptor Distance (Å)	H-Bond Angle (°)	Symmetry Operator	Notes
O42A – H42A --- N7G	2.831	163.32		
O42B – H42B --- N13G	2.793	163.45		
O42B – H42B --- N19G	2.635	152.04		
O44B – H44B* --- N1G	2.889	N/A		* Hydrogen atom not modelled
O45B – H45B* --- N1G	2.971	N/A		
O44A – H44A --- O1W	2.746	172.36	$1 (x, y - 1, z)	
O1W – H1W --- O42B	2.745	165.18		
O1W – H2W --- O44A	2.800	158.04	$2 (2 - x, 2 - y, 2 - z)	

This phenomenon of a disordered hydroxyl group bound to a pyridine guest in a fixed position is mirrored by the inverse phenomenon in which a hydroxyl group in a fixed

position (O42B – H42B) is H-bonded to the nitrogen of a pyridine guest that is disordered in two positions (N13G and N19G). In this case, the site occupancy ratio (N13G: N19G 53%: 47%) indicates a more even distribution than in the case of the disordered hydroxyl groups. One might suppose that, as for the O44B/O45B – N1G interaction described above, there would be a correlation between distance of H-bond interaction and relative site occupancy and thus expect these distances to be roughly equal. In fact they are not. The O42B --- N13G distance is some 0.16Å longer than the O42B --- N19G distance yet, despite a longer H-bond length, the N13G position enjoys slightly more occupancy than its counterpart. This suggests that the relative closeness of H-bonding interactions in different disordered positions is not the predominant factor in determining relative site occupancies of those disordered positions.

Yet another interesting variation on the theme of H-bonding coupled with positional disorder is found in this crystal structure, although as will be shown, this particular case is not so straightforward. The O42A – H42A group interacts with a pyridine molecule through the H-bond accepting N7G. This pyridine guest is modelled with site occupancy of 50%. The molecule's alternative position (not shown in the figure above) is generated by symmetry operator (3 – x, 1 – y, 1 – z). This is only a slight displacement in space, but through a centre of symmetry at coordinates (1½, ½, ½), thus the molecule's orientation is inverted and in its alternative position it interacts with the corresponding O42A atom generated by operator (3 – x, 1 – y, 1 – z).

In other words, a pyridine guest is always present between the O42A atoms of two neighbouring asymmetric units, with an equal probability of finding the orientation of this guest controlled by either O42A atom through hydrogen bonding with the pyridinyl nitrogen N7G. (Note, within the original unit cell the centre of symmetry would have coordinates (½, ½, ½) and the two asymmetric units related to each other through this centre would be generated from the original asymmetric unit (x, y, z) via symmetry operators (x – 1, y, z) and (2 – x, 1 – y, 1 – z) respectively.)

Since the centroid of the two possible positions occupied by the pyridine guest is located in a special position one may regard the disordered pyridine system (in both positions) as existing in two neighbouring asymmetric units simultaneously by virtue

of its location (i.e. the location of its centroid on a special position). This situation is shown more clearly in Figure 3.3.3(d).

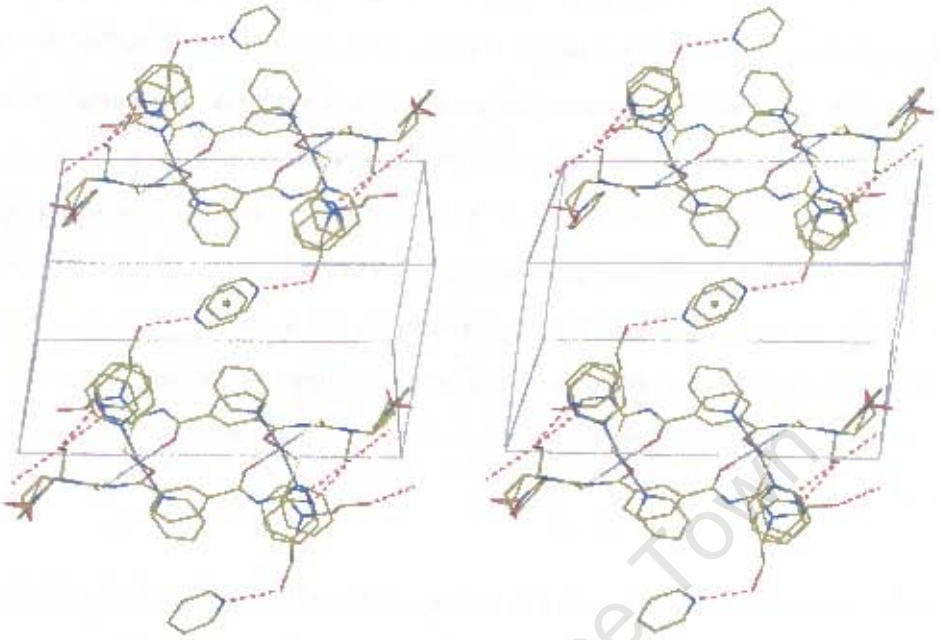

Figure 3.3.3(d) Stereo diagram of two *cis*-[Ni(1-EtOH-*S,O*)(pyridine-*N*)$_2$]$_2$ molecules (with associated guests) related through a centre of symmetry at coordinates (½, ½, ½). The centroid of the disordered pyridine guest system is located on this centre of symmetry.

The final hydrogen bonded guest in this crystal structure is the water molecule. In many ways, the presence of the H_2O guest is an extremely surprising result. The complex was not synthesised in aqueous solution nor was any quantity of water added intentionally during the synthesis. Therefore the water is quite literally an uninvited guest. This is not the surprise; the H-bonding capability of the side chains naturally imparts the compound with a certain degree of hygroscopicity. Although no clear indication of water was noticed in the TGA results for this complex, the gradual mass loss from the sample in the temperature range 100°C – 135°C is likely to involve the removal of the water guest molecules. The presence of water might have been overlooked, however, in this case, the water actually governs the packing of the crystal. As a guest it is paramount, despite its low molecular mass relative to the other components in the crystal structure. This is what is most surprising about the water molecule's presence, and it is precisely what makes this crystal structure so remarkable.

The water molecule is involved in three hydrogen bonds (see Figure 3.3.3(c).). Firstly, it is bound to O42B of the original asymmetric unit through H1W. Note that O42B thus plays a dual role: as H-bond acceptor to the water and as H-bond donor to the disordered N13G / N19G pyridine. Secondly, the water molecule is bound through H2W to O44A of a neighbouring asymmetric unit generated by symmetry operator (2 – x, 2 – y, 2 – z). The third H-bond involving the water molecule is one in which it acts as an acceptor to the O44A – H44A group of another neighbouring asymmetric unit (generated by symmetry operator (x, y + 1, z)). It must be mentioned that this H-bond is listed in Table 3.3.3(c) as O44A – H44A --- O1W $1

In other words, each O1W atom is H-bonded to one O42A atom as well as two O44A atoms of two neighbouring asymmetric units (once as a donor, once as an acceptor). Thus, each O44A atom is H-bonded to two O1W atoms of two neighbouring asymmetric units (once as a donor and once as an acceptor). Since one of these H-bonds links asymmetric units related by a centre of symmetry, i.e. O1W – H2W --- O44A $2 (2 – x, 2 – y, 2 – z), a reciprocal H-bond O1W $2 – H2W $2 --- O44A also exists. This means that pairs of asymmetric units are doubly H-bonded to each other, with each being H-bonded to other asymmetric units as well. The overall result is a 2D Hydrogen bonded network extending throughout the crystal structure. Thus *cis*-[Ni(I-EtOH-*S,O*)(pyridine-*N*)$_2$]$_2$ is in fact a layered solid, with each layer of water-linked metallamacrocyclic adduct units coinciding with the [100] planes of the crystal. Figure 3.3.3(e) illustrates the joining of two neighbouring metallamacrocycles through a centrosymmetric pair of H-bond sets, with O1W and O44A atoms of other hydrogen bonded asymmetric units also shown.

Notice how these other O1W and O44 atoms are H-bonded to each other. A beautiful effect that results from this mode of hydrogen bonding is an almost perfect square formed by two O44A atoms and two O1W atoms of four different asymmetric units. The sides of the square are prescribed by H-bonds that are either 2.800Å or 2.745Å in length, while the internal angles are either 90.37° or the supplementary 89.63°. By virtue of their centrosymmetric relationship, these atoms O44A and O1W atoms must form a parallelogram, but it is by no means dictated that the two different H-bond distances should be so similar, or that the angles between atoms should be so close to 90°.

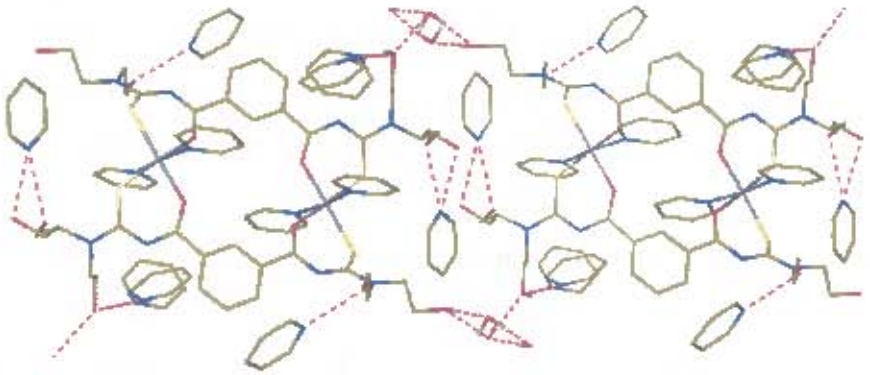

Figure 3.3.3(e). Two *cis*-[Ni(1-EtOH-*S,O*)(pyridine-*N*)$_2$]$_2$ molecules joined by a centrosymmetric pair of H-bond sets that form almost perfect squares. H-bonded atoms from other neighbouring asymmetric units also shown.

This square, being the meeting point of four asymmetric units is continuously reproduced throughout the two-dimensional network; each square is positioned with its centroid lying halfway along the b-axis of a unit cell, i.e. special position (0, ½, 0). However, the H-bonds that join neighbouring *cis*-[Ni(1-EtOH-*S,O*)(pyridine-*N*)$_2$]$_2$ molecules in the network are not parallel with the plane of such a square, but are aligned almost orthogonally with this plane (angle O42B – O1W – O44A $2: 111.62°). Thus, throughout the network, the planes of these squares are not parallel to the planes of the 2D network layers (the [100] planes). Figure 3.3.3(f) shows a portion of a single layer, viewed along the principal axial directions of the unit cell.

View (ii) of Figure 3.3.3(f) shows that channels of H-bonded squares exist throughout the layer. However these channels have a far smaller internal cross-sectional area than that of the central cavity within a metallamacrocyclic unit, and thus cannot be considered in terms of molecular containment or transport systems.

If one considers the H-bonded pyridine guests as being distinct from the water-linked layers of *cis*-[Ni(1-EtOH-*S,O*)(pyridine-*N*)$_2$]$_2$ molecules, then an interesting picture emerges. Two successive *cis*-[Ni(1-EtOH-*S,O*)(pyridine-*N*)$_2$]$_2$ layers could be considered to have a layer of pyridine guests sandwiched between them.

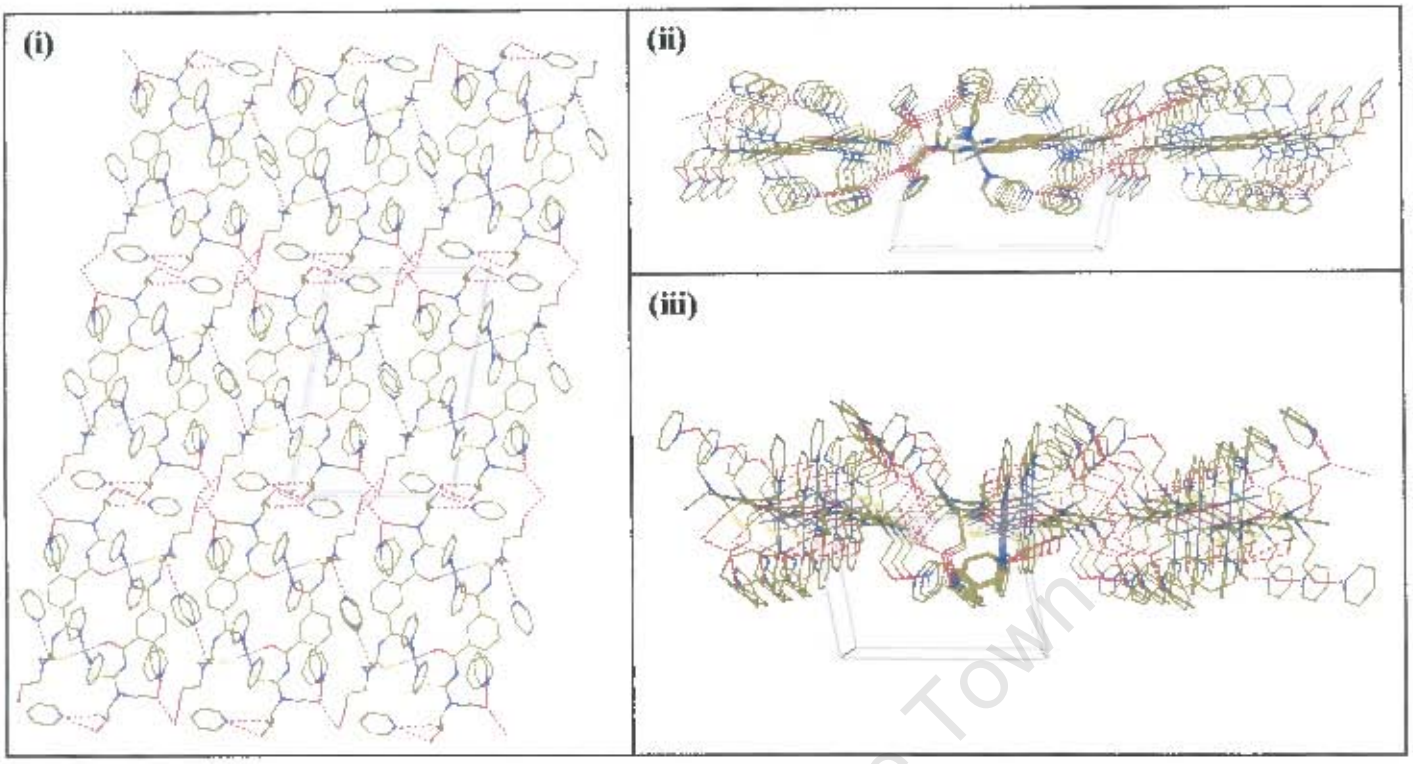

Figure 3.3.3(f). Fragment of the 2-dimensional H-bonded network of *cis*-[Ni(1-EtOH-*S,O*)(pyridine-*N*)$_2$]$_2$ viewed along the (i) [100], (ii) [010] and (iii) [001] directions

Figure 3.3.3(g) shows two such H-bonded layers, omitting the pyridine guests found between the layers. View (ii) of this figure shows that there is some interaction between metallamacrocyclic adducts of different layers. The interaction is a π-π stacking interaction between N5A pyridine ligands of asymmetric units related by symmetry operator (1 – x, 2 – y, 1 – z). The distance between the centroids of these ligands is found to be 4.530Å. This is out of the accepted range of 3.3 – 3.8Å for π-π interactions, but as one can see in the figure, the degree of eclipsing of the planes is quite low and only small regions of each of the pyridine rings (namely the C8A – C9A bonds) seem to be interacting. The distance between the centroids of the C8A – C9A regions of neighbouring asymmetric units is 3.627Å. Thus, despite only a small region of overlap, these two pyridine rings are certainly engaged in a π-π interaction. This type of interaction is blocked for the other pyridine ligands of the adduct because of the eclipsing of the pyridine rings by hydroxyethyl side branches as described above. On the opposite faces, these interacting pyridines seem to also be engaged in weak interactions with N7G pyridine guest molecules (both molecules of the

disordered pair). The shortest distance between atoms in the guest and the ligand is 3.60Å (C10A – C8G (x – 1, y, z)), which suggests that some interaction is occurring, although this interaction is considered very weak, because the planes of the N7G guests are not parallel to the planes of the pyridine ligands. The π-π interactions described here are illustrated in Figure 3.3.3(h) below.

The existence of π-π interactions between successive layers extends the 2D H-bonded network into a 3D supramolecular network. This *cis*-[Ni(I-EtOH-*S,O*)(pyridine-*N*)$_2$]$_2$ / H_2O system can be seen as a framework within which the pyridine guests are trapped, and further held in place by hydrogen bonding interactions with the respective hydroxyl groups. This conception of the crystal structure of *cis*-[Ni(I-EtOH-*S,O*)(pyridine-*N*)$_2$]$_2$ is therefore one in which the pyridine molecules can be said to occupy channels in the framework. These channels run continuously in the [010] and [001] directions throughout the entire crystal. (views (ii) and (iii) of Figure 3.3.3(g).)

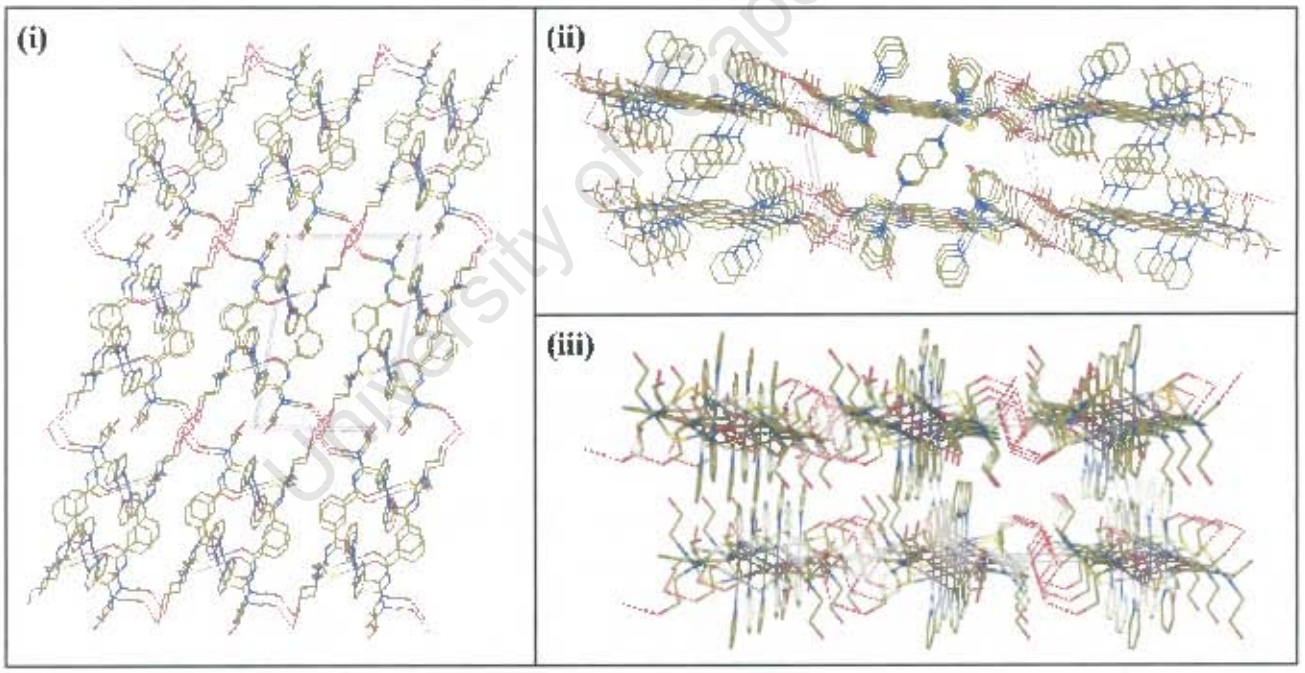

Figure 3.3.3(g). Two successive layers of water-linked H-bonded *cis*-[Ni(I-EtOH-*S,O*)(pyridine-*N*)$_2$]$_2$ units viewed along the (i) [100], (ii) [010] and (iii) [001] directions. Pyridine guests omitted to show channels through framework. Hydrogen atoms omitted; H-bonds shown as D --- A interactions.

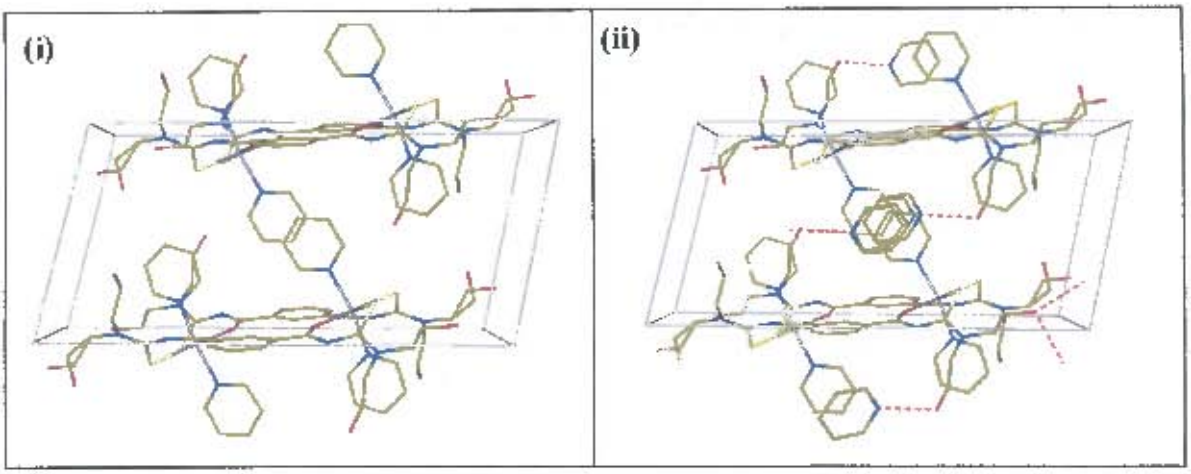

Figure 3.3.3(h). (i) π-π interactions between pyridine ligands of metallamacrocyclic units in different layers and (ii) between these ligands and nearby pyridine guests, forming channel walls in the supramolecular framework. Hydrogen atoms omitted; H-bonds shown as D — A interactions.

Figure 3.3.3(i) below shows the supramolecular framework in stick representation with the pyridine guest molecules in space filling representation. This figure gives a clear perspective of the manner in which the pyridine guests occupy the channels within the supramolecular framework. It can be seen that the channels permeate continuously throughout the crystal structure in the [010] and [001] directions. The channels in both directions are wide enough to accommodate two pyridine molecules abreast, but the guests fill the channel in a staggered manner. This can be seen most clearly in the 'top down' view normal to the [100] plane (i). Note that the N7G pyridines (the disordered pairs shown with no hydrogens) are considered part of the [010] channel walls due to their π-π interaction with the pyridine ligands.

An interesting feature revealed by the perspective in view (i) is that there are channels running diagonally through the crystal, wide enough to accommodate one pyridine molecule, but interrupted after every five pyridine guests by the pyridine ligands of a metallamacrocyclic unit. Thus the crystal structure could also be considered to contain parallel tube-like cavities filled with pyridine guests.

The final depictions of the crystal structure of *cis*-[Ni(1-EtOH-*S,O*)(pyridine-*N*)$_2$]$_2$ are the stereo packing diagrams shown in Figure 3.3.3(j), below. In this figure, the pyridine guests are colour coded in green and the hydrogen bonds between hydroxyl

groups and pyridine guests are not indicated, for the sake of clarity. The three views given in Figure 3.3.3(j) clearly show the channels in the supramolecular framework, occupied by the pyridine guests.

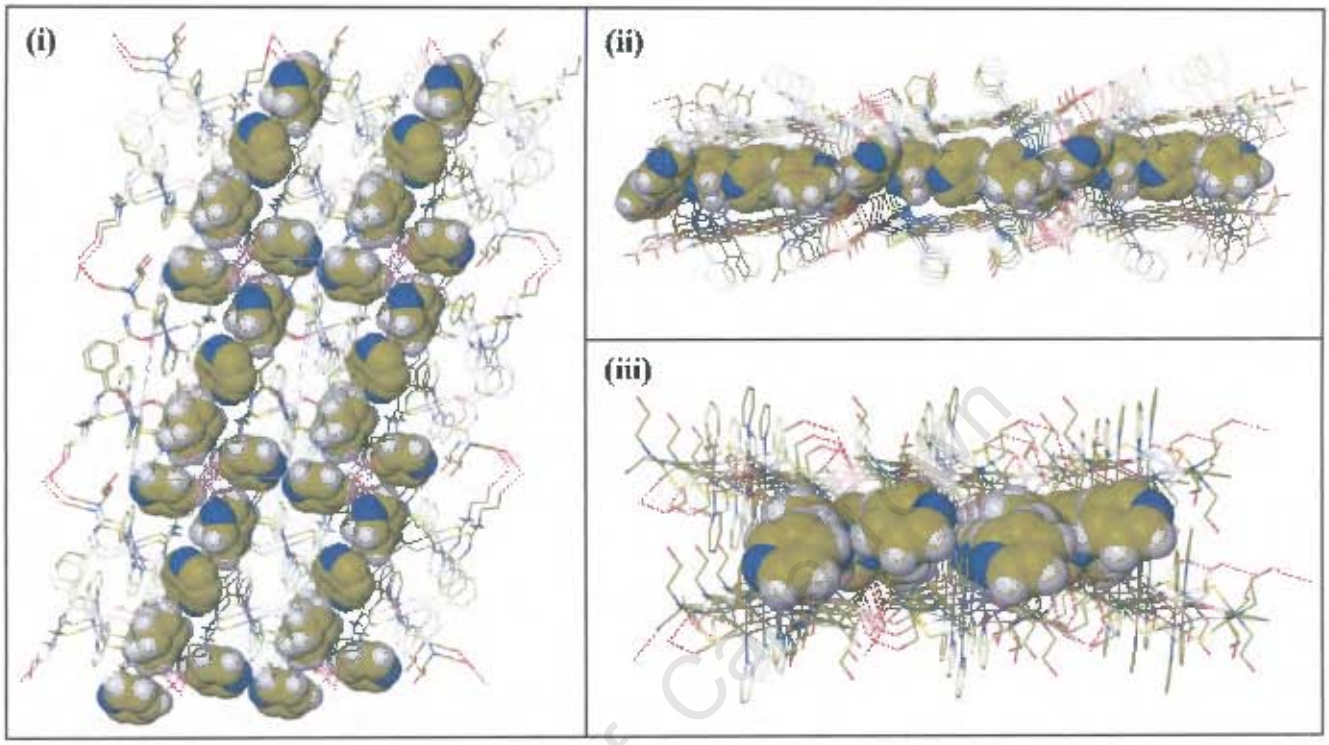

Figure 3.3.3(i). Pyridine guest molecules (space fill) held within a supramolecular framework of *cis*-[Ni(l-EtOH-*S,O*)(pyridine-*N*)$_2$]$_2$ and H_2O units (stick). Hydrogen atoms omitted; H-bonds shown as D — A interactions.

The crystal structure of *cis*-[Ni(l-EtOH-*S,O*)(pyridine-*N*)$_2$]$_2$ can be considered to be a supramolecular framework containing intersecting channels occupied with included pyridine guests. However, it must be remembered that the guests are held to the metallamacrocyclic units by forces that are as strong as those that form the 2-dimensional network layers. Furthermore, these hydrogen bonds are stronger than the π-π interactions that bind successive layers to each other. This structure can therefore be considered to be a layered solid.

However one wishes to construe this crystal structure, it is clear that it does comprise a supramolecular system of complexity belied by the low order of symmetry possessed by the structure. In many ways, this structure is far more complex than that of its parent ligand l-EtOH, but both ligand and adduct owe their complexities in part to the hydrogen bonding capability imparted to them by their hydroxyl groups.

Overall, the most fascinating aspect of the *cis*-[Ni(I-EtOH-*S,O*)(pyridine-*N*)$_2$]$_2$ crystal structure is that its manifestation as a true supramolecular network arises from the unintended presence of that small, initially undetected, and highly versatile water molecule.

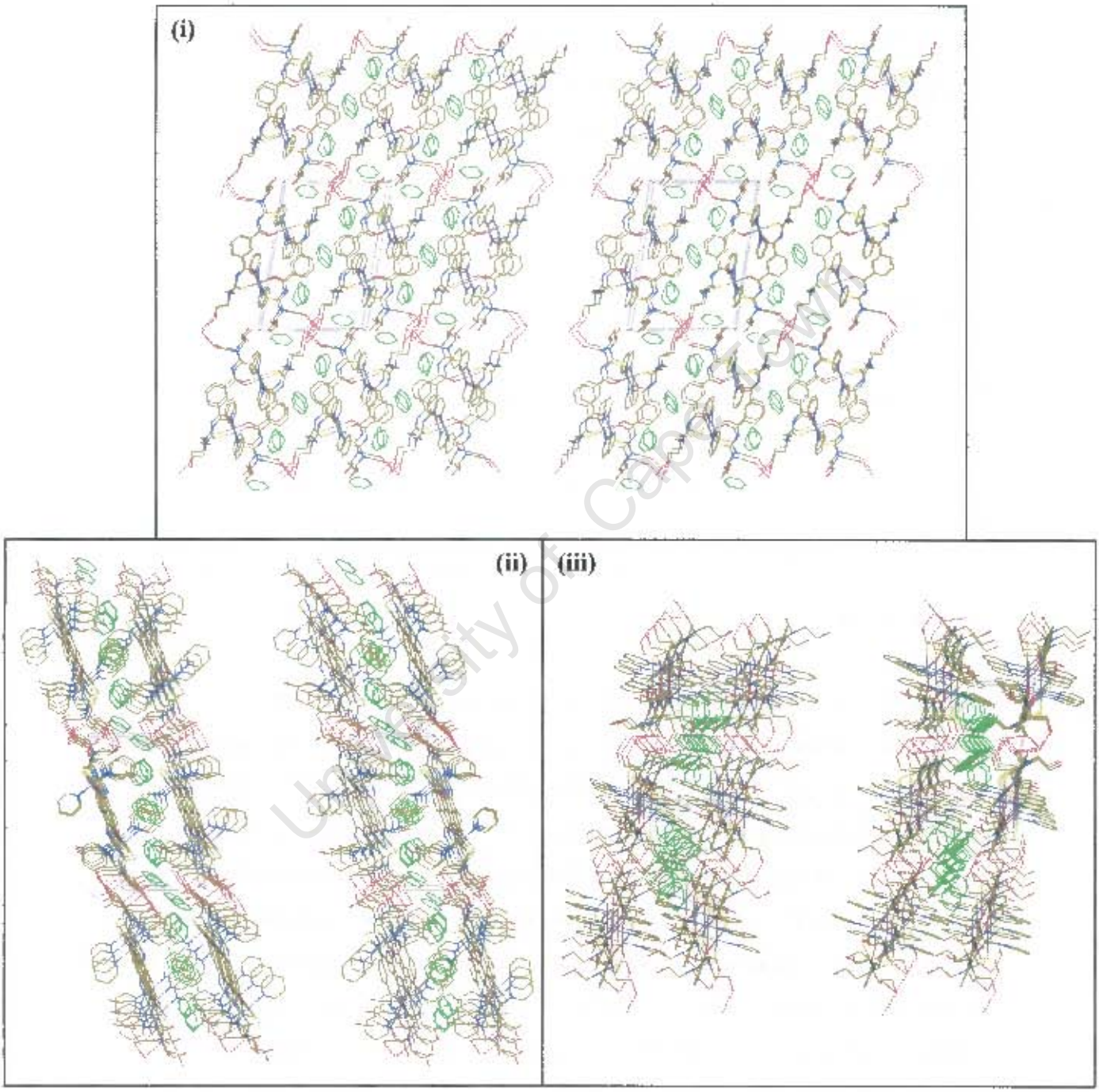

Figure 3.3.3(j). Stereo Packing Diagrams of the crystal structure of *cis*-[Ni(I-EtOH-*S,O*)(pyridine-*N*)$_2$]$_2$ viewed along the principle directions: [100] (i), [010], (ii) and [001] (iii). (Pyridine guest molecules coloured green. H-bonds between OH groups and pyridine guests omitted for clarity.)

3.3.4. [*Cis*-(tris-μ-(3,3,3',3'-tetraethyl-1,1'-terephthaloylbis(thioureato-*S,O*))-tri-nickel(II))-hexa(pyridine-*N*)] (*cis*-[Ni(T-Et-*S,O*)(pyridine-*N*)$_2$]$_3$)

The compound *cis*-[Ni(T-Et-*S,O*)(pyridine-*N*)$_2$]$_3$ is the only octahedral adduct of a 3:3 Ni metallamacrocycle. Thus far, it has been shown that there is much similarity between the 2:2 octahedral adducts *cis*-[Ni(I-Et-*S,O*)(pyridine-*N*)$_2$]$_2$, *cis*-[Ni(I-Et-*S,O*)(4DMAP-*N*)$_2$]$_2$ and *cis*-[Ni(I-EtOH-*S,O*)(pyridine-*N*)$_2$]$_2$. In this section it is shown that there are many substantial differences between the archetypal 2:2 octahedral adduct (*cis*-[Ni(I-Et-*S,O*)(pyridine-*N*)$_2$]$_2$) and its 3:3 analogue *cis*-[Ni(T-Et-*S,O*)(pyridine-*N*)$_2$]$_3$.

Thermal Analysis

The dark brown complex *cis*-[Ni(T-Et-*S,O*)]$_3$ was dissolved in pyridine, forming a yellow adduct in solution. Crystals grown from this solution were dark brown in colour. These *cis*-[Ni(T-Et-*S,O*)(pyridine-*N*)$_2$]$_3$ crystals were subjected to thermogravimetric analysis. The results of the TGA are represented graphically in Figure 3.3.4(a) below. The first thermal event is consistent with the loss of pyridine from the crystal.

Note that the graph indicates that mass loss is not arrested entirely at any point. This prevents the accurate calculation of the composition of the crystals. The three points shown at 195 °C, 237 °C and 270 °C correspond with the loss of 8, 8.5 or 9 pyridine molecules per metallamacrocycle respectively. There are only 6 sites available for the axial coordination of pyridine to the Ni(II) centres of the 3:3 metallamacrocycle. Thus there must also be 2 – 3 pyridine guest molecules per metallamacrocyclic unit in the crystal structure. Calculations are based on the remaining mass percentage following the first thermal event, which is attributed to the square planar metallamacrocycle to which the adduct gradually reverts upon removal from the mother liquor (see Experimental Section 2.3.4). The second thermal event, which has onset temperature of 286 °C, is consistent with the melting of the 3:3 metallamacrocycle *cis*-[Ni(T-Et-*S,O*)]$_3$ (Experimental Section 2.2.3).

As with the other metallamacrocyclic adduct crystals that were grown in pyridine (*cis*-[Ni(I-Et-*S,O*)(pyridine-*N*)$_2$]$_2$ and *cis*-[Ni(I-EtOH-*S,O*)(pyridine-*N*)$_2$]$_2$), there is difficulty in resolving the mass loss into two events, the first attributed to the loss of the guests and the second attributed to the loss of ligands. In this case, the total mass loss – which must occur by way of at least two separate processes – appears as a single thermal event.

The mass loss of pyridine from this adduct continues to higher temperatures than those observed for the 2:2 metallamacrocyclic adducts. This could indicate a stronger binding of the coordinated pyridines to the nickel(II) centres in this complex, or possibly a different diffusivity of the pyridine out of the lattice

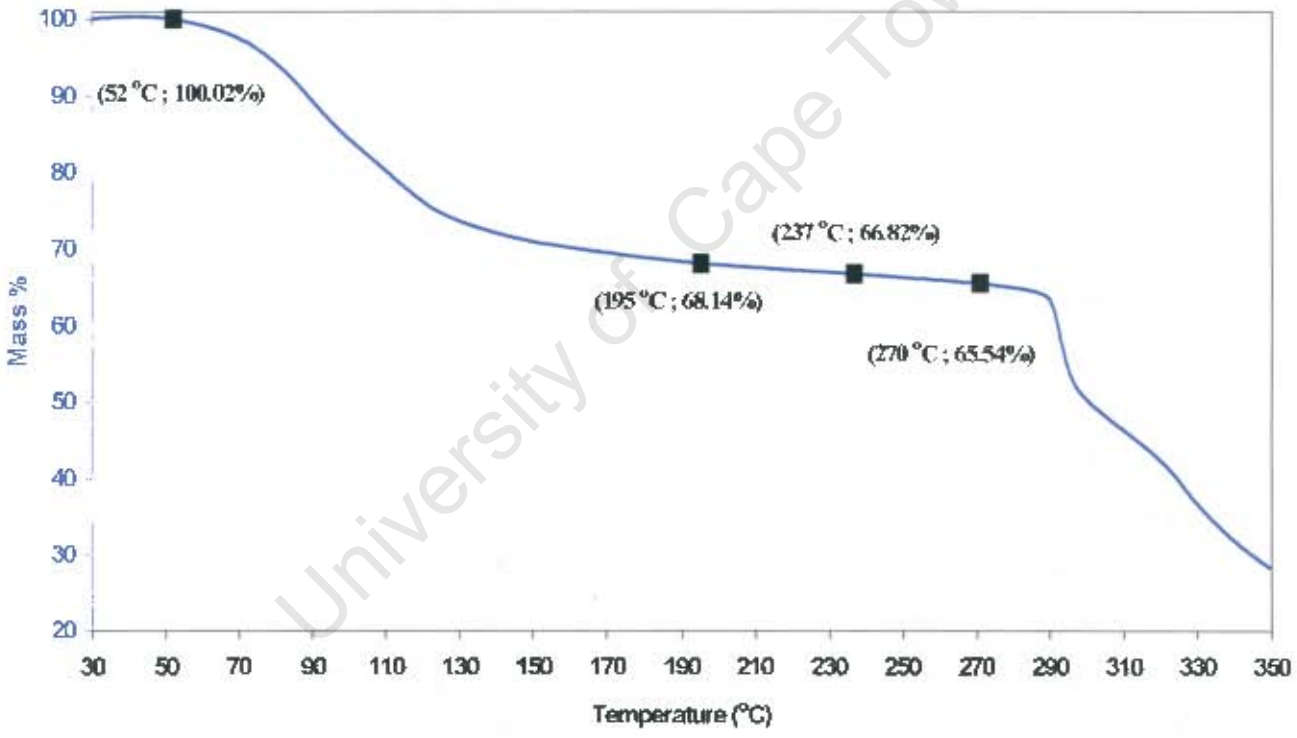

Figure 3.3.4(a) Graph of TGA results for *cis*-[Ni(T-Et-*S,O*)(pyridine-*N*)$_2$]$_3$

The crystal structure of *cis*-[Ni(T-Et-*S,O*)(pyridine-*N*)$_2$]$_3$ was elucidated by single crystal diffractometry. The results correspond well with the TGA results, but reveal far more than the chemical composition of the *cis*-[Ni(T-Et-*S,O*)(pyridine-*N*)$_2$]$_3$ crystal, including the fact that this compound is of the form *cis*-[Ni(T-Et-*S,O*)(Pyridine)$_2$]$_3$.2.5(Pyridine). In other words a total of 8.5 pyridines per metallamacrocycle are to be found in the crystal structure.

Single Crystal Diffractometry

Table 3.3.4(b). Crystal Data and Refinement Parameters for *cis*-[Ni(T-Et-*S,O*)(pyridine-*N*)$_2$]$_3$. 2.5(pyridine)

Molecular Formula	$C_{84}H_{102}N_{12}O_6S_6Ni_3 \cdot 2½(C_6H_6)$ *
Formula Weight (g.mol^{-1})	2023.60
Temperature (K)	173
Wavelength (Å)	0.71070
Crystal System	Monoclinic
Space Group	$P2_1/n$
a (Å)	16.4822(2)
b (Å)	27.7131(3)
c (Å)	22.9061(3)
$\alpha = \gamma$ (°)	90
β (°)	95.793 (1)
Volume (Å^3)	10409.5(2)
Z	4
Calculated Density (g.cm^{-3})	1.291
μ (mm^{-1})	0.717
F(000)	4260
Crystal Size	0.25 x 0.15 x 0.07 mm
θ Range Scanned (°)	1.63 – 25.98
Index Range	$-20 \leq h \leq 19$, $-33 \leq k \leq 31$, $-26 < l < 28$
No. Reflections Collected	48083
No. Unique Reflections	30810 [R(int) = 0.0379]
Completeness	98.5 %
Refinement Method	Full-matrix-block L.S. on F^2
Data / Restraints / Parameters	30810 / 2 / 2354
Goodness-of-fit on F^2	0.952
Final R Indices [$I>2\sigma(I)$]	$R_1 = 0.0533$, $wR_2 = 0.1119$
R Indices (all data)	$R_1 = 0.0863$, $wR_2 = 0.1263$
Largest Diff. Peak and Hole	0.941 and -0.595 e. Å^{-3}

* The pyridine guests were modelled as C_6H_6, as the locations of the nitrogens could not be determined.

Cis-[Ni(T-Et-*S,O*)(pyridine-*N*)$_2$]$_3$ crystallises in the space group P*n*. Unlike the space groups of the 2:2 metallamacrocycle and adducts P*n* is non-centrosymmetric. This reflects a fundamental difference in the point group symmetries of the 2:2 and 3:3 metallamacrocyclic molecules – 2:2 complexes possess a centre of symmetry, while 3:3 complexes do not. In the case of the 2:2 complexes, the asymmetric units invariably consisted of half a metallamacrocycle, with the other half generated via a centre of symmetry. It is evident that the point group symmetries of these complexes play a major role in determining the space group symmetries of their crystal structures. The asymmetric unit of this 3:3 structure consists of two metallamacrocyclic adduct molecules and 5 included pyridine guests. The P*n* space group results in a total of 4 metallamacrocyclic adduct molecules per unit cell. Since the *cis*-[Ni(T-Et-*S,O*)(pyridine-*N*)$_2$]$_3$ molecule is quite large, the unit cell containing four such molecules accompanied by 10 pyridine guests must accordingly be large; the volume of the unit cell is greater than 10 000 Å^3, whereas none of the 2:2 adducts' unit cells exceed 4000 Å^3. Figure 3.3.4(b) shows the atom labelling of the asymmetric unit in two pictures: one omitting all coordinated and included pyridines, and the other with all pyridines shown and labelled. Table 3.3.4(c) lists the average bond lengths around the nickel(II) centres and within the chelate rings of the two metallamacrocyclic adducts (which are referred to as ABC and DEF respectively).

Table 3.3.4(c) Comparison of important bond lengths of ABC and DEF adduct molecules in *cis*-[Ni(T-Et-*S,O*)(pyridine-*N*)$_2$]$_3$ crystal structure

Bond Type	Average Bond Lengths (Å)	
	ABC	DEF
C=O	1.26(1)	1.26(1)
C(O)=N	1.33(1)	1.32(1)
C(S)=N(CO)	1.35(1)	1.35(1)
C=S	1.72(1)	1.72(1)
C(S)=NR2	1.35(1)	1.35(2)
O – Ni	2.03(1)	2.03(4)
S – Ni	2.39(3)	2.38(2)
N – Ni	2.14(2)	2.15(3)

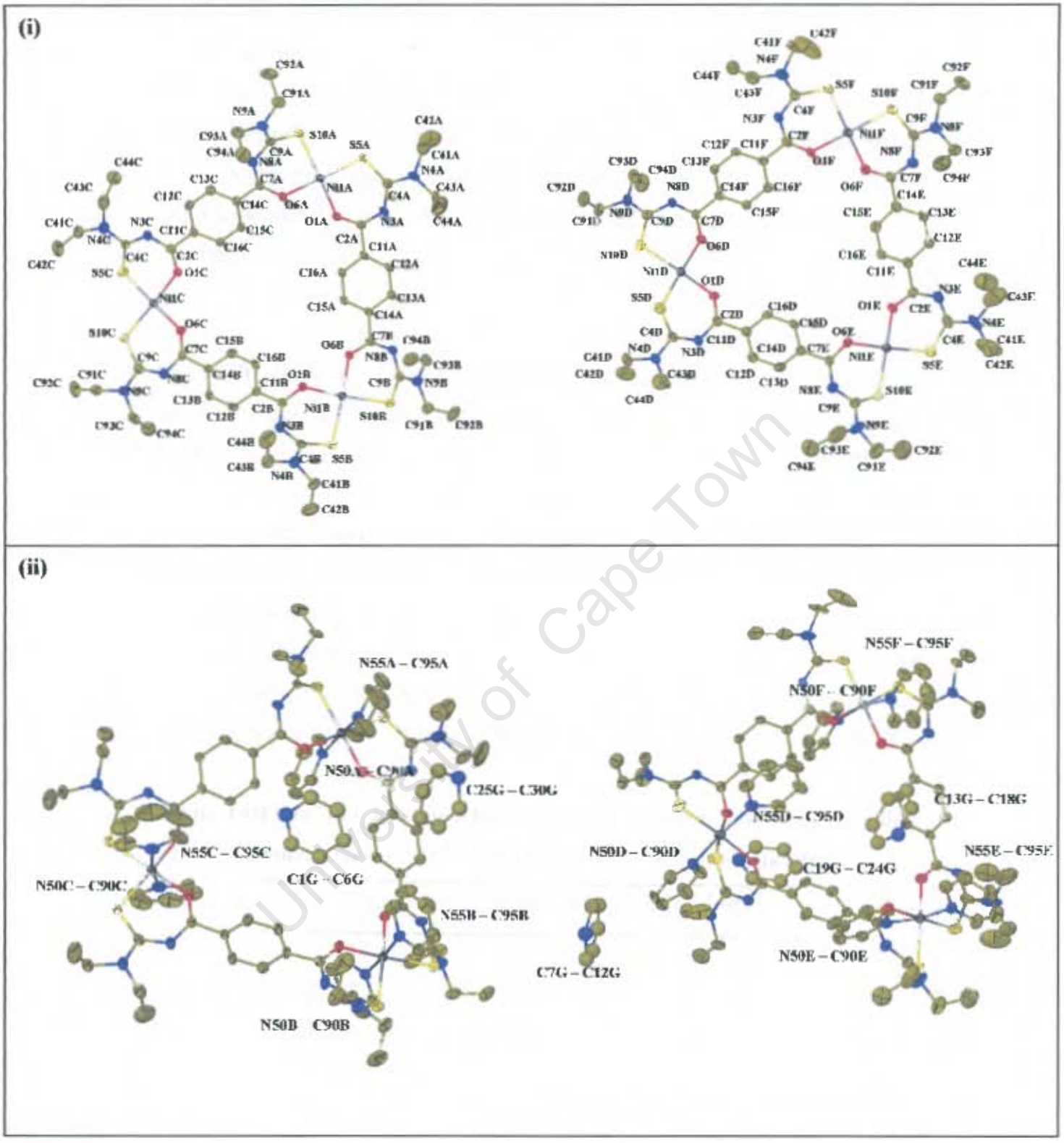

Figure 3.3.4(b). Asymmetric unit contents of *cis*-[Ni(T-Et-*S,O*)(pyridine-*N*)$_2$]$_3$: (i) Pyridine ligands and guests omitted with metallamacrocyclic atom labels indicated, (ii) Pyridine ligands and guests shown and labelled. In each pyridine guest molecule a nitrogen atom is indicated in an arbitrary position – despite being modelled as a carbon. Thermal ellipsoids shown at 50% probability.

The important bond lengths in the two adduct molecules, listed in Table 3.3.4(c), are almost identical. These values are also similar to the bond lengths found for the 2:2 Ni adducts, yet it appears that the two *cis*-[Ni(T-Et-*S,O*)(pyridine-*N*)$_2$]$_3$ molecules assume very different conformations. This is best observed by comparing bond angles, and plane angles. Table 3.3.4(d) lists the bond angles around the Ni(II) centres. While there are far more unique angles in the *cis*-[Ni(T-Et-*S,O*)(pyridine-*N*)$_2$]$_3$ crystal structure than there are in any of the structures of the 2:2 adducts, a perusal of Table 3.3.4(d) yields the following general results.

The *cis*- angles within the *S,O* square planes around the nickel centres are close to 90° (less than 2° deviation) with the exception of the angles O1B – Ni1B – O6B, S5 – Ni1 – S10 and O1E – Ni1E – O6E, which each deviate by more than 3° from orthogonality. The *trans*- angles within the *S,O* square planes deviate from linearity by as little as 0.6° and as much as 5°. The pyridine ligands are axially coordinated to the nickel atoms in such a way that the N – Ni – O and N – Ni – S bond angles are in some cases close to 90° and in other cases deviate by as much as 5.5°. The N50 – Ni1 – N55 bond angles are in most cases close to 170°, indicating that the pyridine ligands are tilted in towards the centre of the metallamacrocyclic cavity. Overall these results do not differ greatly from the bond angles that were observed for the 2:2 Ni adducts.

The main difference in appearance between the 2:2 and 3:3 complexes actually arises from the difference in plane angles. More specifically, in each of the 2:2 adducts, the planes of the two benzoyl rings were found to be parallel, and the two benzoyl planes were found to be virtually coplanar. These results are a consequence of the centrosymmetric nature of the 2:2 metallamacrocyclic complexes. Since the *cis*-[Ni(T-Et-*S,O*)(pyridine-*N*)$_2$]$_3$ molecule lacks this symmetry, it is not surprising that the benzoyl ring planes deviate from coplanarity or even parallelism. Figure 3.3.4(c) shows a stick representation of the two adduct molecules, ABC and DEF, of the *cis*-[Ni(T-Et-*S,O*)(pyridine-*N*)$_2$]$_3$ asymmetric unit. The deviation from coplanarity of the benzoyl rings in the molecule can clearly be seen. Table 3.3.4(e) lists the angles between the benzoyl ring planes in each of the *cis*-[Ni(T-Et-*S,O*)(pyridine-*N*)$_2$]$_3$ asymmetric unit molecules. Note that the root mean square deviation from planarity is no greater than 0.018Å in any of these benzoyl rings and in most cases is significantly lower than this.

Table 3.3.4(d). Comparison of bond angles around the six Ni(II) centres of the two asymmetric unit molecules of *cis*-[Ni(T-Et-*S,O*)(pyridine-*N*)$_2$]$_3$

Bond Type	*cis*-[Ni(T-Et-S,O)(pyridine-N)$_2$]$_3$ Molecule					
	ABC			DEF		
	Molecule Segment					
	A	B	C	D	E	F
	Cis- Angles (°)					
O1 – Ni1 – O6	88.38	86.64	91.22	88.84	87.18	89.59
O1 – Ni1 – S5	90.56	90.91	88.79	90.42	90.39	91.46
O6 – Ni1 – S10	90.25	88.54	90.64	92.84	91.2	90.5
S5 – Ni1 – S10	90.85	93.89	89.38	88.18	91.24	88.45
N50 – Ni1 – O1	88.34	87.08	85.34	85.88	86.69	86.67
N50 – Ni1 – O6	84.35	87.95	86.8	90.54	84.83	84.54
N55 – Ni1 – O1	86.5	90.68	89.5	87.79	87.21	88.20
N55 – Ni1 – O6	86.99	87.95	85.09	82.68	89.3	85.19
N50 – Ni1 – S5	93.06	91.06	91.86	94.44	92.37	95.43
N50 – Ni1 – S10	92.61	91.11	96.41	90.94	93.45	92.72
N55 – Ni1 – S5	95.5	92.96	91.84	92.26	93.25	94.93
N55 – Ni1 – S10	92.37	90.78	93.28	95.55	92.49	92.43
	Trans- Angles (°)					
O1 – Ni1 – S10	178.26	174.91	177.51	176.42	178.35	179.37
O6 – Ni1 – S5	177.23	177.4	178.67	174.91	176.39	178.95
N50 – Ni1 – N55	170.03	175.43	169.7	170.8	171.7	168.54

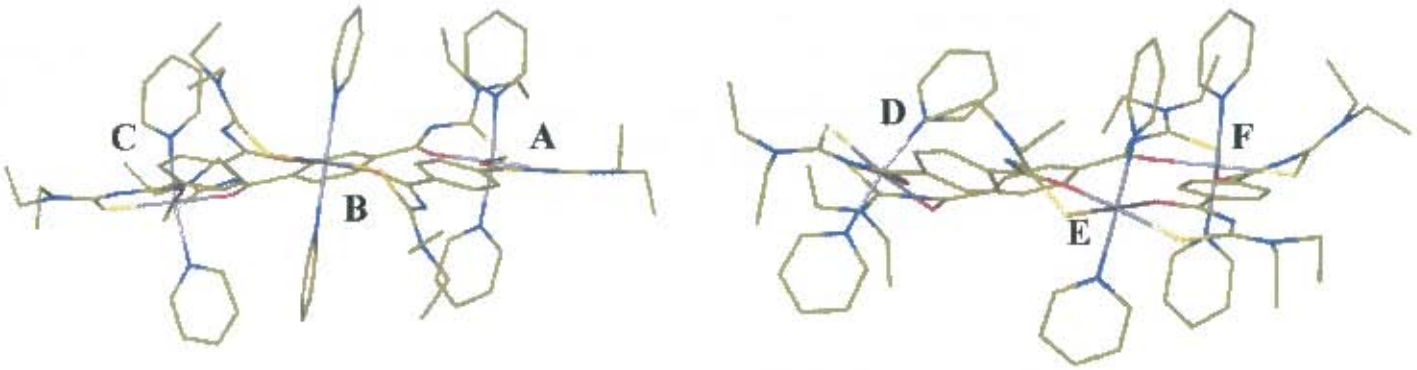

Figure 3.3.4(c). Stick representation of the two *cis*-[Ni(T-Et-*S,O*)(pyridine-*N*)$_2$]$_3$ molecules in the asymmetric unit (with sections of molecules labelled).

This tilting of the benzoyl rings makes the overall conformations of the metallamacrocyclic rings far from planar. The metallamacrocycles could even be said to be slightly reminiscent of the bowl-shaped calixarenes.

The *S,O*- square planes around the Ni (II) centres are also tilted with respect to each other. Table 3.3.4(f) lists the angles between the *S,O*- nickel square planes. In both *cis*-[Ni(T-Et-*S,O*)(pyridine-*N*)$_2$]$_3$ molecules, two of the three Ni square planes are approximately parallel – having an angle of less than 10° between them – while the third square plane lies in an oblique orientation with respect to the other two. In molecule ABC, square plane C makes angles of roughly 20° with the A and B square planes, while in molecule DEF, square plane D makes angles larger than 30° with each of the other square planes. This causes the D pyridine ligands to have very pronounced tilts (one toward the central cavity and the other outward.)

It is clear therefore, that the conformations of the *cis*-[Ni(T-Et-*S,O*)(pyridine-*N*)$_2$]$_3$ molecules are very different from those of their 2:2 analogues, with the larger metallamacrocycle apparently allowed greater conformational deviation from planarity.

Table 3.3.4(e). List of angles between benzoyl ring planes within *cis*-[Ni(T-Et-*S,O*)(pyridine-*N*)$_2$]$_3$ molecules of asymmetric unit

Benzoyl Ring Planes	Plane Angles (°)
Molecule ABC	
A - B	35.24
A - C	26.12
B - C	42.99
Molecule DEF	
D - E	34.52
D - F	47.70
E - F	16.78

Table 3.3.4(f). List of angles between *S,O*- Ni square planes within *cis*-[Ni(T-Et-*S,O*)(pyridine-*N*)$_2$]$_3$ molecules of asymmetric unit

S,O- Ni square planes	Plane Angles (°)
Molecule ABC	
A - B	5.12
A - C	22.29
B - C	19.34
Molecule DEF	
D - E	31.61
D - F	35.41
E - F	8.46

Two pyridine guests are situated in close proximity to each of the *cis*-[Ni(T-Et-*S,O*)(pyridine-*N*)$_2$]$_3$ molecules, while a fifth guest molecule lies approximately halfway between them. It must be emphasised that for each of these guests, it is not possible to determine in which atomic position the nitrogen atom lies, thus the atoms arbitrarily indicated as nitrogen in figure 3.3.4(b(ii)) are actually modelled as carbons in the crystal structure. It must also be mentioned that the C25G pyridine proved difficult to refine anisotropically. The other guest molecules could be refined anisotropically with very little trouble.

The guest molecules appear to be scattered rather haphazardly around the *cis*-[Ni(T-Et-*S,O*)(pyridine-*N*)$_2$]$_3$ molecules, but closer inspection shows that the guest sites have something in common – with one exception. That is the C7G pyridine, which is situated too far from either *cis*-[Ni(T-Et-*S,O*)(pyridine-*N*)$_2$]$_3$ molecule to engage in van der Waals interactions with the hosts. The other four guests are much closer to the various aromatic rings of either host molecule, allowing π-π interactions to occur. The C25G pyridine appears to be involved in edge-to-face type interactions with the C11A – C16A benzoyl ring as well as the N55A and N55B pyridine ligands. The other three pyridine guests are located directly above or below the central cavities of the *cis*-[Ni(T-Et-*S,O*)(pyridine-*N*)$_2$]$_3$ metallamacrocycles, surrounded on three sides by pyridine ligands. One could consider these three guests (C1G, C13G and C19G) as being contained within the host molecules. This is a shift from the type of host-guest interactions observed in the 2:2 metallamacrocyclic adducts' crystal structures. In each previous case, no guest molecules were held within the cavity of the host molecule. This difference in host-guest behaviour between 2:2 and 3:3 complexes can be attributed to the increased size of the 3:3 complex.

Figure 3.3.4(d) shows the two *cis*-[Ni(T-Et-*S,O*)(pyridine-*N*)$_2$]$_3$ molecules in space-filled representation. Two perspectives are shown, one viewing down onto the N50 pyridine ligands and the other down onto the N55 pyridines – i.e. views from 'above' and 'below' the metallamacrocyclic rings. One picture showing the guests and one omitting the guests is shown from each perspective. These views clearly indicate a central cavity running through the molecules. This cavity consists of two different zones – the outer zone between the three-pyridine ligands of each face, and the inner zone passing through the centre of the metallamacrocycle. It can be seen that in both

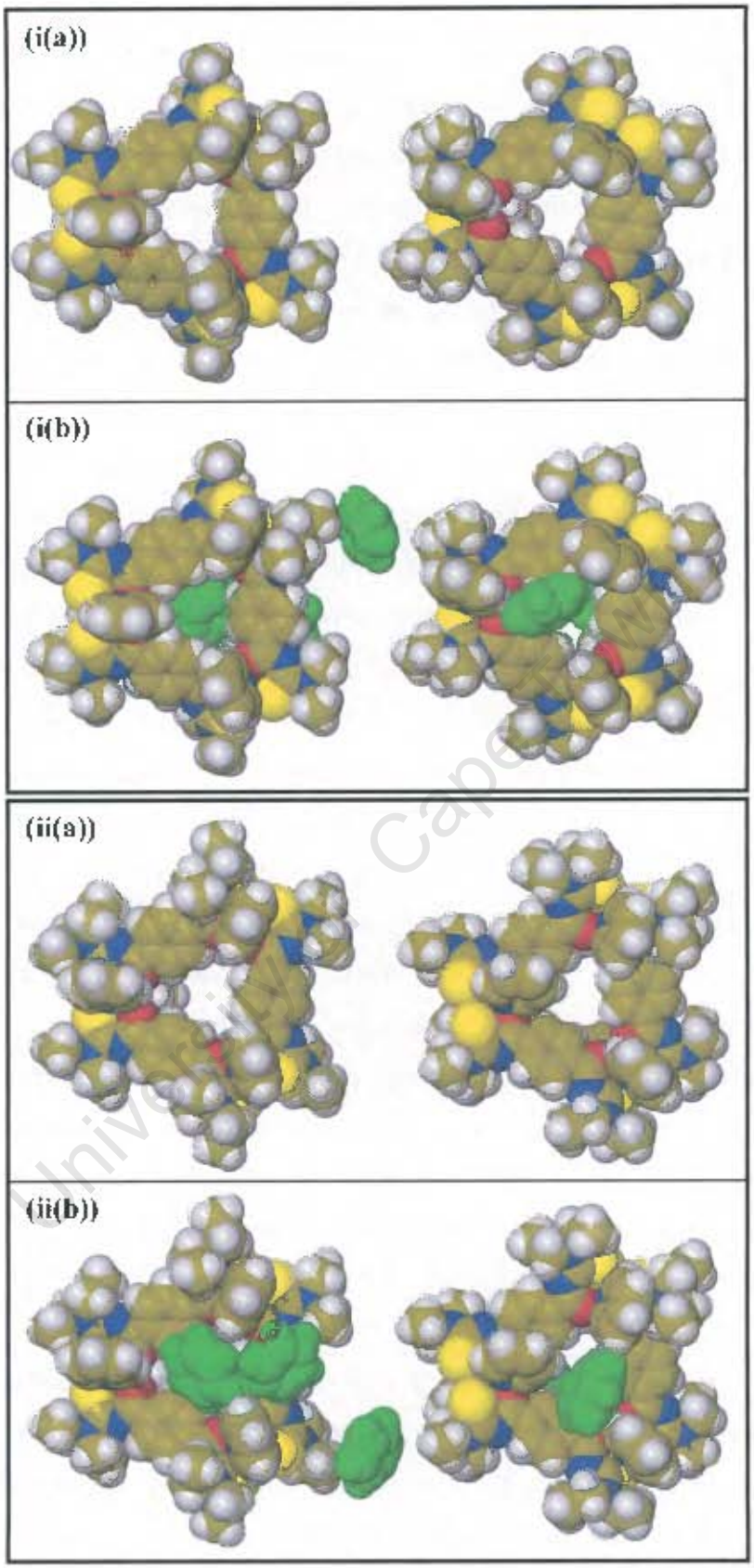

Figure 3.3.4(d). Spacefill representations of *cis*-[Ni(T-Et-*S,O*)(pyridine-*N*)$_2$]$_3$ metallamacrocycles viewed down onto N50 faces (i) and N55 faces (ii) with pyridine guests omitted (a) and shown in (spacefill) colour coded in green (b).

molecules, there is space in the outer zones of the cavity to admit a guest molecule of small size such as pyridine. However, it can also be seen that the inner zone of the cavity is too small to allow the admission of a pyridine molecule. Furthermore, it should be noted that since the pyridine ligands do not form a continuous ring, larger guest molecules can be admitted into the outer cavity zones with part of the guest protruding through a gap between the pyridine ligands, if oriented correctly. This would not be possible for the inner cavity zone. Thus, the inner cavity zone is much less inclusive than the outer zones.

An indication of the size of the outer zones of the cavity can be given by the distances between the nickel atoms in each molecule. In each case this distance is greater than 10.5 Å. For the purposes of a *rough* calculation, one may consider the area of the outer cavity portions of the metallamacrocycle to be a circle that touches each of the three nickel atoms – i.e. the circumscribed circle of an equilateral triangle with sides 10.5Å. Some quick trigonometric manipulation reveals that the radius of such a circle must equal $10.5Å / (\sqrt{3}) \approx 6.0Å$. Thus, one can state that the outer portions of the cavity might be able to admit molecules with a diameter of around 12Å or less. Similarly, the distances between centroids of the benzoyl hydrogen atoms H15 and H16 of each T-Et ligand give an indication of the size of the inner cavity zone. The average distance is approximately 4.9 Å. If we consider the area of the inner cavity zone to be a circle that touches each of the three H15 – H16 bond centroids – i.e. the circumscribed circle of an equilateral triangle with sides 4.9Å, it can be shown that the radius of such a circle will be $4.9Å / (\sqrt{3}) \approx 2.8Å$. Thus, the inner zone of the cavity might admit molecules with a diameter of about 5.6Å or less.

The distances between diametrically opposed hydrogen atoms in each of the pyridine guests are found in this crystal structure to be in the range 4.4 – 4.7Å. If one adds the van der Waals radii of the atoms to this distance (the accepted value for the van der Waals radius of hydrogen is 1.2Å.[109]), one obtains a value that roughly represents the diameter of a pyridine molecule. This value is 6.8 – 7.1Å - small enough to fit into the outer cavity zone, but larger than the inner cavity diameter. Thus pyridine guests are admitted into the outer zones, but not the inner zones of each metallamacrocyclic adduct molecule. This 'back-of-the-envelope' calculation based on the crystal structure data is illustrated in figure 3.3.4(e).

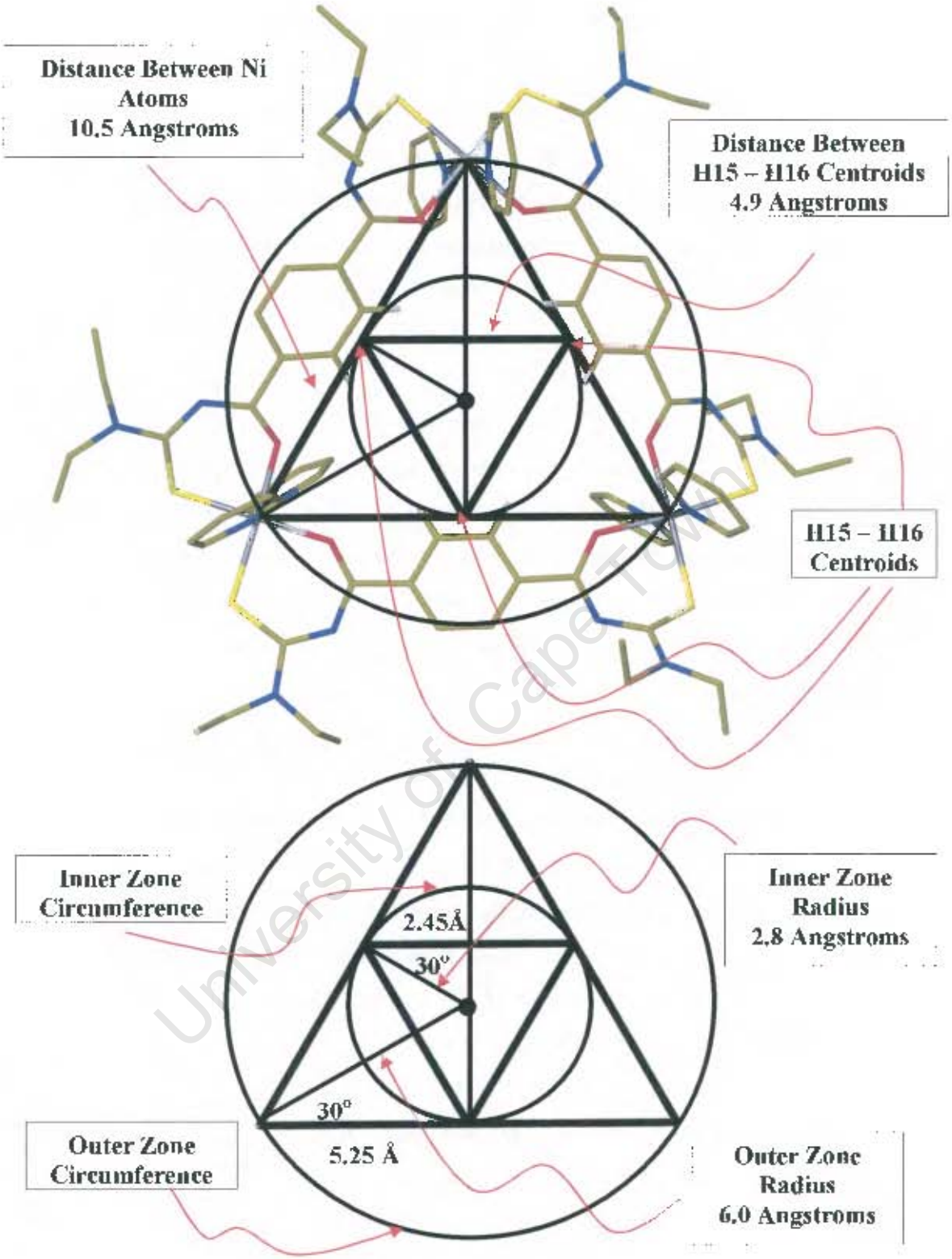

Figure 3.4.4(e). Geometric analysis of size of inner and outer zones of the central cavity within *cis*-[Ni(T-Et-*S,O*)(pyridine-*N*)$_2$]$_3$ molecules.

The packing of the unit cell has a scattered appearance that is due to the fact that the asymmetric unit consists of two adduct molecules and five guest molecules that are all symmetrically unrelated. Were the asymmetric unit to consist of only one molecule (or, as is the case for the 2:2 complexes, half a molecule), there would be a greater semblance of order in the packing diagrams. The very large size of the adduct molecules also obscures the ordered nature of the crystal packing. In the crystal structure of I-Et, which had an asymmetric unit consisting of two molecules, one can make out the order in the packing diagrams. Figure 3.3.4(f) illustrates the packing of the crystal structure with stereo diagrams viewed down the three principle directions of the monoclinic unit cell.

The diagrams do not show much more than has already been discussed. Essentially, the *cis*-[Ni(T-Et-*S,O*)(pyridine-*N*)$_2$]$_3$ crystal structure consists of a large unit cell (16 x 28 x 23 Å^3), containing two very large molecules and five smaller guests. The size of the molecule and the low order of symmetry give rise to this situation, which complicated the elucidation of this structure.

Overall, the crystal and molecular structure of *cis*-[Ni(T-Et-*S,O*)(pyridine-*N*)$_2$]$_3$ resembles that of its 2:2 analogue in many ways, but with two major differences. Firstly, there is a lack of inversion symmetry in the molecule, which in turn results in the lack of inversion symmetry in the crystal structure of *cis*-[Ni(T-Et-*S,O*)(pyridine-*N*)$_2$]$_3$. Secondly, the *cis*-[Ni(T-Et-*S,O*)(pyridine-*N*)$_2$]$_3$ is able to include guests within the centre of the molecule due to the increased molecular size in going from 2:2 to 3:3. This gives rise to a greater number of guest molecules being included in the *cis*-[Ni(T-Et-*S,O*)(pyridine-*N*)$_2$]$_3$ crystal structure. This mode of guest inclusion also suggests that a larger metallamacrocycle (e.g. 4:4 or 6:6) should be able to admit even larger guests internally and possibly allow molecules to pass right through the central cavity.

These properties, used in combination with the coordinative polymerisation of metallamacrocycles could give rise to new supramolecular materials with many interesting properties and applications.

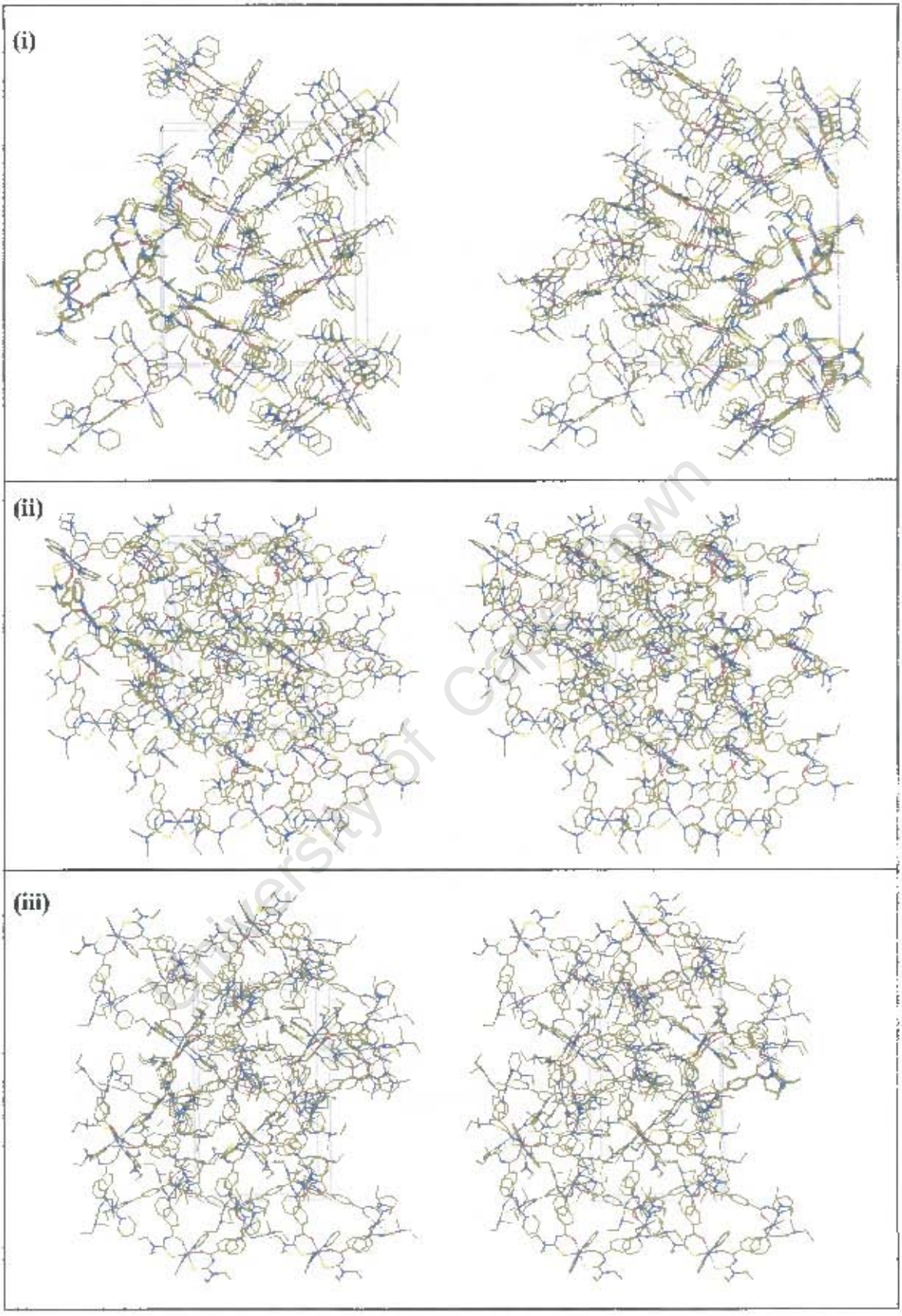

Figure 3.3.4(f). Stereo packing diagrams of *cis*-[Ni(T-Et-*S,O*)(pyridine-*N*)$_2$]$_3$ crystal structure viewed down [100] (i), [010] (ii) and [001] (iii) directions.

3.4 Coordination Polymers

Having shown that the 2:2 and 3:3 Ni(II) metallamacrocycles readily undergo the axial addition of various monodentate pyridines, the next step in a synthetic scheme is the use of bidentate bridging ligands to link metallamacrocyclic units together, and thus give rise to coordination polymers.

The compounds selected for this purpose were: 4,4-bipyridine, pyrazine, 1,2-bis(4-pyridyl)ethane and 1,2-di(4-pyridyl)ethylene. In Section 1.2.2 above, the merits of such compounds as exo-bidentate ligands were discussed and several references to their use given. The structures of these four compounds are represented in Figure 3.4(a).

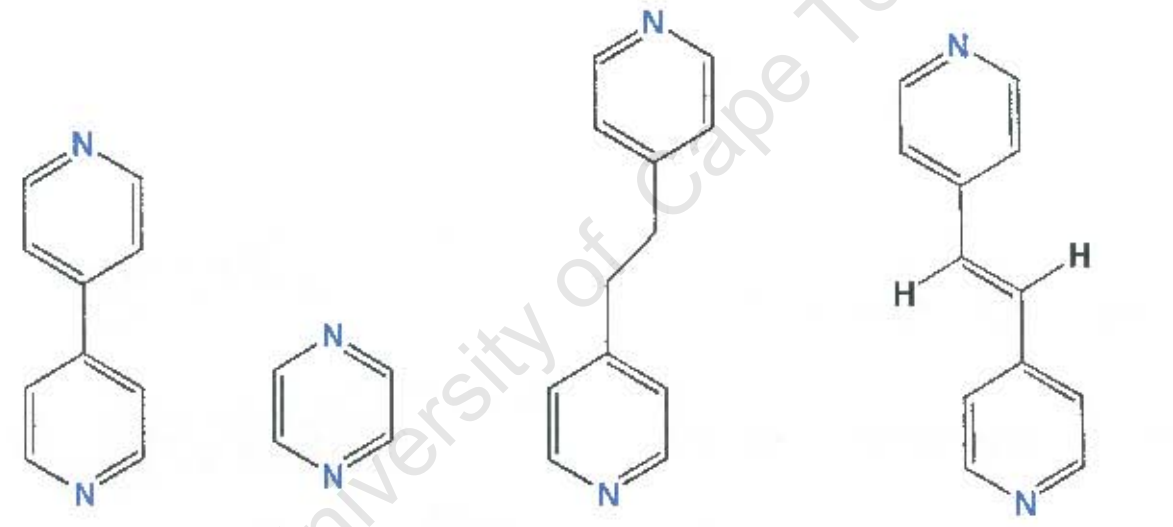

Figure 3.4(a). Structures of compounds used as exo-bidentate ligands to link metallamacrocycles into coordination polymers

As long as the axially coordinated ligand is bidentate, it is expected that the product should be polymeric, but various orientations of the metallamacrocyclic units can conceivably give rise to a number of different types of polymeric structure ranging from a simple linear 1D polymer to a complex 2D array. Three diagrams of possible polymeric structures based on the metallamacrocycle *cis*-[Ni(1-Et-*S*,*O*)]$_2$ are given in Figure 3.4(b).

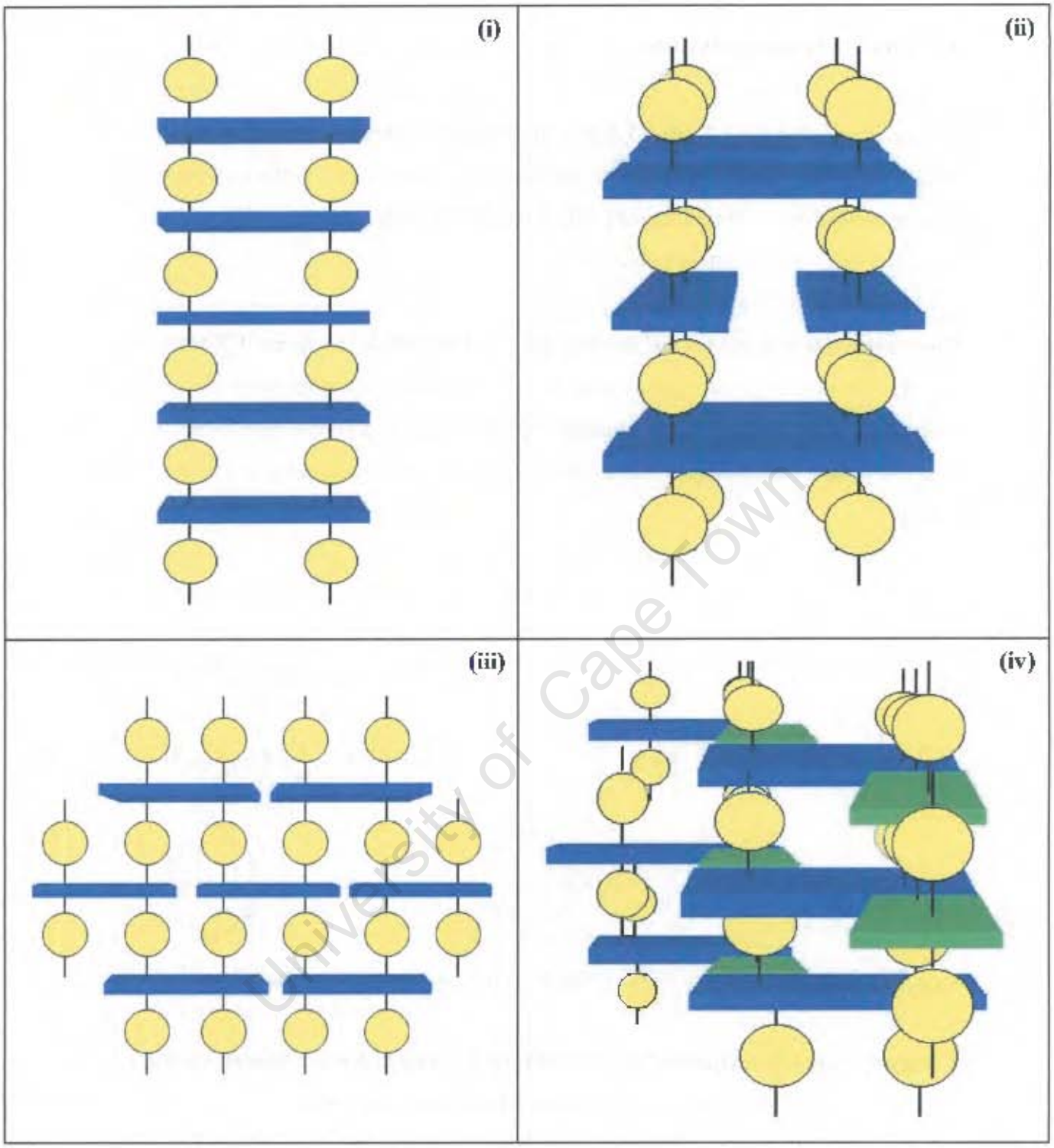

Figure 3.4(b). Schematic diagram of possible polymeric structures based on *cis*-[Ni(I-Et-*S,O*)]$_2$: a simple 1D 'ladder' structure (i), a more complex 1D polymer (ii) a 2D polymeric array (iii) and a more complex 2D polymer (iv).

In the first figure (i), the metallamacrocycles are shown stacking directly above each other, with their major planes in parallel alignments, linked together with two bridging ligands. In the second figure (ii), each layer consists of two

metallamacrocycles, aligned laterally in parallel orientations, with each successive layer stacked one upon the next, with the metallamacrocycles' major planes rotated through 90°. This allows each metallamacrocycle to be connected to 2 metallamacrocycles on either face. The result is a 1D polymeric chain with a greater volume enclosed between each layer, which would possibly give the structure the ability to incorporate a number of guest molecules between layers.

In the third figure (iii), the metallamacrocycles are aligned in parallel orientations but in a staggered arrangement, so that each is connected to two others on either face. The result is an array in which each layer can extend laterally while successive layers stack upon each other.

The final figure (iv) shows a more complex 2D polymeric array. Each layer consists of laterally aligned metallamacrocycles with their major planes set at right angles to create a 'zigzag' line. Successive layers are aligned in a staggered manner with respect to each other so that each metallamacrocycle is connected to two different metallamacrocycles on either face. The resulting structure resembles a zigzagging wall made of parallel ledges in which, going upwards, every second ledge overhangs the one beneath it.

Note that with an arrangement such as in (i), if there are n metallamacrocycles in the polymeric chain – with each coordination site occupied – there will be $2n + 2$ axially coordinated ligands. Thus, the longer the polymer (i.e. the greater the value of n), the more the metallamacrocycle: ligand ratio n: $(2n + 2)$ approaches a value of n: $2n$ – i.e. 1:2. In (ii), it can be seen that the metallamacrocycle to ligand ratio will be n: $(2n + 4)$ – so a large value of n will cause this ratio to also tend to 1: 2. In fact, in any polymeric arrangement in which all coordination sites are occupied by bidentate bridging ligands, each non-terminal ligand will naturally occupy two coordination sites. Thus the coordination site: bridging ligand ratio will be 2:1. Since each *cis*-[Ni(I-Et-*S,O*)]$_2$ molecule possesses 4 coordination sites, it follows that the *cis*-[Ni(1-Et-*S,O*)]$_2$: ligand ratio will tend to 1: 2 as the number of metallamacrocycles increases – provided the number of terminal ligands does not increase. In the case of the 2D polymers ((iii) and (iv)), it can be seen that axial growth of the polymer does not increase the number of terminal ligands, while lateral growth of the polymer will do

so – therefore, a 2D polymeric array should possess a different stoichiometry from that of a 1D polymer.

When considering possible polymeric products, one must take into account the steric restrictions involved in aligning metallamacrocycles laterally (as required in arrangements (ii) - (iv).) Figure 3.4(c) shows a spatial analysis of the *cis*-[Ni(I-Et-*S,O*)]$_2$ molecular structure (i). An 'overhead' view and two lateral views (a 'head-on' view and a 'side-on' view) of the molecule are given, along with measurements of the length and breadth of the molecule. The values given are based on inter-nuclear distances obtained from the crystal structure of *cis*-[Ni(I-Et-*S,O*)]$_2$ (Section 3.2.1). Figure 3.4(c) also includes a representation of the two types of lateral alignment of metallamacrocycles described above (ii).

It is clear that a large amount of spatial superposition of the molecules is required to allow another metallamacrocycle to coordinate to both molecules simultaneously. The possible modes of alignment are 'head-to-head' with the greatest amount of overlap required (ca. 7 Å), 'head to side' – requiring ca. 5 Å of overlap, and 'side-to-side' – requiring ca. 1.5 Å of overlap. The values given for the required amount of overlap are only estimates, as there might be conformational differences between *cis*-[Ni(I-Et-*S,O*)]$_2$ in its free and polymerised forms. The minimal overlap involved in 'side-to-side' alignment (ca. 1.5 Å) might be small enough to be avoided by conformational changes, but even in a polymeric structure requiring this type of orientation (i.e. a 2D polymer of the type shown in Figure 3.4(b)(iii)), there would be a significant amount of steric strain. One must conclude that the only viable type of coordination polymer based on *cis*-[Ni(I-Et-*S,O*)]$_2$ is the 1D 'ladder' type shown in Figure 3.4(b)(i) which does not require any lateral alignment of metallamacrocycles. It is perhaps worth mentioning that the use of long flexible bidentate bridging ligands could obviate these steric limitations.

A similar examination of the possible polymerisation products based on the 3:3 metallamacrocycle, *cis*-[Ni(T-Et-*S,O*)]$_3$, is also presented. Figure 3.4(d) depicts schematic diagrams of potential *cis*-[Ni(T-Et-*S,O*)]$_3$-based polymer types. Diagram (i) represents the simplest 1D polymer. It consists of a chain of 3:3 metallamacrocycles with each aligned directly above the last and linked by 3 axially coordinated bidentate

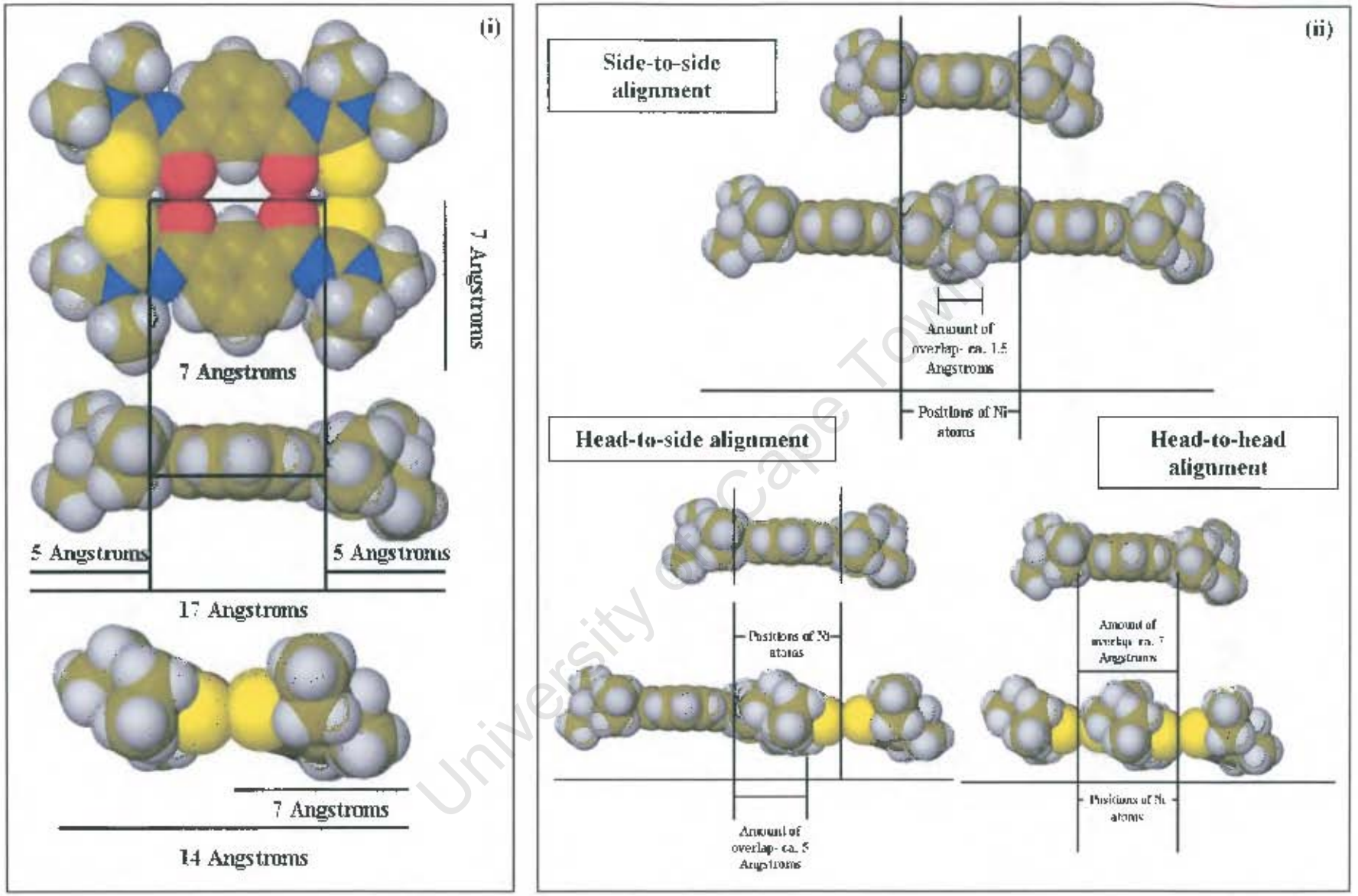

Figure 3.4(c). Spatial analysis of size of *cis*-[Ni(I-Et-*S,O*)]$_2$ (i) and amount of lateral overlap needed for 2 *cis*-[Ni(I-Et-*S,O*)]$_2$ molecules to simultaneously be linked to a third *cis*-[Ni(I-Et-*S,O*)]$_2$ (ii) – a requirement for the formation of complex coordination polymers

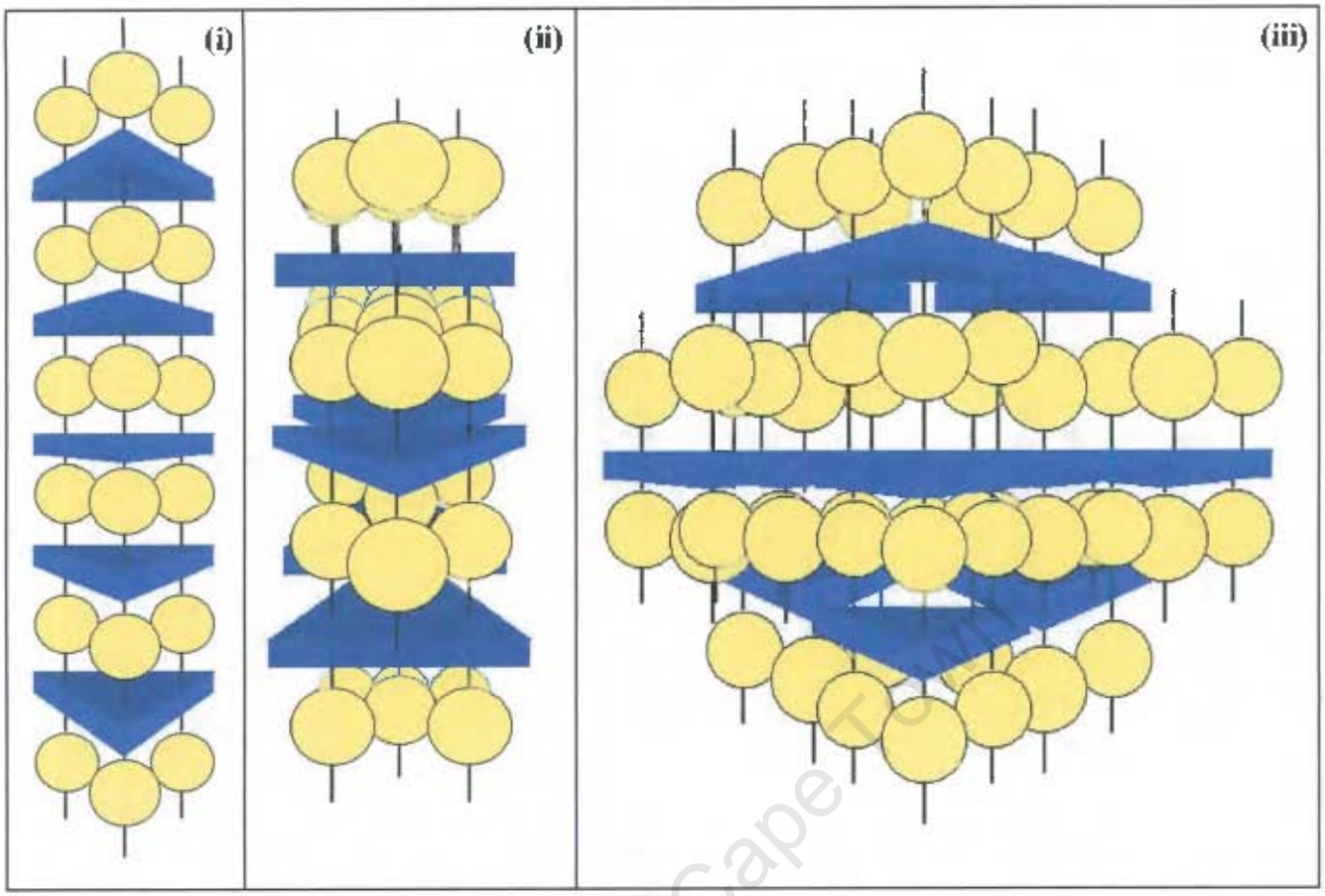

Figure 3.4(d). Schematic diagram of possible polymeric structures based on *cis*-[Ni(T-Et-*S,O*)]$_3$: a simple 1D 'ladder' structure (i) a 2D array (ii) and a complex 3D polymer (iii).

bridging ligands. This is analogous to the 2:2 'ladder' structure shown in Figure 3.4(b)(i). The 2D polymeric array (ii) is made up of layers of metallamacrocycles aligned 'head-to- tail', with successive layers in anti-parallel orientations, one upon the next in a staggered fashion so that each metallamacrocycle is doubly connected to one metallamacrocycle and singly connected to another on either face. The final diagram (iii) shows a 3D coordination polymer in which each metallamacrocycle is positioned in a staggered orientation with respect to the metallamacrocycles in neighbouring layers. In this way, each metallamacrocycle will be bound to 3 different metallamacrocycles on either face. Such a structure will allow layers of laterally aligned metallamacrocycles to extend in 2 dimensions, while axial building of layer upon layer will extend the polymer in the third dimension.

The stoichiometries of these two polymer types will differ in the same way that the proposed *cis*-[Ni(I-Et-*S,O*)]$_2$ coordination polymers would. The 1D polymer would

tend to a metallamacrocycle: bridging ligand ratio of 1:3 as the polymer length increases, while the number of terminal ligands remains constant. The 3D polymer would have an increasing number of terminal ligands as the size of each layer grows, but the number of terminal ligands would not increase with a growth in polymer chain length.

Again, the proposal of possible structures other than a simple 'ladder' appears to be moot, as any such structure requires the lateral alignment of multiple metallamacrocycles in close enough proximity for a metallamacrocycle in a successive layer to connect to them all simultaneously and the steric hindrance owing to the ethyl side branches of the metallamacrocycles would prevent this. Once again, it ought to be mentioned that this difficulty may be circumvented if the bridging ligands used are of a long flexible type.

To be certain that this steric hindrance will occur, a spatial analysis of the *cis*-[Ni(T-Et-*S,O*)]$_3$ metallamacrocycle has been undertaken. All measurements of the *cis*-[Ni(T-Et-*S,O*)]$_3$ molecule are based on the crystallographic results for the 3:3 octahedral adduct *cis*-[Ni(T-Et-*S,O*)(pyridine-*N*)$_2$]$_3$. Figure 3.4(e) shows the results of this analysis. Measurements of the dimensions of the metallamacrocycle are given (i). The inter-nuclear distances between nickel centres is approximately 10.5 Å, while the lengths of each major side of the roughly triangular molecule are about 15.5 Å. The next diagram (ii) gives an illustrated estimate of the amount of spatial overlap required for lateral alignment. Four types of alignment are shown: 'head-to-head' – requiring about 1 Å of spatial overlap to position the molecules correctly; 'side-to-side' – requiring roughly 2.5 Å overlap; 'head-to-side' requiring around 1 Å overlap; and 'head-to-tail' – with some 4 Å of spatial overlap needed. As with the spatial analysis for *cis*-[Ni(I-Et-*S,O*)]$_2$, there is some uncertainty in these values due to possible conformational changes. This means that where the degree of overlap is small (i.e. in 'head-to-head' or 'head-to-side' alignment), there is some possibility that two metallamacrocycles can be aligned laterally to obtain the required Ni – Ni inter-nuclear distance of 10.5 Å without encountering insurmountable steric hindrance. Since 'head-to tail' alignment requires a large degree of overlap, the formation of the 2D array shown in Figure 3.4(d)(ii), which requires this type of alignment, is precluded. The formation of a 3D array could conceivably be possible, if the type of

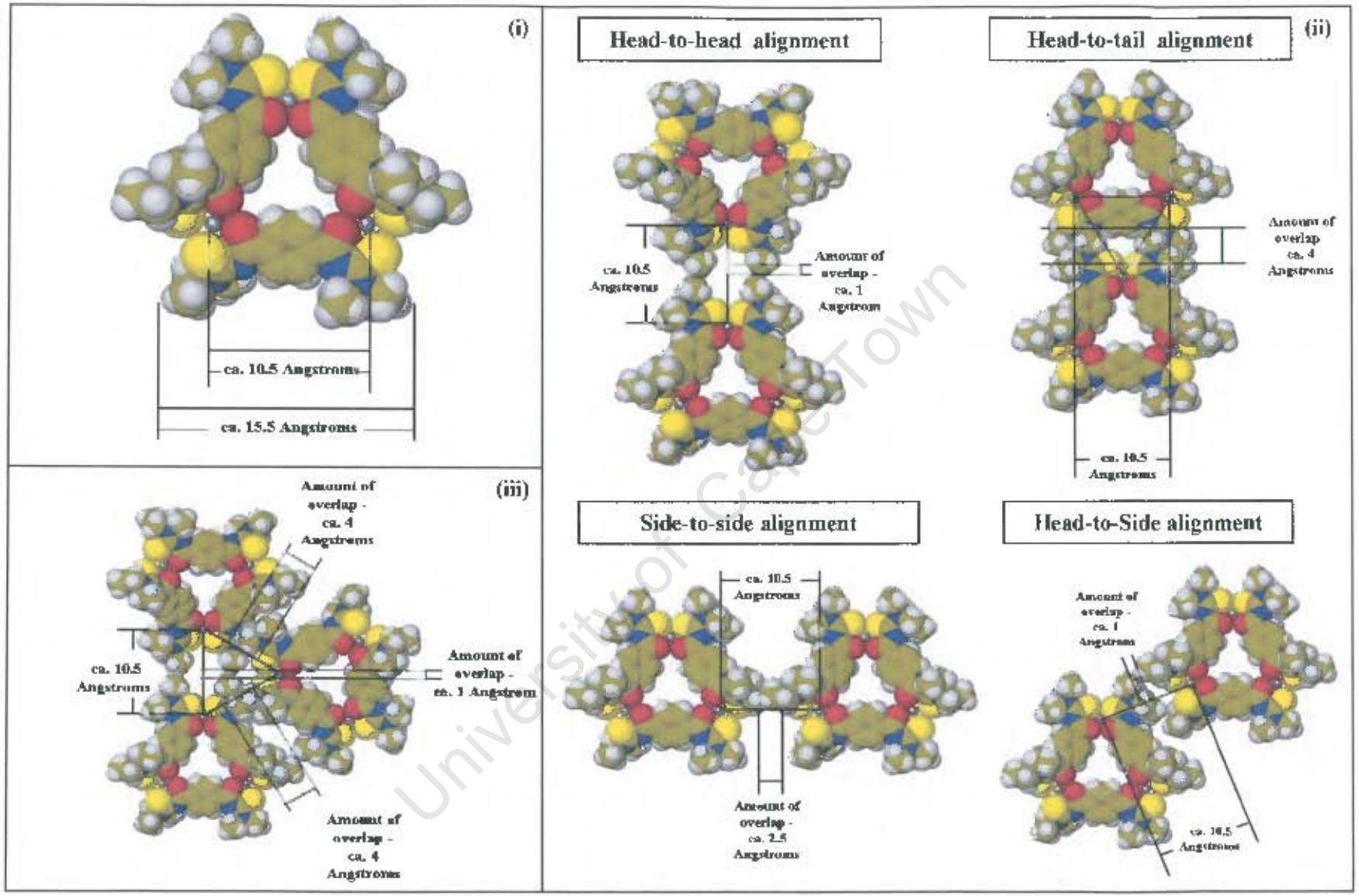

Figure 3.4(c). Spatial analysis of size of *cis*-[Ni(T-Et-*S,O*)]$_3$, (i) and amount of lateral overlap needed for 2 *cis*-[Ni(T-Et-*S,O*)]$_3$, molecules to simultaneously be linked to a third *cis*-[Ni(T-Et-*S,O*)]$_3$, (ii) and for three molecules to do so (iii) – a requirement for the formation of complex coordination polymers

alignment were either' head-to-head' or 'head-to-side'. However the final diagram (iii) of Figure 3.4(e) shows that the correct positioning of a third metallamacrocycle (to form an equilateral triangle of length 10.5 Å between Ni atoms of three different molecules) would require a spatial overlap of about 4 Å between the third molecule and both of the first two.

As with the 2:2 polymeric structures a high degree of spatial superposition seems to be necessary in the case of any 3:3 polymer that requires a lateral orientation of metallamacrocycles. As a result, it would appear to be almost certain that no such structure could be formed. The conclusion that one must draw therefore, is that a polymeric product based on *cis*-[Ni(T-Et-*S*,*O*)]$_3$ or any other 3:3 metallamacrocycle must be of the simple 1D 'ladder' type (with the possible exception of polymers using long flexible bridging ligands).

The results of various analytical techniques for a number of products of reactions between metallamacrocycles (both 2:2 and 3:3) and the bidentate bridging ligands, 4,4-bipyridine, pyrazine, 1,2-bis(4-pyridyl)ethane and 1,2-di(4-pyridyl)ethylene are reported.

The various reactions performed, as described in the Experimental Section, gave rise to products with a range of different physical properties. Preliminary analyses indicate that colour, composition (metallamacrocycle: ligand ratio) and decomposition temperature all appear to vary from one compound to another. One compound even possesses striking molecular recognition properties.

However, one property all of these compounds do have in common: insolubility in a wide range of solvents. Upon mixing a solution of metallamacrocycle with a solution of bidentate ligand, a powdery precipitate rapidly forms. In each case, this precipitate is found to be either insoluble or to revert to the original separate components in solution. This property makes the analysis of these compounds much more difficult. NMR in solution is not an option and since attempts to grow crystals of acceptable size and quality were unsuccessful the use of our most powerful analytical tool – single crystal x-ray diffraction – is thus precluded. The structures of these compounds are therefore not elucidated to the same degree as those of the earlier compounds upon

which they are based. Inferences are drawn from the results of various analytical techniques to obtain an idea of the nature of these compounds. Schematic drawings – as opposed to accurately rendered high-resolution images – will be the mode of illustration in this section. The techniques used to further characterise the compounds were IR spectroscopy, hot stage microscopy (HSM), TGA, MALDI-TOF mass spectrometry (which proved unsuccessful) and x-ray powder diffraction (XRD). The results of this characterisation are presented and discussed compound by compound in this chapter.

3.4.1. Poly-[*cis*-(bis-μ-(3,3,3',3'-tetraethyl-1,1'-isophthaloylbis(thiourcato-*S,O*))-di-nickel(II))-bis-μ-(pyrazine-*N,N'*)] ({*cis*-[Ni(I-Et-*S,O*)(pyrazine-*N,N'*)]$_2$}$_n$)

The reaction of purple *cis*-[Ni(I-Et-*S,O*)]$_2$ with pyrazine yielded a dull green powder. The difference in colour between reagents and product immediately suggests that new coordination bonds have formed, altering the electronic configuration around the Ni(II) centres. This inference is based on the results of the synthesis of octahedral adducts (Section 3.3) in which the colour change from purple to green is invariably observed upon axial coordination of pyridines to 2:2 metallamacrocycles. Since the axially coordinated pyrazine is bidentate, it is expected that the product should be polymeric, and thus of the 'ladder' type described above. Figure 3.4.1(a) represents the proposed structure for {*cis*-[Ni(I-Et-*S,O*)(pyrazine-*N,N'*)]$_2$}$_n$ based on this deduction.

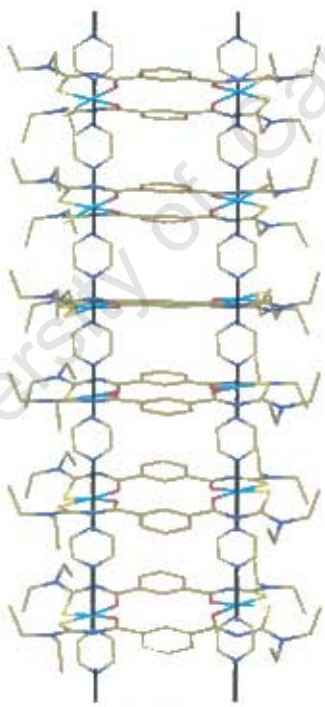

Figure 3.4.1(a). Schematic diagram of proposed polymeric structure of {*cis*-[Ni(I-Et-*S,O*)(pyrazine-*N,N'*)]$_2$}$_n$

If the product is a long chain polymer of this type, then it follows that the *cis*-[Ni(I-Et-*S,O*)]$_2$: coordinated pyrazine ratio should be 1: 2 – as described above. The results of various analytical techniques are reported below to help confirm or refute this proposal and allow a better conception of the product's nature.

Thermogravimetric Analysis

Figure 3.4.1(b) below represents the TGA results for {*cis*-[Ni(I-Et-*S,O*)(pyrazine-*N,N'*)]$_2$}$_n$. Both the mass percentage vs. time function and its first derivative curve are indicated and temperatures of minimum mass loss rate are reported – to allow better indication of poorly resolved, yet separate, thermal events.

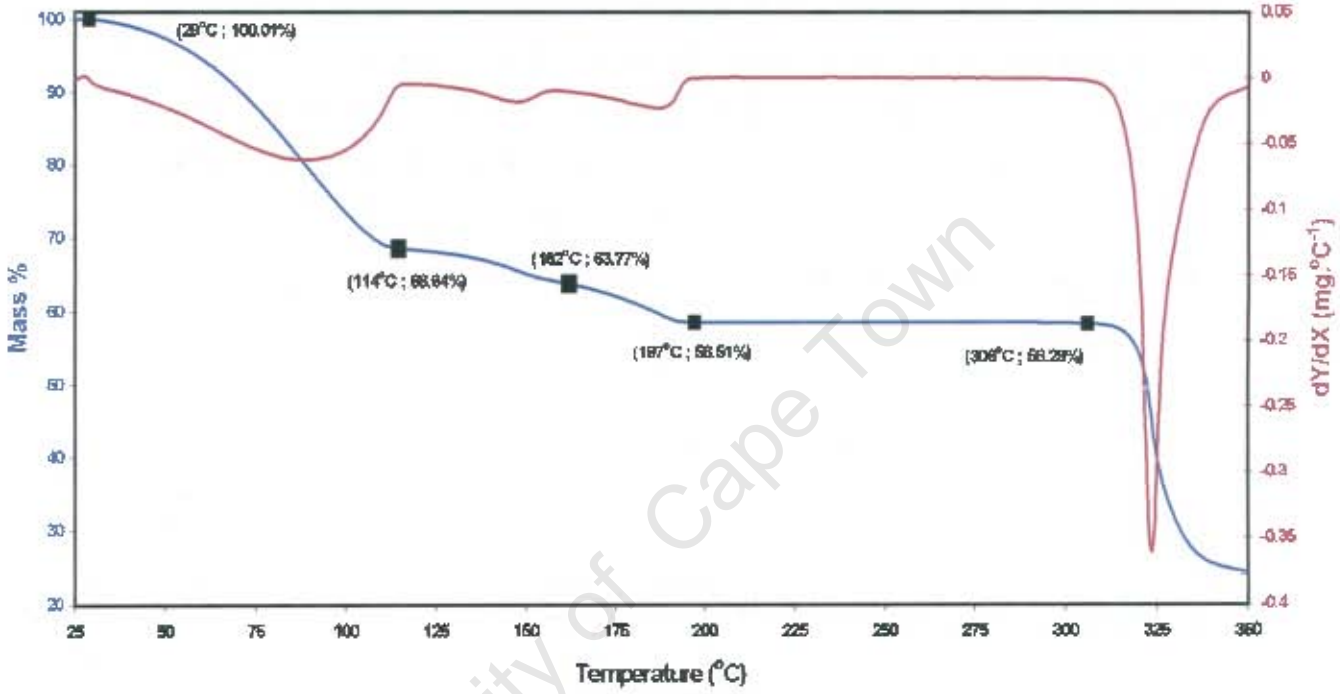

Figure 3.4.1(b). TGA trace for {*cis*-[Ni(I-Et-*S,O*)(pyrazine-*N,N'*)]$_2$}$_n$ with 1st derivative curve indicated.

The graph reveals that the onset of mass loss begins at the starting temperature of the thermal analysis (ca. 30 °C). A series of three distinct mass loss events is recorded, ending in a flat line at 197 °C. This 'plateau' continues with very little loss of mass until about 306 °C, after which a sharp mass loss occurs. The TGA seems to indicate that on heating, {*cis*-[Ni(I-Et-*S,O*)(pyrazine-*N,N'*)]$_2$}$_n$ reverts to the metallamacrocycle *cis*-[Ni(I-Et-*S,O*)]$_2$, which then proceeds to decompose beyond 300 °C. Thus the value of 58.51 % is taken to represent the fraction of the total mass made up by the metallamacrocycle. Table 3.4.1(a) shows the results of molar mass calculations based on this deduction and indicates the components to which each mass loss is attributed. These results correspond well with the loss of an integral number of pyrazine molecules (molar mass = 80.09 g.mol^{-1}). Overall, they suggest a *cis*-[Ni(I-Et-

S,O)]$_2$: pyrazine ratio of 1: 8. Furthermore, the individual mass losses are also close to the molar masses of integral numbers of pyrazine molecules. The first event would thus indicate the loss of 6 pyrazines per *cis*-[Ni(I-Et-*S,O*)]$_2$ unit.

However, the solvent used – dichloromethane – has a molar mass close to that of pyrazine (84.93 g.mol^{-1}). It is therefore also possible that the first mass loss corresponds with the removal of 6 included solvent molecules – although this mass loss would then be expected to be noticeably larger (ca. 1%). The second event indicates a single pyrazine and the third, another single pyrazine. One may infer from this is that there are 2 axially co-ordinated pyrazine molecules per metallamacrocyclic unit and 6 guest molecules (either pyrazine or dichloromethane) held in the structure by weak intermolecular forces.

Table 3.4.1(a). TGA Calculations of Mass Losses for {*cis*-[Ni(I-Et-*S,O*)(pyrazine-*N,N'*)]$_2$}$_n$

Feature on Graph	Temp. Range (°C)	Component Mass %	Molar Mass (g.mol^{-1})	Component Identification
Stable Range	197 – 306	58.51 %	902.51	*cis*-[Ni(I-Et-*S,O*)]$_2$
First Mass Loss	29 – 114	31.37 %	484	6 Pyrazines / 6 CH_2Cl_2
Second Mass Loss	114 – 162	4.87 %	75	1 Pyrazine
Third Mass Loss	162 – 197	5.26 %	81	1 Pyrazine
Combined Mass Loss	29 – 197	41.50 %	640	

Hot Stage Microscopy

Figure 3.4.1(c) is a series of digital photographs of a sample of {*cis*-[Ni(I-Et-*S,O*)(pyrazine-*N,N'*)]$_2$}$_n$, under silicone oil, on a hot stage microscope. The sample was heated rapidly (40 °C.min^{-1}) from room temperature. At ca. 90 °C, the sample begins changing colour from green to orange. This colour change continues – accompanied by the formation of bubbles in the oil – until at ca. 160 °C, the sample

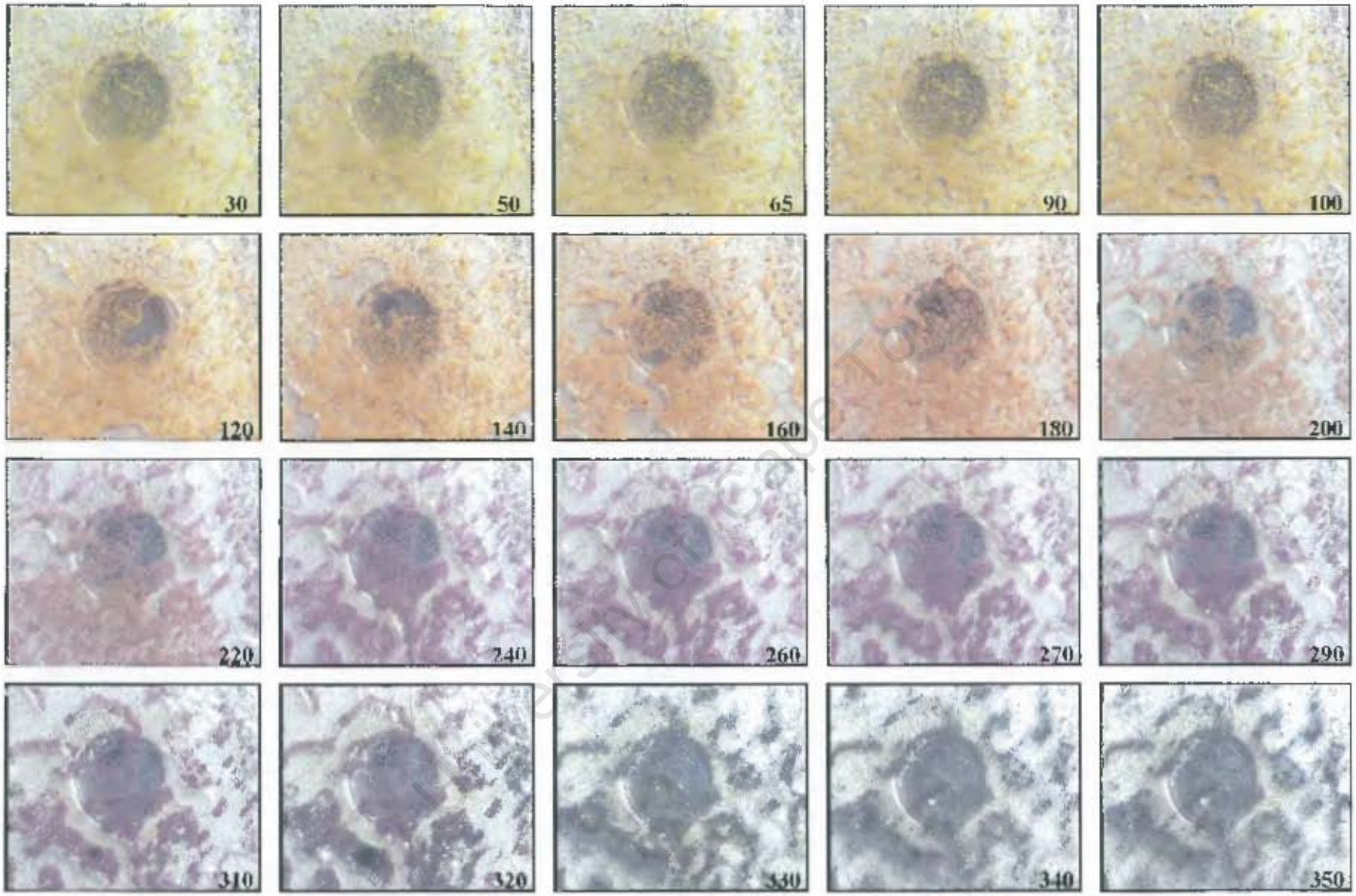

Figure 3.4.1(c). HSM photographs of {*cis*-[Ni(I-Et-*S,O*)(pyrazine-*N,N'*)]$_2$}$_n$ heated under silicone oil. Temperatures reported in degrees Celsius.

can definitely be seen to be orange and no longer green. However, the colour transition is not arrested at this point. The sample continues to darken and gradually change to a deep purple – with bubbling still observed. By 240 °C the sample has completed this colour change and remains purple until about 290 °C, where it begins to rapidly blacken and decompose. By 340 °C the sample is completely black.

This behaviour seems to confirm that {*cis*-[Ni(I-Et-*S,O*)(pyrazine-*N,N'*)]$_2$}$_n$ gradually reverts to the purple metallamacrocycle *cis*-[Ni(I-Et-*S,O*)]$_2$ – which then proceeds to decompose beyond 300 °C. In this regard, {*cis*-[Ni(I-Et-*S,O*)(pyrazine-*N,N'*)]$_2$}$_n$ behaves similarly to the octahedral adducts such as *cis*-[Ni(I-Et-*S,O*)(pyridine-*N*)$_2$]$_2$. What is especially interesting is the intermediate orange colour of the sample. It is possible that this colour is due to the presence of Ni (II) centres in two different electronic configurations: the high-spin paramagnetic configuration of octahedrally coordinated nickel and the low-spin diamagnetic configuration of square planar nickel. In other words, at first, all nickel centres have pyrazine ligands axially coordinated, thus the compound's colour is green. As coordinated pyrazine ligands are gradually removed from the nickel centres, more and more nickel centres change from octahedral to square planar until eventually all pyrazine ligands have been removed and all nickel centres are square planar. During this transition, the presence of nickel atoms in both states gives rise to visible light absorption in the wavelength ranges associated with each electronic state. The result is a distinct orange colour. The various shades of orange are construed as a qualitative indication of the proportion of nickel centres in either electronic state. The bubbles evolved during this transition can be attributed to the expulsion of pyrazine from the sample.

The HSM photographs indicate that from 30 – 100 °C there is some colour change in the sample. However, the most striking colour change occurs in the range 100 – 240 °C. This suggests that the majority of ligand removal from the metal centres occurs in this temperature range. This roughly corresponds with the second and third events observed in the TGA trace, although sample behaviours during HSM and TGA do vary, insomuch as the mass loss during TGA is arrested at 197 °C, whereas the colour change during HSM is only completed by 240 °C.

Elemental analysis results (Section 2.4.1 and Table 3.4.1(b) below) correspond well with elemental mass percentages calculated for a *cis*-[Ni(I-Et-*S,O*)]$_2$: pyrazine ratio of 1: 2 – as shown in the schematic drawing of a 2:2 metallamacrocyclic coordination polymer (Figure 3.4(a) above). This data does not match the data found from TGA, but the discrepancy can be attributed to the preparative techniques used before elemental analysis, which included subjecting the compound to vacuum, possibly removing weakly held pyrazine or dichloromethane molecules from the compound, thus rendering it into a guest-free structure. Note that a *cis*-[Ni(I-Et-*S,O*)]$_2$: pyrazine ratio of 1:4 (i.e. the stoichiometry expected for a monomeric octahedral adduct) does not match the experimental results.

Table 3.4.1(b). Comparison of {*cis*-[Ni(I-Et-*S,O*)(pyrazine-*N,N'*)]$_2$}$_n$ elemental analysis results with values calculated for a monomeric octahedral adduct, a guest-free polymer and a structure containing guest molecules.

Element	Found %	Calculated %		
		Metallamacrocycle: Pyrazine Ratio		
		1:2	1:4	1: 8
C	49.10	49.73	51.07	52.92
H	5.28	5.31	5.28	5.23
N	15.49	15.82	18.33	21.78
S	11.77	12.07	10.49	8.31

IR Spectroscopy

Infrared analyses were performed on the compounds pyrazine, *cis*-[Ni(I-Et-*S,O*)]$_2$ and {*cis*-[Ni(I-Et-*S,O*)(pyrazine-*N,N'*)]$_2$}$_n$ in the range 1000 – 300 cm^{-1}. There are two important observations for the purpose of this characterisation. Firstly, there is a significant increase in absorption at 486 cm^{-1} for {*cis*-[Ni(I-Et-*S,O*)(pyrazine-*N,N'*)]$_2$}$_n$ as compared to *cis*-[Ni(I-Et-*S,O*)]$_2$. Secondly, there is an additional peak at 415 cm^{-1} in the {*cis*-[Ni(I-Et-*S,O*)(pyrazine-*N,N'*)]$_2$}$_n$ spectrum. The shifting of a peak in the free pyrazine IR spectrum at ca. 417 cm^{-1} to 472 – 486 cm^{-1} in the spectrum of a

pyrazine complex is characteristic of pyrazine acting as a bidentate bridging ligand.[110, 111] The increased absorption at 486 cm^{-1} for {*cis*-[Ni(I-Et-*S,O*)(pyrazine-*N,N'*)]$_2$}$_n$ is strong confirmation that pyrazine has coordinated to 2 separate Ni(II) centres. The remaining presence of a peak at 415 cm^{-1} for {*cis*-[Ni(I-Et-*S,O*)(pyrazine-*N,N'*)]$_2$}$_n$ suggests that uncoordinated pyrazine is also present in the sample. A comparison of the spectrum of *cis*-[Ni(I-Et-*S,O*)]$_2$ with that of {*cis*-[Ni(I-Et-*S,O*)(pyrazine-*N,N'*)]$_2$}$_n$ in the C – Cl stretching range (850 – 550 cm^{-1})[112] shows that no new peaks are observed for {*cis*-[Ni(I-Et-*S,O*)(pyrazine-*N,N'*)]$_2$}$_n$. This suggests that dichloromethane is not present as a guest in the sample.

X-ray Powder Diffraction

Figure 3.4.1(d) below shows the x-ray powder diffraction pattern of {*cis*-[Ni(I-Et-*S,O*)(pyrazine-*N,N'*)]$_2$}$_n$, along with those of *cis*-[Ni(I-Et-*S,O*)]$_2$, pyrazine and a pattern generated by superimposing the patterns of *cis*-[Ni(I-Et-*S,O*)]$_2$ and pyrazine (pyrazine reflections weighted by a factor of 0.25 to prevent loss of detail from the *cis*-[Ni(I-Et-*S,O*)]$_2$ pattern.) It is immediately evident that the {*cis*-[Ni(I-Et-*S,O*)(pyrazine-*N,N'*)]$_2$}$_n$ powder pattern is not merely the superposition of the *cis*-[Ni(I-Et-*S,O*)]$_2$ and pyrazine powder patterns. In other words, the green powder {*cis*-[Ni(I-Et-*S,O*)(pyrazine-*N,N'*)]$_2$}$_n$ is not simply a mixture of *cis*-[Ni(I-Et-*S,O*)]$_2$ and pyrazine crystals – although this is already strongly suggested by the difference in the colours of *cis*-[Ni(I-Et-*S,O*)]$_2$ and {*cis*-[Ni(I-Et-*S,O*)(pyrazine-*N,N'*)]$_2$}$_n$.

The powder pattern of {*cis*-[Ni(I-Et-*S,O*)(pyrazine-*N,N'*)]$_2$}$_n$ exhibits much broader peaks than that of *cis*-[Ni(I-Et-*S,O*)]$_2$ – possibly implying that {*cis*-[Ni(I-Et-*S,O*)(pyrazine-*N,N'*)]$_2$}$_n$ is not wholly crystalline. A reduced degree of crystallinity is an indication that the compound could be polymeric. It can be suggested that the rapid coordination of the bidentate bridging ligands results in the formation of a highly insoluble polymeric product that quickly precipitates as a partially amorphous powder.

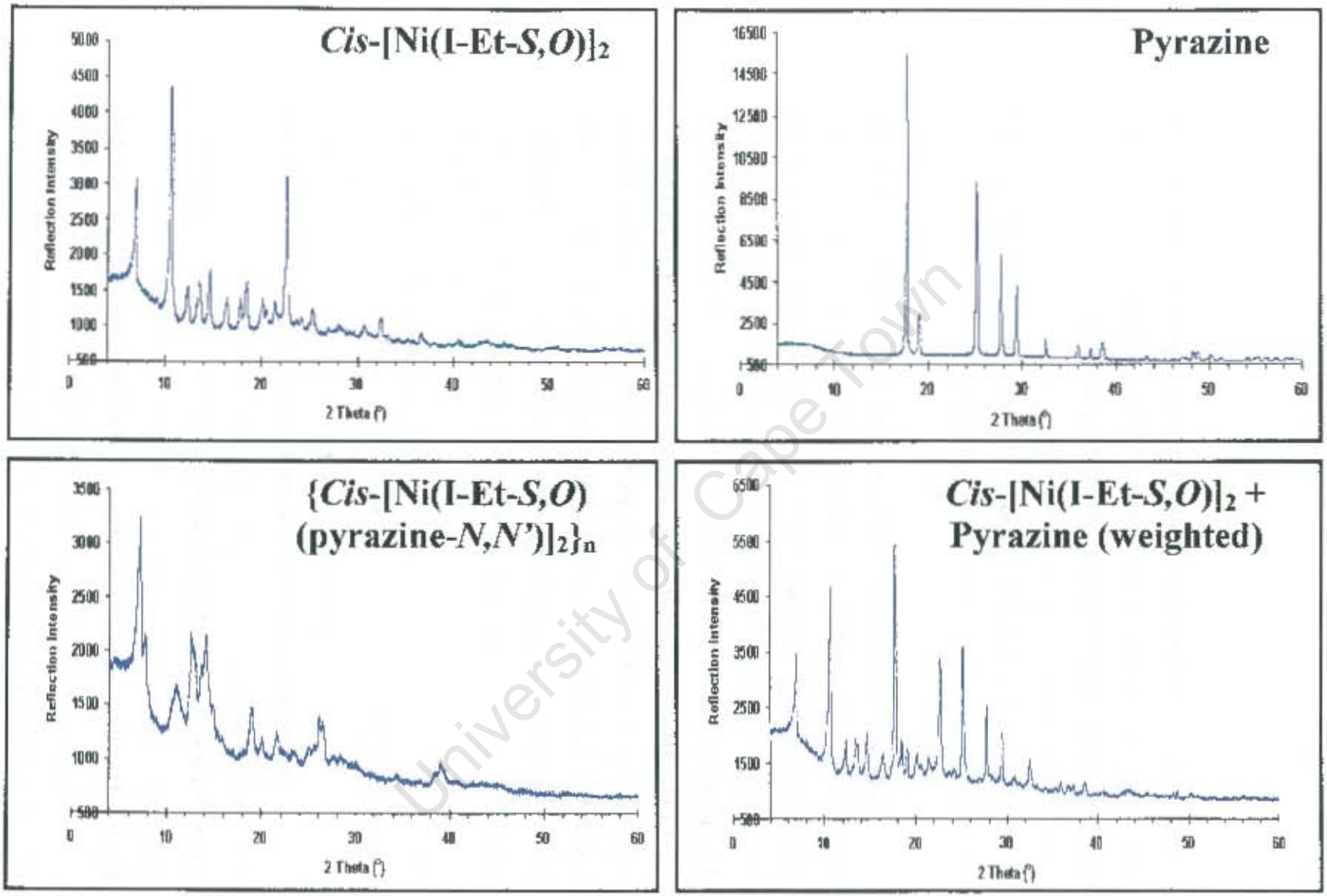

Figure 3.4.1(d). X-ray powder diffraction patterns for {*cis*-[Ni(I-Et-*S,O*) (pyrazine-*N,N'*)]$_2$}$_n$ and its unreacted components - separate and superimposed

Summary

Preliminary observations indicated that the addition of pyrazine to *cis*-[Ni(I-Et-*S,O*)]$_2$ yields a new compound – probably possessing octahedral coordination around the nickel centres. TGA and elemental analysis show that {*cis*-[Ni(I-Et-*S,O*)(pyrazine-*N,N'*)]$_2$}$_n$ has a *cis*-[Ni(I-Et-*S,O*)]$_2$: pyrazine ligand ratio of 1:2 with 6 guest molecules (either pyrazine or dichloromethane) per metallamacrocycle. IR analysis indicates that pyrazine is acting as a bidentate bridging ligand, and also seems to be present as an uncoordinated guest, while there does not seem to be any CH_2Cl_2 present as a guest. XRD indicates that {*cis*-[Ni(I-Et-*S,O*)(pyrazine-*N,N'*)]$_2$}$_n$ is at least partially crystalline, and possesses a crystal structure that is markedly different from those of pyrazine and *cis*-[Ni(I-Et-*S,O*)]$_2$.

{*Cis*-[Ni(I-Et-*S,O*)(pyrazine-*N,N'*)]$_2$}$_n$ is a new compound. The product was expected to be a coordination polymer. Its physical properties, stoichiometry and other analytical evidence bear this out. {*cis*-[Ni(I-Et-*S,O*)(pyrazine-*N,N'*)]$_2$}$_n$ is almost certainly a polymer of the form illustrated in Figure 3.4.1(a), containing 6 pyrazine guest molecules, i.e. {*cis*-[Ni(I-Et-*S,O*)(pyrazine-*N,N'*)]$_2$.6(pyrazine)}$_n$.

3.4.2. Poly-[*cis*-(bis-μ-(3,3,3',3'-tetraethyl-1,1'-isophthaloylbis(thiourcato-*S,O*))-di-nickel(II))-bis-μ-(4,4'-bipyridine-*N,N'*)] ({*cis*-[Ni(I-Et-*S,O*)(bipy-*N,N'*)]$_2$}$_n$)

The reaction of purple *cis*-[Ni(J-Et-*S,O*)]$_2$ with 4,4'-bipyridine (bipy) yielded a dull green powder similar to {*cis*-[Ni(I-Et-*S,O*)(pyrazine-*N,N'*)]$_2$}$_n$. This colour change was again taken as signifying a change in the coordination around the Ni(II) centres from square planar to octahedral. Since bipy has the ability to act as bidentate bridging ligand, the product of a coordination reaction of bipy with a metal complex such as *cis*-[Ni(J-Et-*S,O*)]$_2$ was expected to be polymeric (and therefore of the ladder type similar to the proposed structure for {*cis*-[Ni(I-Et-*S,O*)(pyrazine-*N,N'*)]$_2$}$_n$). The stoichiometry of such a polymer would give a metallamacrocycle: ligand ratio of 1:2. The results of various analytical techniques for {*cis*-[Ni(I-Et-*S,O*)(bipy-*N,N'*)]$_2$}$_n$ are reported below.

Thermogravimetric Analysis

Figure 3.4.2(a) below is a graphical representation of the TGA results for {*cis*-[Ni(1-Et-*S,O*)(bipy-*N,N'*)]$_2$}$_n$. As with {*cis*-[Ni(I-Et-*S,O*)(pyrazine-*N,N'*)]$_2$}$_n$, a first derivative curve is included to allow better identification of poorly resolved thermal events. However, this does not help interpret what turns out to be a complex TGA trace. The mass loss begins at 163 °C and continues past the decomposition point of *cis*-[Ni(I-Et-*S,O*)]$_2$ and is ongoing at the final temperature of the TGA run (350 °C). The first derivative trace resolves what appears to be one continuous mass loss into a few separate thermal events. The mass loss that begins at 163 °C appears to abate somewhat at 220 °C – with some 9.98 % mass having been lost. A second event is already underway at this stage and increases the mass loss rate until another point of inflection (or local maximum in the first derivative trace) at 239 °C (5.29% mass lost). A large mass loss (29.20%) ensues from this temperature until 308 °C, beyond which the mass loss rate increases again and then abates once more at 350 °C having lost 10.52%.

Clearly, the interpretation of this data is troublesome, as there is no temperature range during which the sample is gravimetrically stable, and thus no clear mass percentage upon which to base calculations. It is also difficult to determine accurately how much

mass is lost in each thermal event as the points of inflection represent weakly resolved borders between thermal events and the rate of mass loss at each of these points is still quite high.

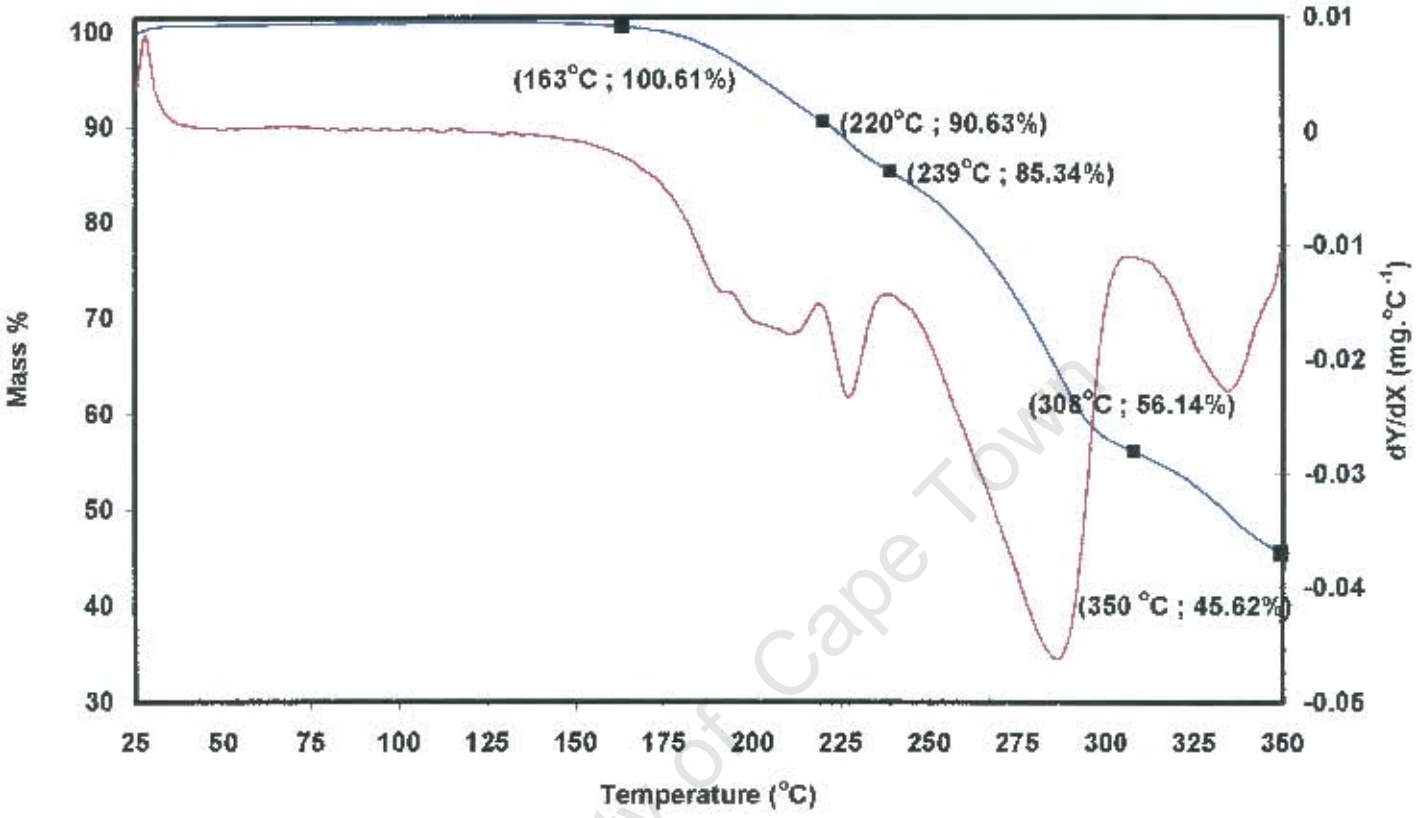

Figure 3.4.2(a). TGA trace for {*cis*-[Ni(I-Et-*S,O*)(bipy-*N,N'*)]$_2$}$_n$ with 1st derivative curve indicated.

With these difficulties in mind, Table 3.4.2(a) below was devised based on two assumptions. In the TGA of {*cis*-[Ni(I-Et-*S,O*)(pyrazine-*N,N'*)]$_2$}$_n$, it was seen that soon past 306 °C, the metallamacrocycle *cis*-[Ni(I-Et-*S,O*)]$_2$ begins to decompose. Thus the assumption is made for {*cis*-[Ni(I-Et-*S,O*)(bipy-*N,N'*)]$_2$}$_n$ that the remaining mass at the point of inflection at 308 °C represents the metallamacrocycle *cis*-[Ni(I-Et-*S,O*)]$_2$ and any mass loss beyond this temperature results from the degradation of the metallamacrocycle itself. Another assumption made is that the masses lost between the points of inflection represent discrete thermal events.

Table 3.4.2(a). TGA Calculations of Mass Losses for {*cis*-[Ni(I-Et-*S,O*)(bipy-*N,N'*)]$_2$}$_n$

Feature on Graph	Temp. Range (°C)	Component Mass %	Molar Mass (g.mol^{-1})	Component Identification
Point of inflection	308	56.14 %	902.51	*cis*-[Ni(I-Et-*S,O*)]$_2$
First Mass Loss	163 - 220	9.98 %	160	1 bipy / 2 CH_2Cl_2
Second Mass Loss	220 – 239	5.29 %	85	1 CH_2Cl_2 / 0.5 bipy
Third Mass Loss	239 - 308	29.20 %	469	3 bipy
Combined Mass Loss	163 - 308	44.50 %	718	

The first thermal event from 163 ~ 220 °C indicates a mass loss of 9.98%. This represents a component with a molar mass of 160 g.mol^{-1} – which corresponds well with the molar mass of 4,4'-bipyridine (156.19 g.mol^{-1}) or alternatively twice the molar mass of dichloromethane (84.93 g.mol^{-1}) – the solvent in which the reaction was conducted. The second event from 220 – 239 °C represents a component with a molar mass of 85 g.mol^{-1}. This corresponds well with the molar mass of dichloromethane or alternatively, with half the molar mass of 4,4'-bipyridine. The final event before decomposition of the metallamacrocycle involves the loss of 469 g.mol^{-1}. This corresponds very well with three times the molar mass of 4,4'-bipyridine.

The data can thus be interpreted in the following way: the first mass loss corresponds with the loss of one molecule of 4,4'-bipyridine The second event could represent the loss of one molecule of dichloromethane per metallamacrocycle – although intuitively one might expect the loss of this molecule prior to the loss of 4,4'-bipyridine. The final mass loss matches well with the molar mass of 3 molecules of bipy per *cis*-[Ni(I-Et-*S,O*)]$_2$ unit.

This data indicates a *cis*-[Ni(I-Et-*S,O*)]$_2$: 4,4'-bipyridine : dichloromethane composition in the ratio: 1 : 4 : 1 – i.e. 4 molecules of bipy and one molecule of CH_2Cl_2 per *cis*-[Ni(I-Et-*S,O*)]$_2$ unit. This raises an interesting issue regarding the nature of the product. A metallamacrocycle: ligand ratio of 1: 4 is characteristic of the

monomeric octahedral adducts of *cis*-[Ni(I-Et-*S,O*)]$_2$ such as *cis*-[Ni(I-Et-*S,O*)(pyridine-*N*)$_2$]$_2$, whereas a 1:2 ratio is expected for a 'ladder'-type coordination polymer. It is therefore possible that {*cis*-[Ni(I-Et-*S,O*)(bipy-*N,N'*)]$_2$}$_n$ is either a coordination polymer with two bipy molecules and 1 CH_2Cl_2 molecule per metallamacrocycle included in the structure or a monomeric octahedral adduct with one CH_2Cl_2 guest per adduct molecule (as was found to be the case for *cis*-[Ni(I-Et-*S,O*)(DMAP-*N*)$_2$]$_2$).

The insolubility of {*cis*-[Ni(I-Et-*S,O*)(bipy-*N,N'*)]$_2$}$_n$, combined with the fact that bipy is a bidentate bridging ligand, suggests that the compound is polymeric, but this is in no way conclusive.

Hot Stage Microscopy

Figure 3.4.2(b) shows a series of photographs of {*cis*-[Ni(I-Et-*S,O*)(bipy-*N,N'*)]$_2$}$_n$ under silicone oil on a hot stage microscope. The sample was heated at 20 °C per minute from room temperature. The photographs indicate that {*cis*-[Ni(I-Et-*S,O*)(bipy-*N,N'*)]$_2$}$_n$ is thermally robust, remaining apparently unchanged until 160 °C – at which point the sample begins to change colour from green to a dullish brown. This colour change continues until about 180 °C, after which, the sample begins changing colour to purple. At around 200 °C, bubbles evolve from the sample, as it continues darkening in colour. By 225 °C, the sample has completed the colour change to deep purple – which is how it remains until past 300 °C, where it rapidly degrades to a black residue (not shown).

These observations seem to indicate something similar to that observed for {*cis*-[Ni(I-Et-*S,O*)(pyrazine-*N,N'*)]$_2$}$_n$. The gradual disappearance of the green colour suggests that the axially coordinated bipy ligands break their bonds with the Ni atoms. The intermediate brown colour can be attributed to the presence of both square planar and octahedral nickel (II) in the sample. As the temperature is further elevated, the colour change continues until all bipy has decoordinated from the Ni(II) centres. The evolution of bubbles from the sample may be attributed to the loss of bipy from the complex, although the fact that there is some delay between what is perceived to be

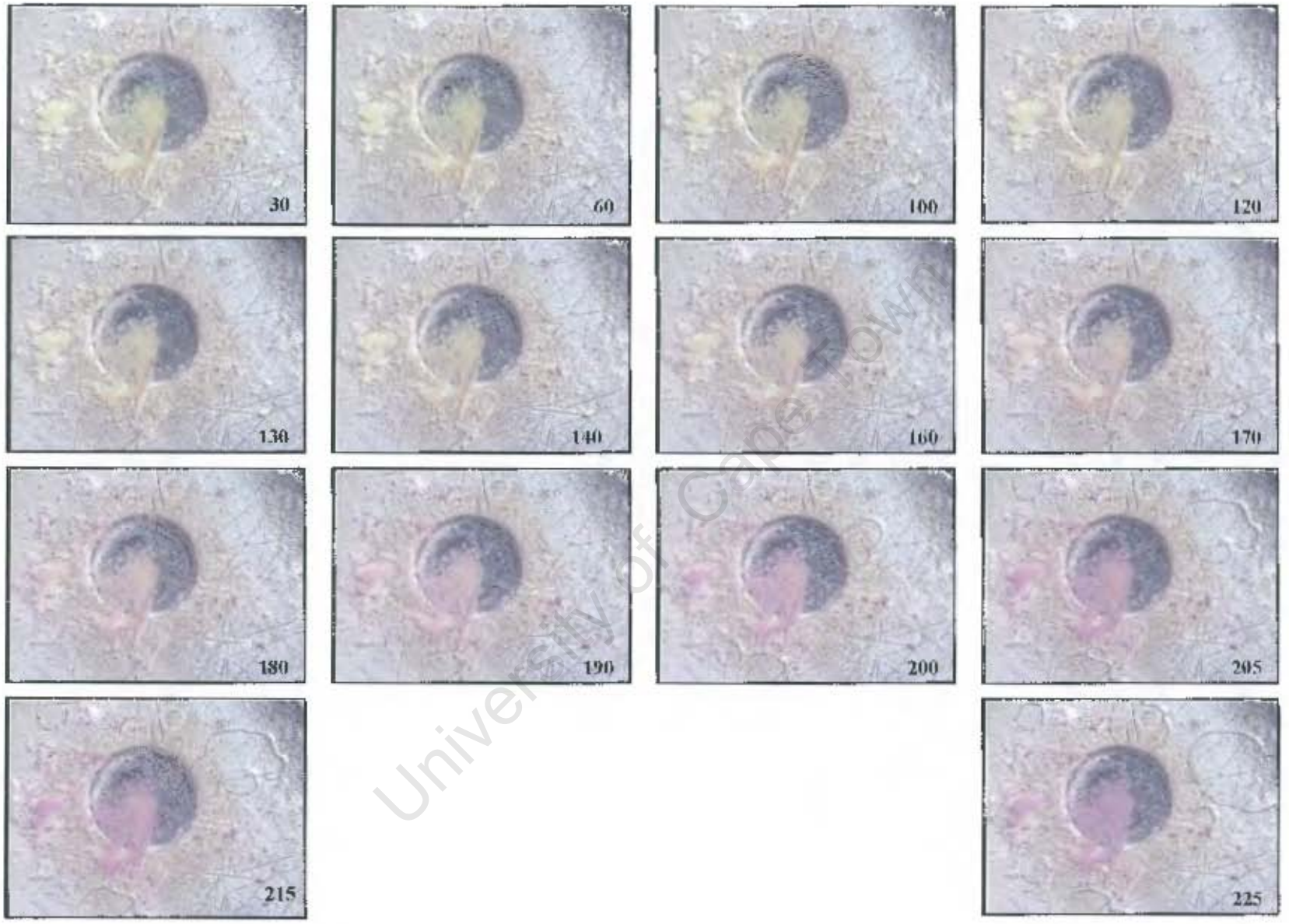

Figure 3.4.2(b). HSM photographs of {*cis*-[Ni(1-Et-*S*,*O*)(bipy-*N*,*N*')]$_2$}$_n$ heated under silicone oil. Temperatures reported in degrees Celsius.

the decoordination of the ligand and its removal could indicate that the bipy remains present with the complex even after decoordination. Note that in {*cis*-[Ni(I-Et-*S,O*)(pyrazine-*N,N'*)]$_2$}$_n$, the evolution of pyrazine was observed to be concomitant with the colour change beginning at ca. 100 °C. This difference could be explained in terms of the melting and boiling points of pyrazine and 4,4'-bipyridine. Pyrazine (m.p. 55 °C and b.p.. 115 °C) would be expected to be removed at a much lower temperature than bipy (m.p. 112 °C and b.p. 305 °C) – provided that the forces holding them in their respective crystal structures are comparable. The colour change from green to purple occurs over similar ranges for both {*cis*-[Ni(I-Et-*S,O*)(pyrazine-*N,N'*)]$_2$}$_n$ and {*cis*-[Ni(I-Et-*S,O*)(bipy-*N,N'*)]$_2$}$_n$ and thus the dative covalent bond strengths do not appear to differ greatly. Once the Ni – N coordination bonds are broken, there is no other strong force (e.g. hydrogen bonding) holding the ligand within the crystal structure.

Once the colour change from green to purple is complete at ca. 225 °C, {*cis*-[Ni(I-Et-*S,O*)(bipy-*N,N'*)]$_2$}$_n$ appears to be thermally stable until around the decomposition point of *cis*-[Ni(I-Et-*S,O*)]$_2$. It is therefore likely that {*cis*-[Ni(I-Et-*S,O*)(bipy-*N,N'*)]$_2$}$_n$ reverts to the metallamacrocycle *cis*-[Ni(I-Et-*S,O*)]$_2$ upon heating.

It is interesting to compare the TGA results with the observations obtained from HSM. However it must be stressed that the TGA and HSM results will not necessarily agree entirely because of the difference in experimental conditions. The initial colour change during HSM begins at roughly the same temperature as the initial onset of mass loss in the TGA – ca. 160 °C. The colour change is completed by 225 °C – well before the decomposition point of *cis*-[Ni(I-Et-*S,O*)]$_2$. This is similar to the observation made for {*cis*-[Ni(I-Et-*S,O*)(pyrazine-*N,N'*)]$_2$}$_n$, where complete colour change had occurred by 240 °C. The difference is that for {*cis*-[Ni(I-Et-*S,O*)(pyrazine-*N,N'*)]$_2$}$_n$, the TGA showed mass loss arrest at 197 °C, whereas for {*cis*-[Ni(I-Et-*S,O*)(bipy-*N,N'*)]$_2$}$_n$, mass loss continued past 300 °C. This can be explained in terms of the difference in melting and boiling points of pyrazine and 4,4'-bipyridine as described above. The expulsion of coordinated bipy ligands of {*cis*-[Ni(I-Et-*S,O*)(bipy-*N,N'*)]$_2$}$_n$ could actually occur at temperatures higher than the decoordination events, hence the continued mass loss well beyond the temperature of the final colour change. This would also explain the poor resolution of the final

thermal events, as the *cis*-[Ni(I-Et-*S,O*)]$_2$ complexes begin decomposing while bipy molecules stubbornly persist within the structure. The loss of dichloromethane at the elevated temperature of 220 °C (as indicated by TGA) would occur if this guest were trapped within layers of the coordination polymer. It would only be able to escape once decoordination of bipy from *cis*-[Ni(I-Et-*S,O*)]$_2$ had occurred. This fits with the HSM indication that the decoordination process occurs from 160 – 225 °C. The possibility of the first two thermal events representing the loss of 1 bipy followed by 1 CH_2Cl_2 molecule per metallamacrocycle is now more appealing. The first mass loss – attributed to a bipy guest – occurs before the decoordination of the two bipy ligands. The second event represents the loss of one enclathrated CH_2Cl_2 per metallamacrocycle, and occurs during decoordination (as the colour change is occurring), as these molecules should be able to escape immediately as the coordination bonds are broken – i.e. throughout the entire temperature range of decoordination. This event is then followed by the loss of the remaining – possibly enclathrated – bipy guest and the 2 decoordinated bipy's as one final event. These results imply the possibility that {*cis*-[Ni(I-Et-*S,O*)(bipy-*N,N'*)]$_2$}$_n$ is a polymeric clathrate complex with one dichloromethane guest and one bipy guest caged between layers of metallamacrocycles by the coordinated bipy ligands.

Elemental Analysis

Table 3.4.2(b) below compares the values obtained from the elemental analysis of {*cis*-[Ni(I-Et-*S,O*)(bipy-*N,N'*)]$_2$}$_n$ with values calculated for a coordination polymer (*cis*-[Ni(I-Et-*S,O*)]$_2$: bipy ratio 1: 2) and a monomeric octahedral adduct (*cis*-[Ni(1-Et-*S,O*)]$_2$: bipy ratio 1: 4) – assuming that all included guests are removed by subjection of the sample to vacuum prior to analysis, as suggested for {*cis*-[Ni(1-Et-*S,O*)(pyrazine-*N,N'*)]$_2$}$_n$ above. The composition that gives calculated values closest to those found by elemental analysis is the 1: 2 ratio. It is most likely therefore, that {*cis*-[Ni(1-Et-*S,O*)(bipy-*N,N'*)]$_2$}$_n$ is a coordination polymer, with all its guest molecules removed on subjection to vacuum (giving a *cis*-[Ni(I-Et-*S,O*)]$_2$: bipy: CH_2Cl_2 ratio of 1: 2: 0). This gives no clear indication as to the original composition of the product as enclathrated guests may have been present but were removed on subjection to vacuum, or possibly no guests were enclathrated at any stage.

Table 3.4.2(b). Comparison of {*cis*-[Ni(I-Et-*S,O*)(bipy-*N,N'*)]$_2$}$_n$ elemental analysis results with values calculated for a monomeric octahedral adduct and a guest-free polymer

Element	Found %	Calculated %	
		cis-[Ni(I-Et-*S,O*)]$_2$: bipy ratio	
		1: 2	1: 4
C	54.76	55.36	59.77
H	5.34	5.31	5.28
N	13.77	13.84	14.67
S	9.86	10.56	8.40

X-ray Powder Diffraction

Figure 3.4.2(c) shows the x-ray powder diffraction pattern of {*cis*-[Ni(I-Et-*S,O*)(bipy-*N,N'*)]$_2$}$_n$ as well as that of *cis*-[Ni(I-Et-*S,O*)]$_2$, 4,4'-bipyridine and a pattern generated by the addition of the reflection data for *cis*-[Ni(I-Et-*S,O*)]$_2$ and 4,4'-bipyridine. It is evident that the prominent peak at $2\theta = 25.5^{\circ}$ in the bipy pattern is absent from the {*cis*-[Ni(I-Et-*S,O*)(bipy-*N,N'*)]$_2$}$_n$ pattern, as is the peak at $2\theta = 10.6^{\circ}$ in the *cis*-[Ni(I-Et-*S,O*)]$_2$ pattern. Furthermore, a new peak is present in the {*cis*-[Ni(I-Et-*S,O*)(bipy-*N,N'*)]$_2$}$_n$ pattern at $2\theta = 8.6^{\circ}$, which is not present in any of the other patterns. Hence, one can deduce that {*cis*-[Ni(I-Et-*S,O*)(bipy-*N,N'*)]$_2$}$_n$ possesses a new crystal structure – it is not simply a mixture of *cis*-[Ni(I-Et-*S,O*)]$_2$ and bipy.

Furthermore, when one compares the powder diffraction patterns of {*cis*-[Ni(I-Et-*S,O*)(bipy-*N,N'*)]$_2$}$_n$ with that of {*cis*-[Ni(I-Et-*S,O*)(pyrazine-*N,N'*)]$_2$}$_n$, one sees remarkable similarity. Figure 3.4.2(d) below shows the powder patterns for these two compounds on the same set of axes.

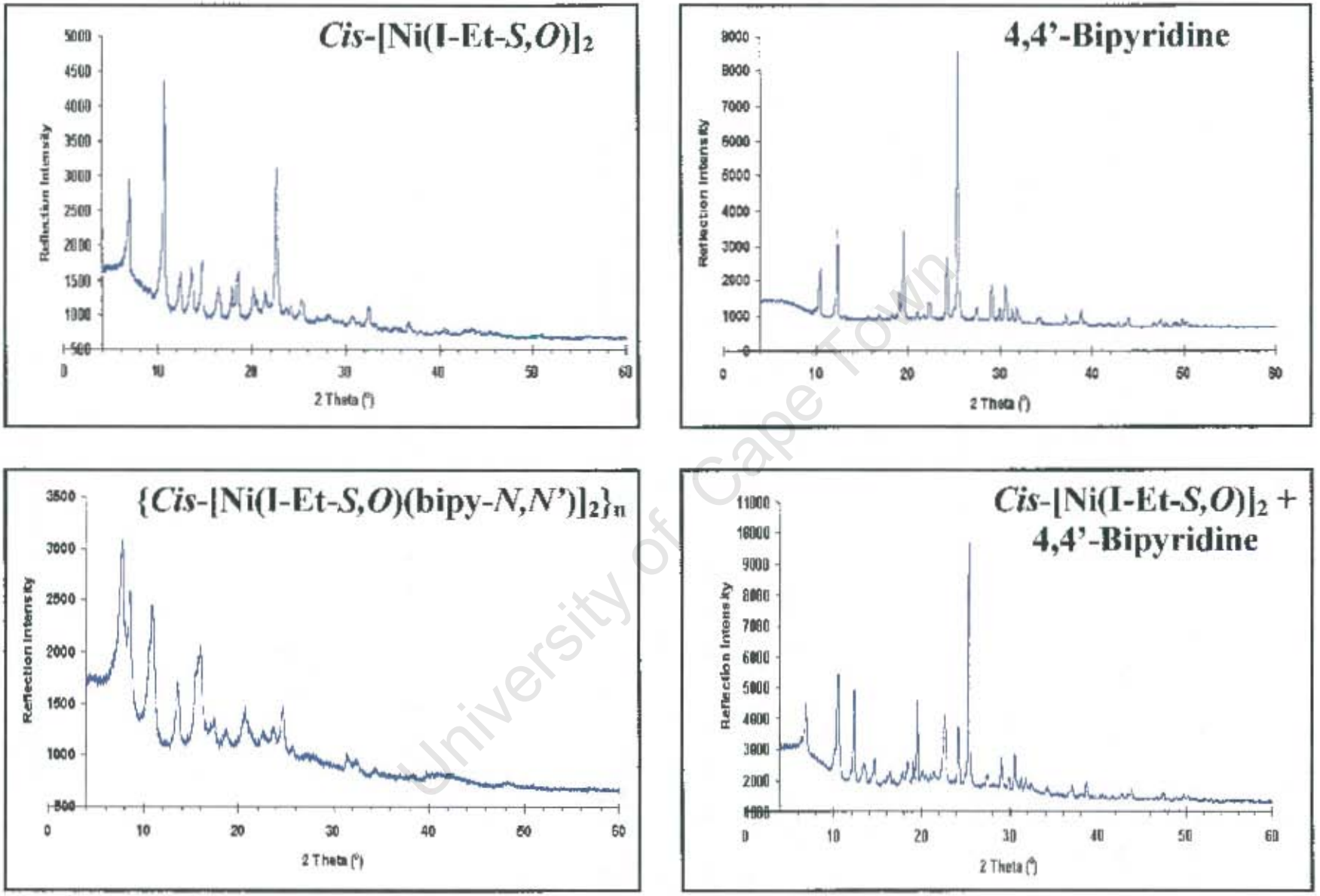

Figure 3.4.2(c). X-ray powder diffraction patterns for {*cis*-[Ni(I-Et-*S,O*) (bipy-*N,N'*)]$_2$}$_n$ and its unreacted components - separate and superimposed

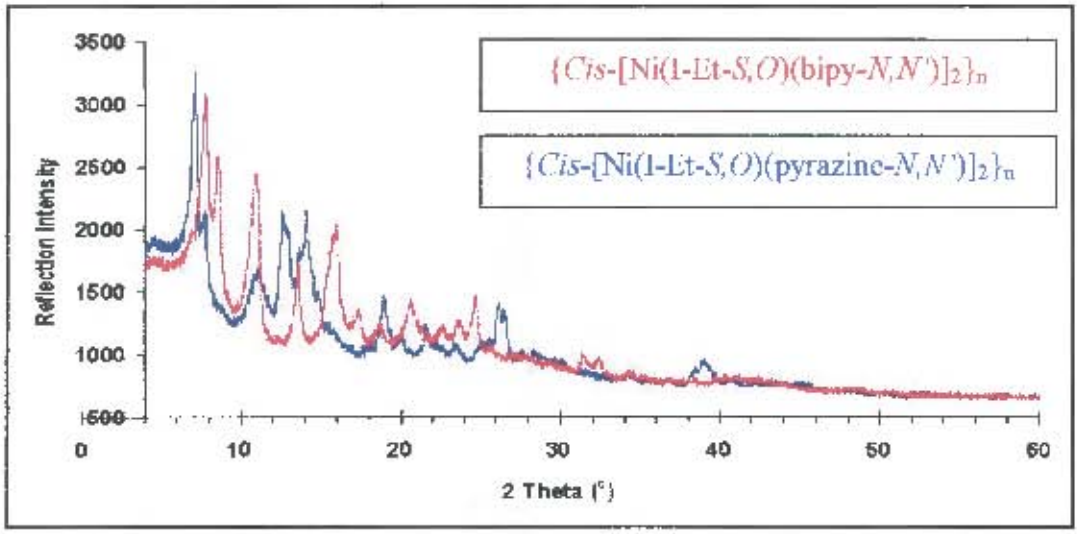

Figure 3.4.2(d) Comparison of x-ray powder diffraction patterns of {*cis*-[Ni(I-Et-*S,O*)(bipy-*N,N'*)]$_2$}$_n$ and {*cis*-[Ni(I-Et-*S,O*)(pyrazine-*N,N'*)]$_2$}$_n$

At low values of 2θ (0 – 20°), the graphs possess the same number of peaks with the same general shapes and similar heights (with the exception of the peaks at ca. 11°, which differ considerably in height). The peaks appear at similar angles, with some slight shifting observed. In two cases (at 2θ = ca. 8° and ca. 15°), where a peak shoulder is observed for {*cis*-[Ni(I-Et-*S,O*)(pyrazine-*N,N'*)]$_2$}$_n$, a similar feature is observed for {*cis*-[Ni(I-Et-*S,O*)(bipy-*N,N'*)]$_2$}$_n$, but with the shoulder amplified so that it appears as a distinct peak (at 2θ = 8.6° and 17.5° respectively). Clearly, the XRD patterns for {*cis*-[Ni(I-Et-*S,O*)(pyrazine-*N,N'*)]$_2$}$_n$ and {*cis*-[Ni(I-Et-*S,O*)(bipy-*N,N'*)]$_2$}$_n$ bear more similarity to each other than they do to the patterns for each of their respective components. This hints to a similarity in the crystal structures of the two products, which might be expected from two analogous coordination polymers.

Summary

Initial observations suggest that the product {*cis*-[Ni(I-Et-*S,O*)(bipy-*N,N'*)]$_2$}$_n$ is a new compound possessing octahedral coordination of 4,4'bipyridine around the Ni(II) centres of 2:2 metallamacrocycles. TGA and elemental analysis agree with the proposal that the product possesses a *cis*-[Ni(I-Et-*S,O*)]$_2$: bipy ratio of 1:4, with one dichloromethane guest per metallamacrocycle present in the structure. Unusual thermal behaviour suggests that the compound may be a clathrate complex. The similarities in properties and XRD results to {*cis*-[Ni(I-Et-*S,O*)(pyrazine-*N,N'*)]$_2$}$_n$ imply that the compound is a ladder-type coordination polymer. The proposed

composition for {*cis*-[Ni(I-Et-*S,O*)(bipy-*N,N'*)]$_2$}$_n$ is thus given as {*cis*-[Ni(l-Et-*S,O*)(bipy-*N,N'*)]$_2$.2(bipy).(CH_2Cl_2)}$_n$. A schematic diagram of this proposed structure is given in Fig 3.4.2(e).

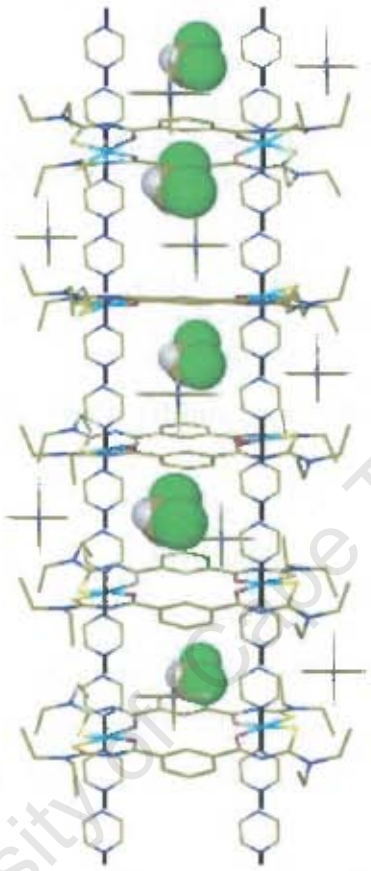

Figure 3.4.2(e). Schematic diagram of proposed structure for {*cis*-[Ni(I-Et-*S,O*)(bipy-*N,N'*)]$_2$}$_n$, illustrating coordinated bipy ligands, external bipy guests and enclathrated bipy and CH_2Cl_2 guests.

3.4.3. Poly-[*cis*-(bis-μ-(3,3,3',3'-tetraethyl-1,1'-isophthaloylbis(thioureato-*S,O*))-di-nickel(II))-bis-μ-(1,2-bis(4-pyridyl)ethane-*N,N'*)] ({*cis*-[Ni(I-Et-*S,O*)(BPE-*N,N'*)]$_2$}$_n$)

The reaction of purple *cis*-[Ni(I-Et-*S,O*)]$_2$ with 1,2-Bis(4-pyridyl)ethane (BPE) yielded a bright green powder with the colour change considered to be a sign of a change in the coordination around the Ni(II) centres from square planar to octahedral. The product of this reaction, {*cis*-[Ni(I-Et-*S,O*)(BPE-*N,N'*)]$_2$}$_n$, is initially expected to be a ladder type coordination polymer analogous to {*cis*-[Ni(I-Et-*S,O*)(pyrazine-*N,N'*)]$_2$}$_n$ and {*cis*-[Ni(I-Et-*S,O*)(bipy-*N,N'*)]$_2$}$_n$. Again, an indicator of the polymeric nature of this compound would be given by metallamacrocycle: ligand ratio of 1:2. The results of the characterisation of {*cis*-[Ni(I-Et-*S,O*)(BPE-*N,N'*)]$_2$}$_n$ are reported below.

Thermogravimetric Analysis

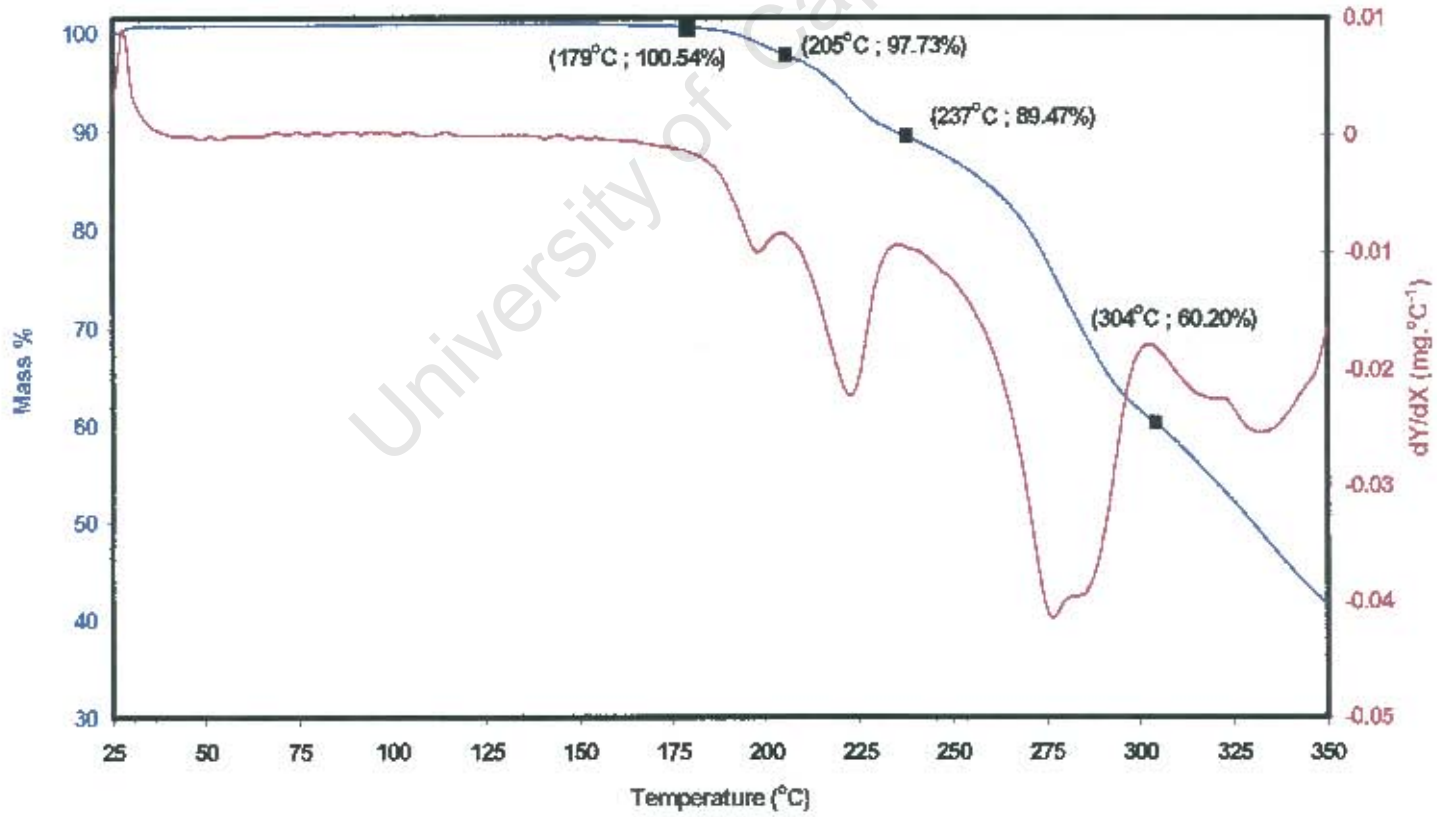

Figure 3.4.3(a). TGA trace for {*cis*-[Ni(I-Et-*S,O*)(BPE-*N,N'*)]$_2$}$_n$ with 1st derivative curve indicated.

Figure 3.4.3(a) illustrates the results of TGA for the product {*cis*-[Ni(I-Et-*S,O*)(BPE-*N,N'*)]$_2$}$_n$. It is immediately clear that a complex process is occurring as the sample is heated. The onset of mass loss occurs at ca.180 °C. The second derivative trace shows that the mass loss rate decreases at 205 °C – by which time less than 3 % of the total mass has been lost – but then increases greatly almost immediately until another point of inflection at 237 °C. This second thermal event involves the loss of 8.26 % of the total mass. After this, the mass loss rate increases again until 304 °C, at which point another 29.27 % of the mass has been lost. Beyond this temperature, the sample continues to lose mass as it decomposes. As a result of this behaviour, one cannot base any calculations on the assumption that the remaining mass at any point is solely attributed to the metallamacrocycle *cis*-[Ni(I-Et-*S,O*)]$_2$, which has been the strategy utilised in previous characterisations.

Hot Stage Microscopy

Figure 3.4.3(b) shows a series of photographs of a sample of {*cis*-[Ni(I-Et-*S,O*)(BPE-*N,N'*)]$_2$}$_n$ under silicone oil as it is heated from room temperature (heating rate 20 °C. min^{-1}). The sample appears to be stable with no observable change until 100 °C, where the appearance of bubbles signifies the removal of some component from the structure. This component removal increases considerably in rate so that by 130 °C the formation of bubbles is extremely rapid. This continues until around 180 °C, where the onset of a colour change suddenly occurs and by which time the bubbling has abated. This change begins at the periphery of the sample and spreads inwards towards the centre. The colour changes from green to purple through an orange intermediate colour. By 205 °C, the sample is completely purple. This is very much the same type of behaviour that was observed for {*cis*-[Ni(I-Et-*S,O*)(pyrazine-*N,N'*)]$_2$}$_n$ and {*cis*-[Ni(I-Et-*S,O*)(bipy-*N,N'*)]$_2$}$_n$ – apparent confirmation that {*cis*-[Ni(I-Et-*S,O*)(BPE-*N,N'*)]$_2$}$_n$ is simply an analogue of those two compounds. But then at around 230 °C, something wholly unexpected begins to happen. The sample appears to become paler in colour. By 250 °C this is much more noticeable and by 280 – 290 °C, the sample has become completely white. Then, by 310 °C, the sample darkens into a grey-green accompanied with the renewed onset of bubbling, which appears to signify the onset of total thermal decomposition, as the sample bubbles rapidly and gradually darkens further until finally, by 450 °C, only a black residue

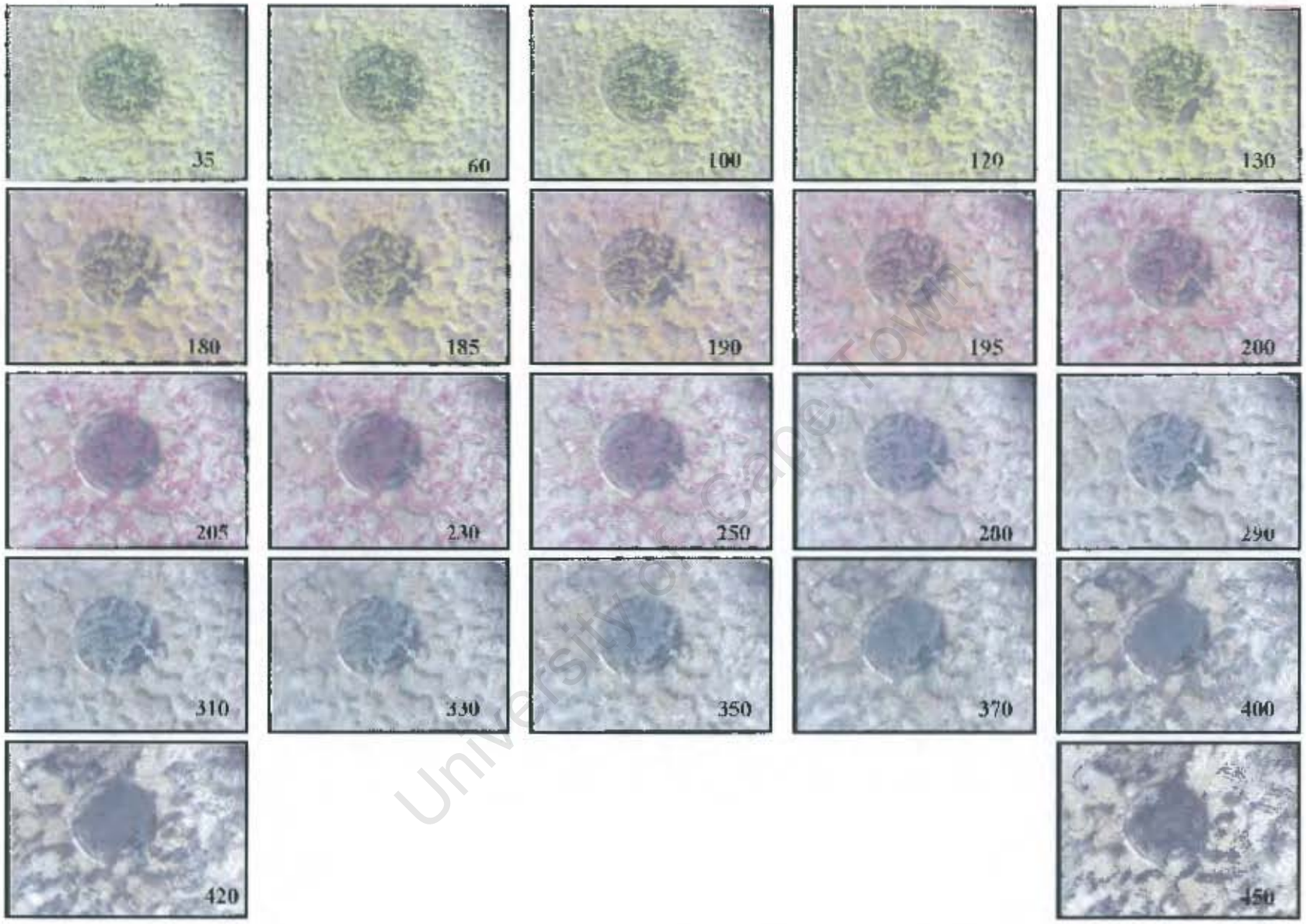

Figure 3.4.3(b). HSM photographs of {*cis*-[Ni(l-Et-*S,O*)(BPE-*N,N'*)]$_2$}$_n$ heated under silicone oil. Temperatures reported in degrees Celsius.

remains. Up till 230 °C, it seems that {*cis*-[Ni(I-Et-*S,O*)(BPE-*N,N'*)]$_2$}$_n$ undergoes the same transition as the first two coordination polymers: removal of guests and decoordination of axial ligands to revert to the metallamacrocycle *cis*-[Ni(I-Et-*S,O*)]$_2$. However the unexpected colour change from purple to white seems to suggest some major transition with respect to the Ni(II) centres. A white or colourless appearance is characteristic of Ni(0) complexes such as tetracarbonyl nickel. This would suggest that the Ni(II) centres have been reduced to Ni(0). However, such a consideration is highly unlikely as no strong reducing agents were employed in this reaction. Another alternative is presented by the reported existence of an interesting octahedral Ni(II) complex, which is polymeric and colourless. Furthermore, this coordination polymer employs 4,4'-bipyridine as a bidentate bridging ligand.[113] It therefore seems likely that a thermally induced rearrangement occurs within the sample to bring about this colour change. This adds more weight to the supposition that {*cis*-[Ni(I-Et-*S,O*)(BPE-*N,N'*)]$_2$}$_n$ (as well as its analogues) is indeed a coordination polymer. However, this phenomenon reinforces the difficulty in the characterisation of {*cis*-[Ni(I-Et-*S,O*)(BPE-*N,N'*)]$_2$}$_n$ by TGA. It is certain that at no time during the TGA is the metallamacrocycle *cis*-[Ni(I-Et-*S,O*)]$_2$ the sole remaining component. Therefore, its molar mass cannot be used as the basis on which the molar masses of other components may be determined. However, it seems that the boundary temperatures of the thermal events during TGA correspond very well with the temperatures of the chromatic transitions observed during HSM, and the conjunction of observations from the two techniques allows certain deductions to be made.

The first thermal event begins at around 180 °C. This event seems to involve a colour change from green through orange to purple as well as a mass loss of some 2.81 %. The mass loss slows down to a local minimum at 205 °C, which is the temperature at which the first colour change has completed. The second mass loss beginning at this temperature and continuing until 237 °C corresponds well with the range in which no colour change is observed during HSM. The next mass loss range (237 -- 304 °C) is the same range in which the sample loses its purple colour. Beyond 304 °C the mass loss increases again, corresponding with the observed gradual blackening of the sample.

The colour change observed at 180 °C can be attributed to the decoordination of 1,2-bis(4-pyridyl)ethane from the Ni(II) centres. However, the mass loss is too small to indicate the loss of these former ligands from the structure. It is more likely that – in a similar manner to that proposed for {*cis*-[Ni(I-Et-*S,O*)(bipy-*N,N'*)]$_2$}$_n$ above – this mass loss is due to the expulsion of an enclathrated dichloromethane guest, which was trapped within the structure until such time as the axial coordination bonds were broken. The purple colour to which the sample reverts from 180 – 205 °C could indicate the presence of the unpolymerised metallamacrocycle *cis*-[Ni(I-Et-*S,O*)]$_2$. However, it is certain that there is also 1,2-bis(4-pyridiyl)ethane present above this temperature, as the later transition would not occur if only *cis*-[Ni(I-Et-*S,O*)]$_2$ remained. The following thermal event from 205 – 237 °C might then represent the removal of BPE or more CH_2Cl_2. The Solver tool in Microsoft Excel was employed to find any viable solutions to the assignment of each percentage mass loss to integral numbers of BPE or CH_2Cl_2 (or combinations of both). This proved fruitless – even at a low accepted level of precision. This confirms that the mass loss from one point of inflection to another does not accurately represent the mass lost in each actual thermal event – a consequence of the fact that the mass loss rate at each point of inflection is still quite high. This especially applies to the point of inflection at 304 °C where the mass loss rate is 0.02 mg °C^{-1}. It is also at this temperature that the transition to the unknown colourless compound appears complete (according to HSM results) and it is therefore problematic that the mass loss is not more completely arrested at this temperature, as such an arrest would allow more accurate calculations to be made.

In short, only qualitative information can be gleaned from the TGA and HSM, because there is no stable or near-stable range of low mass loss rate during the TGA. The results of elemental analysis of {*cis*-[Ni(I-Et-*S,O*)(BPE-*N,N'*)]$_2$}$_n$ are reported below.

Elemental Analysis

Table 3.4.3(a) gives the results of elemental analysis for {*cis*-[Ni(I-Et-*S,O*)(BPE-*N,N'*)]$_2$}$_n$ together with the values calculated for several *cis*-[Ni(I-Et-*S,O*)]$_2$: BPE: CH_2Cl_2 ratios. The stoichiometries which are of interest are those corresponding to a monomeric octahedral adduct (*cis*-[Ni(I-Et-*S,O*)]$_2$: BPE: CH_2Cl_2 ratio 1: 4: 0), a

guest-free ladder-type polymeric structure (1: 2: 0) and then various other possibilities that may result from either of these stoichiometries with guests included in the structure. The results agree well with a ratio of either 1: 2: 0 or 1: 3: 1. This indicates that {*cis*-[Ni(I-Et-*S,O*)(BPE-*N,N'*)]$_2$}$_n$ is a ladder-type coordination polymer that possibly retains its enclathrated guests (one BPE and one CH_2Cl_2 guest per metallamacrocycle), while any non-enclathrated guests are lost on subjection of the sample to vacuum prior to elemental analysis. This means that no accurate information is given as to the original composition of the sample.

Table 3.4.3(a). Comparison of {*cis*-[Ni(I-Et-*S,O*)(BPE-*N,N'*)]$_2$}$_n$ elemental analysis results with values calculated for a monomeric octahedral adduct, a guest-free polymer and various possible structures containing guest molecules.

Element	Found %	Calculated %		
		cis-[Ni(I-Et-*S,O*)]$_2$: BPE: CH_2Cl_2 Ratio		
		1: 2: 0	1: 3: 0	1: 4: 0
C	56.75	56.70	59.43	61.54
H	5.79	5.71	5.82	5.90
N	12.84	13.22	13.48	13.67
S	9.13	10.09	8.81	7.82
		1: 4: 1	1: 3: 1	1: 2: 1
C		59.20	56.93	54.03
H		5.73	5.63	5.50
N		13.00	12.73	12.40
S		7.44	8.33	9.46

X-ray Powder Diffraction

Figure 3.4.3(c) shows the x-ray powder diffraction pattern for {*cis*-[Ni(I-Et-*S,O*)(BPE-*N,N'*)]$_2$}$_n$ as well as the patterns for *cis*-[Ni(I-Et-*S,O*)]$_2$, 1,2-Bis(4-

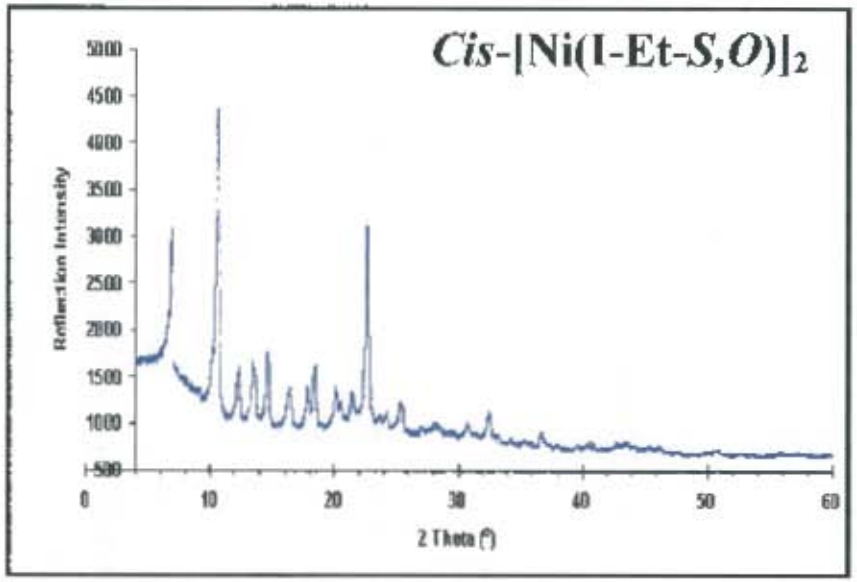

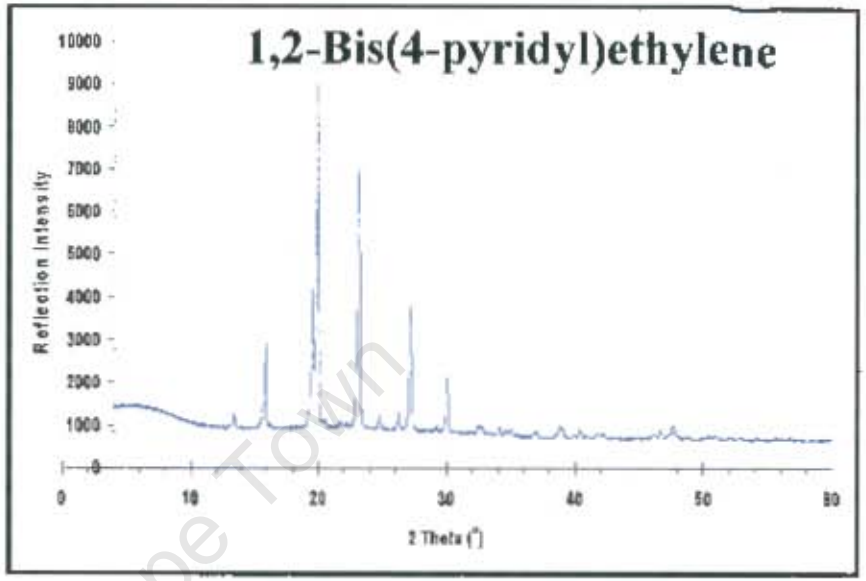

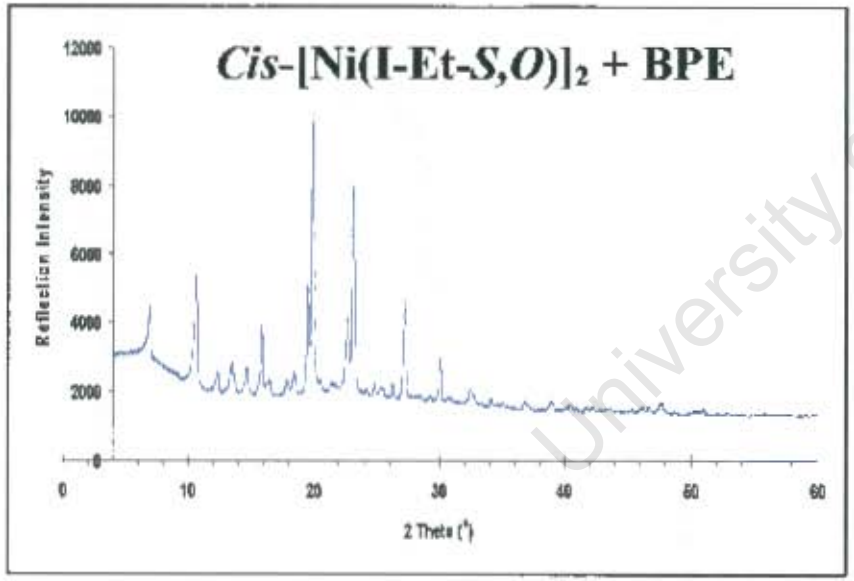

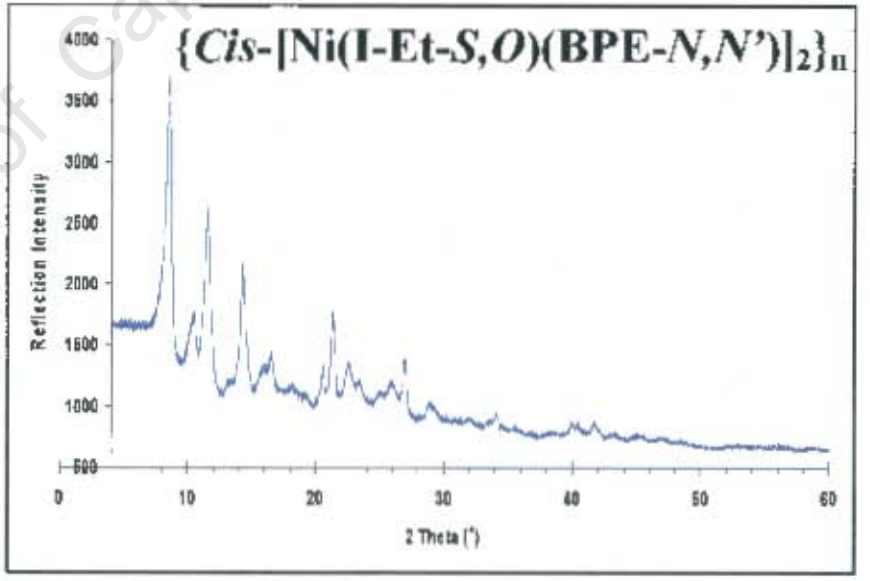

Figure 3.4.3(c). X-ray powder diffraction patterns for {*cis*-[Ni(I-Et-*S,O*) (BPE-*N,N'*)]$_2$}$_n$ and its unreacted components - separate and superimposed

pyridyl)ethane and a pattern generated by the addition of the reflection data for the latter two compounds. As was shown for {*cis*-[Ni(I-Et-*S,O*)(pyrazine-*N,N'*)]$_2$}$_n$ and {*cis*-[Ni(I-Et-*S,O*)(bipy-*N,N'*)]$_2$}$_n$, the XRD analysis of {*cis*-[Ni(I-Et-*S,O*)(BPE-*N,N'*)]$_2$}$_n$ confirms that this product possesses a crystal structure that differs markedly from that of either of its unreacted constituents. The prominent peaks at $2\theta = 19.9°$ and 23.3° in the BPE trace are absent from the {*cis*-[Ni(I-Et-*S,O*)(BPE-*N,N'*)]$_2$}$_n$ trace. Similarly absent from the {*cis*-[Ni(I-Et-*S,O*)(BPE-*N,N'*)]$_2$}$_n$ trace are the major peaks of the *cis*-[Ni(I-Et-*S,O*)]$_2$ trace at $2\theta = 6.9°$, 10.6° and 22.7°. At the same time, there are large peaks at $2\theta = 8.6°$ and 11.6° in the {*cis*-[Ni(I-Et-*S,O*)(BPE-*N,N'*)]$_2$}$_n$ trace that were present in neither the *cis*-[Ni(I-Et-*S,O*)]$_2$ nor the BPE powder diffraction pattern.

Furthermore, the {*cis*-[Ni(I-Et-*S,O*)(BPE-*N,N'*)]$_2$}$_n$ powder diffraction pattern bears much resemblance to that of {*cis*-[Ni(I-Et-*S,O*)(bipy-*N,N'*)]$_2$}$_n$ (which in turn was noticeably similar to that of {*cis*-[Ni(I-Et-*S,O*)(pyrazine-*N,N'*)]$_2$}$_n$ – as mentioned above). Figure 3.4.3(d) shows the powder diffraction pattern of {*cis*-[Ni(I-Et-*S,O*)(BPE-*N,N'*)]$_2$}$_n$ (in blue) together with that of {*cis*-[Ni(I-Et-*S,O*)(bipy-*N,N'*)]$_2$}$_n$ (in red) on the same set of axes.

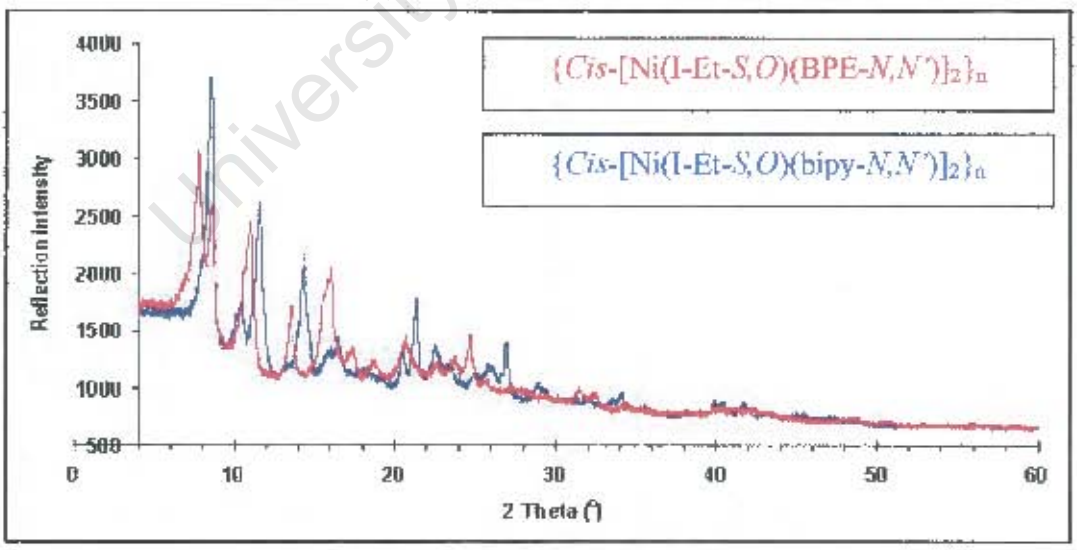

Figure 3.4.3(d) Comparison of x-ray powder diffraction patterns of {*cis*-[Ni(I-Et-*S,O*)(BPE-*N,N'*)]$_2$}$_n$ and {*cis*-[Ni(I-Et-*S,O*)(bipy-*N,N'*)]$_2$}$_n$

square planar Ni(II), but not enough to permanently alter the nature of the product. But perhaps more importantly is the fact that a better understanding of this product and its behaviour can contribute to our ability to design and develop powerful new molecular recognition materials

3.4.5. Poly-[*cis*-(tris-μ-(3,3,3',3'-tetraethyl-1,1'-terephthaloylbis(thioureato-*S,O*))-tri-nickel(II))-tris-μ-(pyrazine-*N,N'*)] ({*cis*-[Ni(T-Et-*S,O*)(pyrazine-*N,N'*)]$_2$}$_n$)

The reaction of the 3:3 metallamacrocycle *cis*-[Ni(T-Et-*S,O*)]$_3$ with pyrazine in chloroform yielded an orange suspension. On filtration, the product possessed a gel-like consistency, but after some time, the product lost this appearance. The final appearance of the product was found to be an orange powder similar in appearance to {*cis*-[Ni(I-Et-*S,O*)(DPE-*N,N'*)]$_2$}$_n$, which was shown above to be a potential coordination polymer, undergoing complete coordination on exposure to various solvents. In this case, the product, {*cis*-[Ni(T-Et-*S,O*)(pyrazine-*N,N'*)]$_2$}$_n$, did not display any such vapochromism. The results of the series of analyses for {*cis*-[Ni(T-Et-*S,O*)(pyrazine-*N,N'*)]$_2$}$_n$ are reported below.

Thermogravimetric Analysis

Figure 3.4.5(a) is a graphical illustration of the results of TGA for the product {*cis*-[Ni(T-Et-*S,O*)(pyrazine-*N,N'*)]$_2$}$_n$. The sample loses some 10.0 % of the total mass by 174 °C. A period of near stability (in gravimetric terms) occurs beyond this temperature. At 236 °C with 87 % of the total mass remaining, the sample is at its most stable – as shown by the first derivative trace, which indicates a local minimum in mass loss rate at this point. By 261 °C, with 85.0% of the total mass remaining, the quasi-stable range has ended and the compound rapidly decomposes.

If the remaining mass just prior to the onset of final decomposition is taken as representing only the 3:3 metallamacrocycle *cis*-[Ni(T-Et-*S,O*)]$_3$, then calculations can be made regarding the composition and the nature of {*cis*-[Ni(T-Et-*S,O*)(pyrazine-*N,N'*)]$_2$}$_n$. This strategy is the same as that employed in previous TGA characterisations. Prior to the final decomposition of the product, two separate thermal events take place, one much faster than the other. Table 3.4.5(a) gives the results of these calculations and assigns the masses lost in each thermal event to components of the compound

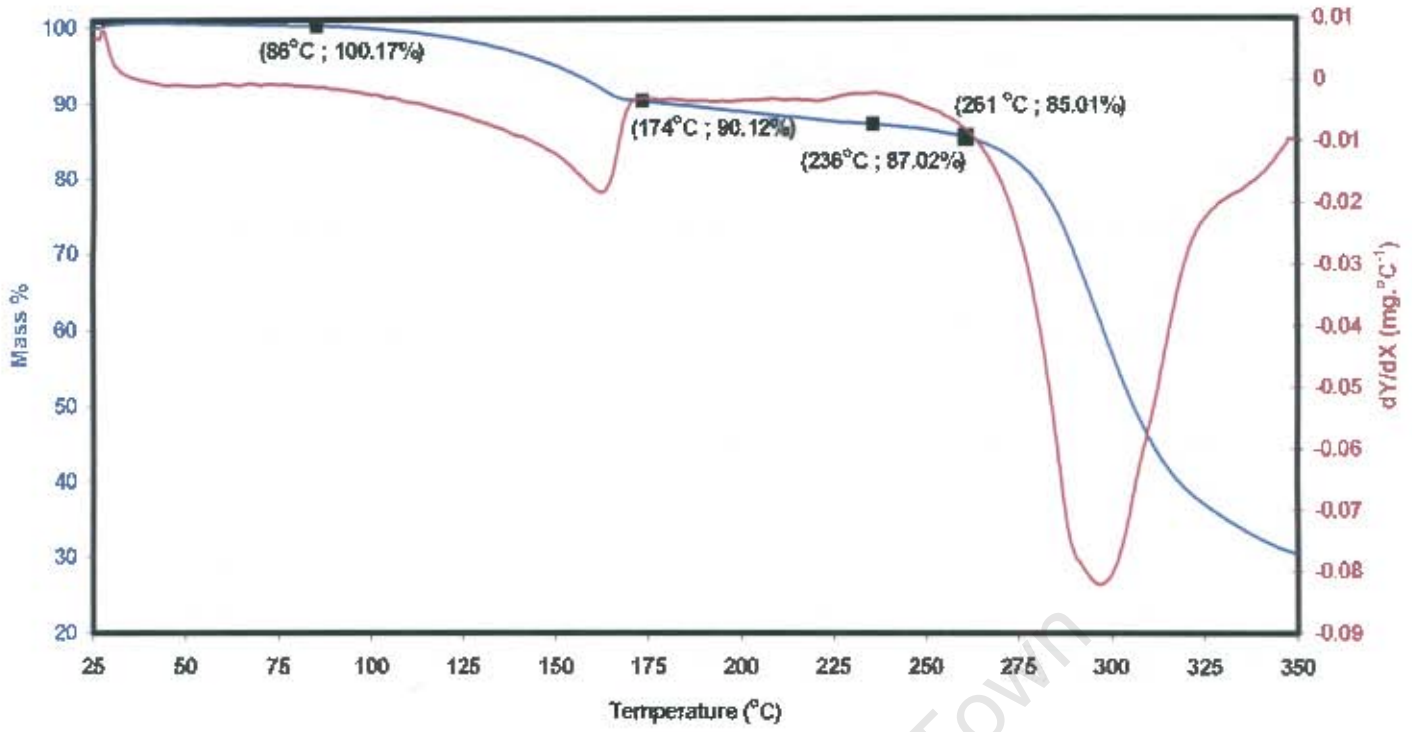

Figure 3.4.5(a) Graph of TGA results for {*cis*-[Ni(T-Et-*S,O*)(pyrazine-*N,N'*)]$_2$}$_n$

Table 3.4.4(a). TGA Calculations of Mass Losses for {*cis*-[Ni(T-Et-*S,O*)(pyrazine-*N,N'*)]$_2$}$_n$

Feature on Graph	Temp. Range (°C)	Component Mass %	Molar Mass (g.mol^{-1})	Component Identification
Onset of final decomp.	261	85.01 %	1353.762	*cis*-[Ni(T-Et-*S,O*)]$_3$
First Mass Loss	86 - 174	10.05 %	160	2 Pyrazines
Second Mass Loss	174 – 261	5.16 %	81	1 Pyrazine
Combined Mass Loss	86 - 261	15.21 %	241	3 Pyrazines

The TGA results clearly point to the loss of three pyrazine molecules per 3:3 metallamacrocyclic unit. The first thermal event is due to the loss of two pyrazine molecules, while the second event is due to the loss of another. There is no ambiguity arising from the similar molar masses of pyrazine and CH_2Cl_2 as there was for {*cis*-[Ni(I-Et-*S,O*)(pyrazine-*N,N'*)]$_2$}$_n$, because the solvent used in this case was chloroform (molar mass 119.38 g.mol^{-1}). The metallamacrocycle to bidentate ligand ratio is 1:3, which is expected for a linear 3:3 metallamacrocyclic coordination polymer as described in the beginning of Section 3.4 above.

Hot Stage Microscopy

A sample of {*cis*-[Ni(T-Et-*S,O*)(pyrazine-*N,N'*)]$_2$}$_n$ was heated under silicone oil from room temperature. A series of photographs taken during the heating process is given in Figure 3.4.5(b). The photographs indicate that the dull orange powder is stable up to ca. 90 °C – as there is no change in the appearance of the sample, and no evidence of gas evolution up to this point. These results agree well with the observations made during TGA, despite the differences in physical environment during the two analyses. During TGA, the onset of mass loss occurs at 86 °C – close to the 90 °C observed as the onset temperature during HSM. Above 90 °C, gas bubbles begin to form, but the appearance of the sample remains unchanged until 160 °C. By this stage, the sample has darkened in colour. At the same time, the rate of gas evolution has increased. The colour change continues as the sample is heated further. By 180 °C, the sample's colour is closer to purple than to orange. By 200 °C the sample is a dusty pink colour and the bubbling has abated somewhat. This colour persists for a while, with some slight darkening observed, but then, by 250 °C, the powder seems to be going paler. This colour change continues rapidly, so that at 270 °C, the sample is grey. The sample then proceeds to darken in colour and at 300 °C the onset of rapid bubbling is observed as the sample decomposes to a blackened residue. This behaviour shows that {*cis*-[Ni(T-Et-*S,O*)(pyrazine-*N,N'*)]$_2$}$_n$ undergoes some transition beginning at around 90 °C – most probably the loss of coordinated pyrazine ligands. By ca. 200 °C, this transition appears to be complete – as evidenced by the subsiding gas evolution. The sample appears to be relatively stable until around 270 °C, an observation that is mirrored by the relative stability in the mass of the sample from 180 °C – 250 °C – as seen during TGA. Beyond 270°C, decomposition begins, as indicated by the colour change to grey. The complete decomposition to a black residue continues beyond this point. This agrees roughly with the temperature for the onset of total decomposition of {*cis*-[Ni(T-Et-*S,O*)(pyrazine-*N,N'*)]$_2$}$_n$ observed during TGA. This thermal behaviour is similar to that of the 3:3 metallamacrocyclic adduct *cis*-[Ni(T-Et-*S,O*)(pyridine-*N*)$_2$]$_3$, which was shown (by TGA) to lose its coordinated ligands and revert to a square planar metallamacrocycle by 200 °C, and then rapidly decompose to a black residue. The onset of this final decomposition was found to occur at 286 °C. The thermal behaviour of {*cis*-[Ni(T-Et-*S,O*)(pyrazine-*N,N'*)]$_2$}$_n$ is also similar to that of

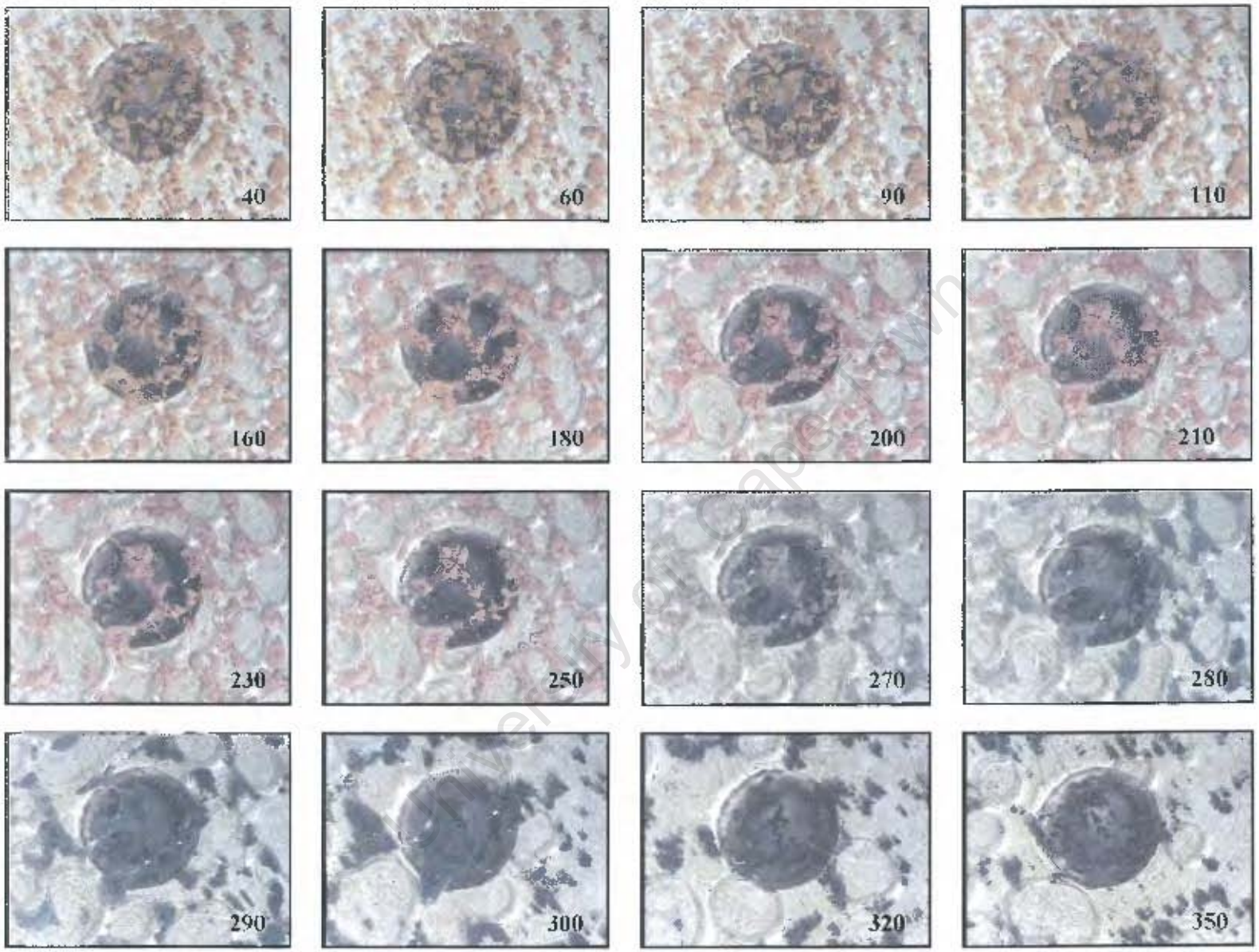

Figure 3.4.5(b). HSM photographs of {*cis*-[Ni(T-Et-*S,O*)(pyrazine-*N,N'*)]$_2$}$_n$ under silicone oil. Temperatures reported in degrees Celsius.

{*cis*-[Ni(I-Et-*S,O*)(pyrazine-*N,N'*)]$_2$}$_n$, the 2:2 coordination polymer formed from the same bidentate ligand.

Elemental Analysis

Table 3.4.5(b) shows the results of elemental analysis found for {*cis*-[Ni(T-Et-*S,O*)(pyrazine-*N,N'*)]$_2$}$_n$, and compares these results to values calculated for metallamacrocycle: ligand ratios of 1:3 and 1:6, which are the ratios expected for a 3:3 coordination polymer and a 3:3 monomeric octahedral adduct respectively.

Table 3.4.5(b). Comparison of {*cis*-[Ni(T-Et-*S,O*)(pyrazine-*N,N'*)]$_2$}$_n$ elemental analysis results with values calculated for a monomeric octahedral adduct and a guest-free polymer

Element	Found %	Calculated %	
		Metallamacrocycle: Pyrazine Ratio	
		1:3	1:6
C	49.66	49.73	51.07
H	5.34	5.31	5.28
N	15.33	15.82	18.33
S	12.57	12.07	10.49

The results correspond much more closely with the values calculated for a *cis*-[Ni(T-Et-*S,O*)]$_3$: pyrazine ratio of 1:3 than they do for a ratio of 1:6. This is further evidence that {*cis*-[Ni(T-Et-*S,O*)(pyrazine-*N,N'*)]$_2$}$_n$ is a linear 3:3 metallamacrocyclic coordination polymer.

IR Spectroscopy

As with the 2:2 coordination polymer, an increased absorption peak is observed in the 472 – 486 cm^{-1} range (at 483 cm^{-1}) that is characteristic of bidentate coordinated pyrazine [110, 111]. The absorption peak at 417 cm^{-1} for free pyrazine is absent from the

IR spectrum of {*cis*-[Ni(T-Et-*S,O*)(pyrazine-*N,N'*)]$_2$}$_n$. This indicates that there is no free pyrazine present as a guest in the structure. {*cis*-[Ni(T-Et-*S,O*)(pyrazine-*N,N'*)]$_2$}$_n$ contains only fully coordinated pyrazine ligands. In other words, it can be conclusively stated that {*cis*-[Ni(T-Et-*S,O*)(pyrazine-*N,N'*)]$_2$}$_n$ is a true coordination polymer.

X-ray Powder Diffraction

Figure 3.4.5(c) shows the x-ray powder diffraction pattern of {*cis*-[Ni(T-Et-*S,O*)(pyrazine-*N,N'*)]$_2$}$_n$ as well as those of its individual components *cis*-[Ni(T-Et-*S,O*)]$_3$ and pyrazine. A pattern generated by the addition of the patterns of the individual components was omitted, as it is immediately clear that {*cis*-[Ni(T-Et-*S,O*)(pyrazine-*N,N'*)]$_2$}$_n$ possesses a powder diffraction pattern that is completely different from those of its components or a combination thereof. {*cis*-[Ni(T-Et-*S,O*)(pyrazine-*N,N'*)]$_2$}$_n$ produces a trace of broad low-intensity peaks at low-to-medium values of 2θ, becoming almost flat and featureless at higher angles of diffraction. The highest peak in the trace occurs at 2θ = 5.0°. This broad-featured trace is characteristic of a compound possessing a low degree of crystallinity. In fact, {*cis*-[Ni(T-Et-*S,O*)(pyrazine-*N,N'*)]$_2$}$_n$ appears to be less crystalline in nature than any of the 2:2 coordination polymers.

It is worth mentioning that the metallamacrocycle *cis*-[Ni(T-Et-*S,O*)]$_3$ also does not give rise to high-intensity peaks of x-ray diffraction – unlike its 2:2 analogue *cis*-[Ni(I-Et-*S,O*)]$_2$ (see XRD sections for any 2:2 coordination polymer (Sections 3.4.1 – 3.4.4) for the *cis*-[Ni(I-Et-*S,O*)]$_2$ powder diffraction trace). The intensities of the *cis*-[Ni(T-Et-*S,O*)]$_3$ diffraction peaks are relatively low. It is uncertain, however, if there is any significance to the fact that *cis*-[Ni(T-Et-*S,O*)]$_3$ gives rise to partially (or – as will be shown below – entirely) amorphous coordination polymers, while the more powerfully diffracting *cis*-[Ni(I-Et-*S,O*)]$_2$ gives rise to coordination polymers possessed of higher degrees of crystallinity.

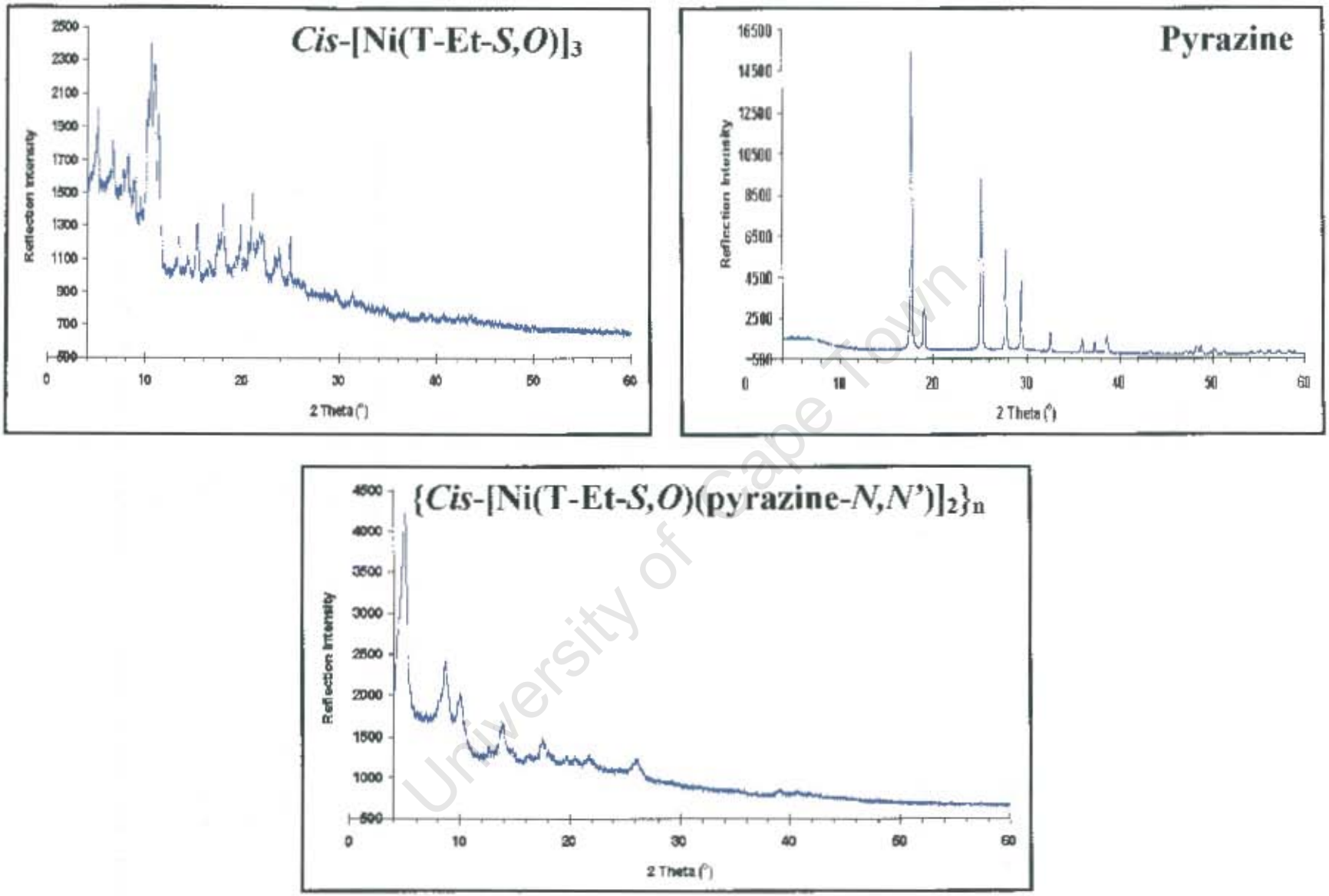

Figure 3.4.5(c). X-ray powder diffraction patterns for {*cis*-[Ni(T-Et-*S,O*)(pyrazine-*N,N'*)]$_2$}$_n$ and its unreacted components

Summary

The product {*cis*-[Ni(T-Et-*S,O*)(pyrazine-*N,N'*)]$_2$}$_n$ has been shown to be composed of three pyrazine molecules per *cis*-[Ni(T-Et-*S,O*)]$_3$ metallamacrocyclic unit. There is evidence of fully coordinated pyrazine and no indication of any free pyrazine in the product. These results are consistent with a 1D triply connected coordination polymer, with no included guests. The product is not highly crystalline and evidently possesses a solid-state structure that differs greatly from the structures of its individual components. Figure 3.4.5(d) below is a schematic diagram of such a polymeric structure of {*cis*-[Ni(T-Et-*S,O*)(pyrazine-*N,N'*)]$_2$}$_n$.

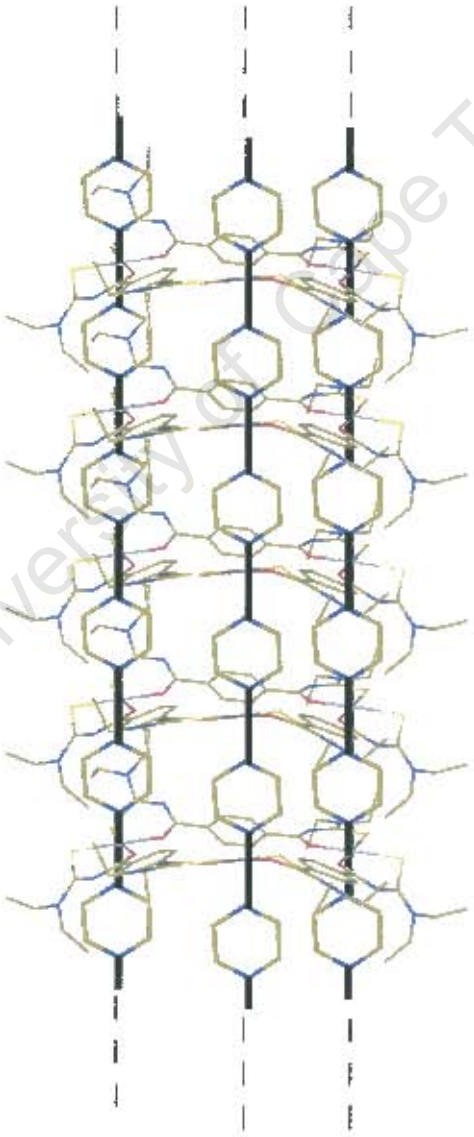

Figure 3.4.5(d). Schematic diagram of the polymeric structure of the 3:3 coordination polymer {*cis*-[Ni(T-Et-*S,O*)(pyrazine-*N,N'*)]$_2$}$_n$

3.4.6. Poly-[*cis*-(tris-μ-(3,3,3',3'-tetraethyl-1,1'-terephthaloylbis(thioureato-*S,O*))-tri-nickel(II))-tris-μ-(4,4'-bipyridine-*N,N'*)] {*cis*-[Ni(T-Et-*S,O*)(bipy-*N,N'*)]$_3$}$_n$

The second attempt at synthesising a coordination polymer of *cis*-[Ni(T-Et-*S,O*)]$_3$ was performed using 4,4'-bipyridine. As with previous reactions of metallamacrocycles with bidentate bridging ligands, a solid product rapidly formed as a suspension in the mother liquor. The colour of this suspension was bright orange. Upon collection from the mother liquor, the product was found to retain solvent and consequently to possess a gelatinous consistency. Upon solvent removal, the product was found to be an orange-brown powder. The results of analysis of this substance are reported below.

Thermogravimetric Analysis

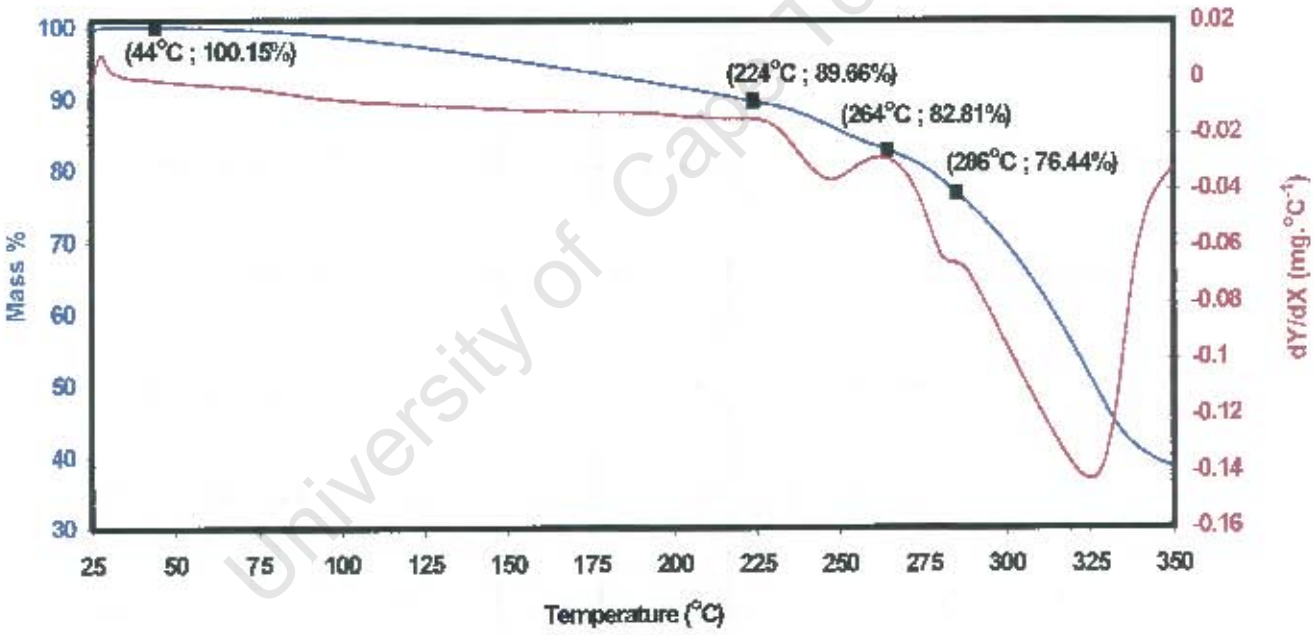

Figure 3.4.6(a). Results of TGA for {*cis*-[Ni(T-Et-*S,O*)(bipy-*N,N'*)]$_3$}$_n$

The results of TGA for {*cis*-[Ni(T-Et-*S,O*)(bipy-*N,N'*)]$_3$}$_n$ are given graphically in Figure 3.4.6(a). The results are unusual. It seems that the sample begins to lose mass almost immediately, but very gradually until 224 °C. At this point the rate of mass loss increases dramatically. At 264 °C the mass loss rate decreases to a local minimum (as shown by the first derivative trace). However, this local minimum is in fact still at quite a high rate of mass loss. Almost immediately after this temperature, the rate of decomposition increases further. At 286 °C the mass loss rate stops

increasing briefly, but then mass loss accelerates even further. By 340 °C less than 40 % of the original mass remains.

The temperature of 224 °C just prior to the acceleration of mass loss seems to correspond with the end of the seemingly stable range during HSM (see below). Beyond this temperature, the mass loss is so rapid that no meaningful calculations can be made. In short, the decomposition process of {*cis*-[Ni(T-Et-*S,O*)(bipy-*N,N'*)]$_3$}$_n$ does not appear to involve an intermediate stage in which only the 3:3 metallamacrocycle *cis*-[Ni(T-Et-*S,O*)]$_3$ is present, and in fact no gravimetrically stable range can be identified. For these reasons, it is not possible to determine the composition or the nature of this product from TGA.

Hot Stage Microscopy

Figure 3.4.6(b) is a series of photographs of {*cis*-[Ni(T-Et-*S,O*)(bipy-*N,N'*)]$_3$}$_n$ under silicone oil while being heated from room temperature. Up to, and beyond, 100 °C, the product appears quite stable. At 130 °C, the product is observed to darken slightly and a slow bubbling can be seen. By 150 °C, the sample has darkened to a brown colour. This colour remains until around 195 °C, where the sample begins to lighten in colour. The slow bubbling is observed throughout this temperature range. By 210 °C, the sample is clearly a much lighter brown than before, but by 230 °C, the sample appears to have acquired a purple tinge. By 240 °C, the sample has begun to take on a pale green colour as the purple-brown colouring disappears. At this point, the rate of gas evolution increases dramatically. By 245 °C the transition in colour has progressed further, and by 250 °C, the entire sample is pale green. Over the next 30 degrees, the sample continues to change colour, so that at 280 °C, the colour is more blue than green. The rapid bubbling is observed to abate at this point. The colour remains unchanged for a short time, but by 340 °C, the product is seen to be undergoing another chromatic transition to a mauve shade. Around 360 °C, the sample can distinctly be seen to be a pale purple. A rapid bubbling has begun at this stage and from 380 °C – 470 °C, this bubbling continues as the sample blackens and decomposes.

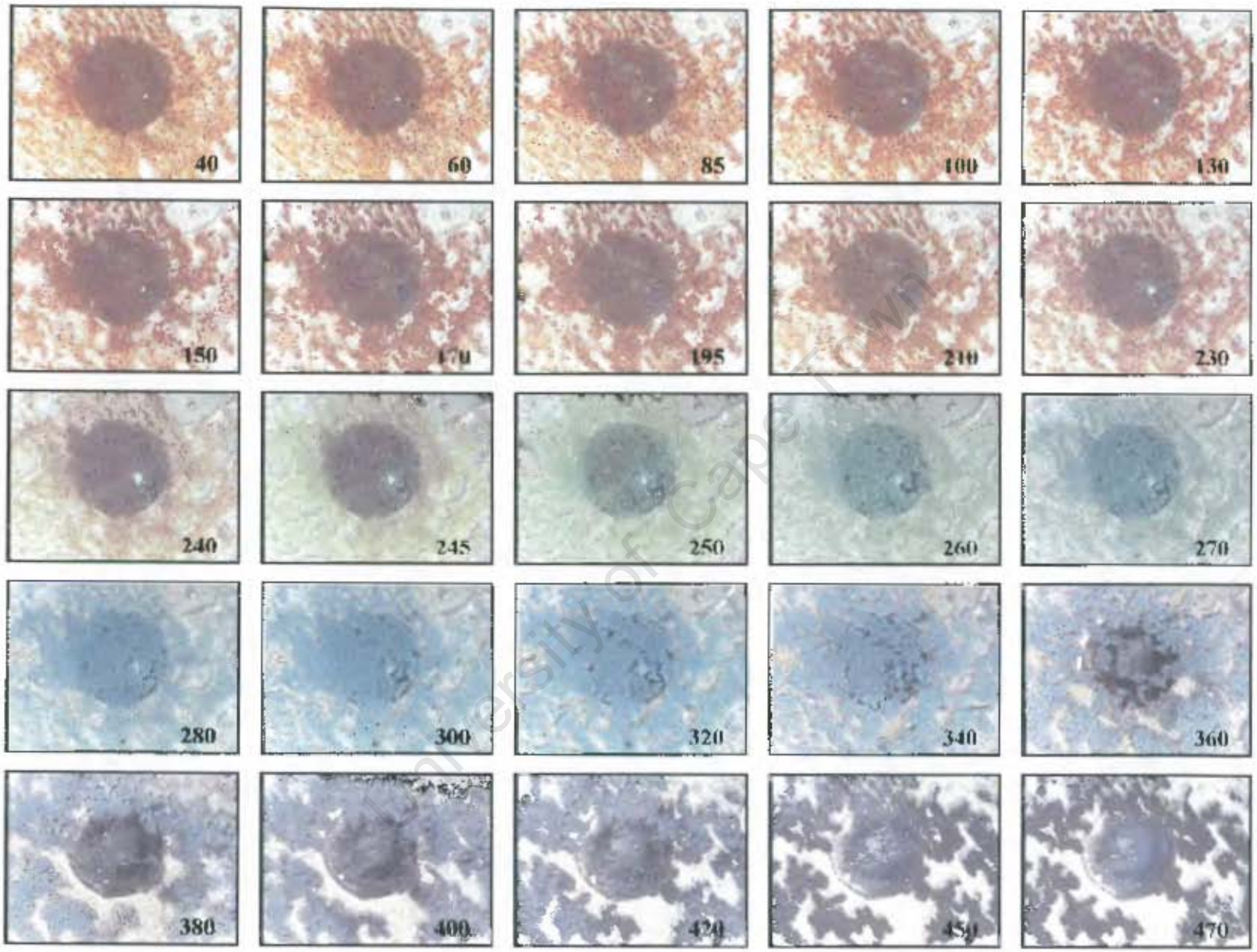

Figure 3.4.6(b). HSM photographs of {*cis*-[Ni(T-Et-*S,O*)(bipy-*N,N'*)]$_3$}$_n$ under silicone oil. Temperatures reported in degrees Celsius.

The number of different colours observed is quite remarkable, and it seems very difficult to identify any temperature range above 100 °C in which the sample is stable. Possibly, the only stable range is from 150 °C – 195 °C, where the colour remains unchanged and the rate of gas evolution appears to be very slow. The appearance of the product during this range is tentatively assigned to monomeric *cis*-[Ni(T-Et-*S,O*)]$_3$, although it is likely that there is still BIPY present that can recoordinate to the metallamacrocycle to give rise to the green colour observed at higher temperatures. Since the metallamacrocycle *cis*-[Ni(T-Et-*S,O*)]$_3$ is itself not stable at temperatures above 270 °C, it seems that the colouring of the sample above this temperature is due to decomposition products of the metallamacrocycle.

There is very little correlation between observations obtained from TGA and HSM, and there is little information that can be inferred from the results of either technique. At this stage, the thermal behaviour of {*cis*-[Ni(T-Et-*S,O*)(bipy-*N,N'*)]$_3$}$_n$ has not been satisfactorily elucidated.

Elemental Analysis

The results of elemental analysis for {*cis*-[Ni(T-Et-*S,O*)(bipy-*N,N'*)]$_3$}$_n$ are given in Table 3.4.6(a). This table also gives the calculated values for various possible compositions including a monomeric octahedral adduct and a 1D coordination polymer.

The observed values are closest to the values calculated for a metallamacrocycle: bipy: $CHCl_3$ ratio of 2:6:1. This is the ratio that would result from a linear 3:3 coordination polymer with one chloroform molecule for every two metallamacrocyclic units. So far, this is the only evidence that {*cis*-[Ni(T-Et-*S,O*)(bipy-*N,N'*)]$_3$}$_n$ is a coordination polymer. It should also be noted that in all previous cases, elemental analysis did not indicate the presence of conventionally included guests due to the subjection of the samples to vacuum prior to analysis. When elemental analysis did indicate the presence of guest molecules, it was inferred that these guests were enclathrated within the structure.

Table 3.4.6(a). Comparison of {*cis*-[Ni(T-Et-*S,O*)(bipy-*N,N'*)]$_3$}$_n$ elemental analysis results with values calculated for a monomeric octahedral adduct a guest-free polymer, and two compositions with included solvent guests.

Element	Found %	Calculated %			
		Metallamacrocycle: Bipy: $CHCl_3$ Ratio			
		1:3:0	1:6:0	1:3:1	2:6:1
C	53.98	55.36	59.77	52.58	53.93
H	5.18	5.31	5.28	5.04	5.17
N	13.20	13.84	14.67	12.98	13.40
S	9.66	10.56	8.40	9.91	10.22

If this is the case for this compound, it is possible that the vacuum has removed any other included guests and the remaining chloroform is strongly held within the central cavity of a metallamacrocycle, or possibly – as the stoichiometry suggests – held partially within the central cavities of two neighbouring metallamacrocycles with inverse orientations. A schematic diagram of such a structure is given in Figure 3.4.6(c) below.

IR Spectroscopy

The infrared spectrum of {*cis*-[Ni(T-Et-*S,O*)(bipy-*N,N'*)]$_3$}$_n$ does not show a peak around 487 cm^{-1}, which would indicate the presence of free *cis*-[Ni(T-Et-*S,O*)]$_3$. Similarly, the characteristic absorption at 500 cm^{-1} for uncoordinated 4,4'-bipyridine is absent from this spectrum. This indicates that the two components of this product are indeed coordinated to each other and therefore strengthens the argument that {*cis*-[Ni(T-Et-*S,O*)(bipy-*N,N'*)]$_3$}$_n$ is a coordination polymer.

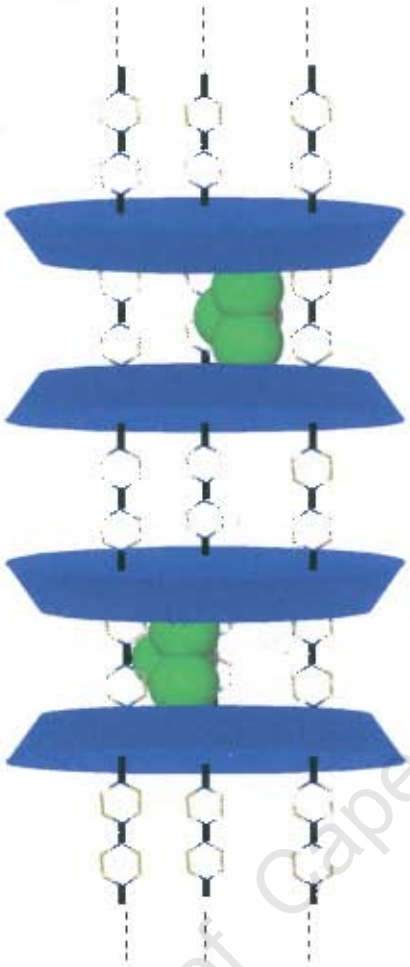

Figure 3.4.6(c) Schematic diagram of a possible polymeric structure of {*cis*-[Ni(T-Et-*S,O*)(bipy-*N,N'*)]$_3$}$_n$ giving rise to a *cis*-[Ni(T-Et-*S,O*)]$_3$: bipy: $CHCl_3$ ratio of 2:6:1 as indicated by elemental analysis

X-ray Powder Diffraction

The x-ray powder diffraction pattern of {*cis*-[Ni(T-Et-*S,O*)(bipy-*N,N'*)]$_3$}$_n$ is given below in Figure 3.4.6(d) along with the powder patterns generated from its individual components. Clearly, {*cis*-[Ni(T-Et-*S,O*)(bipy-*N,N'*)]$_3$}$_n$ is not a highly crystalline material. The broad, almost featureless trace indicates x-ray diffraction of virtually uniform intensity throughout the range $4° < 2\theta < 10°$. Beyond 10°, the reflection intensity drops off until about 15°, where it is seen to increase and then gradually decline as 2θ increases further.

The amorphous nature of the material could be a result of the rapidity of formation during the reaction. Also, the fact that upon formation the solid suspension is

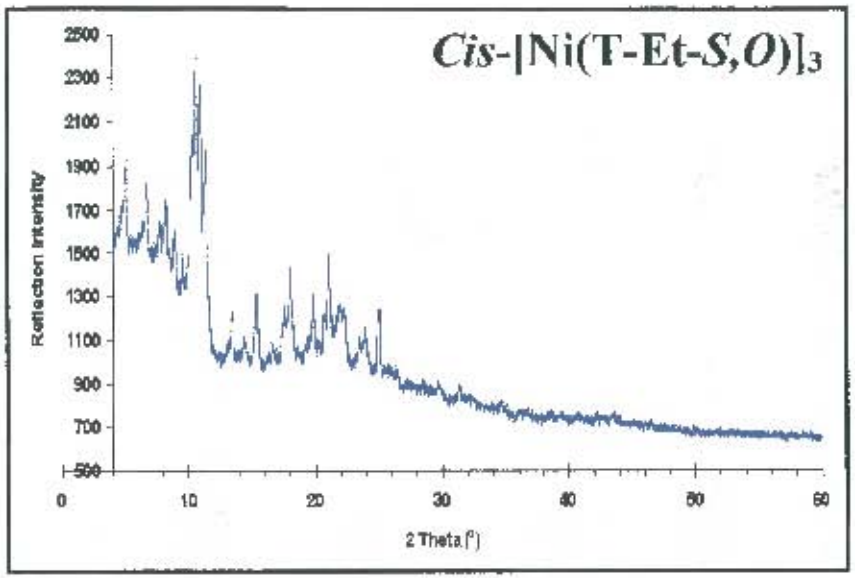

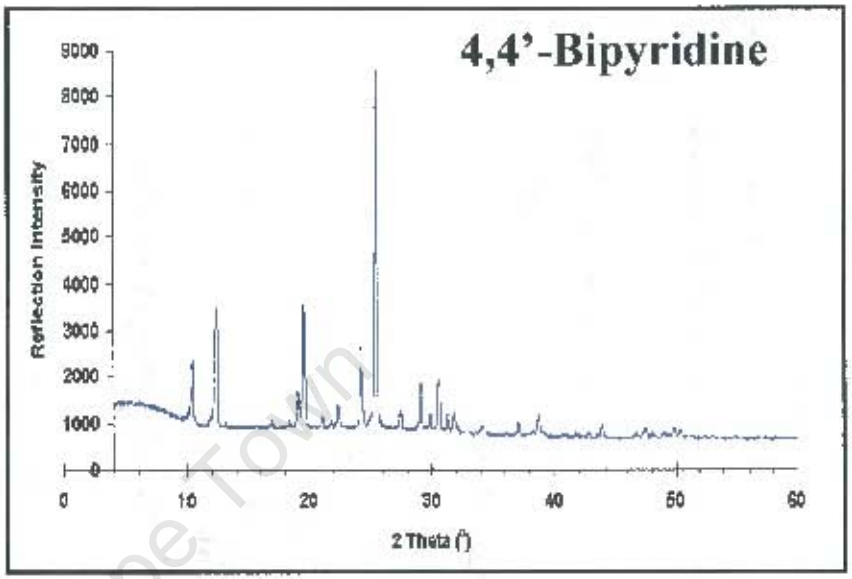

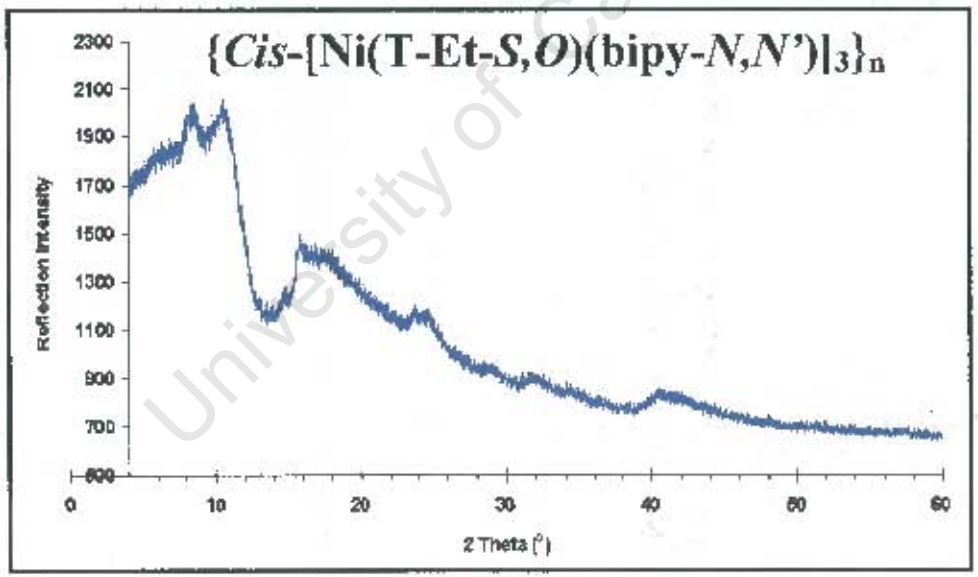

Figure 3.4.6(d). X-ray powder diffraction patterns for {*cis*-[Ni(T-Et-*S*,*O*)(bipy-*N*,*N*')]$_3$}$_n$ and its unreacted components

saturated with solvent – giving it a gel-like nature – could play a role in this phenomenon. As the suspension forms, the inclusion of a very large amount of solvent could result in a high degree of disorder in the solid structure. Alternatively, the suspension that forms could be of a highly ordered nature despite the inclusion of such a large amount of solvent, but upon removal of the retained solvent, the crystal structure of the material is considerably disrupted, resulting in an amorphous residual material.

This explanation would be consistent with what was observed in the case of {*cis*-[Ni(1-Et-*S,O*)(DPE-*N,N'*)]$_2$}$_n$: the presence of solvent molecules plays a vital role in the formation of these coordination polymers. The main difference between this case and that of {*cis*-[Ni(I-Et-*S,O*)(DPE-*N,N'*)]$_2$}$_n$ is that the crystal structure of {*cis*-[Ni(I-Et-*S,O*)(DPE-*N,N'*)]$_2$}$_n$ remains largely intact upon removal of solvent guests. This is almost certainly the result of channels in its crystal structure that allow the solvent to easily permeate the crystal structure – hence the lability of the transformation between guest-included and guest-free states. In the case of {*cis*-[Ni(T-Et-*S,O*)(bipy-*N,N'*)]$_3$}$_n$, the removal of solvent from the originally formed structure is not so labile and certainly is not reversible without completely dissolving the material, which seems to involve the decoordination of the bidentate ligands from the metallamacrocycles. The amorphous nature of this compound makes it very different from the other coordination polymers reported so far. In each case, the XRD data showed at least partial crystallinity of the material studied. This raises the interesting questions of whether {*cis*-[Ni(T-Et-*S,O*)(bipy-*N,N'*)]$_3$}$_n$ can be obtained in a crystalline form and what reaction conditions determine the degree of crystallinity of each of the polymerisation products.

Summary

The product {*cis*-[Ni(T-Et-*S,O*)(bipy-*N,N'*)]$_3$}$_n$ has proven difficult to characterise. It displays unusual thermal behaviour, as observed during hot stage microscopy and thermogravimetric analysis. The TGA results do not allow any accurate calculations and it is only the results of elemental analysis that give any indication of the composition of the material. These results hint at a 3:3 linear coordination polymer containing one strongly held chloroform guest for every two metallamacrocyclic units

– although this is following subjection to vacuum that could have removed more weakly held guests.

Infrared analysis provides further evidence that {*cis*-[Ni(T-Et-*S,O*)(bipy-*N,N'*)]$_3$}$_n$ is a coordination polymer, but XRD reveals that the material is highly amorphous. This could be the result of a disruption of the crystal structure by removal of included guests during post-synthetic treatment of the product. If this is the case, it contrasts greatly with {*cis*-[Ni(1-Et-*S,O*)(DPE-*N,N'*)]$_2$}$_n$, which is able to undergo repeated inclusion and expulsion of solvent guests without any great disruption to its crystal structure.

3.4.7. Poly-[*cis*-(tris-μ-(3,3,3',3'-tetraethyl-1,1'-terephthaloylbis(thioureato-*S,O*))-tri-nickel(II))-tris-μ-(1,2-di(4-pyridyl)ethylene-*N,N'*)] ({*cis*-[Ni(T-Et-*S,O*)(DPE-*N,N'*)]$_3$}$_n$)

The reaction of the metallamacrocycle *cis*-[Ni(T-Et-*S,O*)]$_3$ with the bidentate ligand 1,2-di(4-pyridyl)ethylene in chloroform resulted in the formation of an orange suspension with a gel-like consistency similar to that observed during the synthesis of {*cis*-[Ni(T-Et-*S,O*)(bipy-*N,N'*)]$_3$}$_n$. Once collected, with all solvent evaporated off, the product appeared as an orange-brown powder. The product, {*cis*-[Ni(T-Et-*S,O*)(DPE-*N,N'*)]$_3$}$_n$, was then subjected to the same series of analytical techniques as were the coordination polymers reported above.

{*Cis*-[Ni(I-Et-*S,O*)(DPE-*N,N'*)]$_2$}$_n$, the 2:2 coordination polymer formed with 1,2-di(4-pyridyl)ethylene exhibited vapochromism; there is no evidence of any such behaviour for {*cis*-[Ni(T-Et-*S,O*)(DPE-*N,N'*)]$_3$}$_n$. Exposure to a variety of solvent vapours for considerable periods of time did not result in any visible transformation of the product.

Thermogravimetric Analysis

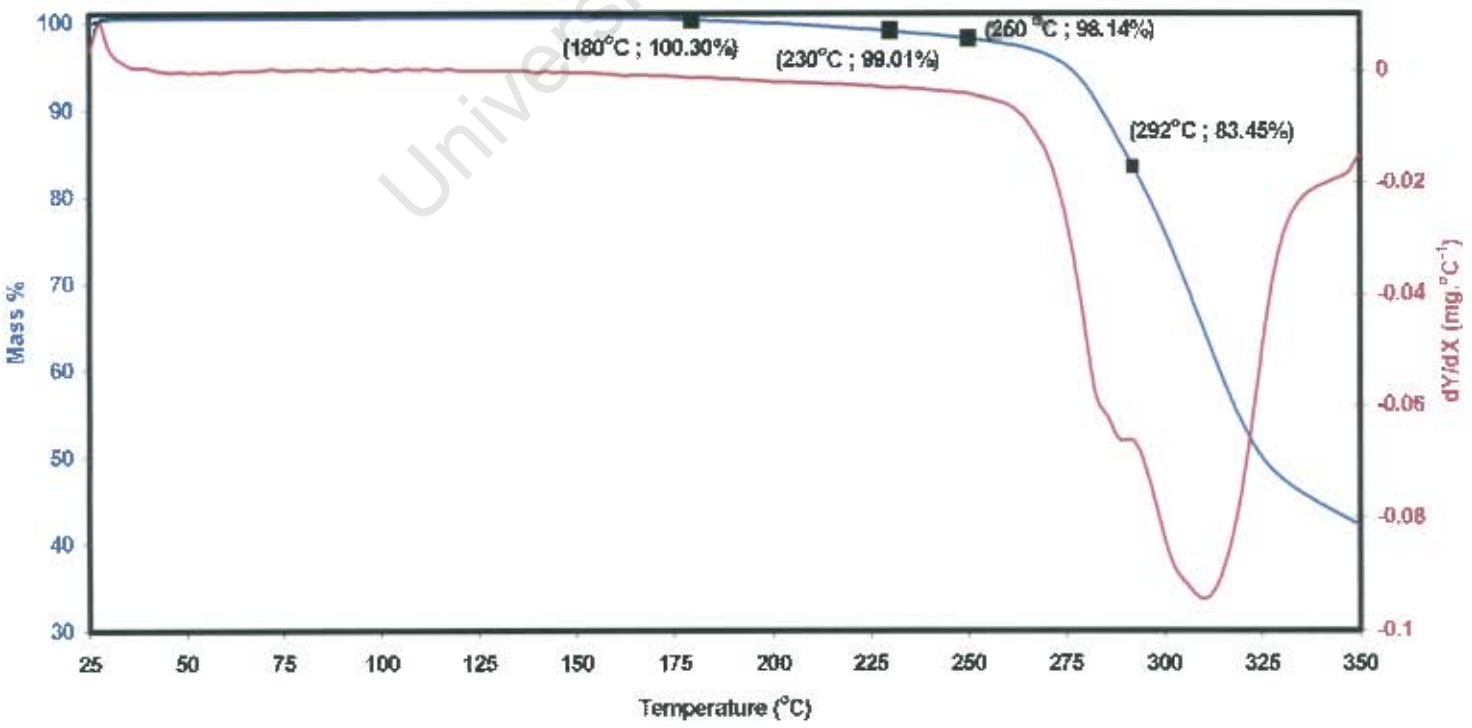

Figure 3.4.7(a). Results of TGA for {*cis*-[Ni(T-Et-*S,O*)(DPE-*N,N'*)]$_3$}$_n$

The results of TGA for {*cis*-[Ni(T-Et-*S,O*)(DPE-*N,N'*)]$_3$}$_n$ are given in Figure 3.4.7(a). The graph indicates one single mass loss of almost 60% of the total mass. The first derivative trace reveals that at 292 °C, the mass loss rate stops increasing. However, at this point the mass loss rate is very high, and no meaningful calculations can be made based on the remaining mass at this temperature.

Note that the mass loss only begins at around 180°C, and even up to 250°C the rate of mass loss is very low, with only about 2% of the total mass being lost over that 70-degree range. This transition could be the result of a decoordination of ligands from the Ni(II) centres without their expulsion from the structure. Beyond 250 °C, the sample begins to decompose, losing mass at an accelerating rate.

Whatever the case may be, the thermal decomposition of {*cis*-[Ni(T-Et-*S,O*)(DPE-*N,N'*)]$_3$}$_n$ does not appear to involve an intermediate phase in which the metallamacrocycle *cis*-[Ni(T-Et-*S,O*)]$_3$ is the sole remaining component; nor is there any evidence of any gravimetrically stable stage in the decomposition process. As a result, the determination of the composition of {*cis*-[Ni(T-Et-*S,O*)(DPE-*N,N'*)]$_3$}$_n$ by TGA is not possible.

Hot Stage Microscopy

A sample of {*cis*-[Ni(T-Et-*S,O*)(DPE-*N,N'*)]$_3$}$_n$ was heated on a hot stage under silicone oil from room temperature. A series of photographs taken during the process are presented in Figure 3.4.7(b). The sample appears to remain unchanged during heating up till ca. 180 °C, where a slight lightening in colour is observed. This process continues till 250 °C, at which point the sample is a light yellow-orange colour. The temperature range in which this gradual colour change occurs corresponds well with the interval of initial gradual mass loss in the TGA trace. This appearance does not persist for long, and from 260 °C, colouring of the sample begins to fade further so that by 280 °C, the sample is pale grey. The sample begins to darken very gradually from 300 °C onward, so that by 400 °C, the sample is a much darker shade of grey; evolution of gas can also be observed at this point. By 450 °C the sample has decomposed to a black residue.

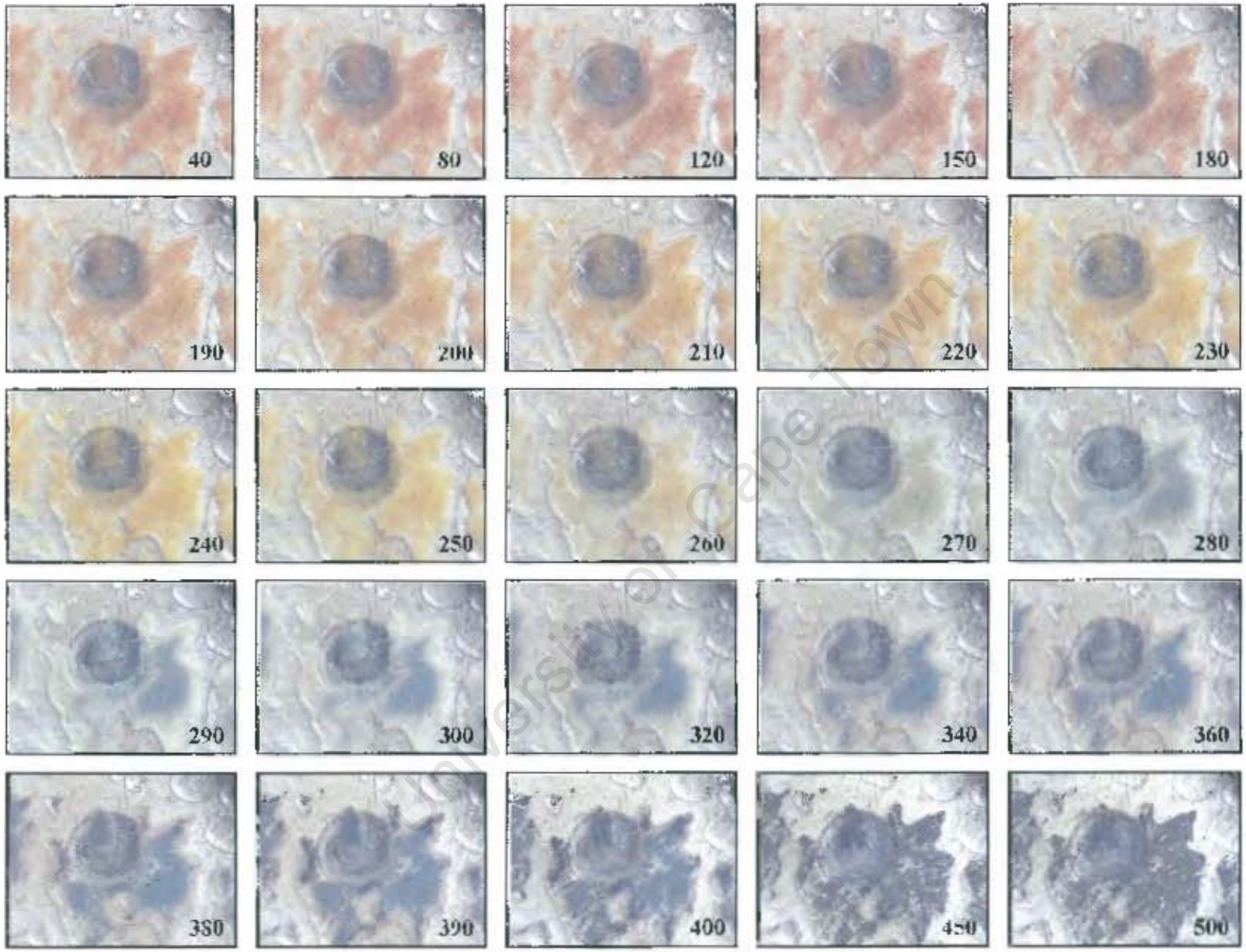

Figure 3.4.7(b). HSM photographs of {*cis*-[Ni(T-Et-*S*,*O*)(DPE-*N*,*N'*)]$_3$}$_n$ under silicone oil. Temperatures reported in degrees Celsius.

The behaviour of the sample suggests that it is stable up to a relatively high temperature. Then, from 180 ° - 250 °C some transition occurs. In most of the cases above, the first transition in colour is due to the decoordination of axial ligands from the metallamacrocycle. In this case, the initial colour of the sample is that of the free metallamacrocycle *cis*-[Ni(T-Et-*S,O*)]$_3$, and the colour after the transition is consistent with an octahedral adduct of *cis*-[Ni(T-Et-*S,O*)]$_3$ (the adduct *cis*-[Ni(T-Et-*S,O*)(pyridine-*N*)$_2$]$_3$ was a yellow-orange colour in solution.) It is also interesting that no bubbling of gas is observed during this transition. Although, counterintuitive, it seems that the sample is undergoing a complexation, not a decoordination as the temperature is raised. From 260 °C onward, the sample undergoes another transition – possibly involving the decomposition of the *cis*-[Ni(T-Et-*S,O*)]$_3$ metallamacrocycle. A very gradual decomposition takes place, and still no bubbling is observed. The absence of any visible gas evolution makes the thermal behaviour of this product very different from any of the coordination polymers reported above

Elemental Analysis

Table 3.4.7(a). Comparison of {*cis*-[Ni(T-Et-*S,O*)(DPE-*N,N'*)]$_3$}$_n$ elemental analysis results with values calculated for a monomeric octahedral adduct a guest-free polymer, and two compositions with included solvent guests.

Element	Found %	Calculated %			
		Metallamacrocycle: DPE: $CHCl_3$ Ratio			
		1:3:0	1:6:0	1:3:1	2:6:1
C	56.74	56.88	61.84	54.11	55.46
H	5.60	5.41	5.44	5.14	5.27
N	13.05	13.27	13.74	12.48	12.86
S	9.62	10.12	7.86	9.52	9.81

The results of the elemental analysis of {*cis*-[Ni(T-Et-*S,O*)(DPE-*N,N'*)]$_3$}$_n$ are given in Table 3.4.7(a), along with values calculated for a monomeric octahedral adduct, a

guest-free linear coordination polymer and two possible compositions of a coordination polymer with included guests.

The results obtained correspond well with the values calculated for a metallamacrocycle: ligand: chloroform ratio of 1:3:0, i.e. a guest-free coordination polymer. Since the sample was subjected to vacuum prior to analysis, it is possible that any included guests were removed and therefore not detected. There is no evidence of any enclathrated guests, and in fact, a compound that contains no volatile guests would be more likely to display the thermal behaviour observed for this compound – specifically the gravimetric stability up to relatively high temperatures.

IR Spectroscopy

The results of infrared analysis are of special interest for {*cis*-[Ni(T-Et-*S,O*)(DPE-*N,N'*)]$_3$}$_n$, because of the possibility that the compound is not a true coordination polymer at room temperature and actually undergoes complexation at elevated temperatures. The indication of free *cis*-[Ni(T-Et-*S,O*)]$_3$ is the characteristic absorption peak at or around 487 cm^{-1}. A peak is observed at 480 cm^{-1}; this is inconclusive. The peak at 670cm^{-1} for free DPE was found to disappear in the spectrum of {*cis*-[Ni(I-Et-*S,O*)(DPE-*N,N'*)]$_2$}$_n$ in its fully coordinated form, and the absence of such a peak is taken as an indicator that no free DPE is present in a sample. No such peak is observed for {*cis*-[Ni(T-Et-*S,O*)(DPE-*N,N'*)]$_3$}$_n$. This suggests that the compound is in a fully coordinated form at room temperature. Despite the unusual colour change and other thermal behaviour, it seems that {*cis*-[Ni(T-Et-*S,O*)(DPE-*N,N'*)]$_3$}$_n$ is a true linear coordination polymer in its powdered form at room temperature.

Despite the fact that its 2:2 analogue displays remarkable molecular recognition properties, {*cis*-[Ni(T-Et-*S,O*)(DPE-*N,N'*)]$_3$}$_n$ appears to be devoid of any such property. Even though it does not contain any included guests, {*cis*-[Ni(T-Et-*S,O*)(DPE-*N,N'*)]$_3$}$_n$ apparently does not possess sites available or accessible for occupation by guest molecules.

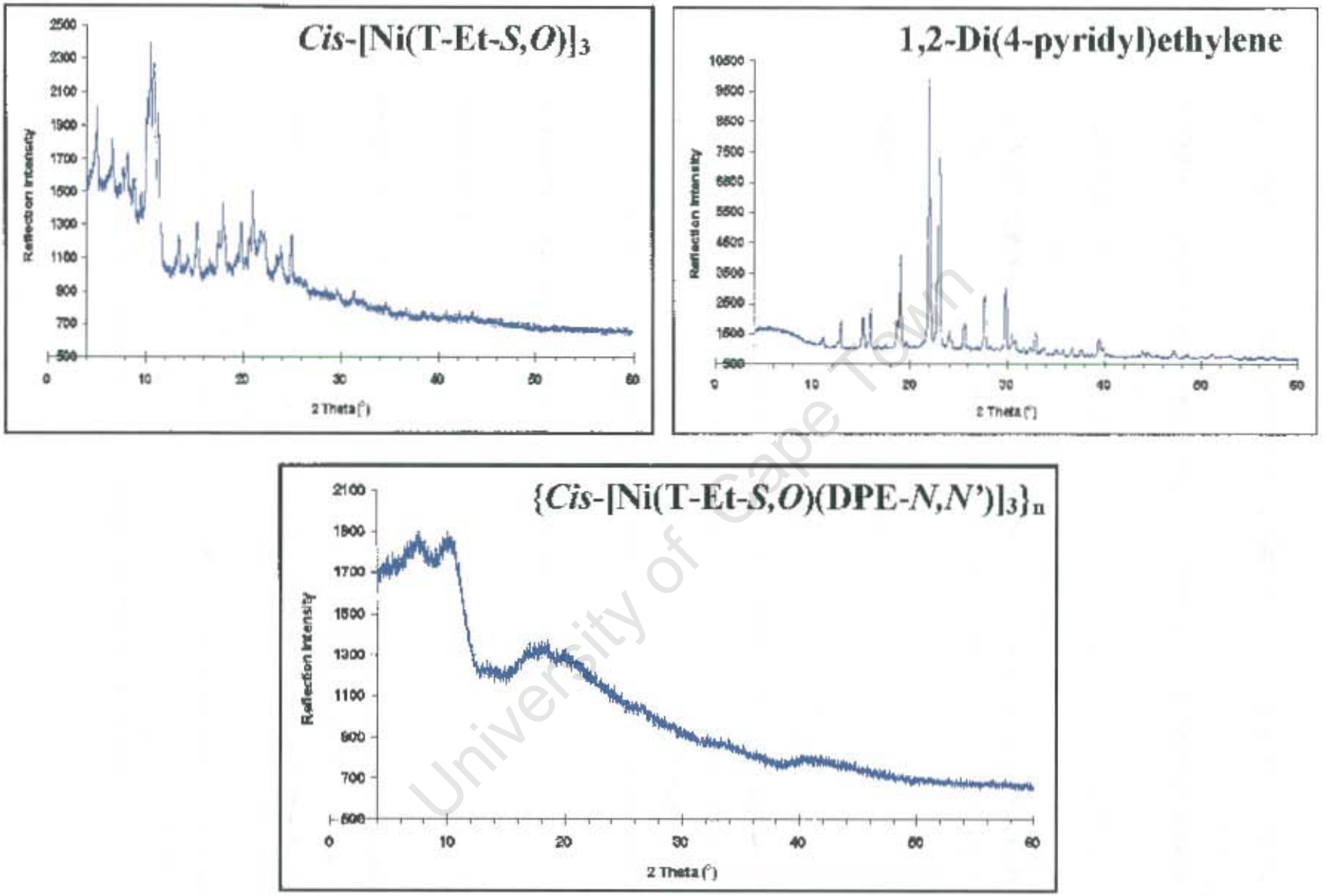

Figure 3.4.7(c). X-ray powder diffraction patterns for {*cis*-[Ni(T-Et-*S,O*)(DPE-*N,N'*)]$_3$}$_n$ and its unreacted components

X-ray Powder Diffraction

The XRD results for {*cis*-[Ni(T-Et-*S,O*)(DPE-*N,N'*)]$_3$}$_n$ are illustrated graphically in Figure 3.4.7(c), along with the powder diffraction patterns for its individual components: *cis*-[Ni(T-Et-*S,O*)]$_3$ and DPE. The results show that {*cis*-[Ni(T-Et-*S,O*)(DPE-*N,N'*)]$_3$}$_n$ is not crystalline. Like {*cis*-[Ni(T-Et-*S,O*)(bipy-*N,N'*)]$_3$}$_n$, this compound gives rise to a broad, practically featureless x-ray diffraction pattern. Again, the amorphous nature of the compound may come about from the rapidity of formation of the solid product, or possibly from disruption to the crystal structure during removal of excess solvent during collection of the product. As mentioned for {*cis*-[Ni(T-Et-*S,O*)(bipy-*N,N'*)]$_3$}$_n$, this disruption of the crystal structure upon expulsion of volatile included solvent molecules contrasts with the ability of {*cis*-[Ni(I-Et-*S,O*)(DPE-*N,N'*)]$_2$}$_n$ to expel solvent molecules with no major disruption to its structure – and readmit them with as much ease.

Whatever the reason, it is evident that 3:3 coordination polymers are more likely to form amorphous solids than their 2:2 counterparts. Whether this is inherent in the nature of the metallamacrocycle, or a result of the solvent used is unclear (chloroform was chosen over dichloromethane for use in the synthesis of the 3:3 coordination polymers as *cis*-[Ni(T-Et-*S,O*)]$_3$ is far more soluble in chloroform).

Summary

The compound {*cis*-[Ni(T-Et-*S,O*)(DPE-*N,N'*)]$_3$}$_n$ is a 3:3 linear coordination polymer. Although it displays unusual thermal behaviour and no calculations based on TGA can be made, the results of elemental analysis and infrared spectroscopy give some insight into the nature of the compound. The possibility – introduced by the unusual colour change observed during HSM – that the compound is not a coordination polymer until heated has been considered and discarded as unlikely, based on the results of IR analysis. X-ray powder diffraction analysis indicates that this product is an amorphous solid. No included guests are indicated for this product and it shows no sign of being able to admit any solvent molecules into its structure. {*cis*-[Ni(T-Et-*S,O*)(DPE-*N,N'*)]$_3$}$_n$ does not possess the molecular recognition abilities of its 2:2 analogue {*cis*-[Ni(I-Et-*S,O*)(DPE-*N,N'*)]$_2$}$_n$, meaning that the latter

remains unique among all the coordination polymers synthesised and studied in this project.

The graphs are not identical. There are some slight shifts in 2θ values and differences in peak height as well as some merging or splitting of peaks. But the overall similarity is unmistakeable. All the features of one graph are present in the other with only relatively small differences. Since their x-ray diffraction behaviours are so similar, it is indeed possible that the compounds {*cis*-[Ni(I-Et-*S,O*)(bipy-*N,N'*)]$_2$}$_n$ and {*cis*-[Ni(I-Et-*S,O*)(BPE-*N,N'*)]$_2$}$_n$ are structurally similar too – possessing the same space group symmetry. If this is the case, then it is highly likely that the asymmetric unit contents would be remarkably similar too.

Summary

From initial observations {*cis*-[Ni(I-Et-*S,O*)(BPE-*N,N'*)]$_2$}$_n$ appears to be a ladder-type coordination polymer, i.e. a homologue of the compounds {*cis*-[Ni(I-Et-*S,O*)(pyrazine-*N,N'*)]$_2$}$_n$ and {*cis*-[Ni(I-Et-*S,O*)(bipy-*N,N'*)]$_2$}$_n$. This proposal is strengthened by the elemental analysis results, which match data calculated for a coordination polymer of this type – and also match the data calculated for such a coordination polymer with one BPE and one CH_2Cl_2 molecule enclathrated within the structure. TGA and HSM support the hypothesis that there is enclathrated dichloromethane present. However TGA does not allow a complete characterisation of the product in this case, because there is no gravimetrically stable temperature range. Added to this is the extra complication of some transformation of the complex at high temperature from a purple coloured sample – thought to be monomeric *cis*-[Ni(I-Et-*S,O*)]$_2$ together with uncoordinated BPE – to a colourless material – possibly a new polymeric form.

The original form of {*cis*-[Ni(I-Et-*S,O*)(BPE-*N,N'*)]$_2$}$_n$ is thought to be a coordination polymer containing some enclathrated guests and possibly other associated guest molecules as well. The polymer would thus be of the form {*cis*-[Ni(I-Et-*S,O*)(BPE-*N,N'*)]$_2$.x(BPE).y(CH_2Cl_2)}$_n$ where x and y are unknown integers of value greater than or equal to 1. XRD results suggest some structural similarity between {*cis*-[Ni(I-Et-*S,O*)(BPE-*N,N'*)]$_2$}$_n$ and {*cis*-[Ni(I-Et-*S,O*)(bipy-*N,N'*)]$_2$}$_n$. A schematic representation of {*cis*-[Ni(I-Et-*S,O*)(BPE-*N,N'*)]$_2$}$_n$ would thus be much the same as that of {*cis*-[Ni(I-Et-*S,O*)(bipy-*N,N'*)]$_2$}$_n$ as shown in Figure 3.4.2(e) above.

3.4.4. Poly-[*cis*-(bis-μ-(3,3,3',3'-tetraethyl-1,1'-isophthaloylbis(thioureato-*S,O*))-di-nickel(II))-bis-μ-(1,2-di(4-pyridyl)ethylene-*N,N'*)] ({*cis*-[Ni(I-Et-*S,O*)(DPE-*N,N'*)]$_2$}$_n$)

The reaction of *cis*-[Ni(I-Et-*S,O*)]$_2$ with 1,2-di(4-pyridyl)ethylene yielded a product that differed markedly from the three 2:2 coordination polymers reported above. In the mother liquor of dichloromethane, the product appeared as a green suspension. However upon filtration, the green powder underwent a colour change to orange as the residual dichloromethane was removed by evaporation. A small portion of dichloromethane was to be used to wash the filtrate, but before the liquid solvent was allowed into contact with the filtrate, it was noticed that the orange powder had transformed in colour back to green. It was quickly established that exposure to vapours of dichloromethane rapidly induced this colour change. Furthermore this vapochromism was found to be fully reversible once exposure to the solvent vapours was halted. Preliminary tests showed that this phenomenon occurred with other solvents, namely chloroform, acetone and dimethylformamide (although in the latter case, the sample had to be immersed in liquid solvent for the colour change to occur). It was also noted that this phenomenon did not occur on exposure of the sample to water or ethanol. In terms of rate of transition, an order of rapidity of colour change on exposure to solvent was established. The order from most rapid to least is: CH_2Cl_2; $CHCl_3$; acetone; DMF. Figure 3.4.4(a) is a series of photographs illustrating this transformation.

An explanation for this phenomenon is that the solvent-free product contains nickel(II) ions with both square planar and octahedral coordination – giving rise to the orange colour similar to that observed for each of the 2:2 coordination polymers at intermediate stages of thermally induced decoordination. The structure can apparently be permeated by solvent molecules, which cause some internal disruption that results in square planar nickel undergoing axial coordination to become octahedral – hence the green colouring that is characteristic of octahedral nickel(II). The difference in size and mobility of solvent molecules may give rise to varying rates of permeation and thus the varying rates at which the colour change occurs.

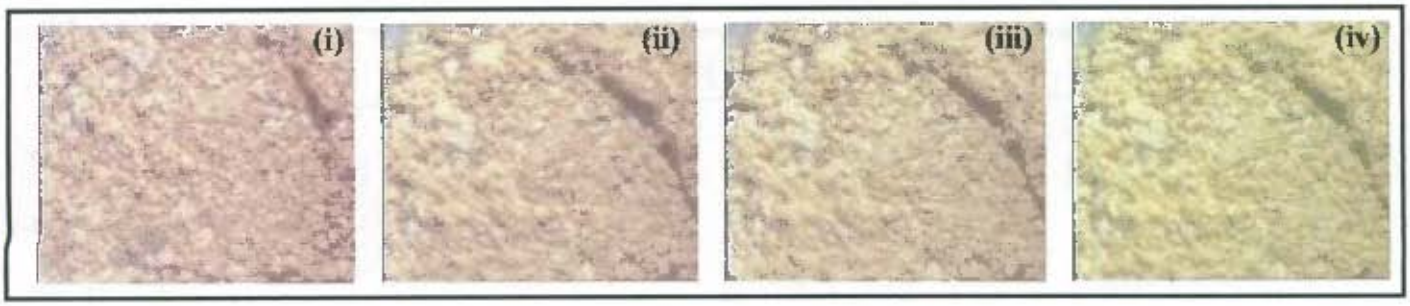

Figure 3.4.4(a). Digital photographs of a sample of {*cis*-[Ni(I-Et-*S,O*)(DPE-*N,N'*)]$_2$}$_n$: (i) as a light orange powder prior initially, (ii) undergoing a colour change immediately upon enclosure in a CH_2Cl_2 saturated chamber, (iii) substantially further in the transition in colour after ca. 5 seconds of exposure and (iv) in the final chromatic state as a pale green powder after 1 minute of exposure. Note: colours appear duller in these pictures than when actually observed.

The same analytical procedures were employed for {*cis*-[Ni(I-Et-*S,O*)(DPE-*N,N'*)]$_2$}$_n$ as were used for the first three coordination polymers above. Another technique using a levitating balance was used to further study the solvent absorption and vapochromism of this compound. The results of these analyses are reported below.

Thermogravimetric Analysis

Figure 3.4.4(b) is a graph obtained from TGA for {*cis*-[Ni(I-Et-*S,O*)(DPE-*N,N'*)]$_2$}$_n$. The initial mass loss begins at ca. 196 °C. By 263 °C this event has ended, with some 19.33 % of the total mass lost. The second thermal event begins soon after 263 °C and continues until 310 °C. The mass lost in this event is 10.40% of the original mass. Beyond 310 °C, a very large and sharp mass loss is observed. By the end of the TGA run at 350 °C, this thermal event is essentially complete, with some 36.20% of the original mass having been lost. In fact, this sharp mass loss at 310 °C shares much similarity with observations made for the 2:2 octahedral adducts and for the coordination polymer {*cis*-[Ni(I-Et-*S,O*)(pyrazine-*N,N'*)]$_2$}$_n$. In each of those cases, the sharp mass loss at around 310 °C was attributed to the decomposition of the metallamacrocycle *cis*-[Ni(I-Et-*S,O*)]$_2$, and the remaining mass just prior to this sharp mass loss was attributed solely to *cis*-[Ni(I-Et-*S,O*)]$_2$.

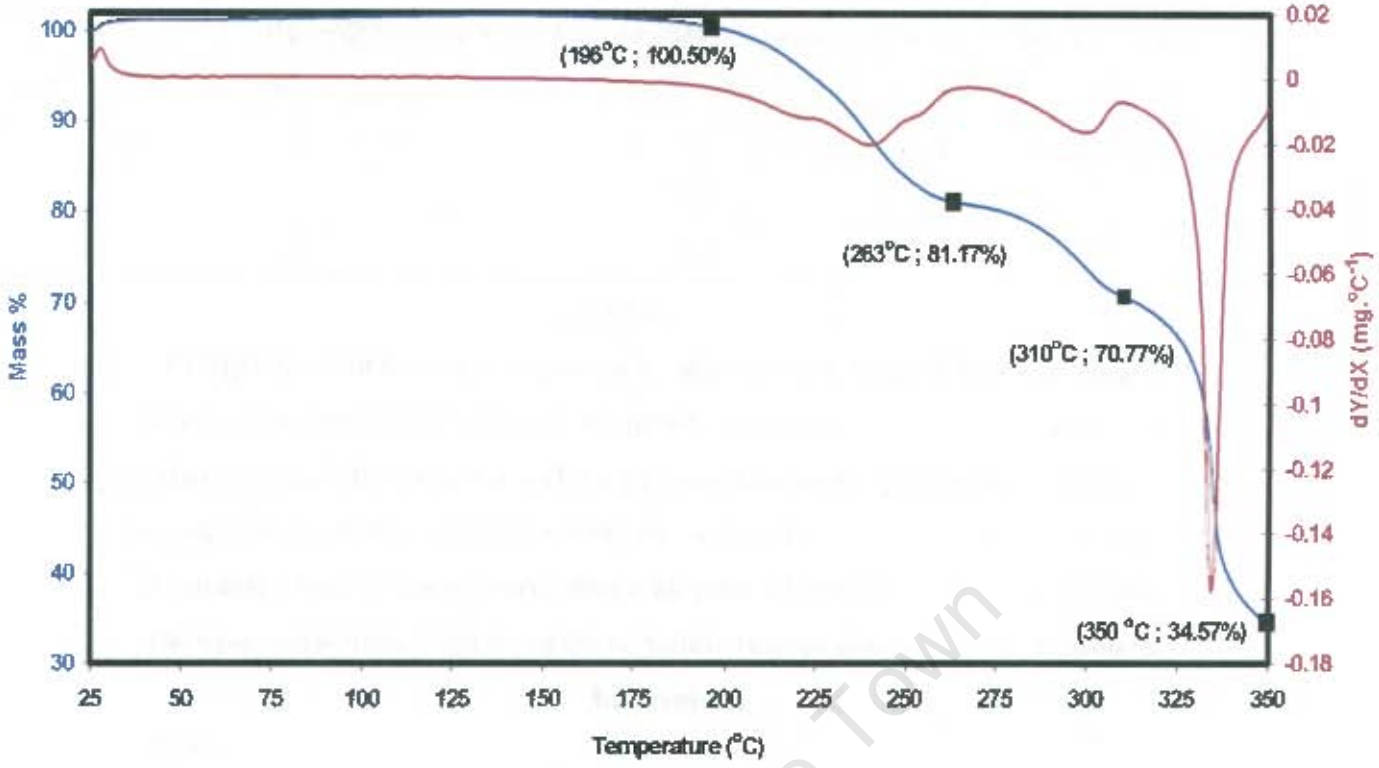

Figure 3.4.4(b). TGA trace for {*cis*-[Ni(I-Et-*S,O*)(DPE-*N,N'*)]$_2$}$_n$ with 1st derivative curve indicated.

It would seem that {*cis*-[Ni(I-Et-*S,O*)(DPE-*N,N'*)]$_2$}$_n$ does revert to *cis*-[Ni(I-Et-*S,O*)]$_2$ during TGA and therefore mass calculations based on this premise can be performed. Furthermore, the first derivative trace indicates that mass loss is practically arrested between the first and second events, and also abates, albeit momentarily, to a very slow rate at the boundary between the second and third thermal events. Therefore, it should be easier to interpret the TGA results for this compound than it was for {*cis*-[Ni(I-Et-*S,O*)(BPE-*N,N'*)]$_2$}$_n$. The results of the mass calculations for {*cis*-[Ni(I-Et-*S,O*)(DPE-*N,N'*)]$_2$}$_n$ and their interpretation are presented in Table 3.4.4(a) below.

The molar mass calculations indicate that in the first two thermal events, a total of 378 g.mol^{-1} is lost. This corresponds fairly well with the molar mass of two 1,2-di(4-pyridyl)ethylene molecules (molar mass 182.2 g.mol^{-1}) per metallamacrocycle. The observed mass loss does seem to be slightly high, but the recorded initial mass gain, of some 0.5% could account for this. The fact that the two thermal events do not individually correspond with the mass of one DPE molecule each is consistent with the originally stated deduction that there are not ligands octahedrally coordinated to

all the nickel(II) centres, yet there must be molecules present as potentially coordinating ligands to allow the octahedral coordination that causes the colour change on exposure to solvent.

Table 3.4.4(a). TGA Calculations of Mass Losses for {*cis*-[Ni(I-Et-*S,O*)(DPE-*N,N'*)]$_2$}$_n$

Feature on Graph	Temp. Range (°C)	Component Mass %	Molar Mass (g.mol^{-1})	Component Identification
Point of inflection	310	70.77 %	902.51	*cis*-[Ni(I-Et-*S,O*)]$_2$
First Mass Loss	196 - 263	19.33 %	246	–
Second Mass Loss	263 – 310	10.40 %	133	–
Combined Mass Loss	163 - 308	29.73 %	378	2 DPE

The TGA results suggest that there is in total enough DPE to octahedrally coordinate to all Ni(II) centres – giving rise to a coordination polymer. The required metallamacrocycle to ligand ratio of 1:2 is indicated, yet the two unequal mass losses suggest that there are two unequal groups of DPE molecules present in the structure under different conditions.

The product {*cis*-[Ni(I-Et-*S,O*)(DPE-*N,N'*)]$_2$}$_n$ therefore must consist of some *cis*-[Ni(I-Et-*S,O*)]$_2$ coordinated to DPE – as well as some free DPE present as guest, but acting as a potential ligand, pending some structural disruption on the part of solvent molecules. According to the ratio of the two mass losses, some 65% of the DPE is present as guest and only 35 % is coordinated to nickel (assuming that the first mass loss is due to the removal of the more weakly held guest molecules.) The results of elemental analysis are given below. As will be seen, they corroborate the findings reported here.

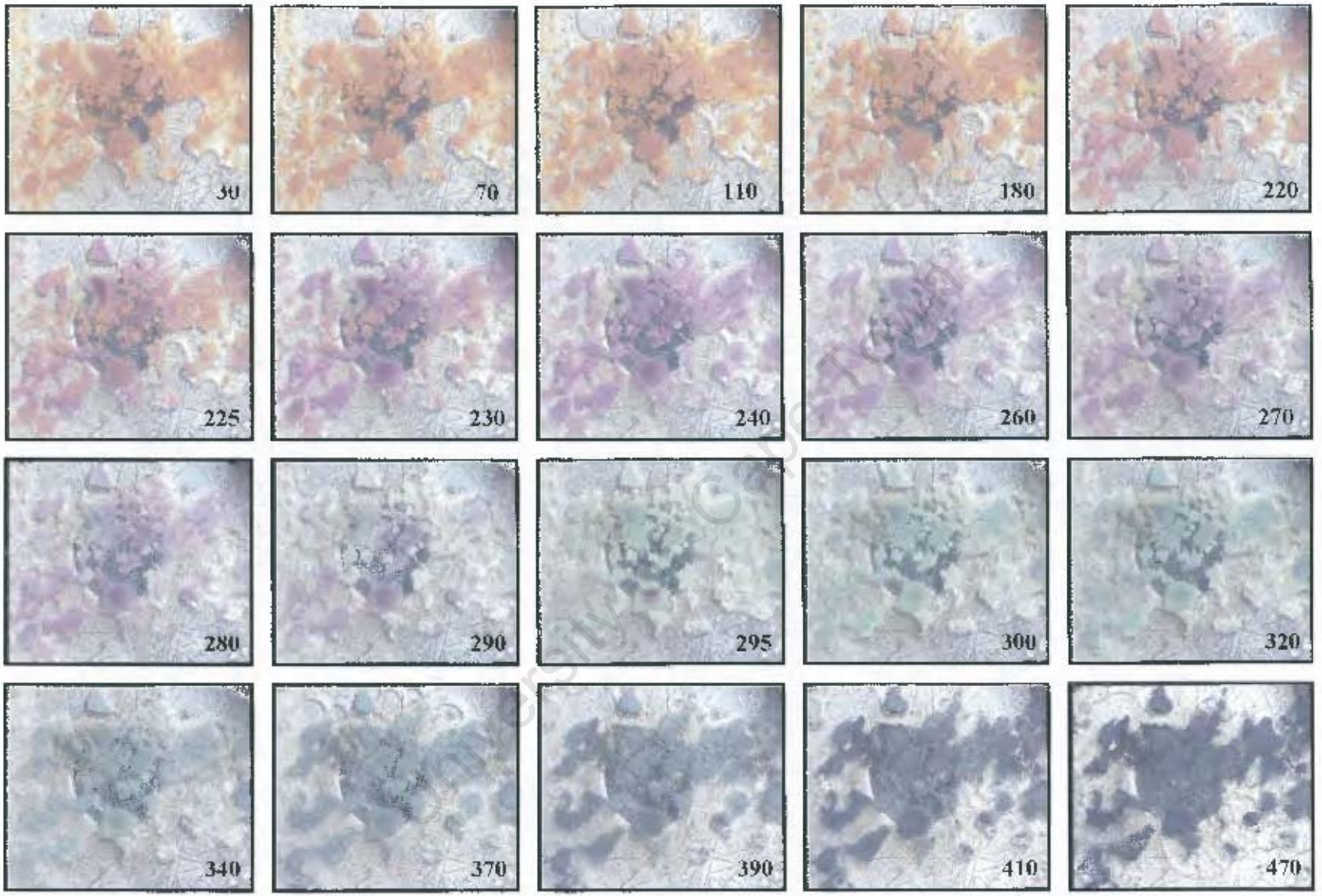

Figure 3.4.4(c). HSM photographs of {*cis*-[Ni(I-Et-*S,O*)(DPE-*N,N'*)]$_2$}$_n$ heated under silicone oil. Temperatures reported in degrees Celsius.

Hot Stage Microscopy

Figure 3.4.4(c) shows a series of photographs of {*cis*-[Ni(I-Et-*S,O*)(DPE-*N,N'*)]$_2$}$_n$ under silicone oil as it is heated. The photographs indicate that the orange sample is stable from room temperature up to 110 °C where the evolution of gas is detected by the formation of bubbles. This bubbling increases in rate up to 180 °C, while the colour remains the same. Beyond this temperature, the colour begins to darken while bubbling continues. By 220 °C, it can be clearly seen that the compound has begun to take on a purple colour. This transition occurs rapidly, until 240 °C, at which point the sample has completed the colour change from orange to purple and gas evolution has abated. This observation corresponds to some extent with the first thermal event on the TGA trace. By 260 °C, the sample is already beginning to undergo another chromatic transition: the purple colour can be seen to become paler. This loss of colour continues until at around 290 °C, almost all of the purple colouring is gone, replaced by a pale grey. The temperature range over which this event is observed roughly matches the temperature range of the second mass loss event during TGA. Over the next 10 degrees, the last vestiges of purple disappear and at the same time, the pale grey colour darkens to a grey-green. Beyond 320 °C, this colour continues to change slowly, becoming more and more grey. By 370 °C, the evolution of gas has begun again and is occurring at a rapid pace. The sample continues to darken accompanied by rapid gas evolution until it has changed to black by 470 °C.

The sharp mass loss event at 310°C during TGA does not correspond with the observations at this temperature in the HSM, where no gas evolution and only some darkening of the sample are observed. The disagreement between what is observed from TGA and HSM can only be explained by the fact that the physical environments during the two techniques are markedly different. It is possible that the loss of colour during HSM is the result of oxidation, which cannot occur in the nitrogen atmosphere under which the sample is heated during TGA. However, this then raises the issue of why the HSM and TGA results for {*cis*-[Ni(I-Et-*S,O*)(BPE-*N,N'*)]$_2$}$_n$ (section 3.4.3 above) appear to agree so well, and why {*cis*-[Ni(I-Et-*S,O*)(BPE-*N,N'*)]$_2$}$_n$ does not seem to revert to *cis*-[Ni(I-Et-*S,O*)]$_2$ during TGA.

The thermal behaviour of this compound is similar to that observed for {*cis*-[Ni(I-Et-*S,O*)(BPE-*N,N'*)]$_2$}$_n$, where, beyond 230 °C, the sample was observed to lose its purple colouring and eventually blacken at temperatures above 400 °C. It appears that {*cis*-[Ni(I-Et-*S,O*)(DPE-*N,N'*)]$_2$}$_n$ also undergoes some transformation – at a comparable temperature – that results in an almost colourless product. As with the product formed from {*cis*-[Ni(I-Et-*S,O*)(BPE-*N,N'*)]$_2$}$_n$, this product seems to be thermally robust.

Elemental Analysis

Table 3.4.4(b) gives the observed percentages of C, H, N and S for {*cis*-[Ni(I-Et-*S,O*)(DPE-*N,N'*)]$_2$}$_n$ as well as the values calculated for various *cis*-[Ni(I-Et-*S,O*)]$_2$: DPE: CH_2Cl_2 ratios.

Table 3.4.4(b). Comparison of {*cis*-[Ni(I-Et-*S,O*)(DPE-*N,N'*)]$_2$}$_n$ elemental analysis results with values calculated for a monomeric octahedral adduct, a guest-free polymer and two possible structures containing guest molecules.

Element	Found %	Calculated %			
		cis-[Ni(I-Et-*S,O*)]$_2$: DPE: CH_2Cl_2 Ratio			
		1: 2: 0	1: 2: 1	1: 3: 1	1: 4: 0
C	56.89	56.88	54.20	57.15	61.84
H	5.50	5.41	5.22	5.26	5.44
N	13.29	13.27	12.43	12.78	13.74
S	9.84	10.12	9.49	8.36	7.86

The agreement between the observed values and those calculated for a guest-free coordination polymer (*cis*-[Ni(I-Et-*S,O*)]$_2$: DPE: CH_2Cl_2 ratio of 1: 2: 0) is excellent. It is almost certain that {*cis*-[Ni(I-Et-*S,O*)(DPE-*N,N'*)]$_2$}$_n$ is a product of the form {*cis*-[Ni(I-Et-*S,O*)(DPE-*N,N'*)]$_2$}$_n$. However this notation is misleading, because it implies that {*cis*-[Ni(I-Et-*S,O*)(DPE-*N,N'*)]$_2$}$_n$ is a guest-free coordination polymer. In fact, {*cis*-[Ni(I-Et-*S,O*)(DPE-*N,N'*)]$_2$}$_n$ is a *potential* coordination polymer in the

guest-free state, and only polymerises completely in the presence of solvent molecules. The correct ratio of metallamacrocycle to bidentate bridging ligand is ensured because the synthesis of the coordination polymer in a solvent medium precedes the formation of the potential coordination polymer upon removal from the solvent.

IR Spectroscopy

Infrared analysis was performed on the compounds *cis*-[Ni(I-Et-*S,O*)]$_2$, 1,2-di(4-pyridyl)ethylene and {*cis*-[Ni(I-Et-*S,O*)(DPE-*N,N'*)]$_2$}$_n$. In order to study the difference between the two states of {*cis*-[Ni(I-Et-*S,O*)(DPE-*N,N'*)]$_2$}$_n$, two samples were prepared – one without solvent and the other mixed with a small amount of dimethylformamide. DMF was used because of its low volatility, which allows it to remain in the sample long enough for analysis to be performed.

There are certain features in the various IR spectra that indicate significant differences in the two states of {*cis*-[Ni(I-Et-*S,O*)(DPE-*N,N'*)]$_2$}$_n$. Primarily, the characteristic absorption peak for free *cis*-[Ni(I-Et-*S,O*)]$_2$ at 487 cm^{-1} is also observed for {*cis*-[Ni(I-Et-*S,O*)(DPE-*N,N'*)]$_2$}$_n$, but is conspicuously absent in the spectrum of {*cis*-[Ni(I-Et-*S,O*)(DPE-*N,N'*)]$_2$}$_n$ with DMF. The absence of such a peak is also noted in the spectra of the 2:2 coordination polymers {*cis*-[Ni(I-Et-*S,O*)(bipy-*N,N'*)]$_2$}$_n$ and {*cis*-[Ni(I-Et-*S,O*)(BPE-*N,N'*)]$_2$}$_n$ (although it is present in the spectrum of {*cis*-[Ni(I-Et-*S,O*)(pyrazine-*N,N'*)]$_2$}$_n$, in that case it is attributed to pyrazine in the bridging mode). From this it is inferred that there is some axially uncoordinated *cis*-[Ni(I-Et-*S,O*)]$_2$ present in the {*cis*-[Ni(I-Et-*S,O*)(DPE-*N,N'*)]$_2$}$_n$ sample – giving rise to the absorption at 487 cm^{-1}. The introduction of DMF, effecting vapochromism, causes the disappearance of this peak, indicating that any free *cis*-[Ni(I-Et-*S,O*)]$_2$ is coordinated to a ligand in the presence of the solvent. The absence of a peak in the spectrum of {*cis*-[Ni(I-Et-*S,O*)(DPE-*N,N'*)]$_2$}$_n$ with DMF at ca. 670 cm^{-1} also strengthens this argument. This peak was observed for pure DPE and also for the solvent-free {*cis*-[Ni(I-Et-*S,O*)(DPE-*N,N'*)]$_2$}$_n$ and apparently arises from a vibrational mode available to free DPE, but not to bidentate coordinated DPE.

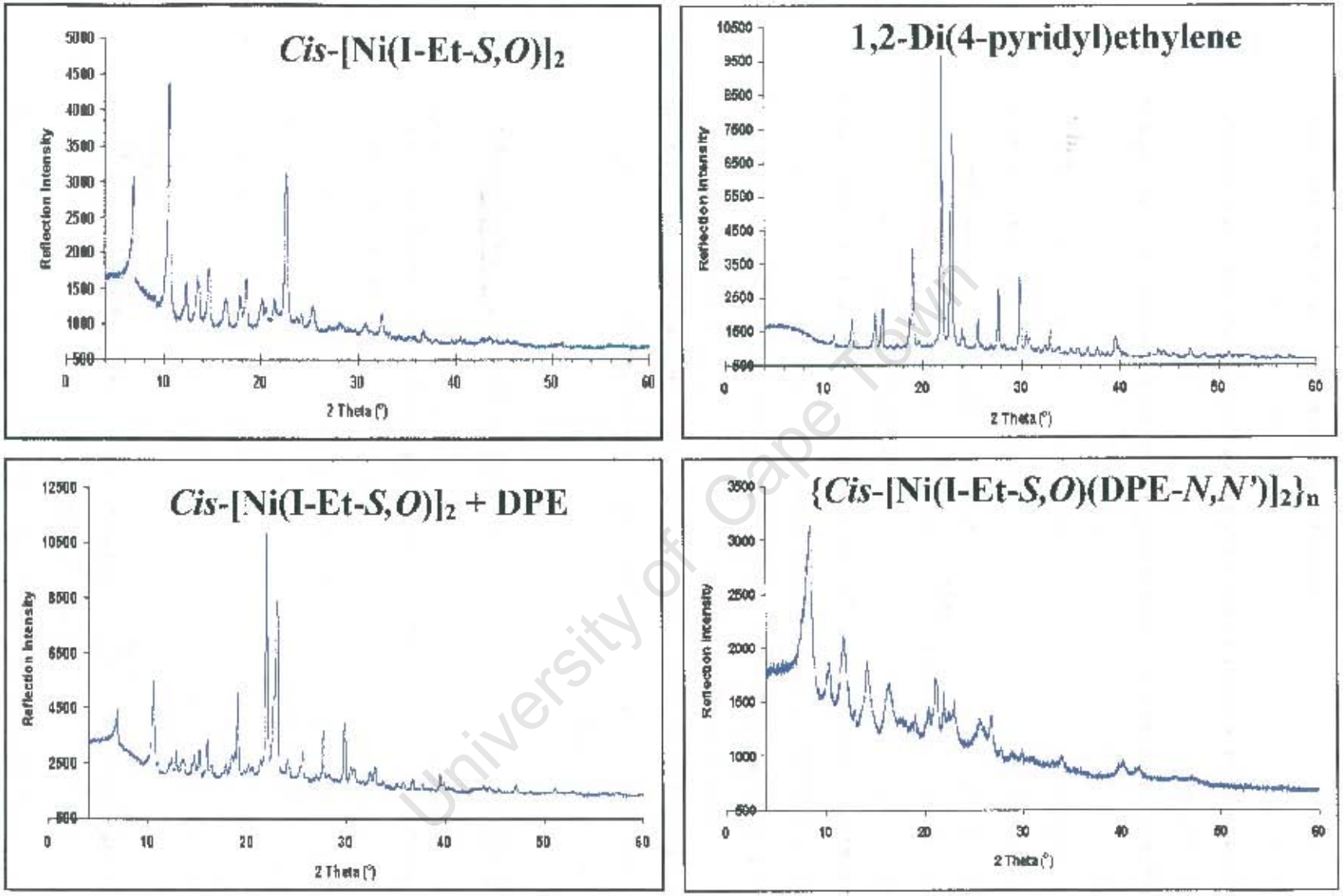

Figure 3.4.4(d). X-ray powder diffraction patterns for {*cis*-[Ni(I-Et-*S,O*) (DPE-*N,N'*)]$_2$}$_n$ and its unreacted components - separate and superimposed

X-ray powder diffraction

As with the previous coordination polymers, powder diffraction studies were conducted for the product {*cis*-[Ni(I-Et-*S,O*)(DPE-*N,N'*)]$_2$}$_n$ as well its component bidentate bridging ligand 1,2-di(4-pyridyl)ethylene.. The x-ray powder diffraction experiment was attempted for {*cis*-[Ni(I-Et-*S,O*)(DPE-*N,N'*)]$_2$}$_n$ in the presence of CH_2Cl_2 vapour – i.e. in the vapochromated state. The result of this experiment was a broad featureless trace – suggesting that the crystal structure of the sample does not remain intact when solvent-activated.

Figure 3.4.4(d) shows the powder patterns for DPE and {*cis*-[Ni(I-Et-*S,O*)(DPE-*N,N'*)]$_2$}$_n$ as well as that of *cis*-[Ni(I-Et-*S,O*)]$_2$ and a pattern generated by the addition of the *cis*-[Ni(I-Et-*S,O*)]$_2$ and DPE patterns. As with the 2:2 coordination polymers above, the {*cis*-[Ni(I-Et-*S,O*)(DPE-*N,N'*)]$_2$}$_n$ trace differs markedly from the powder patterns of either of its components and also differs from the pattern generated by the addition of the *cis*-[Ni(I-Et-*S,O*)]$_2$ and DPE traces. The peaks at $2\theta = 10.6°$ and 22.6° in the *cis*-[Ni(1-Et-*S,O*)]$_2$ trace as well as those at 22.0° and 23.0° in the DPE trace are not present in the {*cis*-[Ni(1-Et-*S,O*)(DPE-*N,N'*)]$_2$}$_n$ trace. This indicates that the product {*cis*-[Ni(I-Et-*S,O*)(DPE-*N,N'*)]$_2$}$_n$, although not a coordination polymer, is not merely a solid-solid mixture of *cis*-[Ni(I-Et-*S,O*)]$_2$ and DPE. The very broad peaks hint at a low degree of crystallinity in this product. Figure 3.4.4(e) is a comparison of the powder patterns of {*cis*-[Ni(I-Et-*S,O*)(DPE-*N,N'*)]$_2$}$_n$ and {*cis*-[Ni(I-Et-*S,O*)(BPE-*N,N'*)]$_2$}$_n$, which is a coordination polymer with a powder diffraction pattern similar to those of the other coordination polymers {*cis*-[Ni(I-Et-*S,O*)(pyrazine-*N,N'*)]$_2$}$_n$ and {*cis*-[Ni(I-Et-*S,O*)(bipy-*N,N'*)]$_2$}$_n$.

Interestingly, the two powder patterns are virtually identical. They are much more similar than any other pair of diffraction patterns for the 2:2 coordination polymers. Almost every peak in the {*cis*-[Ni(I-Et-*S,O*)(BPE-*N,N'*)]$_2$}$_n$ trace is found in that of {*cis*-[Ni(I-Et-*S,O*)(DPE-*N,N'*)]$_2$}$_n$. Only some variation in the peak intensities and some minor shifts distinguish one pattern from the other. This is all the more interesting because the compounds seem to have such different properties and compositions. {*cis*-[Ni(I-Et-*S,O*)(BPE-*N,N'*)]$_2$}$_n$ is a coordination polymer, while solvent-free {*cis*-[Ni(I-Et-*S,O*)(DPE-*N,N'*)]$_2$}$_n$ is not. {*Cis*-[Ni(I-Et-*S,O*)(BPE-

N,N')]$_2$}$_n$ was shown to have included guests, while {*cis*-[Ni(I-Et-*S,O*)(DPE-*N,N'*)]$_2$}$_n$ has none.

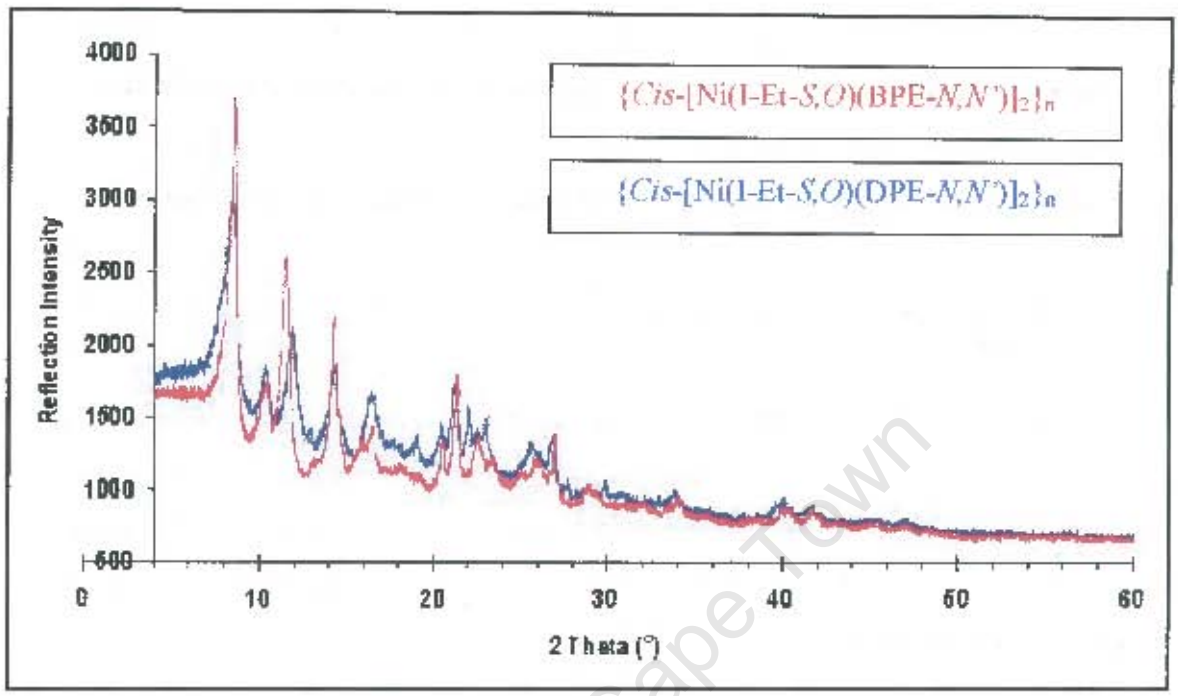

Figure 3.4.4(e) Comparison of x-ray powder diffraction patterns of {*cis*-[Ni(I-Et-*S,O*)(DPE-*N,N'*)]$_2$}$_n$ and {*cis*-[Ni(I-Et-*S,O*)(BPE-*N,N'*)]$_2$}$_n$

It is possible that the crystal structures of the two compounds are analogous, with sites available for occupation by guests. In {*cis*-[Ni(I-Et-*S,O*)(BPE-*N,N'*)]$_2$}$_n$, these sites are occupied, while in {*cis*-[Ni(I-Et-*S,O*)(DPE-*N,N'*)]$_2$}$_n$ these sites are empty. Then upon exposure to potential guest molecules, these sites are filled in the {*cis*-[Ni(I-Et-*S,O*)(DPE-*N,N'*)]$_2$}$_n$ structure, resulting in some subtle structural change that allows a true coordination polymer to form.

The lability of {*cis*-[Ni(I-Et-*S,O*)(DPE-*N,N'*)]$_2$}$_n$ in terms of the incorporation and removal of guest molecules (and formation and breaking of coordination bonds) is remarkable. The rapidity with which the transformation occurs suggests that the solvent molecules are not enclathrated or otherwise strongly held in the structure. This would be a major difference between the solvent-containing form {*cis*-[Ni(I-Et-*S,O*)(DPE-*N,N'*)]$_2$}$_n$ and {*cis*-[Ni(I-Et-*S,O*)(BPE-*N,N'*)]$_2$}$_n$, which is thought to contain some enclathrated guests.

In the case of {*cis*-[Ni(I-Et-*S,O*)(DPE-*N,N'*)]$_2$}$_n$, it can be concluded that the polymerisation occurs by some solvent-mediated mechanism. Upon removal of the product from the mother liquor, any solvent molecules present as guests in the structure are expelled, with a resultant decoordination of some of the axial ligands. These ligands remain in place in the structure as guests, available to recoordinate to the nickel(II) centres upon re-entry of solvent molecules into the system. The similarity between the powder diffraction patterns of solvent-free {*cis*-[Ni(I-Et-*S,O*)(DPE-*N,N'*)]$_2$}$_n$ and the solvent-containing coordination polymer {*cis*-[Ni(I-Et-*S,O*)(BPE-*N,N'*)]$_2$}$_n$ suggests that the crystal structure of {*cis*-[Ni(I-Et-*S,O*)(DPE-*N,N'*)]$_2$}$_n$ remains largely the same upon expulsion of the included guests and decoordination of some of the DPE ligands. The interference that prevents one from obtaining a powder diffraction pattern for {*cis*-[Ni(I-Et-*S,O*)(DPE-*N,N'*)]$_2$}$_n$ in the presence of a potential guest is frustrating. The cause of this interference is possibly due to partial dissolution of the product by the solvent/guest molecules – in this case an undesired side-effect.

Levitating balance measurements

The uptake of solvent molecules by {*cis*-[Ni(I-Et-*S,O*)(DPE-*N,N'*)]$_2$}$_n$ was observed gravimetrically by use of a sensitive levitating balance in a closed system. The sample was weighed (155 mg) and then placed in an evacuated chamber; dichloromethane was then allowed to enter the chamber to a fixed pressure (typically attained within the first few minutes of the experiment) and isobaric measurements of sample mass gain over time were taken. The experiment was repeated at different pressures from 200 – 300 mmHg. The results of these experiments are plotted on the same set of axes – as shown in Figure 3.4.4(f). A slight error is incurred by plotting all three graphs on the same time axis, as the increments in time measurements during each run were not exactly identical. Nevertheless, the amount of mass gained is not affected, nor is the overall pattern of mass gain in each case.

The results indicate that the pressure of the solvent in the chamber affects the amount of solvent sorbed by the sample, so that at 200 mmHg, the sample sorbs a maximum of 53 mg of CH_2Cl_2, at 250 mmHg, the sample sorbs a maximum of 67 mg and at 300

mmHg, the sample sorbs a maximum of 69 mg. The mass of sorbed solvent is not expected to greatly exceed 69 mg at higher pressures.

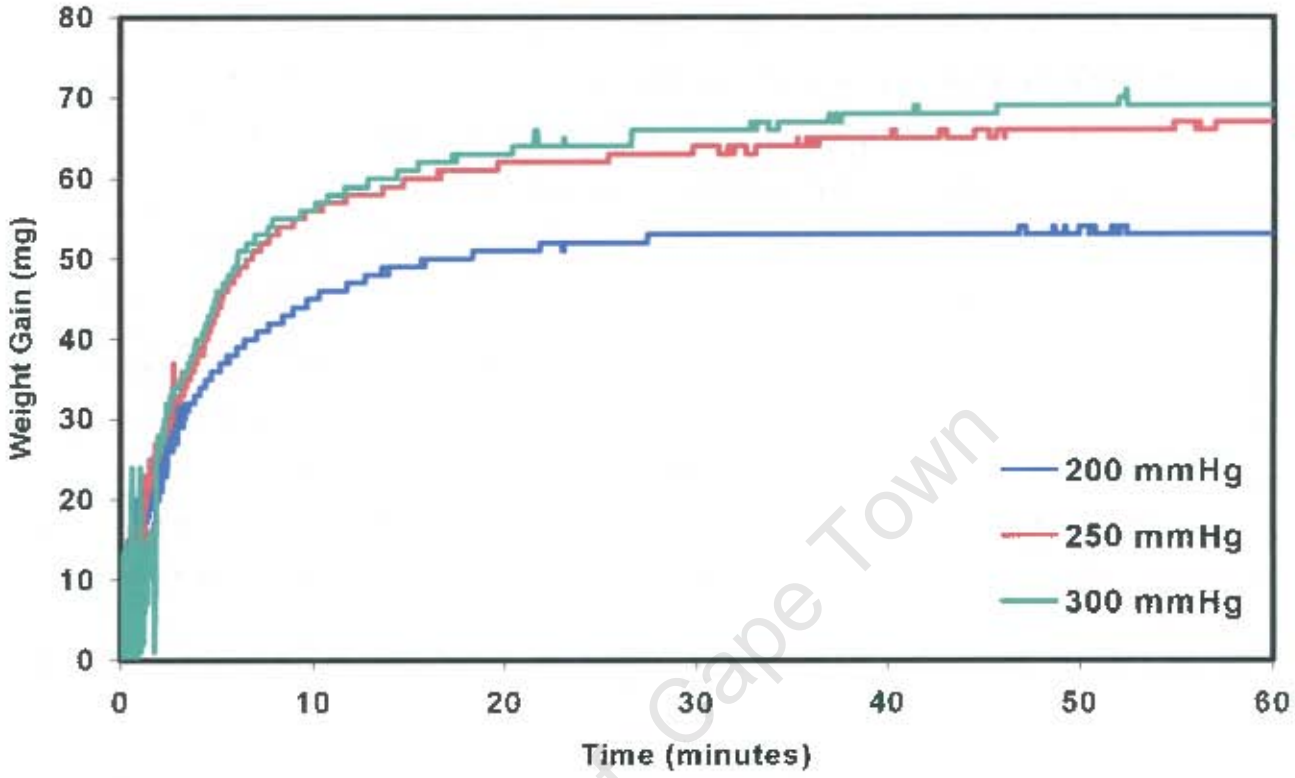

Figure 3.4.4(f). Results of gravimetric study of isobaric sorption of CH_2Cl_2 by $\{cis\text{-}[Ni(1\text{-}Et\text{-}S,O)(DPE\text{-}N,N')]_2\}_n$ performed on a levitating balance

These results reveal that $\{cis\text{-}[Ni(I\text{-}Et\text{-}S,O)(DPE\text{-}N,N')]_2\}_n$ is a strong solvent sorbing agent, able to take up almost half its mass in dichloromethane at the highest pressure. This effect certainly involves the penetration of the $\{cis\text{-}[Ni(I\text{-}Et\text{-}S,O)(DPE\text{-}N,N')]_2\}_n$ structure and is not merely the result of adsorption onto the surface of the sample. This is a strong indication that $\{cis\text{-}[Ni(1\text{-}Et\text{-}S,O)(DPE\text{-}N,N')]_2\}_n$ has a porous structure through which solvent molecules can travel with relative ease. The different amounts of solvent sorbed at different pressures seem to suggest that the dichloromethane molecules do not only occupy fixed sites within the structure, but can fill the structure with varying stoichiometries – possibly even to the point where the product is partially dissolved – as evidenced by XRD.

Table 3.4.4(c) shows a calculation of the number of CH_2Cl_2 molecules sorbed per repeating unit in the $\{cis\text{-}[Ni(I\text{-}Et\text{-}S,O)(DPE\text{-}N,N')]_2\}_n$ structure.

Table 3.4.4(c). Calculation of the ratio of sorbed solvent molecules to repeating units of {*cis*-[Ni(I-Et-*S,O*)(DPE-*N,N'*)]$_2$}$_n$ at various pressures.

Molar mass of *cis*-[Ni(I-Et-*S,O*)]$_2$ (g.mol-1)	902.508
Molar mass of DPE (g.mol-1)	182.226
Molar mass of 1 repeating unit of {*cis*-[Ni(I-Et-*S,O*)(DPE-*N,N'*)]$_2$}$_n$ (g.mol-1)	1266.96
Mass of sample (g)	0.155
No. of moles of repeating units	1.22×10^{-4}
Molar mass of CH_2Cl_2 (g.mol-1)	84.933

Pressure of CH_2Cl_2 (mmHg)	200	250	300
Mass of sorbed CH_2Cl_2 (g)	0.053	0.067	0.069
No. of moles of CH_2Cl_2 sorbed	6.24×10^{-4}	7.89×10^{-4}	8.12×10^{-4}
No. of CH_2Cl_2 molecules sorbed per repeating unit	5.10	6.45	6.64

These values are clearly non-stoichiometric, suggesting that while there are possibly specific sites within the structure which – when occupied by solvent molecules – are responsible for the coordination of DPE to Ni(II), it seems that these sites are not the only positions within the structure available for solvent molecules. The higher the pressure of the solvent vapour, the more solvent molecules penetrate and disrupt the structure. However, upon removal of the vapour, the sorbed solvent molecules exit the structure – leaving it intact – just as easily as they entered.

Summary

The results of analysis of {*cis*-[Ni(I-Et-*S,O*)(DPE-*N,N'*)]$_2$}$_n$ have revealed that in a solvent-rich environment, the product is a ladder-type coordination polymer similar to {*cis*-[Ni(I-Et-*S,O*)(pyrazine-*N,N'*)]$_2$}$_n$, {*cis*-[Ni(I-Et-*S,O*)(bipy-*N,N'*)]$_2$}$_n$ and {*cis*-[Ni(I-Et-*S,O*)(BPE-*N,N'*)]$_2$}$_n$. However, in the absence of solvent, the product undergoes partial decoordination of DPE from the Ni(II) centres, resulting in a mixture of square-planar and octahedral nickel(II). This transition gives rise to a

striking change in colour. In this solvent-free state, {*cis*-[Ni(I-Et-*S,O*)(DPE-*N,N'*)]$_2$}$_n$ still contains all the previously coordinated DPE molecules as guests and potential ligands within its structure. The x-ray powder diffraction pattern shows that the crystal structure of this solvent-free state is possibly analogous to that of the true coordination polymer {*cis*-[Ni(I-Et-*S,O*)(BPE-*N,N'*)]$_2$}$_n$. In this state there are pores or channels through which solvent molecules may permeate the structure.

Furthermore, there are specific sites within the structure, which -- upon occupation by guests such as dichloromethane – result in some subtle shift that allows the DPE potential ligands to recoordinate to the Ni(II) centres and reform a true coordination polymer. The concomitant colour change makes this product a powerful molecular sensor – particularly sensitive to dichloromethane and chloroform.

Figure 3.4.4(g) represents this process schematically. The positions of the dichloromethane guests in the polymeric structure (diagrams (ii) and (vi)) are shown to be close to the DPE bridging ligands, as it is logical to assume that the CH_2Cl_2 guests might occupy such positions and thus somehow influence the DPE ligands by virtue of their proximity. Also note that the guest-free product is represented in diagram (iv) as consisting of square planar metallamacrocycles alternating with octahedral adducts of metallamacrocycles. This is not necessarily the case, as it is also possible that the product consists of oligomeric chains of bonded metallamacrocycles as well as sections of aligned, but unconnected *cis*-[Ni(I-Et-*S,O*)]$_2$ and DPE molecules. Either case would agree with the results of the various analyses performed. One feature that is not indicated is the presence of excess solvent molecules. The results of the levitating balance experiments and the failed attempt at obtaining an XRD powder pattern for {*cis*-[Ni(I-Et-*S,O*)(DPE-*N,N'*)]$_2$}$_n$ in the presence of CH_2Cl_2 indicate that excess solvent molecules are present and cause the partial dissolution of the polymer.

The inability to obtain {*cis*-[Ni(I-Et-*S,O*)(DPE-*N,N'*)]$_2$}$_n$ crystals suitable for single crystal diffractometry is a setback. The crystal structure must possess many interesting features, such as channels for the solvent guests to pass through and occupy. The exact mechanism of the vapochromism is also of great interest, as it involves the disruption of the structure: enough to induce coordination of DPE to

Chapter 4

Conclusion

Having reported the findings of this project, it now remains to summarise these results and consider their overall implications, particularly with respect to the broad context of self-assembly and other aspects of supramolecular chemistry. It is also necessary to consider the aims of the project and whether they have been achieved. It is certainly worthwhile to point out where more work may be done in the area covered by this project and to speculate on where future work could lead.

4.1. Summary of Results

4.1.1. Chelating Ligands

A total of four bipodal 3,3,3',3'-tetraalkyl-1,1'-aroylbis(thiourea) ligands were synthesised by the Douglass and Dains method. These ligands represent the four possible permutations that arise by varying two characteristics (relative substitution and side chain composition) each in two different ways (meta- vs. para- substitution and ethyl vs. 2-hydroxyethyl side chains). The characteristics chosen to be varied were those that had been found to significantly affect the behaviour of the resultant ligands. It was expected that relative substitution would control the outcome of complexation of the ligands, while side chain composition would be paramount in determining the mode of supramolecular interaction of the complexes. The four ligands were synthesised and crystal structures of the two isophthaloyl ligands I-Et and I-EtOH were solved. The difference between these two structures was remarkable, all the more so because it resulted only from the side chain composition. The presence of terminal hydroxyl groups in I-EtOH gave rise to the possibility of new modes of hydrogen bonding, which in turn gave rise to a crystal structure composed of a network of intersecting helical chains of molecules. The crystal structure of I-Et exhibited a much more straightforward mode of hydrogen bonding that gave rise to parallel rectilinear chains of molecules running through the structure.

The difference in ethyl and hydroxyethyl branched aroylbis(thioureas) H-bonding was expected to be of great significance in metal complexes of the ligands, since abstraction of the N – H protons as a prerequisite to chelation would eliminate a

potential donor – hydrogen system in the resulting complexes, rendering complexes of ethyl branched ligands incapable of H-bonding.

4.1.2. Metallamacrocyclic complexes

The four synthesised ligands were each reacted with Ni(II) in an attempt to give rise to metallamacrocyclic complexes via self-assembly. It was expected that the two isophthaloylbis(thioureas) would give rise to 2:2 metallamacrocycles while the terephthaloylbis(thioureas) would form 3:3 metallamacrocycles. General characterisation confirmed the metal: ligand ratio of 1:1 in each case. The 3:3 metallamacrocycle *cis*-[Ni(T-Et-*S,O*)]$_3$ had been synthesised previously by Hoyer *et al*,[39] and crystals of *cis*-[Ni(I-Et-*S,O*)]$_2$ were obtained and its crystal structure determined by single crystal diffractometry – revealing packing in offset stacks of π-π associated 2:2 metallamacrocycles. However, it was not certain that the ligands I-EtOH and T-EtOH had given rise to a 2:2 and a 3:3 metallamacrocycle respectively.

As a result of the failure to obtain good quality single crystals of most of the complexes, this section of the results chapter is brief. However, this failure did not prevent the use of these products as secondary building units (SBUs) in the next step of the building-up process.

4.1.3. Octahedral adducts

The Ni(II) aroylbis(thiourea) complexes were all reacted with pyridine. Attempts to grow crystals of the products of these reactions were successful except in the case of *cis*-[Ni(T-EtOH-*S,O*)(pyridine-*N*)$_2$]$_3$, which did not even yield a solid product. *Cis*-[Ni(I-Et-*S,O*)]$_2$ was also reacted with 4-dimethylaminopyridine, and crystals obtained of the product. The four crystal structures of octahedral adducts constitute a major portion of the results, and a comparison of these structures clearly shows that the initial ligand variations have significant effects on the supramolecular structures of these products.

The two *cis*-[Ni(I-Et-*S,O*)]$_2$ adducts, *cis*-[Ni(I-Et-*S,O*)(pyridine-*N*)$_2$]$_2$ and *cis*-[Ni(I-Et-*S,O*)(DMAP-*N*)$_2$]$_2$ are shown to be remarkably similar. The space group of their

crystal structures are identical. Each structure includes solvent guests in very similar positions. Hence, the crystal packing modes of the two structures both give rise to continuous parallel guest-filled channels.

In contrast to this similarity, the crystal structure of *cis*-[Ni(I-EtOH-*S,O*)(pyridine-*N*)$_2$]$_2$ differs quite remarkably from those of the *cis*-[Ni(I-Et-*S,O*)]$_2$ adducts. The large amount of included solvent and the inclusion of water in the *cis*-[Ni(I-EtOH-*S,O*)(pyridine-*N*)$_2$]$_2$ structure are a direct result of the H-bond capability that arises from the hydroxyethyl side chains. This structure is the result of a self-assembly into two-dimensional H-bonded layers of metallamacrocyclic adduct molecules, that are in turn held together by π-π interactions between pyridine ligands of successive layers. Thus *cis*-[Ni(I-EtOH-*S,O*)(pyridine-*N*)$_2$]$_2$ self-assembles into a 3-dimensional infinite supramolecular architecture, through which parallel guest-filled channels run. The structure is all the more fascinating, because the water guest molecules, which were absorbed from the atmosphere, govern the mode of assembly of the H-bonded layers.

A wholly different crystal structure is observed for the pyridine adduct of the 3:3 metallamacrocycle *cis*-[Ni(T-Et-*S,O*)]$_3$. In this case, the unit cell is found to consist of two adduct molecules and several associated pyridine guests. The higher order crystal symmetry of the 2:2 adducts is absent in the *cis*-[Ni(T-Et-*S,O*)(pyridine-*N*)$_2$]$_3$ structure as a result of the non-centrosymmetric nature of the 3:3 metallamacrocycle itself. However, this crystal structure possesses a feature that the 2:2 adducts lack. The 3:3 metallamacrocyclic adduct has an internal cavity that is large enough to admit pyridine and thus the structure that arises exhibits intramolecular guest inclusion reminiscent of the manner of guest inclusion in cyclodextrin and calixarene compounds. At the same time, extramolecular inclusion of pyridine is also observed. Thus *cis*-[Ni(T-Et-*S,O*)(pyridine-*N*)$_2$]$_3$ demonstrates modes of inclusion that are characteristic of both cavitates and clathrates.[93(b)]

4.1.4 Coordination polymers

A series of reactions coordinating exo-bidentate nitrogen donor ligands to the ethyl branched 2:2 and 3:3 metallamacrocycles *cis*-[Ni(I-Et-*S,O*)]$_2$ and *cis*-[Ni(T-Et-*S,O*)]$_3$ was carried out. Although no single crystals of any of the products could be obtained

due to the tendency of these compounds either to insolubility or to disintegration upon dissolution, a number of other techniques of characterisation were performed. The results of these analyses indicated that the products were coordination polymers – with one notable exception. There were also indications of guests present in most of the products, and proposals were made as to the location of these guests in the coordination polymer structures. In essence, it was proposed that guests could be held weakly in spaces between polymeric chains and more strongly in the spaces between monomeric units within the polymeric chains.

The interaction between host and guest is of much interest and importance in one particular case. The product {*cis*-[Ni(I-Et-*S,O*)(DPE-*N,N'*)]$_2$}$_n$, was shown to have the metallamacrocycle: bidentate ligand stoichiometry expected for a coordination polymer, but differed in appearance and behaviour from the other *cis*-[Ni(I-Et-*S,O*)]$_2$ / bidentate ligand reaction products. Specifically, {*cis*-[Ni(I-Et-*S,O*)(DPE-*N,N'*)]$_2$}$_n$ showed no indication of containing any guests and furthermore exhibited the property of vapochromism, noticeably changing colour in the presence of solvent vapours. Levitation balance experiments showed that {*cis*-[Ni(I-Et-*S,O*)(DPE-*N,N'*)]$_2$}$_n$ could absorb a relatively large amount of chlorinated solvent. Ultimately, it was concluded that {*cis*-[Ni(I-Et-*S,O*)(DPE-*N,N'*)]$_2$}$_n$ in the guest-free state is not a true coordination polymer, but on exposure of the product to certain solvents readily includes the solvent as a guest with a concomitant subtle structural alteration that transforms the product {*cis*-[Ni(I-Et-*S,O*)(DPE-*N,N'*)]$_2$}$_n$ into a true coordination polymer.

No other coordination polymer exhibited this phenomenon. The fact that the corresponding 3:3 polymer {*cis*-[Ni(T-Et-*S,O*)(DPE-*N,N'*)]$_3$}$_n$ did not behave in a similar fashion was taken as further indication that 2:2 and 3:3 metallamacrocycles, although analogous, are in many ways fundamentally different. The inherent symmetry difference between 2:2 and 3:3 metallamacrocycles gives rise to channels within the crystal structures of adducts of the former, but not the latter. This could also apply to 2:2 and 3:3 coordination polymers, and would explain why a 2:2 polymer can act as a solvent sorbing compound, while no 3:3 polymer can do the same. The fact that the 3:3 coordination polymers might be amorphous or of a limited degree of crystallinity – as suggested by XRD – while the 2:2 polymers are clearly

crystalline, is another manifestation of the differences between 2:2 and 3:3 metallamacrocycles.

There still remain certain aspects of the coordination polymers that remain unclear, particularly their thermal behaviour. Hot stage microscopy revealed that some of the products undergo a series of unexpected changes upon heating and thermogravimetric analysis in some cases gave results that are very difficult to interpret. Overall, however, the evidence obtained in this portion of the project strongly indicates that metallamacrocyclic complexes readily assemble with exo-bidentate ligands into linear 1D coordination polymers.

4.2. Project Evaluation

4.2.1. First stage aims: ligand synthesis and characterisation

The most important aim of the project's first stage was the synthesis of the four bipodal ligands I-Et, I-EtOH, T-Et and T-EtOH. This was achieved, as general characterisation indicates. The crystal structure solution of I-Et and I-EtOH were also achieved and the comparison of their structures proved to be of great interest. The crystal structure of T-EtOH could not be obtained and this failure is considered a disappointing setback, because a comparison of this crystal structure with those of the other ligands would have increased our understanding of the effects of variation on ligand structure and behaviour.

4.2.2. Second stage: metallamacrocyclic Ni(II) complexes

Again, the most important aim in this stage was achieved: synthesising Ni(II) metallamacrocycles from the four ligands synthesised in the first stage. The crystal structure of *cis*-[Ni(I-Et-*S,O*)]$_2$ was obtained, successfully demonstrating that 2:2 nickel metallamacrocycles can be synthesised, and thus filling in a gap in the pattern of the d^8 metals to form 2:2 and 3:3 metallamacrocycles with isophthaloyl-and terephthaloyl- bis(thioureas) respectively.

4.2.3. Third stage: octahedral adducts of metallamacrocycles

The extension of square planar metallamacrocycles into octahedral adducts using pyridine was successful in all cases except that of *cis*-[Ni(T-EtOH-*S,O*)(pyridine-*N*)$_2$]$_3$. The various adducts that were obtained in solid form were well characterised allowing a thorough comparison of the influence of the aroylthiourea ligand variations at this level in the progression of assembly. The assembly of the highly organised hybrid 3D open framework of *cis*-[Ni(I-EtOH-*S,O*)(pyridine-*N*)$_2$]$_2$ is an excellent example of the dramatic effect that hydrogen bond capability can have on a system and clearly fulfilled the expectation that the metallamacrocyclic motif could give rise to some type of porous or channel-containing structure.

However, it should be mentioned that throughout every stage of the project, the ligand T-EtOH, its metallamacrocyclic complex *cis*-[Ni(T-EtOH-*S,O*)]$_3$ and now its pyridine adduct *cis*-[Ni(T-EtOH-*S,O*)(pyridine-*N*)$_2$]$_3$ have proved difficult. In fact no crystallographic evidence exists to indicate that any of these products do possess the expected molecular structures. This situation is disappointing, because the 3:3 metallamacrocycle *cis*-[Ni(T-EtOH-*S,O*)]$_3$ and its adducts represent a combined variation that must be explored: hydrogen bonding capability in a non-centrosymmetric complex – not to mention the possible combination of both intra- and extramolecular guest inclusion, as seen in the *cis*-[Ni(T-Et-*S,O*)(pyridine-*N*)$_2$]$_3$ crystal structure.

4.2.4. Fourth stage: polymerisation of metallamacrocycles using bridging ligands

This stage of the project can be said to be generally successful, even though the investigation of the different products was hampered by the nature of the compounds, tending either toward insolubility or disintegration upon dissolution. As a result, single crystal x-ray diffractometry could not be employed to determine the solid state structures of these polymers, nor could MALDI-TOF mass spectrometry be used to determine their sizes. Despite these setbacks, it must be remembered that the main aim of this stage was to synthesise coordination polymers of metallamacrocyclic complexes, and that was achieved – as evidenced by the various other methods of characterisation that were available, namely TGA, elemental analysis, HSM, IR spectroscopy and x-ray powder diffraction.

The inability to elucidate the structures of these products and to determine the polymeric chain lengths is seen as a deficit that must still be addressed by some means. However, the unexpected discovery of the vapochromism of {*cis*-[Ni(I-Et-*S,O*)(DPE-*N,N'*)]$_2$}$_n$ and its subsequent investigation add some weight to the work done in this stage of the project.

4.2.5. Evaluation in terms of the current chemical context

Overall, the majority of the aims of this project have been achieved. A progression from ligand through to coordination polymer has been rationally designed and successfully implemented. The various products obtained along the way have been thoroughly scrutinised and several complex molecular and supramolecular structures have been revealed. Most importantly, some of the potential merits of the aroylthioureas as supramolecular building blocks have clearly been realised.

It has clearly been shown that the isophthaloyl- or terephthaloylbis(thioureas) in conjunction with the Ni(II) ion constitute a system that is pre-programmed to form 2:2 or 3:3 metallamacrocyclic complexes via self-assembly according to the definition by J.-M. Lehn.[42] Similar metallamacrocycles based on bipodal acyl- and aroyl-thioureas had already been synthesised by others using Ni(II) as well as other metals (see Section 1.1.5.) This project has added to those findings; it can now certainly be stated that the aroylthiourea-based metallamacrocyclic motif can be classified with other series of self-assembled metallamacrocyclic complexes (see Section 1.2.1.) Just as many of these other metallamacrocyclic complexes have been employed as secondary building units in further self-assemblies (see Section 1.2.2), so have the aroylthiourea-based metallamacrocycles. By exploiting the coordination modes available to Ni(II), a series of 1D coordination polymers as well as a hybrid 3D supramolecular framework have been synthesised. Furthermore, these new supramolecular architectures display a wide variety of host-guest interactions.

Clearly, this system of compounds involves a whole range of different aspects of supramolecular chemistry including host-guest interactions, hydrogen bonded networks, crystal engineering, self-assembly, metal-organic frameworks, coordination polymers, and reticular synthesis. There is the hint of possible technological application, particularly in light of the molecular sensing property of $\{$*cis*-[Ni(I-Et-*S,O*)(DPE-*N,N'*)]$_2$$\}_n$.

With the knowledge gained from this project, it is hoped and certainly foreseeable that the aroylthiourea motif will become a well-studied and exploited tool in the field of

supramolecular architecture. With this in mind, it is seen as fitting that the final words of this dissertation are given over to discussing the potential for future research.

4.3. The Future

Even within the clearly defined boundaries outlined in the aims of this project, there are spaces that remain to be filled. The most important of these must be the study of the ligand T-EtOH and its products. Despite the difficulty in working with these compounds, it is vital that a clear picture be obtained of the nature of these compounds and the similarities and contrasts that they bear with respect to their already well-characterised analogues. The other gap that must be filled is the elucidation of the coordination polymers' structures. This is particularly important in the case of $\{cis\text{-}[Ni(I\text{-}Et\text{-}S,O)(DPE\text{-}N,N')]_2\}_n$, where the vapochromic phenomenon clearly relies on the ability of the product to readily admit and expel solvent guests with little or no disruption of the crystal structure.

Beyond the scope of the project lies the rich potential for new supramolecular architectures that depend mainly on creative customisation of the aroylthiourea ligands. Only a few such possibilities were discussed in the introduction and then only in general terms. A creative mind can surely come up with a whole host of other possibilities in a short space of time. So long as future research is directed in this area, it is likely that the following advances will be reported in the future:

1) 1-dimensional coordination polymers of *cis*-$[Ni(I\text{-}EtOH\text{-}S,O)]_2$ and *cis*-$[Ni(T\text{-}EtOH\text{-}S,O)]_3$, constituting multi-dimensional frameworks as a result of the additional H-bond capability.

2) 1-dimensional coordination polymers based on *trans*- bis chelation of acyl- or aroylthioureas will be possible, once the rules dictating the formation of *cis*- and *trans*- aroylthiourea isomers are properly deduced.

3) 2-dimensional coordination polymers composed of *trans*- acyl- or aroylthiourea chelate chains linked by axially coordinated bidentate bridging ligands such as 4,4'-bipyridine

4) 1-and 2-dimensional coordination polymers based on tri-and tetrapodal acyl- and aroylthioureas such as those shown in Figure 1.3.1(b), followed by 2- and 3-dimensional coordination polymers formed by linking these chains and layers together using bidentate bridging ligands

5) More coordination polymers with vapochromic capability. These could be tailor made by adjusting characteristics such as the size and polarity of pores. Ultimately, a series of structures, each exclusively admitting only certain guests might emerge, leading to new chemical sensor technology. Additional functionality might be factored into the design so that luminescence or electronic signalling is achieved.

6) Metallamacrocyclic complexes with nanoscale cavity size. These could also be linked as coordination polymers, giving rise to 1-dimensional nanotube structures, which could in turn be linked laterally by coordination or H-bonding to give new 3-dimensional frameworks.

7) Metallamacrocycles with specifically shaped cavities – possibly with chiral designs. These could conceivably have catalytic applications

8) Metallamacrocyclic complexes with long pendant alkyl chains that act as discotic mesogens in liquid crystal formation.

9) Metallamacrocycles that self-assemble into 3-dimensional discrete polyhedral architectures. These can be designed using molecular models. If successfully synthesised, they can then be used as nanoscale secondary building units in the assembly of infinite networks.

10) Multipodal acyl- and aroylthiourea metal complexes with modes of coordination other than square planar and octahedral. Tetrahedrally coordinated products – for example – might give rise to helical chains. The ends of these chains might possibly link up to form large flexible nanocyclic structures.

These are only a few of the options available. The fact is that the acylthiourea motif is so versatile that it could lend itself to almost any desired supramolecular architecture. And of course, these concepts of design have so far ignored the reported use of acylthioureas in chemistry with potential technological application ranging from mining to medicine. It is therefore considered highly likely that supramolecular acylthiourea architectures will spawn new chemical technologies.

It is hoped that this project will make some contribution to achieving that ultimate goal.

References

[1] I.B. Douglass and F.B. Dains, *J. Am. Chem. Soc.*, **1934**, 56, 719

[2] J. Miller, *PhD Thesis*, University of Cape Town, **2000**

[3] K.R. Koch, G Kemp, A. Roodt and W. Purcell, *J. Chem. Soc. Dalton Trans.*, **1997**, 4481

[4] S.A. Bourne and K.R. Koch, *J. Chem. Soc. Dalton Trans.*, **1993**, 2071

[5] K.R. Koch, C. Sacht, T. Grimmbacher and S. Bourne, *S. Afr. J. Chem.*, **1995**, 48(1/2), 71

[6] K R Koch, Y. Wang and A. Coetzee, *J. Chem. Soc. Dalton Trans.*, **1999**, 1013

[7] A. Dago, Y. Shepelev, F. Fajardo, F. Alvarez, R. Pomes, *Acta Crystallogr.*, **1989**, C45, 1192.

[8] K.R. Koch, *Coord. Chem. Rev.*, **2001**, 216–217, 473

[9] G. Fitzl, L. Beyer, J. Sieler, R. Richter, J. Kaiser and E. Hoyer, *Z. anorg. Allg. Chem.*, **1977**, 433, 237

[10] R. Richter, L. Beyer and J. Kaiser, *Z. anorg. Allg. Chem.*, **1980**, 461, 67

[11] L. Beyer, E. Hoyer, H. Hartman and J. Liebscher, *Z. Chem.* 21 **1981** 81.

[12] P. Knuutila, H. Knuutila, H. Hennig and L. Beyer, *Acta Chem. Scand.*, **1982**, A 36, 6, 541

[13] P. Muhl, K. Gloe, F Dietze, E. Hoyer, L. Beyer, *Z. Chem.*, **1986**, 26, 81

[14] J. Sieler, R. Richter, E. Hoyer, L. Beyer, O. Lindqvist and L. Andersen, *Z. Anorg. Allg. Chem.*, **1990**, 580, 167.

[15] W. Bensch and M. Schuster, *Z. Anorg. Allg. Chem.*, **1992**, 615, 93

[16] A. Irving, K.R. Koch and M. Matoetoe, *Inorg. Chim. Acta*, **1993**, 206, 193

[17] K.R. Koch and S. Bourne, *J. Mol. Struc,* **1998**, 441, 11

[18] K.R. Koch, J. Du Toit, M.R. Caira and C. Sacht, *J. Chem. Soc. Dalton Trans.*, **1994**, 785

[19] Basic Principles of HSAB and FMO Theory read from D.F. Shriver, P.W. Atkins, C.H. Langford Inorganic Chemistry, 2nd Ed. **1994**, Ch. 5.14, 212. Original work: (a) R.G. Pearson, *J. Am. Chem. Soc.*, **1963**, 85, 3533. (b) R. G. Pearson, *Science*, **1966**, 151, 172. (c) R. G. Pearson, *Chem. Br.*, **1967**, 3, 103. (d) R. G. Pearson, *J. Chem. Ed.*, 45, 581, 1968. (e) G. Klopman and R. F. Hudson, *Theoret. Chim. Acta*, **1967**, 8, 165. (f) G. Klopman, *J. Am. Chem. Soc.*, **1968**, 90, 223.

[20] K.R. Koch, A. Westra, D. Hannekom, currently unreported

[21] K.-H. Konig, M. Schuster, B Steinbrech, G. Schneeweis and R. Schlodder, *Fresenius Z. Anal. Chem.*, **1985**, 321, 457

[22] P. Vest, M. Schuster and K.-H. Konig, *Fresenius Z. Anal. Chem.*, **1989**, 335, 759

[23] M. Schuster, *Fresenius Z. Anal. Chem.*, **1986**, 324, 127

[24] K.R. Koch, J. Miller, A. Westra, *Proceedings of the International Solvent Extraction Conference,* **2002**, Cape Town, South Africa, *(ISEC-2002)*, C. Sole, P.M. Cole, J.S.

Preston, D.J. Robinson (Eds), The South African Institute of Mining and Metallurgy, Johannesburg.

[25] M. Domınguez, E. Antico, L. Beyer, A. Aguirre, S. Garcıa-Granda and V. Salvado, *Polyhedron*, **2002**, 21, 1429

[26] S. Ringmann and M. Schuster, *Chem. Tech. (Leipzig)*, **1997**, 49 (5), 217.

[27] M. Schuster, *Fresenius Z. Anal. Chem.*, **1992**, 342, 791

[28] A.N. Mautjana, J.D.S. Miller, A. Gie, S.A. Bourne and K.R. Koch, *J. Chem. Soc. Dalton Trans.*, **2003**, 1952

[29] K.R. Koch, *Coord. Chem. Rev.*, **2001**, 216–217, 473

[30] M. Schwarzer and M. Schuster, *Anal. Chim. Acta*, **1996**, 328, 1.

[31] W. Henderson, B.K. Nicholson and C.E.F. Rickard, *Inorg. Chim. Acta*, **2001**, 320, 101

[32] U. Bierbach and N. Farrell, *J. Inorg. Biochem.*, **1995**, 59, 2, 233

[33] C. Sacht and M.S. Datt, *Polyhedron*, **2000**, 19, 1347

[34] B. Rosenberg, L. VanCamp, J. E. Trosko and V. H. Mansour, *Nature*, **1969**, 222, 385.

[35] E. Rodrıguez-Fernandez, E. Garcıa, M.R. Hermosa, A. Jimenez-Sanchez, M. M. Sanchez, E. Monte and J.J. Criado *J. Inorg. Biochem.*, **1999**, 75, 181

[36] R. del Campo, J.J. Criado, E. Garcıa, M.R. Hermosa, A. Jimenez-Sanchez, J.L. Manzano, E. Monte, E. Rodrıguez-Fernandez and F. Sanz, *J. Inorg. Biochem.*, **2002**, 89, 74

[37] T. J. Egan, K. R. Koch, P. L. Swan, C. Clarkson, D. A. Van Schalkwyk and P. J. Smith, *J. Med. Chem.*, **2004**, 47 (11), 2926

[38] Y.-S. Wu, *PhD. Thesis*, University of Cape Town, **2002**

[39] E. Hoyer, R. Kohler, R. Kirmse, R. Richter, J. Sieler and L. Beyer, *Z. Anorg. Allg. Chem.*, **1986**, 537, 133.

[40] K.-H. Konig, M. Kuge, L. Kaul and H.-J. Pletsch, *Chem. Ber.*, **1987**, 120, 1251.

[41] K.R. Koch, S.A. Bourne, A. Coetzee and J. Miller, *J. Chem. Soc. Dalton Trans.*, **1999**, 3157

[42] J.-M. Lehn, *Frontiers in Supramolecular Organic Chemistry and Photochemistry*, H.-J. Schneider and H. Durr (ed.), VCH, Weinheim, **1991**, p.17.

[43] J.L. Atwood, J.E.D. Davies, D.D. MacNicol and F. Vögtle (eds.), *Comprehensive Supramolecular Chemistry*, **1996**, Pergamon, New York. For concepts most applicable to this project, see vols. 6 – 10.

[44] (a) P.J. Stang and D.H. Cao, *J. Am. Chem. Soc.*, **1994**, 116, 11, 4981 (b) J. Manna, J.A. Whiteford and P.J. Stang, *J. Am. Chem. Soc.*, **1996**, 118, 8731 (c) J. Manna, C.J Kuehl, J.A. Whiteford, P.J Stang, D.C. Muddiman, S.A. Hofstadler and R.D. Smith, *J. Am. Chem. Soc.*, **1997**, 119, 11611

[45] C. Muller, J.A. Whiteford and P.J. Stang, *J. Am. Chem. Soc.*, **1998**, 120, 9827

[46] J. Fan, J.A. Whiteford, B. Olenyuk, M.D. Levin, P.J. Stang and E.B. Fleischer, *J. Am. Chem. Soc.*, **1999**, 121, 2741

[47] P.J. Stang, D.H. Cao, K. Chen, G.M. Gray, D.C. Muddiman, R.D. Smith, *J. Am. Chem. Soc.* **1997**, 119, 5163

[48] P.J. Stang, N.E. Persky, J. Manna, *J. Am. Chem. Soc.*, **1997**, 119, 4777.

[49] Y.K. Kryschenko, S.R. Seidel, A.M. Arif, P.J. Stang, *J. Am. Chem. Soc.*, **2003**, 125, 5193

[50] M. Aoyagi, K. Biradha and M. Fujita, *Bull. Chem. Soc. Jpn.*, **1999**, 72, 2603

[51] C.J Matthews, K. Avery, Z. Xu, L.K. Thompson, L. Zhao, D.O. Miller, K. Biradha, K. Poirier, M.J. Zaworotko, C. Wilson, A.E. Goeta and J.A.K Howard, *Inorg. Chem.*, **1999**, 38, 5266

[52] J. Rojo, F.J. Romero-Salguero, J-M. Lehn, G. Baum and D. Fenske, *Eur. J. Inorg. Chem.*, **1999**, 1421

[53] J. Song, D. Moon and M.S. Lah, *Bull. Korean Chem. Soc.*, **2002**, 23, 5, 708

[54] D.T. Puerta and S.M. Cohen, *Chem. Commun.*, **2003**, 11, 1278

[55] H. Piotrowski and K. Severin, *PNAS.*, **2002**, 99, 8, 4997

[56] D.V Soldatov, A.S. Zanina, G.D. Enright, C.I. Ratcliffe and J.A. Ripmeester, *Crystal Growth & Design*, **2003**, 3, 6, 1005

[57] J.-M. Lehn, *Perspect. Coord. Chem.*, **1992**, 447.

[58] J.-M. Lehn, *Pure Appl. Chem.* **1978**, *50*, 871.

[59] G. R. Desiraju *Angew. Chem. Int. Ed.*, **1995**, 34, 2311

[60] (a) First use of the phrase "Molecular Tectonics" S. Mann, *Nature,* **1993**, 365, 499. (b) A list of references to later prominent use of the phrase by Hosseini *et al.* in numerous papers from **1996** can be found at: http://www-chimie.u-strasbg.fr/~lcco/perso/Wais/listepubMWH.html

[61] V.G. Machado, P.N.W. Baxter and J-M. Lehn, *J. Braz. Chem. Soc.*, **2001**, 12, 4 (the authors cite the following references for this definition: Lehn, J.-M. *Angew. Chem. Int. Ed.* **1990**, *29*, 1304 and Lehn, J.-M. *Supramolecular Chemistry*; VCH; Weinheim, **1995**.)

[62] The authors cite G.M. Whitesides, J.P. Mathias and C.T. Seto, *Science* **1991**, *254*, 1312 at this point.

[63] J.-M. Lehn, *Science*, **2002**, 295, 2400

[64] F. M. Tabellion, S. R. Seidel, A. M. Arif, and P. J. Stang *J. Am. Chem. Soc.*, **2001**, 123, 7740

[65] Although metal-ligand bonds are also termed 'dative covalent bonds', the general consensus is that such an interaction is listed among the 'non-covalent' interactions that link molecular units into supramolecular architectures, because they are generally more labile, with lower energy associations than true covalent bonds. See for example: (a) G. M.

Whitesides, J. P. Mathias, and C. T. Seto, *Science,* **1991,** 254, 1312 (b) R. Vaidya, G. López, J. A. López, *Kirk-Othmer Encyclopedia of Chemical Technology: Nanotechnology*, **1998**, Wiley: http://www.mrw.interscience.wiley.com/kirk/articles/nanovaid.a01/sect1 7.html. (c) A. J. Goshe, I. M. Steele, C. Ceccarelli , A. L. Rheingold , and B. Bosnich, PNAS, **2002** , 99, 8, 4823. (d) J.-M. Lehn, *Science*, **2002**, 295, 2400 (ref. 64). (e) J.V. Barth, J. Weckesser, N. Lin, A. Dmitriev and K. Kern, *Appl. Phys. A*, **2003**, 76, 645.

[66] (a) M. Fujita, S. Nagao, K. Ogura, *J. Am. Chem. Soc* **1995**, *117*, 1649. (b) T. Kusukawa, M. Fujita, *Angew. Chem., Int. Ed.,* **1998**, *37*, 3142. (c) M. Fujita, *Chem. Soc. Rev* **1998**, *27*, 417. (c) N. Takeda, K. Umemoto, K. Yamaguchi, and M. Fujita, *Nature* **1999**, *398*, 794. (d) M. Fujita, N. Fujita, K. Ogura, and K. Yamaguchi, Nature **1999**, *400*, 52

[67] (a) R. W. Saalfrank, I. Bernt, F. Hampel, *Chem. Eur. J.* **2001,** *7*, 2770. (b) R. W. Saalfrank, H. Glaser, B. Demleitner, F. Hampel, M. Chowdhry, V. Schünemann, A. X. Trautwein, G. B. M. Vaughan, R. Yeh, A. V. Davis, K. N. Raymond, *Chem. Eur. J.*, **2002**, 8, 493. (c) R. W. Saalfrank, I. Bernt, F. Hampel, A. Scheurer, T. Nakajima, S. H. Z. Huma, F. W. Heinemann, M. Schmidtmann, A. Müller, *Polyhedron,* **2003**, 22, 2985.

[68] (a) S.R. Seidel, P.J. Stang, *Accounts Chem. Res.* **2002**, 35, 972. (b) C.J. Kuehl, Y.K. Kryschenko, U. Radhakrishnan, S.R. Seidel, S.D. Huang, P.J. Stang. *PNAS.*, **2002**, 4932.(c) S. Leininger, J. Fan, M. Schmitz, P.J. Stang, *PNAS.*, **2000**, 97, 1380. (d) B. Olenyuk, M.D. Levin, J.A. Whiteford, J.E. Shield, P.J. Stang, *J. Am. Chem. Soc.* **1999**, 121, 10434. (e) B. Olenyuk, J.A. Whiteford, A. Fechtenkötter, P.J. Stang, *Nature,* **1999**, 398, 796

[69] M. Eddaoudi, J. Kim, J. B. Wachter, H. K. Chae, M. O'Keeffe and O. M. Yaghi, *J. Am. Chem. Soc.* **2001.**

[70] (a) B. Moulton, J. Lu, A. Mondal and M. J. Zaworotko, *Chem. Commun.*, **2001,** 863. (b) J. Lu, A. Mondal, B. Moulton and M. J. Zaworotko, *Angew. Chem., Int. Ed.*, **2001**, 40, 2113,

[71] G. R. Desiraju, *Crystal Engineering: The Design of Organic Solids*, Elsevier, Amsterdam, **1989**

[72] B. Moulton and M.J. Zaworotko, *Chem. Rev.*, **2001**, 101, 6, 1629

[73] C. V. K. Sharma and R.D. Rogers, *Crystal Engineering Perspectives,* http://www.bama.ua.edu/~rdrogers/webdocs/XE/XEWeb.html

[74] S. L. James *Chem. Soc. Rev.*, **2003**, 32, 276

[75] M. J. Zaworotko, *Chem. Comm.* **2001**, 1, 1

[76] (a) O.M. Yaghi, H. Li and T.L. Groy, *J. Am. Chem. Soc.*, **1996**, 118, 9096. (b) L. Carlucci, G. Ciani, D. M. Proserpio and A. Sironi. *J. C. S. Dalton Trans.*, **1997**, 1801. (c) C.B. Aakeroy, A.M. Beatty and D.S. Leinen, *Angew. Chem. Int. Ed.*, **1999**, 38, 12, 1815. (d) I. Boldog, E.B. Rusanov, A.N. Chernega, J. Sieler and K.V. Domasevitch, *J. Chem. Soc.*

Dalton Trans., **2001**, 6, 893. (e) D.G. Kurth, K.M. Fromm, and J-M. Lehn, *Eur. J. Inorg. Chem.*, **2001**, 1523. (f) S.A. Bourne, A. Mondal and M. J. Zaworotko, *Crystal Engineering*, **2001**, 4, 25. (g) J.W. Ko, K.S. Min and M.P. Suh, *Inorg. Chem.*, **2002**, 41, 2151. (h) J-H. Luo, M-C. Hong, R. Cao, Y-C. Liang, Y-J. Zhao, R-H. Wang and J-B. Weng, *Polyhedron*, **2002**, 21, 893. (i) D. Vujovic, H.G. Raubenheimer and L.R. Nassimbeni, *J. Chem. Soc. Dalton Trans.*, **2003**, 631.

[77] H.W. Roesky and M. Andruh *Coord. Chem. Rev.*, **2003**, 236, 91

[78] A. F. Wells (a) *Three-dimensional Nets and Polyhedra*, Wiley-Interscience, New York, 1977. (b) *Further Studies of Three-dimensional Nets*, ACA Monograph No. 8, American Crystallographic Association, 1979. (c) *Structural Inorganic Chemistry*, Clarendon Press, Oxford, **1984** – (references to Wells cited in references 79 and 80 below)

[79] S.R. Batten and R. Robson, *Angew. Chem. Int. Ed.* **1998**, 37, 1460

[80] S. Decurtins, R. Pellaux, G. Antorrena and F. Palacio, *Coord. Chem. Rev.*, **1999**, 841

[81] K-Y. Choi, H. Ryu, Y-M. Lim, N-D Sung, U-S. Shin and M. Suh, *Inorg. Chem. Comm.*, **2003**, 6, 412

[82] A few examples of 4,4'-bipyridine as *exo*-bidentate ligand: (a) P.N. Taylor and H.L. Anderson, *J. Am. Chem. Soc.*, **1999**, 121, 11538. (b) K. Biradha, K.V. Domasevitch, C. Hogg, B. Moulton, K.N. Power, and M.J. Zaworotko, *Cryst. Eng.*, **1999**, 2, 37. (c) M. Aoyagi, K. Biradha and M. Fujita, *Bull. Chem. Soc. Japan*, **2000**, 73, 6, 1369. (d) B-W. Sun, S. Gao, and Z-M. Wang, *Chem. Letters*, **2001**, 2. (e) M.J. Plater, M.R. St J. Foreman, R.A. Howie and J.M.S. Skakle, *Inorg. Chim. Acta*, **2001**, 318, 175. (f) H. Hou, Y. Wei, Y. Fan, C. Du, Y. Zhu, Y. Song, Y. Niu and X. Xin, *Inorg. Chim. Acta*, **2001**, 319, 212. (g) C. Seward and S. Wang, *Can. J. Chem.*, **2001**, 79, 7, 1187. (h) H. Wei, Y. Wei, Y. Fan, C. Du, Y. Zhu, Y. Song, Y. Niu and X. Xin, *Inorg. Chim. Acta*, **2001**, 319, 212. (i) C-D. Wu, C-Z. Lu, S-F. Lu, H-H. Zhuang and J-S. Huang, *Inorg. Chem. Comm.*, **2002**, 5, 171.

[83] Some examples of pyrazine as bidentate bridging ligand: (a) D.B. Leznoff, B-Y. Xue, C.L. Stevens, A. Storr, R.C. Thompson and B.O. Patrick, *Polyhedron*, **2001**, 20, 1247. (b) C.R. Choudhury, S. K. Dey, S. Sen, B. Bag, S. Mitra, and V. Gramlich, *Z. Naturforsch.*, **2002** 57 b, 1191. (c) S. A. Bourne, M. L. Kilkenny, L. R. Nassimbeni, *J. Chem. Soc., Dalton Trans.* **2001**, 1172.

[84] Examples of 1,2-bis(4-pyridyl)ethane as a flexible bridging ligand: (a) C.S. Hong and Y. Dong, *Inorg. Chem.*, **1998**, 37, 4470. (b) R. Atencio, K. Biradha, T.L. Hennigar, K.M. Poirier, K.N. Power, C.M. Seward, N.S. White and M.J. Zaworotko, *Cryst Eng*, **1998**, 1, 3/4, 203. (c) J.Y. Lu and A. Babb, *Inorg. Chim. Acta*, **2001**, 318, 186 (d) M.J. Plater, M.R. St J. Foreman and J.M.S. Skakle, *Cryst. Eng.*, **2001**, 4, 293. (e) Y.K. Lee and S.W. Lee, *Bull. Korean Chem. Soc.*, **2003**, 24, 7, 906

[85] G. J. McManus, Z. Wang, and M. J. Zaworotko *Crystal Growth & Design,* **4** (1), 11, 2004 citing (a) A. Muller, S.K. Das, M.O. Talismanova, H. Bogge, P. Kogerler, M. Schmidtmann, S.S. Talismanov, M. Luban and E. Krickemeyer, *Angew. Chem., Int. Ed.,* **2002**, 41, 579. (b) A. Muller, S.K Das, P. Kogerler, H. Bogge, .M. Schmidtmann, A.X. Trautwein, V. Schunemann, E. Krickemeyer and W. Preetz, *Angew. Chem., Int. Ed.,* **2000**, 39, 3413

[86] O. M. Yaghi, M. O'Keefe, N. W. Ockwig. H.K. Chae, M. Eddaoudi and J. Kim, *Nature,* **2003**, 423, 705

[87] (a) H. Li, J. Kim, T. Groy, M. O'Keeffe, O. M. Yaghi, *J. Am. Chem. Soc.* **2001,** 123, 4867 (b) M. Eddaoudi, J. Kim, N. Rosi, D. Vodak, J. Wachter, M. O'Keeffe and O.M. Yaghi, Science, **2002**, 295, 469.

[88] S.A. Bourne, J. Lu, A. Mondal, B. Moulton and M.J. Zaworotko, *Angew. Chem. Int. Ed.,* **2001**, 40, 2111

[89] G. J. McManus, Z. Wang, and M. J. Zaworotko, *Crystal Growth & Design,* **2004**, 4 (1), 11

[90] L. Brammer, M. D. Burgard, C. S. Rodger, J.K. Swearingen and N.P. Rath, *Chem. Commun.*, **2001**, 2468

[91] M.S. Lah, I. Kim and M. Moon: http://service2.area.fi.cnr.it/kimic/lah1.pdf.

[92] J.F. Stoddart research group publications list can be found at http://www.chem.ucla.edu/dept/Faculty/stoddart/new/index.php

[93] (a) First use of the term clathrate: H.M. Powell, J. Chem. Soc., **1948**, 61. Also see: (b) E. Weber, *Topics in Current Chemistry*, **1987**, vol. 140, Springer; (c) J.E.D. Davies, J. Incl. Phen & Mol. Recog. Chem., **1998**, 32, 499.

[94](a) B. Chen, M. Eddaoudi, S.T. Hyde, M. O'Keeffe and O.M. Yaghi, *Science,* **2001**, 291, 1021. (b) K. Biradha, Y. Hongo, M. Fujita, *Angew. Chem., Int. Ed.* **2000**, 39, 3843. (c) M. P. Suh, J. W. Ko, H. J. Choi J. Am. Chem. Soc. **2002**, 124, 37, 9.

[95] M. Baron and R. F. T. Stepto, *Pure Appl. Chem.*, **2002**, 74, 3, 493

[96] H.J. Choi and M.P. Suh, *Inorg. Chem.*, **2003**, 42, 1151.

[97] (a) B.K Cho, and M.S. Lee, *J. Am. Chem. Soc.* **2001**, *123*, 9677 and (b) J.H. Jung, Y. Ono, K. Sakurai, M. Sano, and S. Shinkai, *J. Am. Chem. Soc.* **2000**, *122*, 8646.

[98] K.R. Koch, C. Sacht and S. Bourne *Inorg. Chim. Acta*, **1995**, 232, 109

[99] K.R. Koch, O. Hallale, S.A. Bourne, J. Miller and J. Bacsa, *J. Mol. Struc.*, **2001**, 561, 185

[100] Z. Otwinowski, W. Minor, DENZO and SCALEPACK. In *International Tables for Crystallography, Vol F.*, ed.; M. G. Rossman, E. Arnold, Kluwer: Dordrecht, **2000**

[101] G. M. Sheldrick, SHELXS97 and SHELXL97, suite of programs for crystal structure determination and refinement, University of Göttingen, **1997**.

[102] L.J. Barbour, X-Seed, University of Missouri – Columbia, **1999**.

[103] R.A. Bailey, K.L Rothahupt and R.K. Kullnig, *Inorg. Chim. Acta*, **1988**, 147, 233

[104] (a) F. H. Allen, O. Kennard, D.G. Watson, L. Brammer, A. G. Orpen and R. Taylor, *J. Chem. Soc. Perkin Trans. II*, (1987) S1; (b) A. G. Orpen, L. Brammer, F. H. Allen, O. Kennard, D.G. Watson, and R. Taylor, *J. Chem. Soc. Dalton Trans.*, (1989) S1.

[105] C. Janiak, *J. Chem. Soc. Dalton Trans.*, **2000**, 3885.

[106] C. A. Hunter and J. K. M. Sanders, *J. Am. Chem. Soc.*, **1990**, 112, 5525.

[107] K.R. Koch, A. Westra currently unreported.

[108] M. Howe-Grant (Ed.), *Kirk – Othmer Encyclopaedia of Chemical Technology*, 4th ed., **1996**, 20, 644

[109] L. Pauling, *The Nature of the Chemical Bond*, 3rd ed. **1960**, Cornell University Press, Ithaca, New York.

[110] C. R. Choudhury, S. K. Dey, S. Sen, B. Bag, S. Mitra, and V. Gramlich. *Z. Naturforsch*, **2002,** 57 b, 1191

[111] D.B. Leznoff, B-Y Xue, C.L. Stevens, A. Storr, R.C. Thompson, B.O. Patrick *Polyhedron*, **2001**, 20, 1247

[112] http://www.chemistry.ccsu.edu/glagovich/teaching/472/ir/table.html

[113] J. Greve and C. Näther, *Acta Crystallogr.* **2002**, E58, m653

Table A2. Atomic coordinates (x 10^4) and equivalent isotropic displacement parameters (A^2 x 10^3) for **I-EtOH**. U(eq) is defined as one third of the trace of the orthogonalized Uij tensor.

Atom	x	y	z	U(eq)
O(1)	7757(1)	3900(1)	1579(1)	40(1)
C(2)	8877(1)	3315(1)	1702(1)	28(1)
N(3)	10207(1)	3681(1)	1508(1)	31(1)
S(4)	9568(1)	4758(1)	538(1)	39(1)
N(4)	11643(1)	5529(1)	1218(1)	29(1)
C(4)	10508(1)	4700(1)	1109(1)	29(1)
C(11)	8927(1)	2130(1)	2108(1)	25(1)
C(12)	7868(1)	2132(1)	2500	25(1)
C(13)	9990(1)	1069(1)	2106(1)	27(1)
C(14)	9991(1)	10(1)	2500	28(1)
C(41)	12221(2)	6517(1)	811(1)	32(1)
O(42)	11439(2)	8614(1)	1313(1)	55(1)
C(42)	11422(2)	7938(2)	805(1)	41(1)
C(43)	12322(2)	5623(2)	1752(1)	36(1)
O(44)	12822(1)	3167(1)	1945(1)	44(1)
C(44)	13496(2)	4514(2)	1844(1)	40(1)

Table A3. Atomic coordinates (x 10^4) and equivalent isotropic displacement parameters (A^2 x 10^3) for ***Cis*-[Ni(I-Et-*S,O*)]$_2$**. U(eq) is defined as one third of the trace of the orthogonalized Uij tensor.

Atom	x	y	z	U(eq)
Ni(1)	7015(1)	7647(1)	6816(1)	16(1)
O(1a)	8786(1)	8635(1)	6987(1)	21(1)
C(2a)	9580(2)	8581(1)	7778(1)	17(1)
N(3a)	9239(1)	8023(1)	8775(1)	21(1)
S(4a)	6560(1)	6738(1)	8440(1)	24(1)
N(4a)	7740(1)	6916(1)	10207(1)	22(1)
C(4a)	7947(2)	7281(1)	9154(1)	19(1)
C(11a)	11163(2)	9261(1)	7559(1)	17(1)
C(12a)	12187(2)	9120(2)	8361(1)	20(1)
C(13a)	13678(2)	9691(2)	8162(1)	22(1)
C(16a)	11651(2)	9993(1)	6566(1)	17(1)
C(41a)	8848(2)	7347(2)	10886(1)	25(1)
C(42a)	10271(2)	6257(2)	11041(1)	37(1)
C(43a)	6441(2)	6048(2)	10755(1)	25(1)
C(44a)	4883(2)	6935(2)	11032(1)	36(1)
O(1b)	7284(1)	8494(1)	5393(1)	19(1)
C(2b)	6286(2)	8643(1)	4702(1)	16(1)
N(3b)	4805(1)	8223(1)	4772(1)	17(1)
S(4b)	5119(1)	6372(1)	6604(1)	23(1)
N(4b)	2606(1)	7047(1)	5513(1)	17(1)
C(4b)	4145(2)	7301(1)	5567(1)	16(1)
C(11b)	6842(2)	9431(1)	3638(1)	16(1)
C(12b)	5828(2)	9602(1)	2832(1)	19(1)
C(41b)	1719(2)	7801(2)	4640(1)	22(1)
C(42b)	2014(2)	7096(2)	3650(1)	35(1)
C(43b)	1743(2)	6003(2)	6289(1)	21(1)
C(44b)	2143(2)	4492(2)	6071(1)	33(1)

Table A4. Atomic coordinates (x 10^4) and equivalent isotropic displacement parameters (A^2 x 10^3) for *Cis*-[Ni(I-Et-*S,O*)(Pyridine-*N*)$_2$]$_2$. U(eq)is defined as one third of the trace of the orthogonalized Uij tensor.

Atom	x	y	z	U(eq)
Ni(1)	4732(1)	852(1)	1735(1)	26(1)
O(1A)	4482(2)	1356(1)	797(1)	28(1)
C(2A)	3494(4)	1789(2)	604(2)	25(1)
N(3A)	2867(3)	2312(2)	946(2)	33(1)
S(4A)	3720(1)	1875(1)	2254(1)	35(1)
N(4A)	2691(4)	3142(2)	1793(2)	45(1)
C(4A)	3105(4)	2462(2)	1615(2)	30(1)
N(5A)	2787(3)	311(2)	1409(2)	33(1)
C(6A)	2706(4)	-41(2)	808(2)	38(1)
C(7A)	1523(5)	-411(2)	540(2)	46(1)
C(8A)	359(5)	-425(3)	910(3)	55(1)
C(9A)	404(5)	-74(3)	1528(3)	51(1)
C(10A)	1655(5)	291(2)	1768(2)	42(1)
C(11A)	2953(4)	1748(2)	-138(2)	26(1)
C(12A)	3477(4)	1199(2)	-552(2)	25(1)
C(15A)	1517(4)	2201(2)	-1113(2)	38(1)
C(16A)	1958(4)	2241(2)	-426(2)	34(1)
C(41A)	2887(5)	3432(2)	2490(2)	48(1)
C(42A)	1659(5)	3313(3)	2910(2)	59(1)
C(43A)	2062(9)	3656(3)	1281(3)	91(2)
C(44A)	2727(14)	4131(7)	1013(6)	90(5)
C(45A)	740(11)	3580(6)	1034(5)	47(3)
O(1B)	5685(3)	-55(1)	1356(1)	29(1)
C(2B)	6449(4)	-535(2)	1667(2)	24(1)
N(3B)	6933(3)	-575(2)	2323(2)	30(1)
S(4B)	4861(1)	277(1)	2830(1)	37(1)
N(4B)	7233(4)	-267(2)	3432(2)	47(1)
C(4B)	6438(4)	-203(2)	2838(2)	31(1)
N(5B)	6788(3)	1317(2)	1841(2)	32(1)
C(6B)	7543(4)	1355(2)	1300(2)	40(1)
C(7B)	8885(5)	1638(3)	1323(3)	51(1)
C(8B)	9491(5)	1889(3)	1933(3)	59(1)
C(9B)	8740(5)	1860(3)	2497(3)	60(1)
C(10B)	7392(5)	1575(2)	2432(2)	45(1)
C(11B)	6982(4)	-1150(2)	1242(2)	25(1)
C(16B)	7957(4)	-1666(2)	1520(2)	32(1)
C(41B)	8541(5)	-711(3)	3480(2)	62(2)
C(42B)	8264(7)	-1518(3)	3591(3)	83(2)
C(43B)	6794(6)	24(4)	4090(2)	78(2)
C(44B)	7438(11)	723(5)	4259(4)	146(4)
N(1G)	3481(7)	7406(4)	328(3)	105(2)
C(2G)	4369(9)	6864(5)	499(4)	108(2)
C(3G)	3993(10)	6222(6)	829(5)	129(3)
C(4G)	2633(9)	6200(5)	952(4)	121(3)
C(5G)	1708(9)	6647(4)	777(4)	104(2)
C(6G)	2032(9)	7282(5)	456(4)	109(2)

Table A5. Atomic coordinates (x 10^4) and equivalent isotropic displacement parameters (A^2 x 10^3) for *Cis*-[Ni(I-Et-*S,O*)(DMAP-*N*)$_2$]$_2$. U(eq) is defined as one third of the trace of the orthogonalized Uij tensor.

Atom	x	y	z	U(eq)
Ni(1)	7724(1)	964(1)	9825(1)	22(1)
O(1A)	8616(1)	1245(2)	9270(1)	26(1)
C(2A)	8530(2)	1310(3)	8679(2)	23(1)
N(3A)	7893(2)	1657(3)	8252(1)	26(1)
S(4A)	6651(1)	1537(1)	8990(1)	28(1)
N(4A)	6648(2)	2410(3)	7839(1)	32(1)
C(4A)	7107(2)	1880(3)	8343(2)	25(1)
N(5A)	7962(2)	2716(3)	10194(1)	28(1)
C(6A)	7380(2)	3524(3)	10282(2)	30(1)
C(7A)	7542(2)	4635(3)	10541(2)	34(1)
C(8A)	8369(3)	4996(3)	10742(2)	34(1)
N(9A)	8569(2)	6088(3)	11005(2)	48(1)
C(9A)	8978(2)	4140(3)	10664(2)	36(1)
C(10A)	8747(2)	3045(3)	10396(2)	32(1)
C(11A)	9274(2)	993(3)	8377(2)	22(1)
C(12A)	10030(2)	-456(3)	11264(2)	23(1)
C(15A)	9964(2)	904(3)	7465(2)	31(1)
C(16A)	9283(2)	1223(3)	7738(2)	27(1)
C(41A)	5773(2)	2717(4)	7805(2)	44(1)
C(42A)	5214(3)	1772(6)	7461(3)	87(2)
C(43A)	7005(3)	2684(4)	7265(2)	43(1)
C(44A)	7530(3)	3794(4)	7314(2)	55(1)
C(91A)	7937(3)	7000(4)	11021(2)	52(1)
C(92A)	9417(3)	6422(5)	11216(3)	69(2)
O(1B)	8622(1)	423(2)	10545(1)	26(1)
C(2B)	8598(2)	390(3)	11127(2)	26(1)
N(3B)	8024(2)	808(3)	11450(2)	32(1)
S(4B)	6702(1)	552(1)	10493(1)	33(1)
N(4B)	6836(2)	1752(3)	11570(2)	39(1)
C(4B)	7241(2)	1080(3)	11203(2)	31(1)
N(5B)	7694(2)	-841(2)	9527(1)	27(1)
C(6B)	6985(2)	-1438(3)	9358(2)	31(1)
C(7B)	6943(3)	-2631(3)	9195(2)	35(1)
C(8B)	7672(2)	-3297(3)	9202(2)	31(1)
N(9B)	7658(2)	-4475(3)	9037(2)	41(1)
C(9B)	8420(2)	-2656(3)	9382(2)	33(1)
C(10B)	8396(2)	-1468(3)	9537(2)	30(1)
C(11B)	9344(2)	-142(3)	11535(2)	23(1)
C(16B)	9355(2)	-360(3)	12177(2)	29(1)
C(41B)	5972(2)	2109(5)	11396(2)	49(1)
C(42B)	5384(3)	1268(6)	11644(3)	72(2)
C(43B)	7256(3)	2181(5)	12197(2)	49(1)
C(44B)	7671(3)	3381(5)	12156(2)	61(1)
C(91B)	6871(3)	-5085(4)	8866(2)	51(1)
C(92B)	8409(3)	-5113(4)	8990(2)	51(1)
Cl(1G)	4751(5)	3383(8)	9899(4)	64(3)
C(1G)	4521(10)	2523(16)	9299(8)	32(4)
Cl(2G)	4123(3)	3411(5)	8621(2)	57(1)
Cl(1H)	4805(5)	3660(8)	9889(4)	56(2)
C(1H)	4585(9)	2205(14)	9467(7)	22(3)
Cl(2H)	4099(4)	2477(6)	8662(3)	70(1)

Table A6. Atomic coordinates (x 10^4) and equivalent isotropic displacement parameters (A^2 x 10^3) for *Cis*-[Ni(I-EtOH-*S,O*)(Pyridine-*N*)$_2$]$_2$. U(eq) is defined as one third of the trace of the orthogonalized Uij tensor.

Atom	x	y	z	U(eq)
Ni(1)	9069(1)	9212(1)	6792(1)	23(1)
O(1A)	9842(2)	8523(1)	5939(1)	27(1)
C(2A)	10192(2)	7645(2)	5835(1)	23(1)
N(3A)	10474(2)	6999(2)	6327(1)	29(1)
S(4A)	8602(1)	7524(1)	7215(1)	29(1)
N(4A)	10901(2)	6625(2)	7502(1)	32(1)
C(4A)	10089(3)	7061(2)	6994(1)	26(1)
N(5A)	7011(2)	8875(2)	6027(1)	30(1)
C(6A)	6963(3)	9040(3)	5328(2)	46(1)
C(7A)	5670(4)	8811(4)	4800(2)	73(1)
C(8A)	4380(4)	8383(4)	5001(2)	71(1)
C(9A)	4417(3)	8216(3)	5715(2)	54(1)
C(10A)	5746(3)	8471(2)	6213(2)	40(1)
C(11A)	10402(2)	7282(2)	5062(1)	23(1)
C(15A)	10794(3)	5962(2)	4119(2)	39(1)
C(16A)	10689(3)	6289(2)	4851(1)	32(1)
C(41A)	12126(3)	6165(2)	7321(2)	39(1)
O(42A)	14671(2)	6555(2)	7263(1)	63(1)
C(42A)	13504(3)	7005(3)	7439(2)	48(1)
C(43A)	10677(3)	6635(2)	8267(1)	35(1)
O(44A)	9518(3)	5635(2)	9100(1)	53(1)
C(44A)	9663(4)	5628(2)	8343(2)	45(1)
O(1B)	9505(2)	10605(1)	6402(1)	30(1)
C(2B)	9522(3)	11530(2)	6699(1)	24(1)
N(3B)	9560(2)	11908(2)	7408(1)	29(1)
S(4B)	8122(1)	10065(1)	7760(1)	30(1)
N(4B)	9756(2)	11805(2)	8638(1)	31(1)
C(4B)	9239(3)	11309(2)	7926(1)	25(1)
N(5B)	11281(2)	9614(2)	7404(1)	30(1)
C(6B)	12349(3)	9953(2)	7048(2)	43(1)
C(7B)	13808(3)	10146(3)	7371(2)	57(1)
C(8B)	14216(4)	9997(3)	8089(2)	64(1)
C(9B)	13141(4)	9659(3)	8470(2)	54(1)
C(10B)	11691(3)	9483(2)	8109(2)	36(1)
C(11B)	9548(3)	12337(2)	6183(1)	24(1)
C(12B)	9692(2)	12032(2)	5456(1)	23(1)
C(16B)	9341(3)	13358(2)	6398(1)	33(1)
C(41B)	10570(3)	12916(2)	8799(1)	36(1)
O(42B)	12879(3)	14068(2)	8960(1)	64(1)
C(42B)	12148(3)	12975(3)	8783(2)	53(1)
C(43B)	9586(3)	11285(2)	9285(1)	42(1)
O(44B)	7976(4)	10946(3)	10136(2)	64(1)
C(44B)	8134(7)	11544(4)	9536(3)	50(1)
O(45B)	7174(10)	11097(7)	9419(5)	62(3)
C(45B)	8659(11)	11509(7)	9736(5)	28(2)
N(1G)	6534(3)	8788(2)	9478(2)	65(1)
C(2G)	7107(4)	8135(3)	9068(2)	56(1)
C(3G)	6684(4)	7070(3)	8951(2)	64(1)
C(4G)	5540(4)	6618(3)	9252(2)	68(1)
C(5G)	4871(4)	7291(3)	9658(2)	58(1)
C(6G)	5409(4)	8348(3)	9759(2)	58(1)
N(7G)	14512(7)	5458(5)	5814(4)	55(2)
C(8G)	15780(9)	5741(5)	5572(4)	41(2)
C(9G)	16063(10)	5268(7)	4906(5)	65(2)
C(10G)	14918(14)	4480(8)	4445(5)	70(2)
C(11G)	13632(10)	4203(7)	4717(6)	66(2)

Table A6. continued.

C(12G)	13448(9)	4666(7)	5387(5)	65(2)
N(13G)	15073(11)	13945(6)	8145(4)	62(2)
C(14G)	15064(11)	14152(8)	7468(5)	86(3)
C(15G)	15646(10)	13567(8)	6932(5)	76(3)
C(16G)	16320(8)	12797(6)	7190(5)	49(2)
C(17G)	16372(8)	12613(6)	7893(4)	58(2)
C(18G)	15759(9)	13181(8)	8336(5)	66(2)
N(19G)	14473(10)	13876(6)	7939(5)	60(2)
C(20G)	13986(13)	13658(9)	7222(6)	86(3)
C(21G)	14616(13)	13153(8)	6720(6)	84(3)
C(22G)	15850(15)	12899(11)	6949(8)	90(4)
C(23G)	16511(12)	13086(10)	7702(7)	86(3)
C(24G)	15728(12)	13615(10)	8221(6)	72(3)
O(1W)	12078(3)	15446(2)	9988(1)	48(1)

Table A7. Atomic coordinates (x 10^4) and equivalent isotropic displacement parameters (A^2 x 10^3) for T-Et-Ni-Py. U(eq) is defined as one third of the trace of the orthogonalized Uij tensor.

Atom	x	y	z	U(eq)
Ni(1A)	8914(1)	-1310(1)	9108(1)	32
O(1A)	8004(2)	-867(2)	9297(2)	41
C(2A)	7906(3)	-608(2)	9736(3)	32
N(3A)	8407(3)	-488(2)	10197(2)	43
N(4A)	9531(3)	-472(2)	10844(3)	64
C(4A)	9155(4)	-681(2)	10354(3)	42
S(5A)	9666(1)	-1117(1)	10013(1)	42
O(6A)	8228(2)	-1492(1)	8352(2)	32
C(7A)	8432(3)	-1737(2)	7926(2)	26
N(8A)	9176(3)	-1799(2)	7759(2)	33
N(9A)	10527(3)	-1610(2)	7814(2)	37
C(9A)	9879(3)	-1727(2)	8107(3)	31
S(10A)	9997(1)	-1833(1)	8851(1)	36
C(11A)	7084(3)	-364(2)	9714(3)	30
C(12A)	6811(4)	-136(2)	10202(3)	36
C(13A)	6058(4)	57(2)	10190(3)	38
C(14A)	5529(3)	46(2)	9666(2)	26
C(15A)	5799(3)	-161(2)	9173(3)	29
C(16A)	6565(3)	-363(2)	9198(3)	30
C(41A)	10391(6)	-585(3)	11105(4)	75
C(42A)	10291(7)	-942(3)	11520(6)	103
C(43A)	9150(5)	-73(4)	11146(4)	97
C(44A)	9318(8)	415(4)	10905(6)	127
N(50A)	8281(3)	-1893(2)	9482(2)	36
C(50A)	7485(4)	-1934(3)	9354(3)	45
N(55A)	9354(3)	-717(2)	8636(2)	42
C(55A)	8842(4)	-462(3)	8267(4)	58
C(60A)	7040(4)	-2324(3)	9525(3)	51
C(65A)	9073(6)	-75(3)	7941(5)	86
C(70A)	7420(5)	-2675(3)	9845(4)	60
C(75A)	9889(6)	59(3)	8005(5)	92
C(80A)	8267(5)	-2638(3)	9999(4)	62
C(85A)	10431(5)	-198(3)	8369(4)	72
C(90A)	8669(4)	-2241(2)	9807(3)	45
C(91A)	11338(4)	-1539(3)	8111(3)	49
C(92A)	11882(5)	-1984(3)	8124(5)	77
C(93A)	10439(4)	-1528(3)	7175(3)	50
C(94A)	10177(5)	-1018(3)	7026(4)	67
C(95A)	10140(4)	-578(2)	8671(4)	55
Ni(1B)	3217(1)	562(1)	8831(1)	25
O(1B)	3209(2)	114(1)	8132(2)	34
C(2B)	2714(3)	95(2)	7674(3)	28
N(3B)	2222(3)	437(2)	7439(2)	40
N(4B)	1861(4)	1228(2)	7340(2)	44
C(4B)	2029(4)	843(2)	7716(3)	36
S(5B)	1914(1)	896(1)	8452(1)	34
O(6B)	4299(2)	255(1)	9126(2)	27
C(7B)	4671(3)	246(2)	9635(2)	24
N(8B)	4399(3)	355(2)	10140(2)	30
N(9B)	3394(3)	554(2)	10704(2)	37
C(9B)	3727(3)	618(2)	10196(3)	27
S(10B)	3314(1)	1046(1)	9704(1)	31
C(11B)	2716(3)	-354(2)	7318(3)	27
C(12B)	2202(4)	-416(2)	6803(3)	33
C(13B)	2234(4)	-830(2)	6468(3)	33
C(14B)	2792(3)	-1193(2)	6627(3)	27

Table A7. continued (iii).

C(60E)	6912(4)	3879(2)	18817(4)	54
C(65E)	9342(5)	6424(3)	17909(4)	64
C(70E)	7310(4)	3661(2)	19305(4)	55
C(75E)	9090(5)	6867(3)	18110(4)	63
C(80E)	7892(5)	3913(2)	19648(4)	55
C(85E)	8564(6)	6877(3)	18515(4)	66
C(90E)	8055(4)	4377(2)	19504(3)	48
C(91E)	5658(6)	6399(3)	17953(4)	67
C(92E)	6090(7)	6821(3)	18198(5)	95
C(93E)	6215(7)	6210(3)	16978(4)	79
C(94E)	5517(6)	5923(3)	16618(4)	84
C(95E)	8262(5)	6450(2)	18723(3)	51
Ni(1F)	13722(1)	3609(1)	18471(1)	30
O(1F)	13004(2)	3438(1)	17721(2)	34
C(2F)	13135(3)	3155(2)	17313(3)	31
N(3F)	13826(3)	2996(2)	17136(2)	34
N(4F)	15180(3)	2950(2)	17075(2)	43
C(4F)	14581(4)	3059(2)	17408(3)	33
S(5F)	14850(1)	3208(1)	18136(1)	38
O(6F)	12766(2)	3956(1)	18774(2)	37
C(7F)	12788(4)	4301(2)	19134(3)	34
N(8F)	13414(3)	4512(2)	19436(3)	42
N(9F)	14726(3)	4729(2)	19628(3)	45
C(9F)	14207(4)	4377(2)	19460(3)	36
S(10F)	14563(1)	3801(1)	19356(1)	39
C(11F)	12387(3)	2961(2)	16950(3)	29
C(12F)	12454(3)	2639(2)	16494(3)	31
C(13F)	11765(3)	2465(2)	16160(3)	28
C(14F)	10996(3)	2615(2)	16262(3)	28
C(15F)	10923(3)	2938(2)	16723(3)	35
C(16F)	11618(4)	3104(2)	17062(3)	36
C(41F)	16048(4)	2955(3)	17291(4)	70
C(42F)	16430(6)	3430(5)	17175(5)	133
C(43F)	14999(4)	2791(3)	16466(3)	53
C(44F)	14880(5)	2248(3)	16421(4)	68
N(50F)	13225(3)	2979(2)	18853(2)	37
C(50F)	12443(4)	2861(2)	18711(3)	43
N(55F)	13970(3)	4288(2)	18077(2)	39
C(55F)	13333(5)	4559(2)	17845(3)	49
C(60F)	12049(4)	2488(2)	18968(3)	48
C(65F)	13430(5)	5014(2)	17612(4)	67
C(70F)	12482(5)	2223(2)	19396(4)	59
C(75F)	14224(6)	5188(3)	17607(4)	77
C(80F)	13291(5)	2336(2)	19546(4)	62
C(85F)	14872(5)	4911(3)	17831(4)	69
C(90F)	13634(4)	2713(2)	19263(3)	49
C(91F)	15619(4)	4676(2)	19656(3)	46
C(92F)	15994(5)	4580(3)	20281(4)	70
C(93F)	14425(4)	5224(2)	19733(4)	63
C(94F)	14280(6)	5494(3)	19153(5)	99
C(95F)	14721(4)	4469(3)	18065(3)	50
N(1G)	6292(7)	-737(3)	7079(5)	121
C(2G)	5571(6)	-643(3)	7274(4)	80
C(3G)	5432(6)	-241(3)	7567(3)	72
C(4G)	6002(6)	104(3)	7669(4)	74
C(5G)	6744(6)	3(4)	7471(4)	85
C(6G)	6908(6)	-380(4)	7208(5)	89
N(7G)	5119(12)	3181(3)	10785(4)	192
C(8G)	4494(6)	3044(4)	11232(7)	120
C(9G)	4758(3)	2867(2)	11697(2)	90
C(10G)	5389(3)	2809(2)	11826(2)	121
C(11G)	5999(8)	2873(4)	11583(8)	150
C(12G)	5920(3)	3041(2)	11088(2)	116
N(13G)	10035(9)	5612(5)	16660(7)	171

Table A7. continued (iv).

C(14G)	9712(10)	5178(6)	16829(8)	175
C(15G)	10208(9)	4885(6)	17107(7)	151
C(16G)	11034(12)	5020(6)	17249(7)	177
C(17G)	11360(8)	5406(4)	17078(5)	108
C(18G)	10889(10)	5691(5)	16792(7)	140
N(19G)	8441(7)	2216(5)	17526(6)	148
C(20G)	8926(7)	2591(5)	17383(5)	111
C(21G)	9029(8)	3001(4)	17678(5)	105
C(22G)	8619(7)	3088(5)	18122(6)	116
C(23G)	8147(9)	2749(5)	18302(6)	137
C(24G)	8029(3)	2329(2)	17994(2)	152
N(25G)	8400(13)	979(7)	9443(11)	250
C(26G)	8440(16)	977(9)	8822(12)	249
C(27G)	7777(3)	979(2)	8435(2)	141
C(28G)	7087(3)	891(2)	8657(2)	126
C(29G)	7003(12)	941(6)	9165(8)	184
C(30G)	7628(3)	1025(2)	9588(2)	155

Table A7. Atomic coordinates (x 10^4) and equivalent isotropic displacement parameters (A^2 x 10^3) for T-Et-Ni-Py. U(eq) is defined as one third of the trace of the orthogonalized Uij tensor.

Atom	x	y	z	U(eq)
Ni(1A)	8914(1)	-1310(1)	9108(1)	32
O(1A)	8004(2)	-867(2)	9297(2)	41
C(2A)	7906(3)	-608(2)	9736(3)	32
N(3A)	8407(3)	-488(2)	10197(2)	43
N(4A)	9531(3)	-472(2)	10844(3)	64
C(4A)	9155(4)	-681(2)	10354(3)	42
S(5A)	9666(1)	-1117(1)	10013(1)	42
O(6A)	8228(2)	-1492(1)	8352(2)	32
C(7A)	8432(3)	-1737(2)	7926(2)	26
N(8A)	9176(3)	-1799(2)	7759(2)	33
N(9A)	10527(3)	-1610(2)	7814(2)	37
C(9A)	9879(3)	-1727(2)	8107(3)	31
S(10A)	9997(1)	-1833(1)	8851(1)	36
C(11A)	7084(3)	-364(2)	9714(3)	30
C(12A)	6811(4)	-136(2)	10202(3)	36
C(13A)	6058(4)	57(2)	10190(3)	38
C(14A)	5529(3)	46(2)	9666(2)	26
C(15A)	5799(3)	-161(2)	9173(3)	29
C(16A)	6565(3)	-363(2)	9198(3)	30
C(41A)	10391(6)	-585(3)	11105(4)	75
C(42A)	10291(7)	-942(3)	11520(6)	103
C(43A)	9150(5)	-73(4)	11146(4)	97
C(44A)	9318(8)	415(4)	10905(6)	127
N(50A)	8281(3)	-1893(2)	9482(2)	36
C(50A)	7485(4)	-1934(3)	9354(3)	45
N(55A)	9354(3)	-717(2)	8636(2)	42
C(55A)	8842(4)	-462(3)	8267(4)	58
C(60A)	7040(4)	-2324(3)	9525(3)	51
C(65A)	9073(6)	-75(3)	7941(5)	86
C(70A)	7420(5)	-2675(3)	9845(4)	60
C(75A)	9889(6)	59(3)	8005(5)	92
C(80A)	8267(5)	-2638(3)	9999(4)	62
C(85A)	10431(5)	-198(3)	8369(4)	72
C(90A)	8669(4)	-2241(2)	9807(3)	45
C(91A)	11338(4)	-1539(3)	8111(3)	49
C(92A)	11882(5)	-1984(3)	8124(5)	77
C(93A)	10439(4)	-1528(3)	7175(3)	50
C(94A)	10177(5)	-1018(3)	7026(4)	67
C(95A)	10140(4)	-578(2)	8671(4)	55
Ni(1B)	3217(1)	562(1)	8831(1)	25
O(1B)	3209(2)	114(1)	8132(2)	34
C(2B)	2714(3)	95(2)	7674(3)	28
N(3B)	2222(3)	437(2)	7439(2)	40
N(4B)	1861(4)	1228(2)	7340(2)	44
C(4B)	2029(4)	843(2)	7716(3)	36
S(5B)	1914(1)	896(1)	8452(1)	34
O(6B)	4299(2)	255(1)	9126(2)	27
C(7B)	4671(3)	246(2)	9635(2)	24
N(8B)	4399(3)	355(2)	10140(2)	30
N(9B)	3394(3)	554(2)	10704(2)	37
C(9B)	3727(3)	618(2)	10196(3)	27
S(10B)	3314(1)	1046(1)	9704(1)	31
C(11B)	2716(3)	-354(2)	7318(3)	27
C(12B)	2202(4)	-416(2)	6803(3)	33
C(13B)	2234(4)	-830(2)	6468(3)	33
C(14B)	2792(3)	-1193(2)	6627(3)	27

Table A7. continued (i).

C(15B)	3302(4)	-1137(2)	7139(3)	34
C(16B)	3262(4)	-726(2)	7487(3)	33
C(41B)	1547(4)	1692(2)	7543(3)	46
C(42B)	647(5)	1695(3)	7498(4)	80
C(43B)	1980(5)	1186(3)	6715(3)	58
C(44B)	2879(6)	1288(3)	6598(4)	81
N(50B)	2628(3)	-2(2)	9263(2)	31
C(50B)	2886(4)	-451(2)	9235(3)	42
N(55B)	3879(3)	1084(2)	8399(2)	32
C(55B)	4582(5)	977(2)	8205(3)	51
C(60B)	2518(4)	-834(2)	9506(4)	53
C(65B)	5085(5)	1317(3)	7982(4)	66
C(70B)	1850(5)	-735(3)	9792(4)	61
C(75B)	4848(5)	1784(3)	7945(3)	60
C(80B)	1577(4)	-270(2)	9820(4)	53
C(85B)	4120(5)	1905(2)	8127(4)	55
C(90B)	1984(4)	85(2)	9555(3)	42
C(91B)	2678(4)	826(3)	10847(3)	45
C(92B)	2906(5)	1292(3)	11170(4)	65
C(93B)	3723(4)	206(2)	11139(3)	47
C(94B)	3275(5)	-275(3)	11096(4)	63
C(95B)	3656(4)	1544(2)	8351(3)	42
Ni(1C)	3980(1)	-2448(1)	5971(1)	28
O(1C)	5072(2)	-2373(1)	6463(2)	36
C(2C)	5758(3)	-2523(2)	6365(3)	27
N(3C)	5988(3)	-2822(2)	5963(2)	29
N(4C)	5865(3)	-3357(2)	5217(2)	40
C(4C)	5480(3)	-3096(2)	5603(3)	30
S(5C)	4451(1)	-3179(1)	5608(1)	42
O(6C)	3566(2)	-1831(1)	6297(2)	39
C(7C)	2890(3)	-1626(2)	6237(2)	29
N(8C)	2220(3)	-1708(2)	5873(2)	38
N(9C)	1407(3)	-2030(2)	5118(3)	55
C(9C)	2108(4)	-2064(2)	5472(3)	40
S(10C)	2745(1)	-2546(1)	5367(1)	36
C(11C)	6462(3)	-2328(2)	6774(2)	23
C(12C)	7275(3)	-2451(2)	6704(3)	34
C(13C)	7903(3)	-2264(2)	7078(3)	33
C(14C)	7760(3)	-1954(2)	7531(2)	27
C(15C)	6953(3)	-1855(2)	7617(3)	33
C(16C)	6318(3)	-2041(2)	7246(3)	32
C(41C)	5448(4)	-3713(2)	4810(3)	48
C(42C)	5164(6)	-3485(3)	4223(4)	80
C(43C)	6773(4)	-3315(3)	5166(3)	53
C(44C)	7258(5)	-3657(3)	5577(4)	74
N(50C)	3585(3)	-2802(2)	6737(2)	43
C(50C)	3791(4)	-2611(3)	7261(3)	54
N(55C)	4538(3)	-2035(2)	5318(3)	41
C(55C)	5019(4)	-1657(2)	5481(4)	65
C(60C)	3627(5)	-2833(4)	7776(4)	75
C(65C)	5484(5)	-1431(4)	5072(6)	108
C(70C)	3278(6)	-3265(4)	7751(5)	91
C(75C)	5455(7)	-1583(5)	4497(7)	119
C(80C)	3051(5)	-3480(4)	7209(5)	82
C(85C)	4955(7)	-1949(4)	4354(5)	102
C(90C)	3224(4)	-3237(3)	6721(4)	54
C(91C)	1145(4)	-2394(3)	4664(4)	59
C(92C)	1418(6)	-2267(4)	4088(4)	88
C(93C)	830(5)	-1618(3)	5161(4)	67
C(94C)	245(6)	-1745(5)	5590(5)	112
C(95C)	4492(5)	-2176(3)	4753(4)	67
Ni(1D)	8863(1)	2948(1)	15241(1)	33
O(1D)	8367(2)	3386(1)	15820(2)	33

Table A7. continued (ii).

C(2D)	7806(3)	3688(2)	15722(3)	29
N(3D)	7233(3)	3723(2)	15273(2)	33
N(4D)	6543(3)	3514(2)	14397(2)	37
C(4D)	7277(4)	3538(2)	14740(3)	34
S(5D)	8140(1)	3368(1)	14439(1)	45
O(6D)	9575(2)	2628(1)	15948(2)	34
C(7D)	10271(4)	2456(2)	15862(3)	33
N(8D)	10426(3)	2140(2)	15469(2)	33
N(9D)	10070(3)	1562(2)	14786(2)	42
C(9D)	9967(4)	2015(2)	14970(3)	40
S(10D)	9366(1)	2410(1)	14541(1)	50
C(11D)	7736(3)	4062(2)	16197(3)	31
C(12D)	7260(4)	4467(2)	16092(3)	40
C(13D)	7208(4)	4813(2)	16520(3)	42
C(14D)	7624(3)	4760(2)	17067(3)	29
C(15D)	8117(4)	4352(2)	17172(3)	33
C(16D)	8176(4)	4009(2)	16738(3)	34
C(41D)	6490(5)	3382(3)	13765(3)	52
C(42D)	6527(6)	3827(4)	13388(4)	82
C(43D)	5789(4)	3654(2)	14620(3)	44
C(44D)	5372(5)	3235(3)	14878(4)	75
N(50D)	7890(3)	2472(2)	15360(2)	40
C(50D)	7754(4)	2351(3)	15892(3)	56
N(55D)	9859(3)	3433(2)	15270(2)	39
C(55D)	10062(4)	3702(2)	15750(3)	46
C(60D)	7112(5)	2069(3)	16026(4)	72
C(65D)	10717(4)	4001(3)	15824(3)	53
C(70D)	6575(5)	1902(3)	15572(4)	64
C(75D)	11200(4)	4041(3)	15378(4)	61
C(80D)	6696(4)	2028(2)	15019(4)	59
C(85D)	11014(4)	3781(3)	14875(4)	56
C(90D)	7359(4)	2312(2)	14918(4)	53
C(91D)	9656(5)	1376(3)	14232(3)	58
C(92D)	10168(5)	1468(3)	13718(4)	66
C(93D)	10547(4)	1212(2)	15171(3)	49
C(94D)	10060(6)	989(3)	15609(4)	78
C(95D)	10337(4)	3482(2)	14841(3)	47
Ni(1E)	8007(1)	5343(1)	18816(1)	31
O(1E)	9155(2)	5134(2)	18991(2)	38
C(2E)	9674(4)	5180(2)	19427(3)	32
N(3E)	9619(3)	5382(2)	19944(3)	45
N(4E)	9055(4)	5818(4)	20651(4)	114
C(4E)	8948(4)	5581(3)	20131(3)	51
S(5E)	7984(1)	5611(1)	19788(1)	47
O(6E)	8059(2)	5075(1)	18001(2)	34
C(7E)	7545(3)	5113(2)	17552(3)	28
N(8E)	6953(3)	5435(2)	17442(2)	32
N(9E)	6209(4)	6102(2)	17612(3)	52
C(9E)	6643(4)	5716(2)	17844(3)	34
S(10E)	6631(1)	5590(1)	18577(1)	33
C(11E)	10490(3)	4966(2)	19349(3)	33
C(12E)	11137(4)	5012(2)	19788(3)	44
C(13E)	11887(4)	4806(2)	19704(3)	48
C(14E)	11992(4)	4529(2)	19205(3)	34
C(15E)	11337(4)	4482(2)	18790(3)	36
C(16E)	10602(4)	4704(2)	18851(3)	34
C(41E)	8394(6)	6097(4)	20921(5)	89
C(42E)	8028(8)	5762(6)	21288(6)	141
C(43E)	9906(8)	5843(4)	21026(7)	129
C(44E)	9931(7)	5360(4)	21255(6)	119
N(50E)	7667(3)	4610(2)	19040(2)	40
C(50E)	7122(4)	4359(2)	18703(3)	39
N(55E)	8477(3)	6020(2)	18528(2)	36
C(55E)	9006(4)	6008(3)	18134(3)	50

Table A7. continued (iii).

C(60E)	6912(4)	3879(2)	18817(4)	54
C(65E)	9342(5)	6424(3)	17909(4)	64
C(70E)	7310(4)	3661(2)	19305(4)	55
C(75E)	9090(5)	6867(3)	18110(4)	63
C(80E)	7892(5)	3913(2)	19648(4)	55
C(85E)	8564(6)	6877(3)	18515(4)	66
C(90E)	8055(4)	4377(2)	19504(3)	48
C(91E)	5658(6)	6399(3)	17953(4)	67
C(92E)	6090(7)	6821(3)	18198(5)	95
C(93E)	6215(7)	6210(3)	16978(4)	79
C(94E)	5517(6)	5923(3)	16618(4)	84
C(95E)	8262(5)	6450(2)	18723(3)	51
Ni(1F)	13722(1)	3609(1)	18471(1)	30
O(1F)	13004(2)	3438(1)	17721(2)	34
C(2F)	13135(3)	3155(2)	17313(3)	31
N(3F)	13826(3)	2996(2)	17136(2)	34
N(4F)	15180(3)	2950(2)	17075(2)	43
C(4F)	14581(4)	3059(2)	17408(3)	33
S(5F)	14850(1)	3208(1)	18136(1)	38
O(6F)	12766(2)	3956(1)	18774(2)	37
C(7F)	12788(4)	4301(2)	19134(3)	34
N(8F)	13414(3)	4512(2)	19436(3)	42
N(9F)	14726(3)	4729(2)	19628(3)	45
C(9F)	14207(4)	4377(2)	19460(3)	36
S(10F)	14563(1)	3801(1)	19356(1)	39
C(11F)	12387(3)	2961(2)	16950(3)	29
C(12F)	12454(3)	2639(2)	16494(3)	31
C(13F)	11765(3)	2465(2)	16160(3)	28
C(14F)	10996(3)	2615(2)	16262(3)	28
C(15F)	10923(3)	2938(2)	16723(3)	35
C(16F)	11618(4)	3104(2)	17062(3)	36
C(41F)	16048(4)	2955(3)	17291(4)	70
C(42F)	16430(6)	3430(5)	17175(5)	133
C(43F)	14999(4)	2791(3)	16466(3)	53
C(44F)	14880(5)	2248(3)	16421(4)	68
N(50F)	13225(3)	2979(2)	18853(2)	37
C(50F)	12443(4)	2861(2)	18711(3)	43
N(55F)	13970(3)	4288(2)	18077(2)	39
C(55F)	13333(5)	4559(2)	17845(3)	49
C(60F)	12049(4)	2488(2)	18968(3)	48
C(65F)	13430(5)	5014(2)	17612(4)	67
C(70F)	12482(5)	2223(2)	19396(4)	59
C(75F)	14224(6)	5188(3)	17607(4)	77
C(80F)	13291(5)	2336(2)	19546(4)	62
C(85F)	14872(5)	4911(3)	17831(4)	69
C(90F)	13634(4)	2713(2)	19263(3)	49
C(91F)	15619(4)	4676(2)	19656(3)	46
C(92F)	15994(5)	4580(3)	20281(4)	70
C(93F)	14425(4)	5224(2)	19733(4)	63
C(94F)	14280(6)	5494(3)	19153(5)	99
C(95F)	14721(4)	4469(3)	18065(3)	50
N(1G)	6292(7)	-737(3)	7079(5)	121
C(2G)	5571(6)	-643(3)	7274(4)	80
C(3G)	5432(6)	-241(3)	7567(3)	72
C(4G)	6002(6)	104(3)	7669(4)	74
C(5G)	6744(6)	3(4)	7471(4)	85
C(6G)	6908(6)	-380(4)	7208(5)	89
N(7G)	5119(12)	3181(3)	10785(4)	192
C(8G)	4494(6)	3044(4)	11232(7)	120
C(9G)	4758(3)	2867(2)	11697(2)	90
C(10G)	5389(3)	2809(2)	11826(2)	121
C(11G)	5999(8)	2873(4)	11583(8)	150
C(12G)	5920(3)	3041(2)	11088(2)	116
N(13G)	10035(9)	5612(5)	16660(7)	171